# Time series analysis of data measured in the nearshore area

by

Rosa Mphasha

*Thesis presented in partial fulfilment of the requirements for the degree of Master of Science in Applied Mathematics in the Faculty of Science at Stellenbosch University*


Department of Mathematical Sciences,
Applied Mathematics Division,
Stellenbosch University,
Private Bag X1, Matieland 7602, South Africa.

Supervisors:

Dr. G.P.J. Diedericks & Dr. S. Fidder-Woudberg

March 2016

# Declaration

By submitting this thesis electronically, I declare that the entirety of the work contained therein is my own, original work, that I am the sole author thereof (save to the extent explicitly otherwise stated), that reproduction and publication thereof by Stellenbosch University will not infringe any third party rights and that I have not previously in its entirety or in part submitted it for obtaining any qualification.

Date: March 2016

# Abstract

Factors that lead to the generation of currents in the nearshore area within the Natal Bight were investigated. The investigation was carried out on data that spans from the 6th June 2012 to the 16th January 2013. The data comprised current measurements, wave measurements, water level measurements, as well as wind measurements. The measurements were decomposed into different direction components in order to study their impacts on corresponding current measurements. Current measurements were resolved into tidal currents and non-tidal currents through the use of harmonic analysis. Stokes drift was estimated using a monochromatic spectrum to obtain the wave induced current. The effect of the wind on the currents was analysed through the use of wind roses and duration analysis. The study was completed with an exploration of the contribution of the Agulhas current. It was found that the waters are characterized by a semi-diurnal, micro-tidal system and tides have a limited contribution to the generation of currents. The contribution of Stokes drift to the overall currents is less than that of tides. Wind is the most significant generator of the nearshore currents.

# Opsomming

Faktore wat lei tot die opwekking van strome in die kusgebied binne die Natal Bog (Eng. Natal Bight) was ondersoek. Die ondersoek is uitgevoer op data wat strek vanaf die 6de Junie 2012 tot die 16de Januarie 2013. Die data bestaan uit stroom metings, golf metings, watervlak metings asook wind metings. Die metings word ontbind in verskillende komponente ten einde die impak daarvan op die ooreenstemmende stroom metings te bestudeer. Stroom metings was onderskeidelik in gety strome en nie-gety strome verdeel deur gebruik te maak van harmoniese analise. Stokes dryf was bereken deur van 'n monochromatiese golfspektrum gebruik te maak. Die uitwerking van die wind op die strome is analiseer deur die gebruik van wind rose en 'n analise van die duurte waaroor winde uit spesifieke rigtings gewaai het. Die studie is voltooi met 'n ondersoek na die bydrae van die Agulhas-stroom tot die gemete strome. Daar is gevind dat die waters gekenmerk word deur 'n twaalf-uurlikse, mikro-gety stelsel en dat getye 'n beperkte bydrae tot die opwekkinging van strome het. Die bydrae van Stokes dryf tot die algehele strome is minder as die bydrae van getye. Wind is die belangrikste stroomopwekker van die strome langs die kus.

# Acknowledgements

I would like to acknowledge:

- My family, especially my mother, grandmother and sister for providing me with unfailing support and continuous encouragement throughout my years of study and through the process of researching and writing this thesis. This accomplishment would not have been possible without them.
- My supervisors, Dr. G.P.J. Diedericks and Dr. S. Fidder-Woudberg for the patient guidance, encouragement and advice that they provided throughout my time as their student.
- The financial assistance of the National Research Foundation (NRF) towards this research is hereby acknowledged. Opinions expressed and conclusions arrived at, are those of the author and are not necessarily to be attributed to the NRF.

# Contents

# List of Figures

# List of Tables

# Nomenclature

### Variables

| | |
|---|---|
| $\alpha$ | Power in wind power law |
| $x_i$ | Observation at position $i$ |
| $y_i$ | Observation at position $i$ |
| $\bar{x}$ | Mean |
| $s$ | Standard deviation |
| $s^2$ | Variance |
| $r$ | Correlation coefficient |
| $t$ | Time step |
| $x_t$ | observation at time step $t$ |
| $m$ | Lag or time offset |
| $C_m$ | Auto-covariance at lag m |
| $n$ | Particular position of observation in series |
| $N$ | Length of series |
| $\Delta t$ | Time interval |
| $X_t$ | Fourier Transform |
| exp | Exponential |
| $\Delta t$ | Time interval |
| $t_n$ | Time interval at position $n$ in series |
| $s_m$ | Smoothed series |
| $w_m$ | Window function |
| $w_R$ | Rectangular window function |
| $y_m$ | Time series |
| $\hat{\mathbf{e}}^{\mathrm{w}}$ | Unit vector |
| $C_{xy}(m)$ | Cross-variance between series $x$ and $y$ at lag $m$ |
| $r_{xy}(m)$ | Cross correlation between series $x$ and $y$ at lag $m$ |
| $C_{xx}(0)$ | Covariance of series $x$ |
| $k$ | Wavenumber |

**Variables with units**

| | | |
|---|---|---|
| $\lambda$ | Wavelength | [m] |
| $f$ | Frequency | [Hz] |
| $f_D$ | Frequency of received signal | [Hz] |
| $f_s$ | Frequency of sound when objects are stationary | [Hz] |
| $f_n$ | Nyquist frequency | [Hz] |
| $C$ | Speed of sound | [m/s] |
| $v_x$ | East-west velocity component | [cm/s] or [m/s] |
| $v_y$ | North-south velocity component | [cm/s] or [m/s] |
| $v_c$ | Cross-shore velocity component | [cm/s] or [m/s] |
| $v_l$ | Longshore velocity component | [cm/s] or [m/s] |
| $\beta$ | Scientific notation wave direction | [°] |
| $\theta$ | Incoming wave direction | [°] |
| $u_r$ | Speed of wind at given height | [m/s] |
| $zr$ | Given height of wind measurement | [m/s] |
| $u$ | Speed of wind at new height (10 m ) | [m/s] |
| $z$ | New height (10 m) | [m] |
| $V_i$ | Wind intensity | [m/s] |
| $\phi_i$ | Incoming wind direction | [°] |
| $\vec{U}_s$ | Stokes drift velocity | [m/s] |
| $\omega$ | Angular wave frequency | [rad/s] |
| $z$ | Depth from surface | [m] |
| $h$ | Average water level | [m] |
| $H_s$ | Significant wave height | [m] |
| $T_p$ | Peak wave period | [m] |
| $T_{mean}$ | Mean wave period | [s] |
| $D_p$ | Peak wave direction | [°] |
| $D_{mean}$ | Mean peak wave direction | [°] |
| $f_p$ | Peak wave frequency | [1/s] |

**Acronyms**

| | |
|---|---|
| DFT | Discrete Fourier Transform |
| FFT | Fast Fourier Transform |
| PSD | Power spectral density |
| NNE | North North East |
| ENE | East North East |
| ESE | East South East |

SSE South South East
SSW South South West
WSW West South West
WNW West North West
NNW North North West

# Chapter 1

# Introduction

## 1.1 The nearshore area

The coastal zone is the area where the land meets the ocean. The coastal zone is under pressure from both the land side and the sea side. Climate change with its accompanying sea level rise and increased storms, is a natural process that puts pressure on the coastal zone. On the other hand, the coastal zone is utilised as a residential area, used for tourism, serves as a location for harbours and marine protected areas. The coastal zone is therefore a subject of interest in many fields. Any information that aids in the understanding of the coast may be of value to society.

When a person walks towards the ocean, advancing through the coastal zone, the first area the person comes across is the surf zone. This is the zone where waves are unstable and break, creating a bubbly surface. Farther seawards past this zone, is a wave shoaling zone where conditions are stable relative to the surf zone. This is the area that is of interest in this study. This zone is referred to as the nearshore zone. Figure 1.1 illustrates the structure of the nearshore area.

The nearshore area is the area that extends from the surf zone to the inner shelf edge. The nearshore is characterised by shallow depths, typically less than 30 m as opposed to more than 4000 m in the open ocean. It connects the inner continental shelf and the coast. On coasts that have steep slopes the nearshore zone may be less than 100 m in width, while at coasts with a less steep slope it may extend to 5 km offshore. On many coasts the width spans 0.5 to 2.5 km (Davidson-Arnott & Greenwood, 2003).

Ecologically, the nearshore is a complicated and dynamic environment. There is adequate sunlight to support and maintain the growth of plants attached to the seabed. The nearshore zone supports ecological communities, such as

those related with sea grass and coral reefs (Davidson-Arnott & Greenwood, 2003).

The nearshore is also the area where waves undergo transformation due to the geometry, depth, and man-made protective structures present at some coasts.

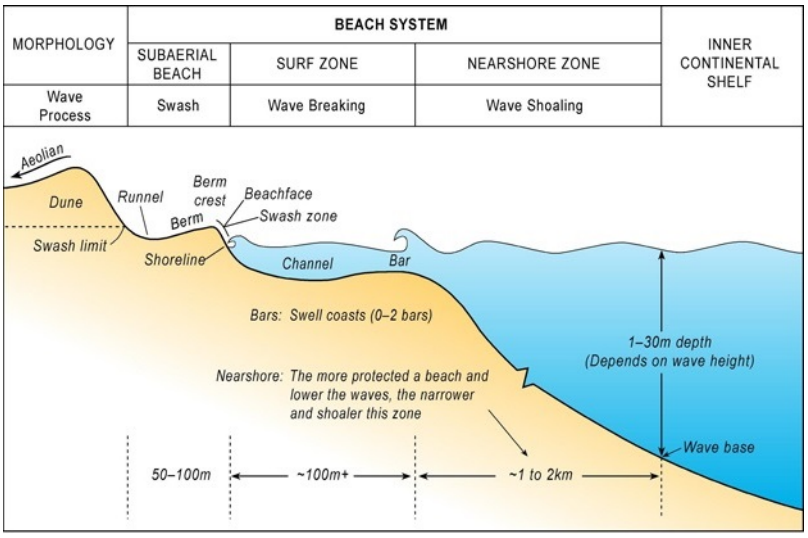


**Figure 1.1:** Diagram representing the nearshore area (Short, 2012).

The proximity of the nearshore to the land allows for inland water to seep or flow into ocean water. With the inflow of water from inland, some nearshore waters have reduced density and salinity (Bowden, 1983) relative to the deepest ocean sections. The dynamic nature of the nearshore makes it important to understand the processes that take place here from a scientific, environmental and engineering perspective.

## 1.2 Problem definition

To understand the different processes in the nearshore area it is important to understand the movement of the waters in this area. The movement of water from one position to the other produces a current. It is thus crucial to understand how currents are generated in the nearshore area.

### 1.2.1 Research question

The main research topic addressed in this study, is to determine what the driving forces that contribute to the generation of currents in the nearshore

area are.

Currents may be driven by various processes such as water density differences, tides, winds, and waves. According to the Coastal Engineering Manual (CEM, 2001), the magnitude of currents generated by different processes can be expressed linearly as follows:

$$u = u_w + u_t + u_s + u_b, \tag{1.2.1}$$

where $u$ is the total current magnitude, $u_w$ is the magnitude of the currents driven by wind, $u_t$ is the magnitude of the current driven by tidal action, $u_a$ is the magnitude of the currents driven by waves and $u_b$ is the magnitude of the currents driven by background phenomena such as ocean currents, respectively.

The extent of the effect that each of the driving forces can have on the generation of currents depends on the geographical location. In this study the location is on the East coast of South Africa, which, apart from the processes mentioned in equation (1.2.1),is also affected by the Agulhas current. The linear superposition of forcing mechanisms given in equation (1.2.1) is taken as an assumption, and this study seeks to determine the forcing mechanisms at a specific location.

This research addresses the driving forces of currents in the nearshore and to what degree each one of them accounts for the generation of currents.

### 1.2.2 Motivation

The nearshore provides opportunities for recreational activities such as boating, fishing and surfing. This area is also a habitat to a variety of flora and fauna. Coastal residential areas are increasing. There are also industries that are built on the coast; these include nuclear power stations, desalination plants and power station plants that could harness energy from waves for the generation of electricity. All of which are factors to highlight the importance of the nearshore or coastal areas.

Water in the nearshore isprone to degradation and deterioration due to maltreated sewage disposal and the resulting release of nutrients. These nutrients overfeed the fauna in the area, causing overpopulation which results in the exhaustion of oxygen and the blocking of sunlight. Run-off of toxic metals, leakage of oil from ships and tanksas well as dumping of waste by humans pose a threat to nearshore areas.

To maintain nearshore areas as life supporting environments, an understanding of the processes that take place in this zone is crucial. A methodology on how

to approach the study of coastal zones and the processes that occur hereis necessary. This research focuses on finding the driving forces of currents in the nearshore area by using time series analysis techniques.

### 1.2.3 Aim and objectives

#### 1.2.3.1 Aim

The aim of this study is to find the driving forces of currents in the study location and to evaluate to what degree each one of them accounts for the generation of currents by analysing time series of measured currents.

#### 1.2.3.2 Objectives

The objectives of this study are divided into general objectives that include the application of general research and oceanographic techniques;and specific ones, more focused objectives that take location and climatological factors into consideration.

**General objectives**

- Apply general data interrogation techniques.
- Apply general oceanographic data analysis techniques to nearshore data.
- Gather information about the processes in the nearshore area.

**Specific objectives**

- To use the collected data on water levels and currents to evaluate the effect of tides on currents and remove such tidal effects with a tidal analysis software.
- To use the collected wind speed and direction with current velocities to evaluate how wind affects currents.
- To use the measured wave heights, mean direction and peak periods to calculate the contribution of Stokes drift to the current.
- To identify the order of importance of each of the driving forces of currents.

### 1.2.4 Approach

Data which include current speed and directions through the water column from the bottom to the surface, water level measurements, wave mean directions, significant wave heights and peak periods as well as wind speed and directions are used in this study. The water level and current data were measured by means of an Acoustic Doppler Current Profiler (ADCP), wave data were measured by means of a SEACAT which was attached to the ADCP in the nearshore and the wind data was measured at the Durban port. The data has been provided by WSP Africa Coastal Engineers in Stellenbosch. The data spans from the $6^{th}$ of June 2012 at 09H00 to the $16^{th}$ of January 2013 at 10H00.

The first step in this study is to construct data summary diagrams. These diagrams allow for the identification of erroneous values and missing values. The data is checked and measuring units are adjusted to oceanographic and meteorologicalconvention. Wind and current data are resolved into north-south and east-west components as well as cross-shore and longshore components.

Derived statistics, such as the means, variances and correlation coefficients are estimated from the data. Such statistical estimates provide information on the quality and variability of the data.

The data series is also examined for frequency content. Fast Fourier Transforms and harmonic analysis are applied to the data for detection of dominant periodicities and preprocessing before filtering.

The tidal effect is removed from the current data with the use of a tidal analysis software developed by Pawlowicz et al. (2002). The de-tided (with the tide removed) data is then used with wind data to evaluate the impact of wind as a driving force. The de-tided data will also be studied with wave data to identify the effect of the Stokes drift on the current. The investigation of the effect of the Agulhas currentfollows. Finally, conclusions are drawn.

## 1.3 Structure of thesis

The following chapters cover an analysis of measured currents and an explanation of the driving forces of currents in the nearshore area. The order of importance of the different driving forces in the generation of currents is also highlighted.

- Chapter 2: Introduces currents, the different types and how they are generated. Different techniques for measuring currents are also provided with an elaborate introduction to the working of an ADCP.

- Chapter 3: Provides details about the measured data. The data is presented graphically. Progressive vector diagrams are provided and the current magnitudes and directions are resolved into vector components. Autocorrelation analysis is performed on the data as well as power spectral analysis.

- Chapter 4: Provides information on tides and tidal analysis. The tided signals present in the current and water level measurements are studied and then removed from the current data.

- Chapter 5: Wave data is introduced and graphically presented. Wave heights, peak periods and directions are used to compute and investigate the effect of Strokes drift on currents.

- Chapter 6: Provides wind data and techniques to be used in the study of the wind impact on the current. Wind roses and progressive vector diagrams of the current and wind data are presented and compared to each other. cross-correlation is also performed and applied on wind and current data. in addition, power spectral analysis is performed on the wind data.

- Chapter 7: Provides information on the Agulhas current. The presence of the Agulhas current is investigated and discussed.

- Chapter 8: A summary and conclusions of the study are given here.

# Chapter 2

# Nearore processes and measurement techniques

## 2.1 Introduction

In this chapter various processes that lead to the generation of currents are presented. It starts with the discussion of these different processes, which is followed by a discussion of different types of currents that are found in the nearshore zone and the types of instruments that can be employed to measure currents. A background review of studies on the KwaZulu-Natal coast of South Africa concludes the chapter.

## 2.2 Nearshore processes

To understand any particular activity in the nearshore area it is crucial to understand the processes that are constantly at work in this area. This chapter introduces some of the different processes that are active in the nearshore area.

The processes are responsible for the form and structure of the coast and also generate coastal currents. In various coastal systems, the main source of energy comes from waves. On some coasts tidal processes and their variability are significant, while on others ocean currents dominate.

Climatological conditions also play a role in the structure of a coastal system. These processes are not isolated, but they may act in sequence or simultaneously. Under certain conditions one process enhances the other, for instance a rising tide may generate a movement of water in a shoreward direction, setting up a current. The rising tide may also increase the height and potency of waves that arrive at the shore. Under other conditions, one process may inhibit the other, for instance the flow of a tidal current in one direction may diminish the velocity of waves moving in an opposite direction (nonetheless, it

is advantageous to separate the processes for the purpose of discussion).

Firstly, tides are briefly discussed, followed by waves, climate, and then ocean currents. Only a brief discussion is given here since an in depth study will be mad in later chapters.

### 2.2.1 Tides

Tides are the motion of the ocean produced mainly by the gravitational forces of the moon and the sun on the earth. Tides are important in the nearshore as they cause a regular variation in sea level along the shore and generate tidal currents. In the open sea, tides are long waves that become altered as they move across continental shelves.Tides that occur during new moon, i.e., when the moon and sun are in alignment and yielding compound gravitational effects, are large and are called spring tides. The tides that occur in the first or third quarters of the moon, when the moon and sun are perpendicular to each other, do not experience the amalgamated gravitational forces. These tides are relatively small and are called neap tides (Bird, 1984; Woodroffe, 2002).

The tidal range in the open ocean is within the order of 0.5 m, but increases as the tides enter coastal waters which are relatively shallow (Bird, 1984). Different coastal environments have difference tidal ranges. An environment with a spring tidal range less than 2 m is called microtidal, one with a tidal range from 2 to 4 m is called mesotidal, one with 4 to 6 m, macrotidal, and one with up to 8 m, megatidal (Woodroffe, 2002). South African coastal waters are characterised by a microtidal range (Harris, 1978b).

As the tides rise and fall, they generate currents. Tidal currents associated with spring tides may have large velocities and are called spring currents. Tidal currents associated with neap tides have lower velocities and are called neap currents.

### 2.2.2 Waves

Waves are undulations on the surface and they move across the water surface transmitting energy in the process with a relatively small movement of net mass. There are different types of waves, such as trans-tidal waves, tides, storm surges, tsunamis, infragravity waves, wind-generated waves and capillary waves. The waves listed here are ordered in terms of frequency, from lowest frequency to highest frequency and illustrated in Figure 2.1 (Holthuijsen, 2007). Waves that are likely to be encountered in the nearshore zone include tide and wind generated waves with a period of at most 20 seconds.

Some waves that break on the beach are caused by distant winds. Waves that result from wind, increase in size depending on the speed of the wind. Their maximum limit is set by gravity and surface tension. Some factors that influence the generation of wind waves include fetch (distance over which the wind is blowing), duration of the wind and the depth of the water (Woodroffe, 2002). Deep water waves can travel through the open ocean to the shore. These waves that travel away from the area where they were generated until they are not influenced by local winds any more, are called swell. In comparison with wind waves, swell is produced by longer waves with gentler crests. After some time, swell covers long distances and coincides with different waves brought on by farther storms going in varying directions, until they reach coastlines.

As deep water waves move into shallow water they undergo transformation. The waves interact with the ocean bed and wave speed decreases. Refraction is likely to take place, where the wave crest becomes close to being parallel to the shore. For refraction, the portion of the wave in shallow depth is slowed more than the portion in deeper waters, thus the wave bends towards the shallow water.

Another process of transformation is called diffraction, which occurs when waves interact with obstructions in their path. The wave spreads and changes direction as it reaches an obstruction that is comparable in size to its wavelength. Wave energy is transferred to the area behind the obstruction. The diffraction process is weak on open beaches (Bowden, 1983).

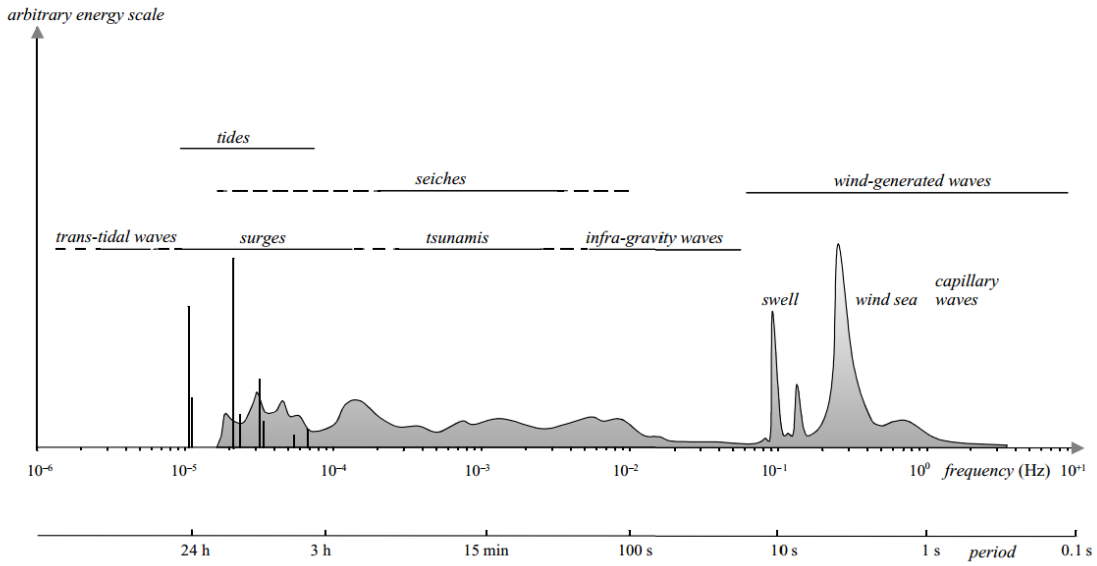


**Figure 2.1:** Frequencies and periods of the undulations of the ocean surface (Holthuijsen, 2007).

As waves enter shallow water, especially over a shoal bottom, their wavelengths decrease and their heights increase until they break. At the break point, the wave will either spill, collapse, plunge or surge (Bowden, 1983). Longshore currents and some cross-shore currents result from the breakers. Cross-shore currents comprise rip currents and undertow.

#### 2.2.2.1 Longshore currents

When waves approach the shore at an angle and break they can drive longshore currents. The flow of water that result after the breaking of waves, on the shore, drives a longshore current which moves parallel to the shore in the direction of the parallel component of the wave (Bowden, 1983). These currents may also be driven by variation in wave height. Large waves may also cause large setups (increase in mean water level) at the shoreline, which in turn cause pressure gradients alongshore and the pressure gradient drives currents towards areas with smaller wave heights (Cushanick, 2005). The strength of longshore currents is only appreciable in the surf zone.

#### 2.2.2.2 Rip currents

When longshore currents converge from opposite directions they form a jet. The jet shoots away from the shoreline in a seaward direction and is called a rip current (Bowden, 1983). These currents are narrow, horizontally constricted, and they have sporadic large velocities. They are usually created in intermediate moderate wave energy coasts (Aagaard & Vinther, 2008). Moderate wave energy coasts are defined by an annual significant wave height of 0.3 to 1 m and the coasts tend to have swamps and deltas, and are partially cliffed (Bird, 1984).

#### 2.2.2.3 Undertow

An undertow is a homogeneous current that flows seaward from the surf zone close to the sea bed. The mean speed of an undertow is approximately 0.5 m/s. An undertow occurs in high energy wave conditions and carries an extensive volume of sediment offshore (Aagaard & Vinther, 2008).

### 2.2.3 Atmospheric conditions

Wind is one of the factors responsible for the generation of waves and currents in coastal zones. Although some coasts are heavily affected by swell related to storms coming from offshore locations, there are also significant waves and currents generated by local winds. Some winds are particularly associated with the coast, which include land breezes and sea breezes. A land breeze occurs during the night when the sea remains warm and the land cools down, so that the wind blows from the land towards the sea. Sea breezes occur during the day when the land is warmer than the sea and then the wind blows from the sea landwards (Woodroffe, 2002).

Wind affects the sea through stress on the sea surface, transferring momentum from the wind to the water. This results in surface waters being driven to move at a speed of approximately 3% (rule of thumb) that of the wind speed at 10 m above the sea surface (Bowden, 1983). Eventually currents that travel in the same direction as the wind are generated which are referred to as wind driven currents. These currents rapidly decrease in speed with increasing depth (Harris, 1978b). Owing to the Coriolis force, the drift induced by the wind is deflected to the left of the wind direction in the southern hemisphere. The deflection is minimized in shoaling waters. When the coast is at the left of the wind, the result is a pile up of water on the shore and, when the coast is to the right, upwelling occurs.

**Upwelling**

Strong winds blowing over the sea surface push water far away from its original position. At the position where the water is removed, water ascends from underneath the surface to replace the surface water that is moving away. The water that is brought up is rich in nutrients, colder and denser than the water it is replacing (Meyer et al., 2002).

Upwelling can occur in coastal waters and also in the open sea. Coastal upwelling contributes to the sustainment of fisheries. For instance, the upwelling of nutrient rich water on the Agulhas bank, on the south coast of South Africa, has made the coast popular for fishermen. Upwelling can be a seasonal process in some areas while being a year-round process in other areas.

### 2.2.4 Ocean currents

Large scale movements of water that occur in the oceans are referred to as ocean currents. This process carries water from the equator towards the poles, redistributing heat around the globe. They make up the ocean circulation which has developed over the course of the movement of plate tectonics as the land masses embraced their present positions. Some parts of the ocean circulation have changed in the quartenary as sea level has varied. Examples include the re-opening of the Torres Strait and English Channel following the flooding of land platforms by the risen Holocene sea level (Woodroffe, 2002).

Surface ocean currents are kept in motion by wind stresses (from prevailing winds) on the surface of the open sea. These currents are also in part (especially deep currents) driven by density variation as a result of variations in temperature and salinity. The variations in temperature and salinity are referred to as thermohaline. These currents are different to those associated with tides and waves or those that are created in coastal waters during strong wind conditions. These currents are slow in motion and can travel for thousands of kilometers.

Atmospheric circulations and thermohaline patterns influenced by the rotation of the earth and the arrangement of land masses maintain the circulation of ocean currents observed today. The circulation is counter-clockwise in the southern hemisphere and clockwise in the northern hemisphere. Ocean currents have a variety of impacts on coastal environments, including climatological conditions and sea surface temperatures (Woodroffe, 2002). They also bring warm or cold water to coastal environments influencing coastal ecological systems (Bird, 1984).

The Agulhas current is one of the ocean currents. It is a deep and progressive current that travels southwards along the east coast of Africa. It drains water accumulated from the Trade wind current and other waters towards the poles. It causes cyclonic eddies in coastal waters, and in areas where it follows close to the coast the waters also move in its direction. Contrary currents are also created in its presence between the current and coast and the water it transports sets up a pressure gradient in coastal waters (Harris, 1978b).

## 2.3 Instruments used to measure currents

The need to understand ocean processes has led to the development of instruments that can be used to measure the different processes that take place in the ocean. These processes include water level variations, wave conditions and currents. There are various instruments available to measure currents and these instruments are constantly being improved. Most instruments are equipped with a compass, a speed sensor, built-in data averaging algorithm and a data storage device (Emery & Thomson, 2004). There are various types of current meters and they use different types of sensors. The variety of sensors includes:

- Savonious rotors,
- Propellers,
- Electronic sensors and
- Acoustic detectors.

All the current meters discussed in this section record speed and direction measurements at a fixed position. These type of measurements at a specific location are referred to as Eulerian measurements.

### 2.3.1 Rotor type current meter (RCM)

The rotor type current meter uses a Savonious rotor. The Savonious rotor comprises six axis-symmetric curved blades in a casing that is aligned with the flow direction. It records data on small magnetic tapes (Emery & Thomson, 2004). The RCM does not average internally and post processing has to follow to obtain the averaged samples. Improvements in their operation has resulted in a series of RCMs having been developed. Their popularity is owed to their simplicity of use since operation and calibration can be performed with ease. They are also reliable and of relatively low cost. It is easy to add other sensors to the RCM for measuring conductivity, depth and temperature on the same data logger.

### 2.3.2 Vector averaging current meter (VACM)

This current meter also uses a Savonious rotor for speed measurement. It employs burst sampling: It measures small samples of closely-packed data, and these samples are separated with long periods of no data. The rapidly collected direction and speed measurement samples are averaged and then used for horizontal and vertical components of velocity computation. Each component is then averaged separately and a single value of the velocity vector is produced for each burst of data collection.

### 2.3.3 Vector measuring current meter (VMCM)

A vector measuring current meter has two orthogonal cosine response propeller sensors to measure horizontal velocity components directly. Cosine response means that the recorded speed is proportional to the cosine of the angle of the current vector with respect to the horizontal. The instrument orientation with respect to magnetic north is sensed with an electronic compass. North-south and east-west velocity components are computed, averaged, and then the averages are recorded on a storage device. In laboratory comparison tests, the VMCM performed better than other current meters when measuring a combination of small mean currents with oscillatory flows of high frequency (Weller & Davis, 1980).

### 2.3.4 Electromagnetic current meters (ECM)

An electromagnetic current meter uses an electronic sensor which employs Faraday's law of electromagnetic induction. As a conductor (the ocean current) moves through an electromagnetic field (produced by the instrument), it generates a voltage that is measured by the sensor electrodes. This voltage is directly proportional to the speed of the ocean current and it is orthogonal to the direction of the electromagnetic field. An electromagnetic meter and compass are employed to produce horizontal components in earth coordinates, which are north, south, east and west.

### 2.3.5 Acoustic Doppler Current Profiler (ADCP)

An acoustic Doppler current profiler was used for the measurements of current velocities used in this study. A detailed description of the workings of an ADCP is therefore provided. The description of an ADCP is provided in the section is mostly from RDI (1996). Specific information with regards to the exact ADCP that collected data for this data is beyond the scope of this study, since it was not made available.

An ADCP is a hydroacoustic current meter, used to measure water current velocities over a depth range using the Doppler effect of sound waves scattered back from particles within the water. These particles are called acoustic scatterers (or scatterers for short) and include zoo-planktons and phyto-planktons.

An ADCP can be moored horizontally on seawalls or bridge pilings in rivers and canals to measure the current profile from shore to shore. It can also be moored to the bottom of ships to take current measurements as they move. In deep areas, they can be lowered on a cable from the surface. The ADCP that was used to collect the data that is used in this study was moored at the sea bed and measured horizontal currents at different heights from the bottom to the surface.

Based on the manner in which ADCPs transmit, receive and process signals, they are classified into three types, namely, broadband, narrowband and pulse-to-pulse coherent. Amongst the three types of ADCPs, the narrowband ADCP has the lowest precision and resolution, and its profiling range and velocity range are the lowest. The broadband ADCP technology was introduced in the 1990s. Its precision is about 3 to 4 times higher and its resolution is about 10 times higher than those of narrowband ADCPs (Huang et al., 2009). The ADCP that was used to collect the data that is used for this study was a broadband ADCP.

An ADCP transmits sound at a fixed frequency and then registers echoes from the sound scatterers in the water which is then used to calculate velocity. This is a direct application of the Doppler effect. The Doppler effect is the change in the observed sound pitch that occurs as a result of relative motion. Sound waves have characteristics similar to those of shallow water ocean waves. The frequency of a sound wave is defined as:

$$C = f\lambda, \tag{2.3.1}$$

where $C$ is the speed of sound, $f$ is the frequency and $\lambda$ is the wavelength. An example of the Doppler effect is the sound made by the siren of a car as it passes. The siren has a higher pitch as the car approaches and a lower pitch as it moves away from the observer. If the pitch and its change are measured, the velocity of the car can be computed.

Figure 2.2 is a depiction of the Doppler effect. Here $f$ is the frequency of the transmitted pulse while $f_D$ is the frequency of the received signal. In the first case the scatterer is moving towards the sound and the wave period of the sound received by the scatterer is decreased. The wave period of the scattered sound is further decreased by movement of the scatterer, as a secondary source of sound, towards the co-located source and receiver. The combined effect is

an increase in frequency, thus $f_D > f$ (since frequency is the inverse of the wave period). In the second case the motion of the scatterer is away from the source and the co-located receiver. It therefore has an effect of a decrease in frequency, thus $f_D < f$. In the third case, the motion of the scatterer is perpendicular to the source or in a stationary state and has no effect on the scatterer or receiver, thus $f_D = f$.

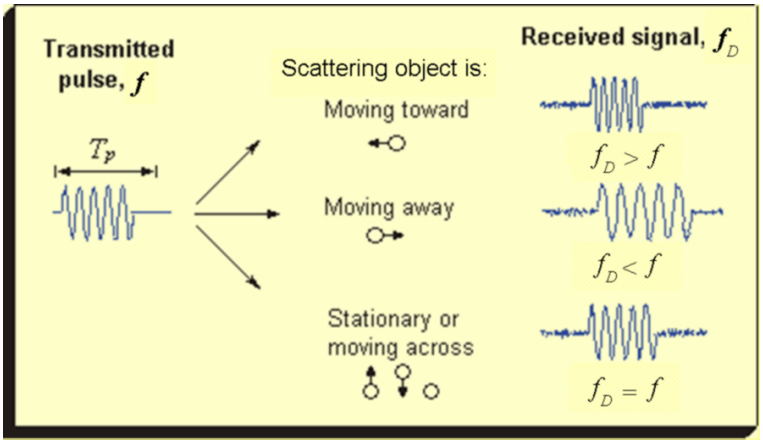


**Figure 2.2:** Depiction of the Doppler effect (GoMA, 2013)

The Doppler shift is the difference between the frequency received by a stationary scatterer and that received by a moving one. The equation for the Doppler shift is

$$f_D - f = f_s(V/C),$$

where $f_s$ is the frequency of sound when objects are stationary, $V$ is the relative velocity between a sound source and receiver. Setting $F_d = f_D - f$ yields

$$F_d = f_s(V/C). \tag{2.3.2}$$

However, an ADCP both receives and transmits sound, so the Doppler shift has to be doubled, equation (2.3.2) then becomes

$$F_d = 2f_s(V/C). \tag{2.3.3}$$

In applications where ADCPs are fixed, both the receiving and transmitting transducers are stationary. The Doppler effect only uses radial motion in line with the transmitted ADCP signal. Angular motion results in no Doppler shift. If a particle is moving both radially and in an angular direction a new term $\cos(X)$ has to be included in equation (2.3.3) to restrain the Doppler shift to the radial component and the equation becomes

$$F_d = 2f_s(V/C)\cos(X), \tag{2.3.4}$$

where $X$ is the angle from the radial direction measured clockwise from the horizontal beam (Boiten, 2003). The angle $X$ is illustrated in Figure 2.3.

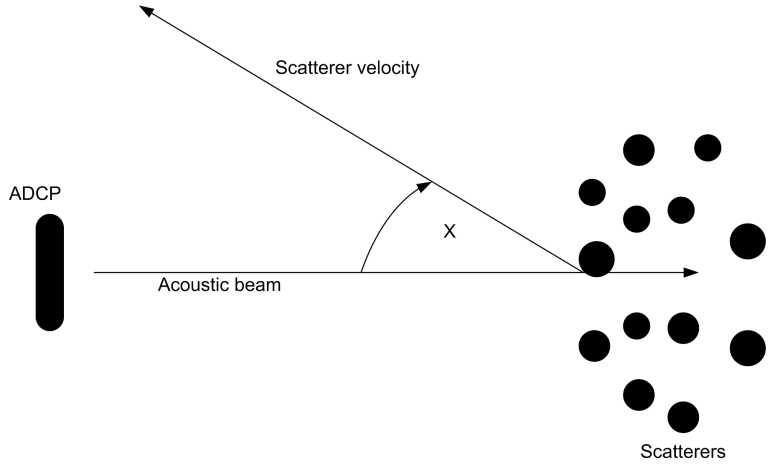


**Figure 2.3:** Vector of relative velocity. $X$ is the angle between the water velocity and acoustic beam.

ADCPs measure velocity using one of two method. They may either use the Doppler shift or use the principle of Doppler time dilation. The latter makes use of the fact that sound takes longer to travel back and forth when a receiver is farther from a sound source. Sound waves that strike particles far from the transducer take longer to come back than those that are reflected from close by.

When a particle is stationary the echoes coming from it will all look identical. If the particle is moved slightly away from a transmitter, it will take slightly longer for sound to travel back and forth. A further increase in the distance between the two implies that it will take even longer for the sound to travel back and forth. This increase in travelling time, owing to an increase in distance, is called propagation delay.

An ADCP may also use phase change to detect propagation delay: Since echoes from the same stationary particle look identical, they also have the same phase. An increase in distance between a transmitter and the particle results in a delayed echo. This echo will have a phase delay relative to the first echo. A further increase in distance causes an even further phase delay relative to the first. These phase delays are measured in degrees and are directly proportional to particle displacements. If propagation delay is measured and the speed of sound is known then the distance that the particle has moved can be computed. Given the time lags between successive pulses, the velocity of the particle can also be computed. The two methods of velocity measurement are mathematically equivalent (RDI, 1996). The ADCP that was used in the

collection of data for this study used time dilation.

An ADCP uses four beams to compute current velocities in three dimensions. Each beam computes the velocity component parallel to it. Earth directions, namely, north-south and east-west are used in the final processing of the measurements. If the beams do not face these directions, trigonometric relations are used to convert the current velocities. This conversion requires that currents be homogeneous in the horizontal layer and the homogeneity is verified by using the third and fourth beam. The third and fourth beams both measure vertical velocity. Measurements from the fourth beam are used for error calculations. The error here is the difference between two estimates of vertical velocity. For example, if one beam points east and another points north, the ADCP can measure the east-west and north-south current components. The difference between the two vertical components produces an error velocity that helps to determine whether the water currents are horizontally homogeneous and whether all four beams are operating properly. Horizontal homogeneity is an assumption that all four beams are sampling the same velocity at the same depth. Recording current measurements in earth coordinates lessens the effort and time needed for post-processing and assures that beam pointing angles are properly corrected.

When an ADCP measures current profiles (at different depths), it divides the current velocity profiles into uniform segments known as depth cells or bins. These are uniformly spaced for ease of processing and interpretation of results. As mentioned earlier, an ADCP sends out pulses and receives echoes in return. Echoes from farther distances take longer to travel back than those travelling from close by. When a signal is received, it is broken into successive segments, which are processed separately. These segments are the bins and the segmentation is called range gating. In this way successive range gates correspond to echoes from increasing distances. The velocity in each gate cell is then averaged over the whole range of the depth cell, thus reducing measurement uncertainties.

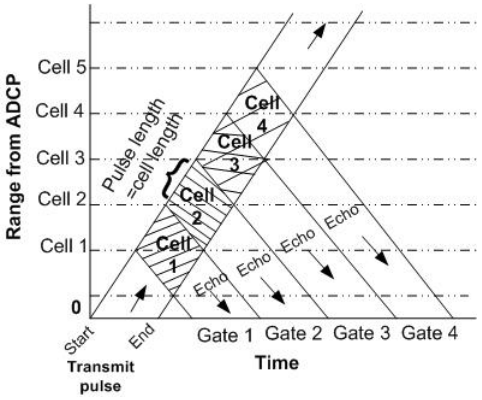


**Figure 2.4:** ADCP depth cells and range-gating RDI (1996)

Figure 2.4 illustrates range gating and how the ADCP averages velocities over the range of each depth cell.

An ADCP sends out pings in a series or a single ping at a time. Single ping velocity errors may be too large to meet most measurement requirements. These velocity errors comprise bias and random error. Random errors are reducible through ensemble averaging which reduces the standard deviation of the random error by the square root of the number of pings. Bias depends on several factors: temperature, mean current speed, signal/noise ratio and beam geometry. An ensemble of measurements of the exact current is averaged until the average error becomes smaller than the bias. It is preferable to have the ADCP average data into ensembles before storing it, although this slows down ping processing. All the measured data is stored in a memory card or disc on the ADCP (RDI, 1996).

The intensity of the signals returning from the ADCP transmitted pulse vary in strength. This signal strength or echo intensity depends on:

- Sound absorption: This causes exponential decay of echo intensity with increasing range and increases in proportion to frequency.
- Beam spreading: It reduces echo intensity by a proportion of the range squared.
- Transmitted power: Longer pulses put more energy into the water.
- Scatterers: More scatterers reflect more sound and vice versa.
- Bubbles: They are generated by breaking waves and may block signals or reduce the profiling range.

The quality of the ADCP transducer also has an effect on data quality. A transducer has to be both directional and efficient. Obstructions in front of

transducers can interfere with acoustic beams and thus reduce data quality. A region of a 15° cone must be kept free from obstructions to minimize the interference. Echoes from the sea surface or the bottom are very strong and can overwhelm transducers, thus they need to be rejected. The velocity at the bottom or surface is on average zero. If it contaminates data, the data is detectable by a bias towards zero and can thus be rejected.

Ringing can also compromise data quality. It occurs when energy from a transmitted pulse lingers long after the transmitted pulse is finished (RDI, 1996). It becomes problematic when there are few scatters, as the ringing energy stays above the weak echo signal for long, thus delaying travelling to the transducer. ADCP measurements are unaffected by thermoclines.

## 2.4 Background review of study area

This section of the study reviews the location where measurements were collected for use in this study. The physical nature of the area and the weather system is summarised. Waves are also discussed and a review of tides concludes the section.

### 2.4.1 Natal Bight and Agulhas current

The measurements were taken just north of Durban, in the Natal Bight on the east coast of South Africa. The Natal Bight is a shallow region between Cape St. Lucia and Durban and it is approximately 160 km long and up to 50 km wide. This is very wide in comparison with the rather narrow continental shelf of the rest of the east coast of South Africa (Lutjeharms et al., 2000).

An important feature of the east coast of South Africa is the Agulhas current. The Agulhas current flows south-westwards from the north-east: from 27°S to 40°S (Gordon, 1985). It flows close to the shore along the narrow shelf until it reaches the Natal Bight where it diverges from the shore. The configuration of the Bight causes the Agulhas current to deviate offshore (Pearce, 1977). The divergence and destabilization results in the formation of Natal pulses in the Natal Bight (Lutjerharms & De Ruijter, 1994; Meyer et al., 2013). These are large, irregular and desolate meanders that progress at 5 $cm.s^{-1}$ in the Natal Bight (Lutjerharms & Roberts, 1988).

Another feature that is found in the Natal Bight is the Natal gyre, which is an extensive cyclonic circulation. The Natal gyre causes anticyclonic circulations that are smaller in size relative to it (Van der Westhuysen, 2002). Nearshore currents in the Natal Bight do not experience significant direct effects from the Agulhas current, although the nearshore currents are influenced by the

Natal gyre system and the counter-clockwise current formed in the Natal Bight (Harris, 1978b).

### 2.4.2 Weather system

The KwaZulu-Natal coastal climate is classified as warm to hot with a humid sub-tropical climate. The region is also characterised by a high annual rainfall (Pearce, 1977; Schumann, 1988).

The shoreline lies approximately north-east and winds that blow along the coast tend to be dominant. South-westerly and north-easterly winds occur with equal frequencies, but, during summer, north-easterly winds tend to dominate. The exact directions of the prevailing winds are north-north-east, north-east, south-south-west and south-west (Schumann, 1988; DN & SDCEA, 2004; Cooper, 1991). The average speed is estimated to be 11.1 m/s and the maximum speed is 16.6 m/s. These were made from measurements taken at Ballito (Cooper, 1991). The period from May to July experiences calmer winds while windy periods begin in August (DN & SDCEA, 2004).

Pearce (1977) described the weather system of the Natal coast as "regular and well-defined", since the weather is controlled by motion of cyclonic depressions approaching the coast from the south-west direction. This happens every few days. The manner in which the cyclonic depressions affects the wind is described by Pearce (1977) as follows: cyclonic depressions originates in the south-west direction and approaches some location along the coast. As this occurs the pressure system along the shore starts to fall and a north-easterly wind results and blows along the shore. A passing of the depression results in a rise in pressure which in turn causes the wind to swing to from the south-west. The wind slowly returns to the north-east as the pressure system stabilizes. The intensity of the wind depends on the propagation attributes and structure of the pressure system.

The KwaZulu-Natal coast is furthermore characterized by a weak sea breeze circulation. It is rare for a sea breeze front to develop with quick changes in temperature and wind. In summer, sea breezes begin at 9h00 and blow until 20h00 while in winter they begin at 11h00 and continue until 17h00. The sea breeze is stronger in the afternoon, and it is generally weak during winter periods.

Land breezes are also important on the Natal coast, especially in winter. Schumann (1988) estimated that land breezes blow from 21h00 to 7h00 while DN & SDCEA (2004) estimated it to commence at 19h00. Land breezes are believed to be augmented by mountain plain winds, and these occur when atmospheric conditions are calm and stable over the ocean (DN & SDCEA, 2004; Schu-

mann, 1988).

Based on time series analysis results by Schumann (1988) made on data measured inshore, there is close correspondence between winds and currents. An 18 hour lag from the onset of the wind to the response from the currents was also established. Harris (1978b) also concluded that direct wind stress is a crucial factor in the Natal Bight region.

### 2.4.3 Waves

Waves tend to mainly approach the shore from the south-eastern direction during summer and spring. Other wave approach directions include east and east-north-eastern directions. This indicates that waves approach the coast at a small angle or in a parallel direction (Cooper, 1991). Longshore currents generated by surface gravity waves are significant features in the KwaZulu-Natal coast. However their significance is restricted to the surf zone (Harris, 1978b).

### 2.4.4 Tides

Schumann & Perrins (1982) measured currents on the Natal coast off the Natal Bight region. They concluded that the tidal circulation was made up of significant diurnal (daily) and semi-diurnal tides. However, the tidal circulation played an insignificant role in the dynamics and motion of currents. A similar conclusion was reached by Harris (1978b).

## 2.5 Summary

This chapter presented processes that occur in the nearshore area, instruments that can be used to measure currents and a review of the study area.

The processes include tides, waves and atmospheric conditions. These processes may take place simultaneously, or in sequence. One process may enhance another or oppose it. These processes play a role in the generation of nearshore currents.

Instruments that can be employed for the measurements of currents include rotor type current meters, vector averaging current meters, electromagnetic current meters, vector measuring current meters and acoustic Doppler current profilers. The difference in these current meters is based on the type of speed sensor each uses. An acoustic Doppler current profiler was used for the collection of data that is used in this study. It was moored to the ocean bed and measured current velocity components in three dimensions along a water

column.

A background review of the study area where the ADCP was positioned highlighted factors that play a role in nearshore waters. The Agulhas current does not have significant direct effects on nearshore currents. However, it has indirect effects in the form of the Natal gyre and the counter currents that are formed from the interaction of the Agulhas current with the structure of the Natal Bight that affect nearshore currents (Van der Westhuysen, 2002; Harris, 1978b)

The KwaZulu-Natal coast is characterized by a humid and hot climate with high rainfall. Even though land breezes and sea breezes are weak, their diurnal periodicity cannot be ignored. Coast-wise winds are predominant and they have been established to have impacts on currents in the Natal Bight region (Schumann, 1988; Pearce, 1977; Harris, 1978b).

Waves tend to approach the coast at a near parallel direction, which is south-east followed by east and east-north-eastern directions (Cooper, 1991). The effect of the waves is mainly significant in the surf zone (Harris, 1978b). The region is also characterized by a micro-tidal range. The tidal circulation plays an insignificant role in the dynamics of currents (Schumann & Perrins, 1982; Harris, 1978b).

# Chapter 3

# Time series analysis of current data

## 3.1 Introduction

This chapter introduces and presents current data. It also presents techniques of univariate time series analysis. Current data is presented using graphs and summary statistics. Missing records are identified and ways to treat data gaps are explored. Current speed and direction measurements are resolved into velocity components that are then analysed. Progressive vector diagrams are constructed from the velocity components and explored. Autocorrelation coefficients are computed from the velocity data and spectral analysis is also performed on the data.

## 3.2 Definition of time series analysis

A time series is a collection of observations of well-defined data that is made consecutively in time. Time series analysis encompasses techniques that can be used to analyse time series data for the purpose of extracting important statistics and other attributes. Time series analysis techniques can be categorized into time domain techniques and frequency domain techniques. The former include, but are not limited to autocorrelation and cross-correlation, and the latter include spectral analysis and cross-spectral analysis (Chatfield, 2004).

Time series analysis can furthermore be divided into descriptive, explanatory and forecasting analysis. This study employs descriptive and explanatory analysis. The descriptive analysis comprises plotting and making visual diagrams of the data. The plots reveal any trend, seasonal variation, possible outliers and turning points. The explanatory part comes is used when observations

are measured on more than one variable. The variation in one series is used to explain the variation in another series (Chatfield, 1989).

### 3.2.1 Variation in time series

There are different types of variations that can occur in a time series. The types of variation include seasonal variation, trend, cyclic variation and irregular fluctuations. Seasonal variations are fluctuations that are repeated on a constant basis in a given period or annually. A trend is a long term pattern of steady change in an average or a general tendency of a series of data points to move in a certain direction. Cyclic variation encompasses variations that are not seasonal, but occur at fixed periods. An example is the daily temperature variation. Irregular fluctuations are what remains after the removal of seasonal variations, cyclic variations and a trend, as noted by Chatfield (1989).

## 3.3 Current data

The main data set to be used comprises current speeds and directions. The current data was measured by the use of an ADCP and the data was provided to be used in this study by WSP Africa Engineers, Stellenbosh. The ADCP was deployed with the aid of divers and moored 0.8 m off the bottom of the sea bed. The data was collected every 20 minutes from the 8th of June 2012 at 9h00 to the 16th of January 2013 at 10h00. Directions are given in degrees, measured clockwise from True North and speed in $mm.s^{-1}$, which are converted to $cm.s^{-1}$. The data was collected over 29 depths ranging from 2.42 m to 16.42 m, from the bottom upwards. A segment of the data is given in Figure A.1 in Appendix A to show how the data looked from the original file of measurements.

### 3.3.1 Data presentation

Data presentation gives a visual overview of data. There are various methods that can be used to present data, such as graphs, scatter plots, and progressive diagrams.

It would be cumbersome to display the data over all 29 depths or bins. To avoid this, some depths are selected and used as representative of the 29 bins. To make the selection, time series plots of current speeds across all depth levels were constructed. The plots indicated that graphs of currents near the surface tend to cluster around similar magnitudes. The same applies to graphs of currents near the sea bed and those at mid-depth. The current

speeds for the upper most bins for the majority of the measurement period are shown in Figure 3.1 which illustrates how currents near surface (14.92 m, 15.42 m, 15.92 m and 16.42 m) tend to cluster around the same magnitudes. The measurements at 14.92 m and 15.42 m do not cluster with 16.42 m and 15.92 m, indicating that only 15.92 m and 16.42 m qualify as surface currents. The plots are representatives for the entire period. A graph of current speeds at the smallest depth (14.92 m) from Figure 3.1 is included in Figure 3.2, as a reference for visual comparison. Figure 3.2 shows how currents at mid-depth levels cluster around the same magnitudes and Figure 3.3 demonstrates how currents at the bottom cluster around the same magnitudes (a graph of current speed measurements at 7.92 m from the ADCP is also included in Figure 3.3 as a reference). Three depths were chosen, one at the near surface (15.92 m away from the ADCP), one at the mid-depth (8.92 m away from the ADCP) and one at the bottom (2.42 m away from the ADCP), to be representative of the 29 depths. The depth of 15.92 m was randomly selected instead of 16.42 m. The speed measurements at the selected depths are displayed in Figure 3.4. The graphs in Figure 3.4 show an increase in speed with increasing distance from the ocean bed. The speed measurements at 2.42 m are the slowest while the speed measurements at 15.92 are the fastest. Also, included is a water level graph which can be seen on the vertical right hand side axis in Figure 3.4.

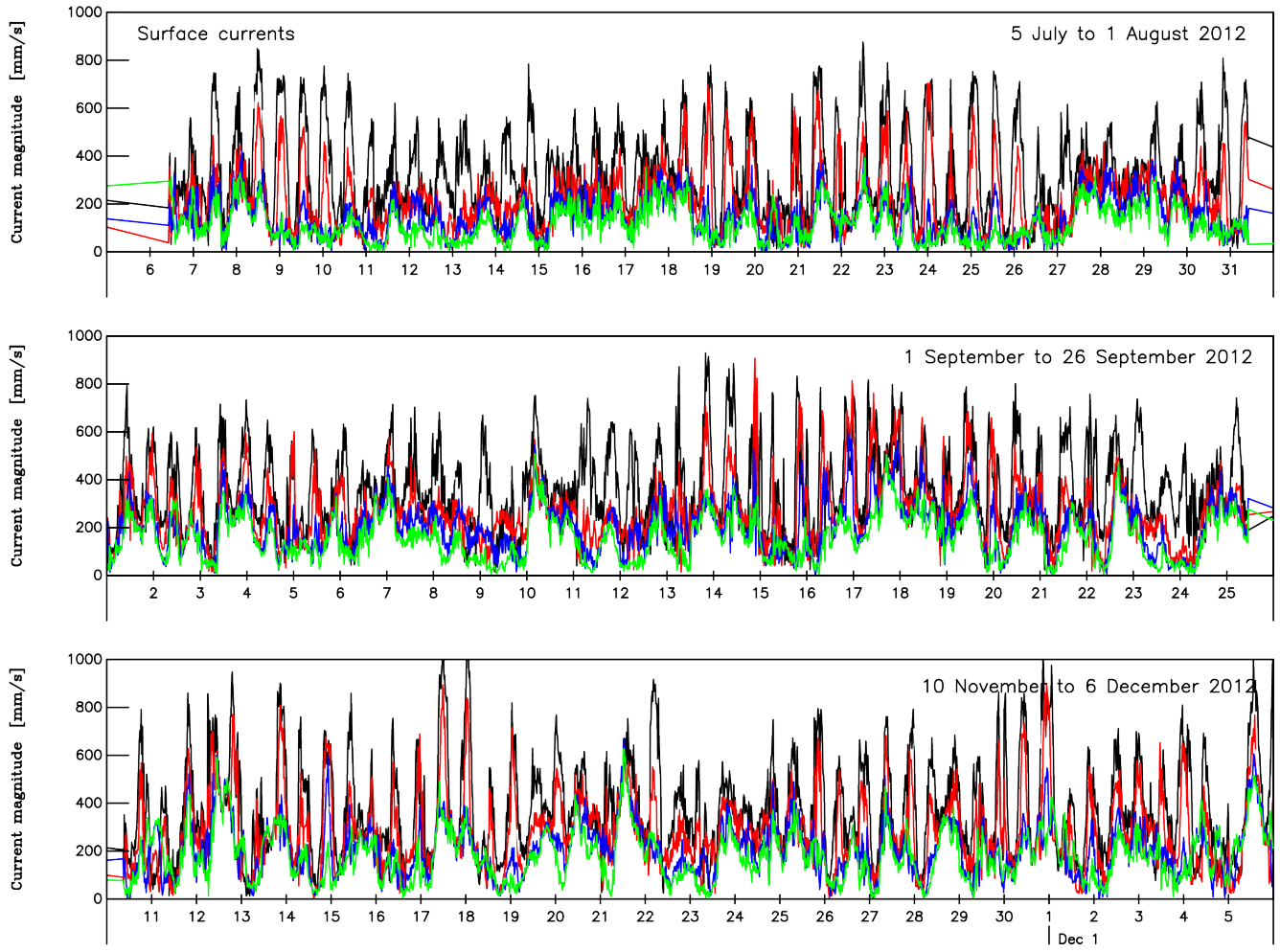


**Figure 3.1:** Four graphs of current speed measurements near the surface, namely, 16.42 m (black), 15.92 m (red), 15.42 m (blue) and 14.92 m (green). The distances are away from ADCP.

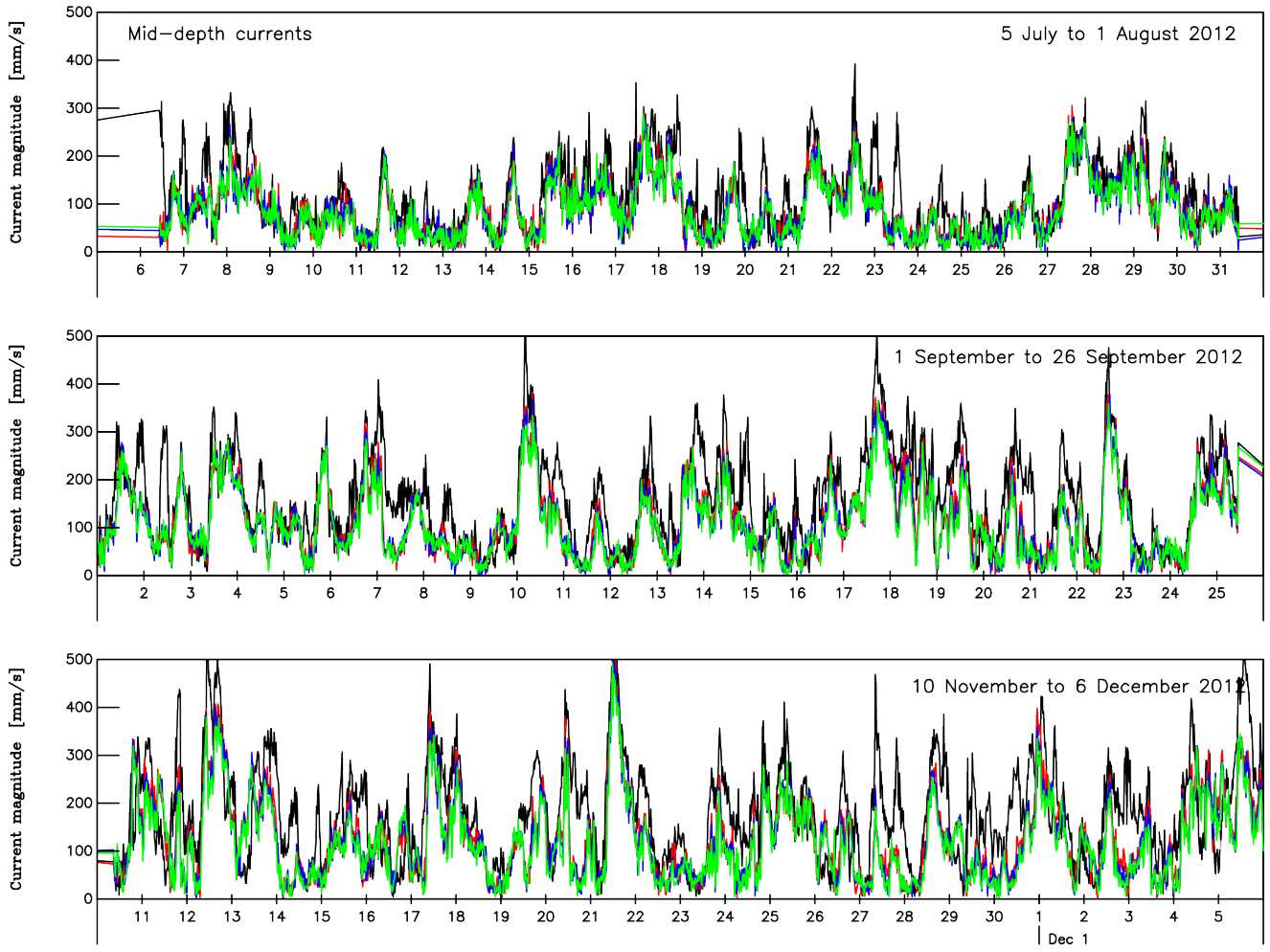


**Figure 3.2:** Graphs of three current speed measurements at middle depths, namely, 9.92 m (red), 8.92 m (blue) and 7.92 m (green) with 14.92 m (black) as reference.

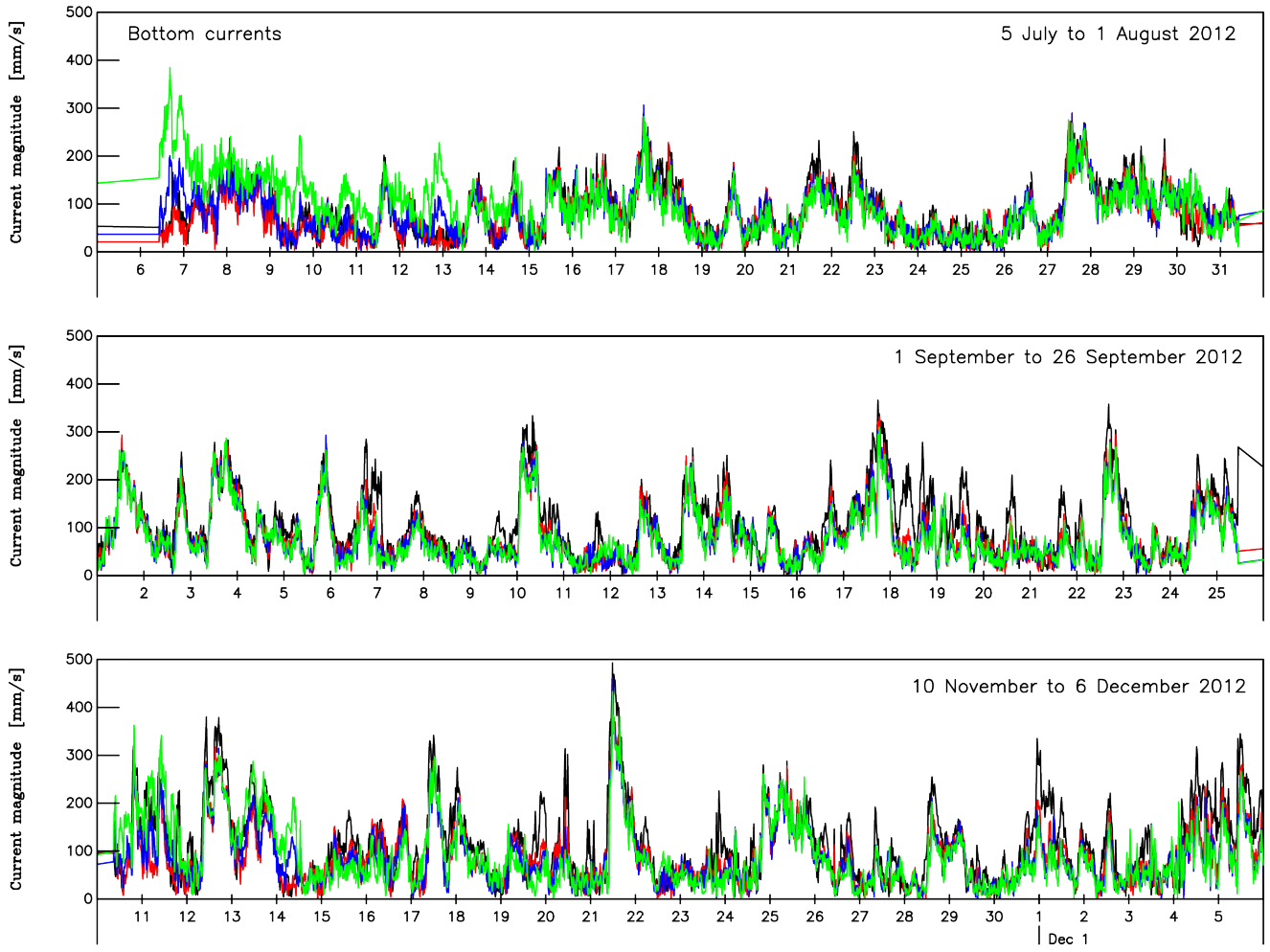


**Figure 3.3:** Graphs of current speed measurements at bottom depths, namely, 3.92 m (black), 2.92 m (blue) and 2.42 m (red) with 7.92 m (green) as reference.

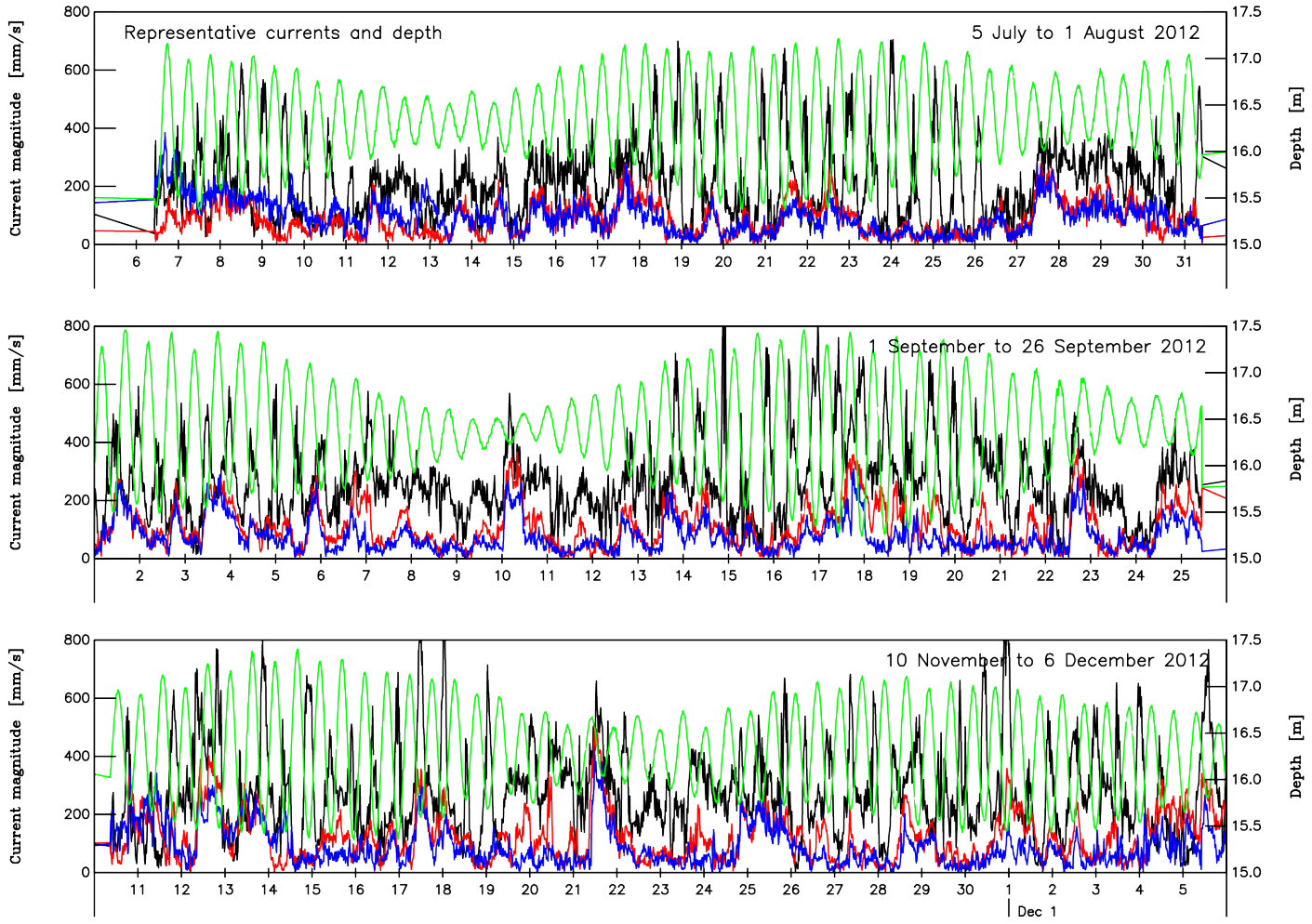


**Figure 3.4:** Three selected current speed measurements at three depths starting 5th July 2012 to 6th December 2012 are shown on the left axis, i.e. 15.92 m (black), 8.92 m (red) and 2.42 m (blue). On the right hand side axis, water level measurements (green) are shown for the same period.

The time series plots show a presence of missing data. The first occurrence of missing data is 14 days in June/July and 2 or 3 days in subsequent months. The missing periods are given in Table 3.1.

**Table 3.1:** Periods of missing records.

| Period | Start | End | Duration |
|---|---|---|---|
| 1 | 2012/06/21 22:59:56 | 2012/07/06 10:20:00 | 14 days, 23 hours, 20 minutes & 4 seconds |
| 2 | 2012/07/31 10:20:00 | 2012/08/03 08:00:00 | 2 days, 21 hours & 40 minutes |
| 3 | 2012/08/28 11:20:00 | 2012/08/31 08:00:00 | 2 days, 20 hours & 40 minutes |
| 4 | 2012/09/25 11:00:00 | 2012/09/28 09:40:00 | 2 days, 22 hours & 40 minutes |
| 5 | 2012/11/06 11:00:00 | 2012/11/10 08:40:00 | 3 days, 21 hours & 40 minutes |
| 6 | 2012/12/12 12:00:00 | 2012/12/15 07:20:00 | 2 days, 19 hours & 20 minutes |

The missing records are discussed further in later sections with regards to possible techniques that can be used to deal with them.

### 3.3.2 Summary statistics

Summary statistics provide a summary of a given set of observations, in order to communicate the largest amount of information as compactly and simply as possible. They include, but are not limited to the mean, standard deviation, variance and range.

The mean is the average of observations. It is one of the measures of central tendency and the most sensitive one. Measures of central tendency are measures of position in a distribution. They provide a summary using one value, the one observation that best depicts the centrality of the data. It is calculated by taking the sum of the observations and dividing it by the total number of observations,

$$\bar{x} = \frac{\sum_{n=1}^{N} x}{N}, \tag{3.3.1}$$

where $\bar{x}$ is the sample mean, $n$ is the position of an observation, $x$ is an observation and $N$ is the total number of observations (Steinberg, 2011).

The variance and standard deviation are two measures of variability or spread. They give an indication of how observations vary or spread out around the mean. The variance is defined as the average of the squared deviations of

observations around the sample mean. It is calculated using the equation,

$$s^2 = \frac{\sum_{n=1}^{N-1}(x - \bar{x})^2}{N-1}, \tag{3.3.2}$$

where $s^2$ is the variance and $N-1$ is used in this case so that the sample variance can provide a good estimate of the population variance. The standard deviation is the square root of the variance. A useful property of the standard deviation is that, unlike the variance, it is expressed in the same units as the data (Ross, 2010).

**Table 3.2:** Summary statistics of current speed for the selected bins, namely, 2.42 m, 8.92 m and 15.92 m. Length refers to the number of observations.

| Period | Depth (m) | Mean (cm/s) | $s^2$ $(\text{cm/s})^2$ | $s$ (cm/s) | Min (cm/s) | Max (cm/s) | Length (20 min) |
|---|---|---|---|---|---|---|---|
| 0 | 2.42 | 7.54 | 18.87 | 4.34 | 0.2 | 26.7 | 979 |
| | 8.92 | 9.61 | 42.73 | 6.54 | 0.1 | 30.8 | |
| | 15.92 | 23.03 | 264.41 | 16.26 | 0.9 | 86.5 | |
| 1 | 2.42 | 9.81 | 33.93 | 5.83 | 0.1 | 38.5 | 1801 |
| | 8.92 | 8.80 | 31.79 | 5.64 | 0.0 | 27.8 | |
| | 15.92 | 21.89 | 165.92 | 12.88 | 0.6 | 87.6 | |
| 2 | 2.42 | 6.68 | 20.86 | 4.57 | 0.1 | 28.6 | 1811 |
| | 8.92 | 8.05 | 34.30 | 5.86 | 0.1 | 42.0 | |
| | 15.92 | 20.69 | 150.78 | 12.28 | 0.4 | 74.8 | |
| 3 | 2.42 | 7.63 | 30.36 | 5.51 | 0.1 | 31.0 | 1810 |
| | 8.92 | 10.93 | 54.88 | 7.41 | 0.0 | 37.8 | |
| | 15.92 | 36.67 | 299.98 | 17.32 | 1.3 | 92.9 | |
| 4 | 2.42 | 5.85 | 19.77 | 4.45 | 0.1 | 35.5 | 2813 |
| | 8.92 | 8.89 | 47.39 | 6.88 | 0.0 | 50.0 | |
| | 15.92 | 25.36 | 228.77 | 15.13 | 0.8 | 112.4 | |
| 5 | 2.42 | 8.76 | 41.15 | 6.42 | 0.1 | 43.3 | 2315 |
| | 8.92 | 12.26 | 66.78 | 8.17 | 0.2 | 50.6 | |
| | 15.92 | 27.71 | 241.45 | 15.54 | 0.4 | 89.8 | |
| 6 | 2.42 | 8.20 | 30.41 | 5.51 | 0.3 | 34.6 | 2313 |
| | 8.92 | 11.67 | 60.64 | 7.79 | 0.0 | 42.9 | |
| | 15.92 | 24.87 | 241.94 | 15.55 | 0.1 | 95.1 | |

Summary statistics of current speeds are given in Table 3.2 for seven periods, the seven periods used are separated by the periods of missing records listed in Table 3.1. In all the seven periods, the mean indicates that speed increases with increasing distance from the sea bed, except for period 1 where the mid-depth mean is less than the bottom mean. The slowest speed occurs at the 8.92 m level and it is 0 cm/s in period 1, 3, 4 and 6, while the fastest

speed is 112.4 cm/s at 15.92 m away from ADCP in period 4. The means for all the twenty-nine levels and seven periods are given in Table A.1 in Appendix A.

The variances and standard deviations at shallower levels, i.e., at 2.42 m and 8.92 m are much smaller compared to those at the surface, 15.92 m. There is thus, more variability at the surface compared to the bottom. However, the variation at all levels is large. This is supported by the large differences between the minimum and maximum values.

### 3.3.3 Dealing with missing data

There is more than 10% missing records in the time series according to the missing records that were provided earlier in Table 3.1. This implies that the missing data can affect the accuracy of the deductions that can be made from the data (Croninger & Douglas, 2005; Dong & Peng, 2013). Whether the missing records are random or not determines the methods that can be used to deal with the missing data.

Table 3.3 shows periods with continuous data records, the missing records given in Table 3.1 occur in between the continuous data records. The mean number of missing records is approximately 4days and the mode is 2 days and a number of hours. The missing records occur once after approximately 13 days, once every month after approximately 25 days on three occasions, then once after approximately 39 days and after approximately 32 days on two occasions. It can be concluded that the records are missing completely at random. Records missing completely at random means that the probability that an observation $X_i$ is missing is unrelated to the value of $X_i$ or to the value of any other variable, i.e. the "missingness" of a variable has no relationship with the variable itself or any other variable in the record (Croninger & Douglas, 2005). The periods of missing data can be explained as the times when the ADCP was removed for cleaning and maintenance.

**Table 3.3:** Periods with available data.

| Period | Start | End | Duration |
|---|---|---|---|
| 0 | 2012/06/08 09:00:00 | 2012/06/21 23:00:00 | 13 days &14 hours |
| 1 | 2012/07/06 10:20:00 | 2012/07/31 10:20:00 | 25 days |
| 2 | 2012/08/03 08:00:00 | 2012/08/28 11:20:00 | 25 days, 3 hours & 20 minutes |
| 3 | 2012/08/31 08:00:00 | 2012/09/25 11:00:00 | 25 days & 3 hours |
| 4 | 2012/09/28 09:40:00 | 2012/11/06 11:00:00 | 39 days & 20 hours |
| 5 | 2012/11/10 08:40:00 | 2012/12/12 12:00:00 | 32 days, 3 hours & 20 minutes |
| 6 | 2012/12/15 07:20:00 | 2013/01/16 10:00:00 | 32 days, 2 hours & 40 minutes |

List-wise deletion is a convenient method to handle the data in period 0, shown in Table 3.3. The data in this period is too short to analyse and make deductions from; and the missing records that follow are long. The data in period 0 is thus deleted and not considered in the rest of this study. The rest of the missing records are not interpolated but the individual periods 1 to 6 as given in Table 3.3 are analysed separately.

### 3.3.4 Velocity components

East-west and north-south velocity components were constructed from the current speed and direction data. The components were constructed as follows,

$$\begin{aligned} v_x &= v \sin \alpha \quad \text{and} \\ v_y &= v \cos \alpha, \end{aligned} \tag{3.3.3}$$

where $v_x$ is the east-west component, $v_y$ is the north-south component and $\alpha$ is the direction angle measured clockwise from True North. Figures A.2, A.3 and A.4 show north-south velocity components and east-west velocity components at three different depths, namely, 2.42 m, 8.92 m and 15.92 m respectively. The velocity components at 15.92 m have a large range compared to the velocity components at 8.92 m and 2.42 m.

### 3.3.5 Cross-shore and longshore velocity components

In the nearshore area, the coast forms a solid boundary that may cause currents to move parallel to the coast. Furthermore, the nearshore area has currents that receive their energy from the breaking of waves at the shoreline. It is thus customary to decompose currents into longshore and cross-shore components.

Given the north-south and east-west velocity components, the axes were rotated through a 52° angle to obtain longshore and cross-shore components. A picture of the orientation of the coast is given in Figure A.5, from which the 52° angle was measured. The rotations were done using,

$$\begin{aligned} v_l &= v_x \cos 52^\circ + v_y \sin 52^\circ \text{ and} \\ v_c &= -v_x \sin 52^\circ + v_y \cos 52^\circ, \end{aligned} \tag{3.3.4}$$

where $v_l$ is the longshore component and $v_c$ is the cross-shore component. Long-shore currents travel parallel to the shoreline while cross-shore currents flow perpendicular to the shoreline. Figures A.6, A.7 and A.8 show time series plots of longshore and cross-shore currents at the three corresponding depths as in Figures A.2, A.3 and A.4. Cross-shore velocity components are slower and less variable relative to longshore velocity components at all depths.

## 3.4 Progressive vector diagrams

A progressive vector diagram (PVD) gives the virtual displacement that a water particle would travel from its initial position $(x_0, y_0)$ if the current would be invariant wherever the particle went. All the PVDs in this study begin at $(0, 0)$. To compose a PVD, time-integrated displacements along the orthogonal directions $(x, y)$ are calculated from corresponding velocity components using the equation,

$$(x, y) = (x_0, y_0) + \sum (u_i, v_i) \triangle t_i, \tag{3.4.1}$$

where $i = 1, 2, 3, ...$, $x_0$ is the original east-west velocity component, $y_0$ is the original north-south velocity component, $u_i$ is the east-west velocity component at position $i$, $v_i$ is the north-south velocity component at position $i$ and $\triangle t_i$ is the change in time corresponding to position $i$. The resulting vectors are plotted to produce a PVD (Emery & Thomson, 2004).

PVDs are presented in Figures 3.5, 3.6 and 3.7 for the depths 2.42 m, 8.92 m and 15.92 m away from the ADCP, respectively. The PVDs are constructed from currents in period 5. The period was chosen randomly. In all three figures, the current mainly moves in a north-east direction or in the opposite direction, south-west. In Figure 3.5, the main direction is north-east, and north with short reversals into the south-western direction. In Figure 3.6, the change in direction of the current into north-east and south-west directions seem to be rather quasi-periodic, although the dominant direction is still north-east. In Figure 3.7, the change in direction is more frequent and random, the distance covered is also much longer, relative to the changes at 2.42 m and 8.92 m away from the ADCP. The PVDs for the remaining periods are included in Appendix A, as Figures A.9 to A.23.

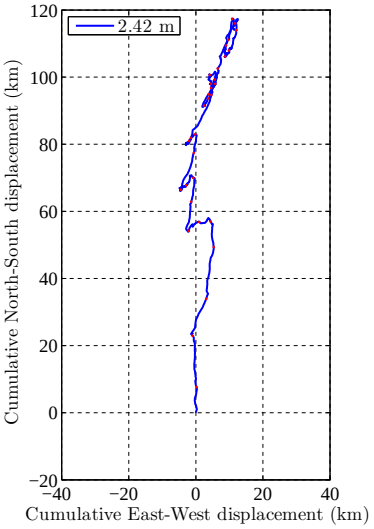


**Figure 3.5:** PVD of the east-west and north-south velocity components at 2.42 m.

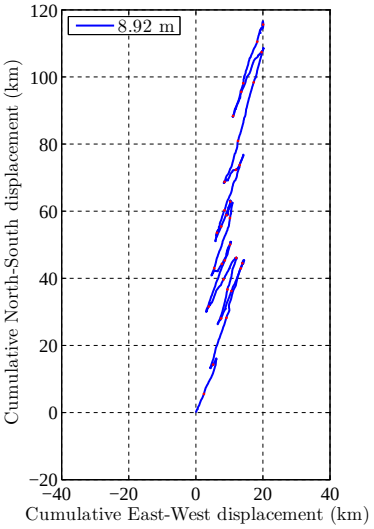


**Figure 3.6:** PVD of the east-west and north-south velocity components at 8.92 m.

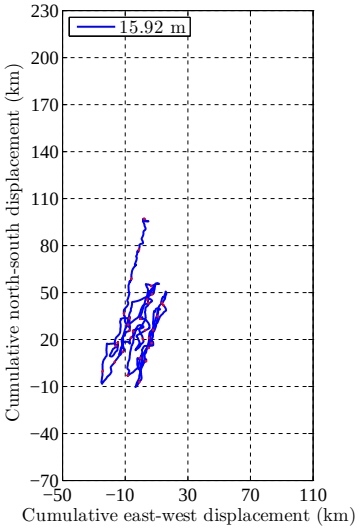


**Figure 3.7:** PVD of the east-west and north-south velocity components at 15.92 m.

## 3.5 Autocorrelation

Autocorrelation is a technique that measures the correlation between observations at different time steps within a time series. It tests for randomness and reveals cyclic as well as seasonal behaviour (Chatfield, 1989). Autocorrelation can also be described as indicating persistence in a signal, where persistence is the tendency of the signal to remain the same from observation to observation. For example, if the current speed recorded at 10:20 is large, the likelihood of the next current speed measured at 10:40 being large, is greater than if the current speed measured at 10:20 was small. Measurements of currents may exhibit persistence due to inertia and tides.

Autocorrelation is analogous to the correlation coefficient which is given by,

$$r = \frac{\sum(x_i - \overline{x})(y_i - \overline{y})}{\sqrt{[\sum(x_i - \overline{x})^2 \sum(y_i - \overline{y})^2]}}. \tag{3.5.1}$$

In equation (3.5.1), $x_i$ is an observation from one data set and $\overline{x}$ is the mean of the observations in the same data set. Similarly, $y_i$ is an observation from another data set and $\overline{y}$ is the corresponding mean.

Given $N$ observations $x_1$,...,$x_N$ of a discrete time series, $N-1$ pairs of observations can be generated, i.e. $(x_1, x_2)$, $(x_2, x_3)$,..., $(x_{N-1}, x_N)$. By treating the first observation in each pair as belonging to one series and the second one as belonging to a second series, the correlation coefficient between $x_t$ and $x_{t+1}$ at lag 1 is given by:

$$r_1 = \frac{\sum_{t=1}^{N-1}(x_t - \overline{x}_{(1)})(x_{t+1} - \overline{x}_{(2)})}{\sqrt{[\sum_{t=1}^{N-1}(x_t - \overline{x}_{(1)})^2 \sum_{t=1}^{N-1}(x_{t+1} - \overline{x}_{(2)})^2]}}. \tag{3.5.2}$$

In Equation (3.5.2), $x_t$ is an observation from one series and $\overline{x}_{(1)}$ is the corresponding mean of that series; $x_{t+1}$ is from the same series at a lag 1 and $\overline{x}_{(2)}$ is the corresponding mean at this lag. Equation (3.5.2) gives an autocorrelation coefficient at lag 1. The equation is rather involved, but $\overline{x}_{(1)} \approx \overline{x}_{(2)}$,

$$r_1 = \frac{\sum_{t=1}^{N-1}(x_t - \overline{x})(x_{t+1} - \overline{x})}{\sqrt{[\sum_{t=1}^{N-1}(x_t - \overline{x})^2 \sum_{t=2}^{N}(x_t - \overline{x})^2]}}. \tag{3.5.3}$$

Further, assuming that,

$$\sum_{t=1}^{N-1}(x_t - \overline{x}) \approx \sum_{t=2}^{N}(x_t - \overline{x}),$$

then Equation (3.5.2) can be approximated by,

$$r_1 = \frac{\sum_{t=1}^{N-1}(x_t - \overline{x})(x_{t+1} - \overline{x})}{\sum_{t=1}^{N}(x_t - \overline{x})^2}. \tag{3.5.4}$$

The generalized equation for the autocorrelation between $x_t$ and $x_{t+m}$ is thus given by:

$$r_m = \frac{\sum_{t=1}^{N-m}(x_t - \overline{x})(x_{t+m} - \overline{x})}{\sum_{t=1}^{N-1}(x_t - \overline{x})^2}, \tag{3.5.5}$$

where $m$ is the time lag (Chatfield, 1989). Autocorrelation coefficients can assume any value between 1 and $-1$. An autocorrelation coefficient of 1 indicates a perfect positive linear relationship between the two variables, 0 indicates the non-existence of a linear relationship, while $-1$ indicates a perfect negative linear relationship between the two variables.

For ease of computation, autocorrelation coefficients are computed from auto-covariance coefficients $c_m$. The auto-covariance coefficient measures the strength of correlation between two variables in the same sample. The auto-covariance is defined as,

$$c_m = \frac{1}{N}\sum_{t=1}^{N-m}(x_t - \bar{x})(x_{t+m} - \bar{x}), \tag{3.5.6}$$

where $c_m$ is the auto-covariance at lag $m$. To compute the autocorrelation coefficient at lag $m$, the following equation is used:

$$r_m = \frac{c_m}{c_0}, \tag{3.5.7}$$

where $m = 1, 2, ..., M$ and $M < N$. The autocorrelation is calculated for up to $\frac{N}{4}$ lags. Any length longer than this is unreliable as the number of pairs used in the estimation of $r_m$ decreases (Reddy, 1997).

Autocorrelation coefficients are presented in plots called correlograms, where the autocorrelation coefficients are plotted at different lags. In the present study, the lags correspond to 20 minutes. Also included in the correlograms are 95% confidence bands. These bands are of the form $\frac{1}{N} \pm \frac{1.96}{\sqrt{N}}$, where $N$ is the length of the time series. The value 1.96 is the 95% standard normal percentile. These limit bands are indicated by horizontal red lines in the correlograms included in Figure F.29, F.30 and 3.10 in Appendix A. These bands are principally included as is convention since none of the six time series are stationary thus the autocorrelation coefficients cannot assume a normal distribution. Equations (3.5.6) and (3.5.7) were used in MATLAB to calculate the autocorrelations and plot the correlograms. The code written in MATLAB is given in Appendix B.

### 3.5.1 Results

Coastal data tend to have periodic phenomena, so it is to be expected that the correlograms exhibit periodic occurrences. Correlograms are provided in Figure F.29, F.30 and 3.10 for six periods as indicated in Table 3.1.

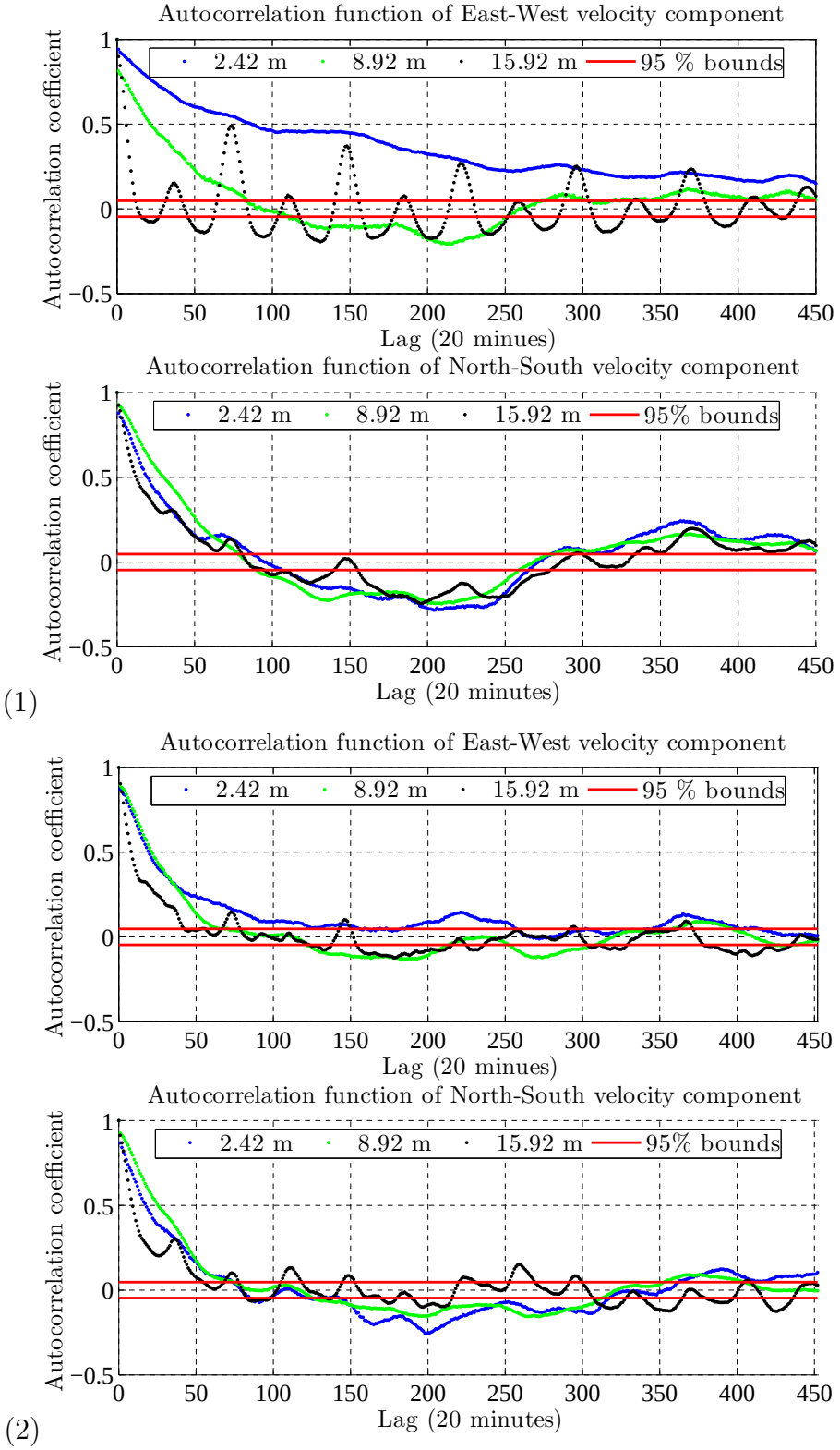


**Figure 3.8:** Correlograms of currents for period one (1) and period two (2). Each of the figures depict correlograms at distance 2.42 m (blue), 8.92 m (green) and 15.92 m (black) from ADCP.

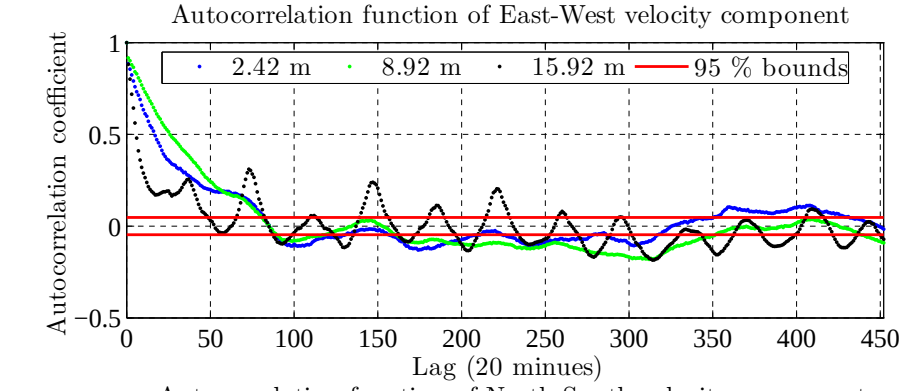


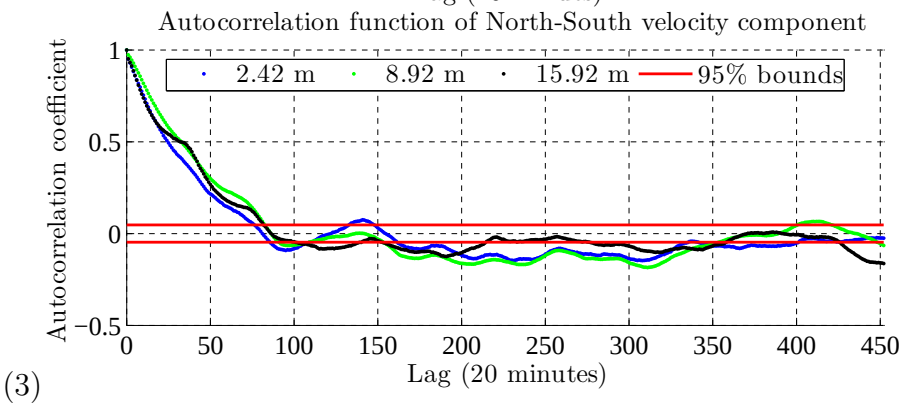


(3)

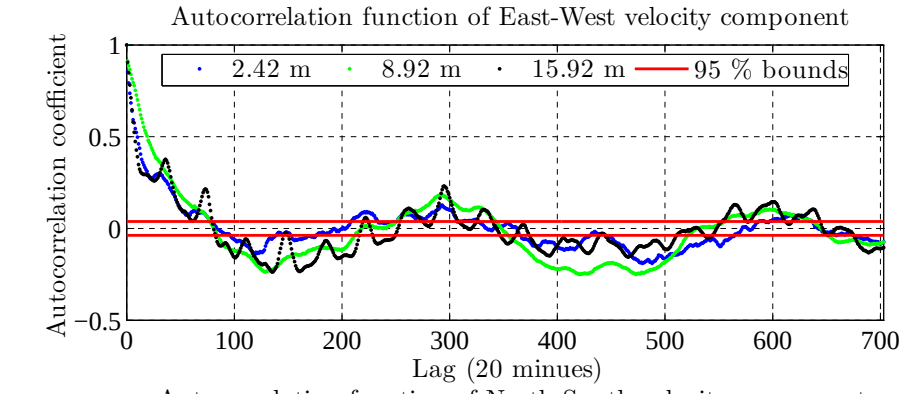


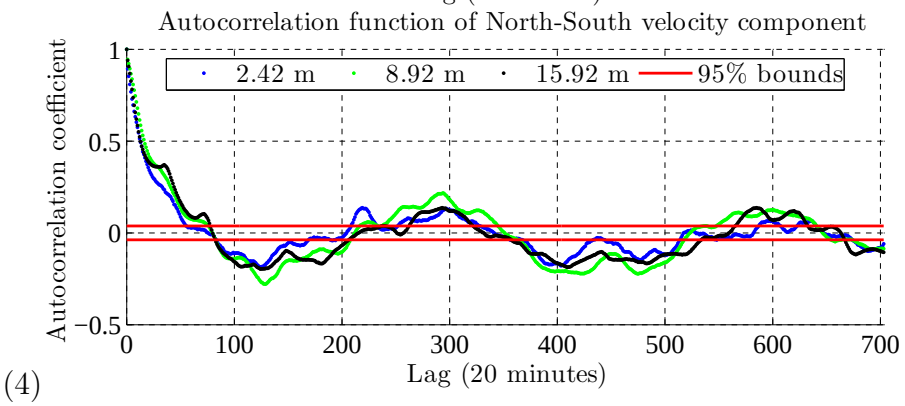


(4)

**Figure 3.9:** Correlograms of currents for period three (3) and period four (4). Each of the figures depict correlograms at distance 2.42 m (blue), 8.92 m (green) and 15.92 m (black) from ADCP.

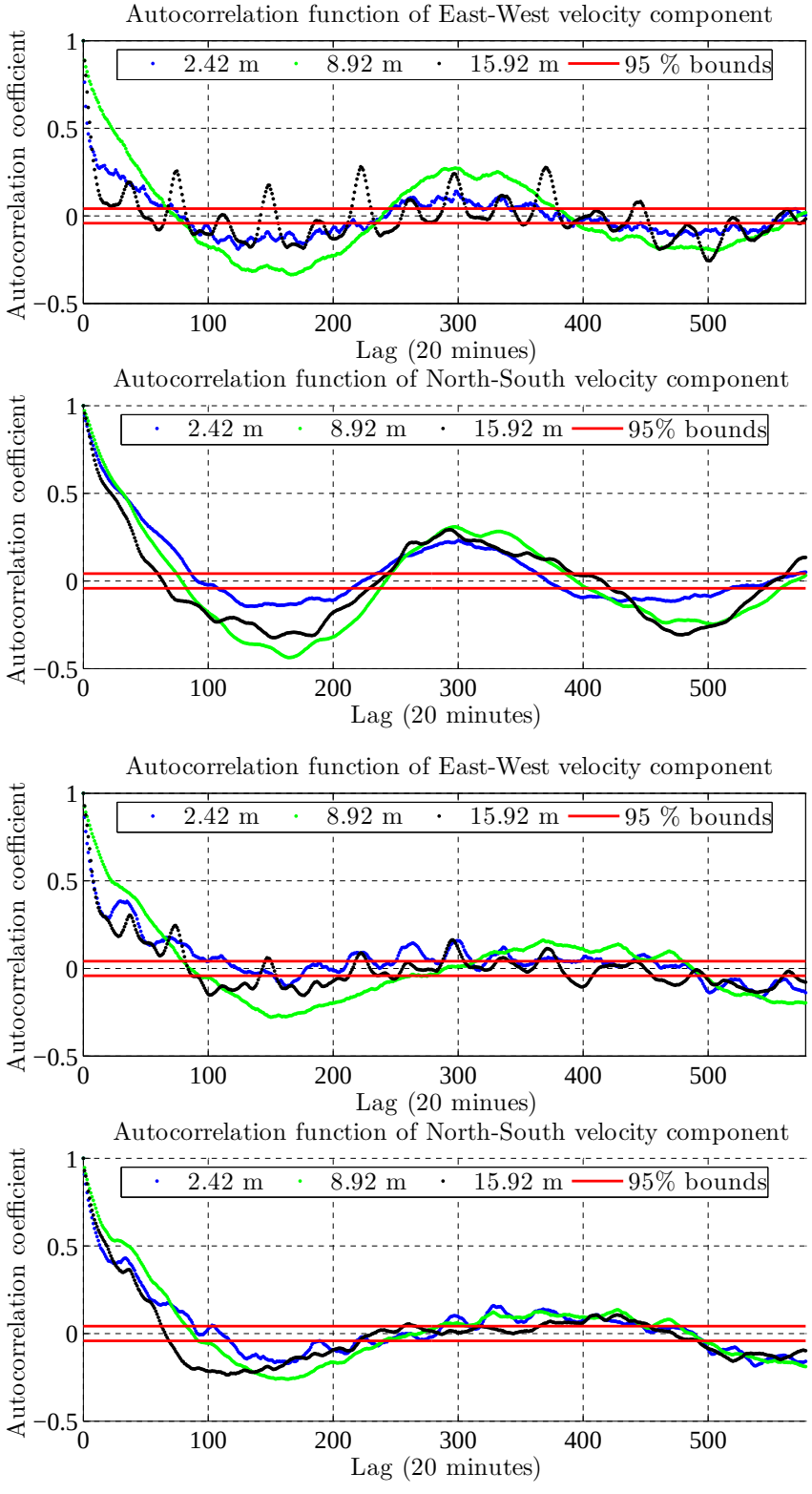


**Figure 3.10:** Correlograms of currents for period five (5) and period six (6). Each of the figures depict correlograms at distance 2.42 m (blue), 8.92 m (green) and 15.92 m (black) from ADCP.

All the correlograms in the figures reveal a 12.3 hourly cycle near the surface (15.92 m) especially in the east-west velocity components. The first one hourly cycle occurs at $\frac{37\times20}{60} = 12.3$. The 12.3 hour cycles disappear with depth, being undetectable in the correlograms at 8.92 m and 2.42 m. These 12.3 hour cycles correspond to periods of semi-diurnal tides.

For period 4, in addition to the 12.3 hour cycle, there is another cycle of approximately 2 days. There are 2 days between one trough to the next and between one crest to the next. The cycle is visible in both east-west and north-south velocity components. Period 5 is also characterized by an additional cycle of approximately 4 days.

Since the corellograms are dominated by periodic patterns no extra information can be deduced from them at this stage. However, the time scales that it takes for autocorrelation coefficients to become insignificant have been computed to provide a reference that can be used later in the study. The time scales are provided in Table 3.4.

**Table 3.4:** Length of significant autocorrelation.

| Period | Component | Lag (time offset) | | |
|---|---|---|---|---|
| | | 15.92 m | 8.92 m | 2.42 m |
| 1 | E-W component | 4 hours | 28 hours | 6.25 days |
| | N-S component | 21 hours | 26 hours | 28 hours |
| 2 | E-W component | 14 hours | 20 hours | 40 hours |
| | N-S component | 18 hours | 22 hours | 24 hours |
| 3 | E-W component | 15 hours | 28 hours | 28 hours |
| | N-S component | 28 hours | 28 hours | 25 hours |
| 4 | E-W component | 19 hours | 26 hours | 19 hours |
| | N-S component | 26 hours | 26 hours | 18 hours |
| 5 | E-W component | 7 hours | 22 hours | 24 hours |
| | N-S component | 20 hours | 25 hours | 28 hours |
| 6 | E-W component | 21 hours | 22 hours | 26 hours |
| | N-S component | 32 hours | 27 hours | 28 hours |

Autocorrelation coefficients become insignificant once they cross the positive confidence band, $\frac{1}{N} + \frac{1.96}{\sqrt{N}}$. The longest time scales occur at 2.42 m, followed by 8.92 m with the shortest time scales observed at 15.92 m. The longest significant time scale is 6.25 days at 2.42 m. The shortest significant time scale is 4 hours at 15.92 m. Significant time scales for the 8.92 m level range from 20 up to 28 hours.

## 3.6 Spectral analysis

Spectral analysis is a mathematical technique that describes how the total power of a signal is distributed over frequency. It involves the transformation of a signal from a time domain to a frequency domain (Emery & Thomson, 2004; Kantz & Schreiber, 2003). Distribution of power over different frequency constituents are measured by means of a power spectral density (PSD) function. There are two methods of performing spectral analysis, namely, parametric and non-parametric methods. The former is data-tailored and assign a pre-defined model to a time series while non-parametric methods are based on Fourier transforms and are not data-tailored (Emery & Thomson, 2004). This study employs non-parametric techniques only.

The transformation of a signal from the time domain to the frequency domain involves the application of Fourier transforms. A brief description of Fourier transforms (discrete Fourier transform and fast Fourier transform) are thus provided in the next subsections. How power spectral densities are computed from discrete Fourier transforms then follows. A graph of frequency versus power spectral densities is called a periodogram. The construction of a periodogram is discussed along with its shortcomings and possible modifications. This section is concluded with a discussion of the results of the power spectral analysis as applied to the nearshore current data.

### 3.6.1 Fourier transforms

A time series can be assumed to be a combination of periodic and pseudo-periodic parts that are superimposed on random noise and a long-term trend. The objective of data analysis in the frequency domain is to separate periodic oscillations from non-periodic and random fluctuations (Baher, 2012). Non-periodic fluctuations may include a trend and random noise. A trend is characterized by long term variability. A trend has not been found in the current measurements used in this study. Random noise may include noise from measuring instruments and any ranges of frequency that are not of interest. This separation of periodic oscillations from non-periodic fluctuations is done through Fourier transforms. Since the data in this study is discrete and of finite length, discrete Fourier transform is applicable and it is discussed.

### 3.6.2 Discrete Fourier Transform

The data in this study has a finite duration, with total period $T = N\Delta t$, where $N$ is the length of the time series and $\Delta t$ is the measuring time interval, which is 20 minutes. The data can be treated as a time series, $y_n = y(t_n)$ with $t_n = n\Delta t$ where $n$ is an integer referring to the particular position of $y$ in the signal. The discrete Fourier transform converts a finite length sample

of equally spaced observations into coefficients of a finite sum of sinusoids as follows:

$$\begin{aligned} Y_m &= \Delta t \sum_{n=0}^{N-1} y_n \mathrm{e}^{-\mathrm{i}2\pi f_m n \Delta t} \\ &= \Delta t \sum_{n=0}^{N-1} y_n \mathrm{e}^{-\mathrm{i}\frac{2\pi mn}{N}}, \end{aligned}$$

with inverse,

$$y_n = \frac{1}{T} \sum_{m=0}^{N-1} Y_m \mathrm{e}^{\mathrm{i}\frac{2\pi mn}{N}},$$

where $f_m = \frac{m}{N\Delta t}$ and $m = 0, 1, 2, ..., N$. The frequencies $f_m$ only go up to the Nyquist frequency. The Nyquist frequency refers to half the sampling rate of a series. It is also the highest frequency that can be used to reconstruct a series from the discrete Fourier transform.

$$f_n = \frac{1}{2\Delta t} \tag{3.6.1}$$

The result of the discrete Fourier transform is used to construct a periodogram of a times series. The construction is based on Parseval's theorem. This theorem relates the average power of a signal to the sum of the squares of the amplitudes of the complex Fourier coefficients. For a finite duration, Parseval's theorem is expressed as follows:

$$\sum_{n=1}^{N} |y_n|^2 = \frac{1}{N} \sum_{n=1}^{N} |Y_m|^2. \tag{3.6.2}$$

The squared amplitudes of the Fourier coefficients are called the power spectral amplitudes and a plot of these divided by frequency versus frequency is called the periodogram of the signal (Baher, 2012; Emery & Thomson, 2004). In practise Fast Fourier transforms are used to compute the discrete Fourier transforms in a timely manner. A description of Fast Fourier Transform is provided in Appendix C.

### 3.6.3 The periodogram

To compute periodograms for each of the time series for the selected six periods, the mean is first removed, the means are provided in Table 3.2. Using MATLAB, Fast Fourier transform was applied to the demeaned series to obtain discrete Fourier transforms, and power spectral densities are obtained following the description in Section 3.6.2. Each of the time series was padded with

$m < N$ zeros to reduce Gibb's phenomenon and to make Fast Fourier transform faster. A description of Gibb's phenomenon is described in Appendix C.

As much as the periodogram can reveal distribution of power in a signal over different frequencies it has disadvantages. It is biased, its variance does not decrease with an increase in the size of the signal and lastly it has fast fluctuations (Buttkus, 2012). The fast fluctuations of the periodogram make it difficult to identify important periodicities. To counter these shortcomings, a periodogram can be smoothed.

A periodogram is smoothed through the use of a window function. This function is applied to a finite series or its Fourier transform to reduce Gibb's phenomenon in spectral estimates. An ideal window allows the least amount of energy to leak from the central lobe to the side lobes. In this way it prevents distortion of spectral estimates. Window functions include the Hamming window, Hanning window, Kaisser window, rectangular window, etc (Harris, 1978a).

In this study, the Hanning window is applied to the data prior to computing discrete Fourier transforms. The smoothed result is obtained through

$$s_m = w_m y_m,$$

where $s_m$ is the windowed series, $w_m$ is the window function and $y_m$ is the time series. The Hanning window is defined as,

$$w_m \quad = \quad 0.5[1 + \cos(\frac{m\pi}{n})]. \tag{3.6.3}$$

The Hanning window was chosen because of its common usage and attractive features. It causes minimal aliasing and has good frequency resolution. Terms are also easy to generate and takes little computation time (Harris, 1978a).

### 3.6.4 Methodology

Power spectra for the six periods are computed using two methods, namely, the periodogram and the modified periodogram. The modified periodogram is a periodogram which is computed with some smoothing. Computation of the periodogram is explained in Section 3.6.2. The computation of the modified periodogram involved demeaning the time series, padding it with zeroes and then applying a Hanning window. After the application of the Hanning window, discrete Fourier transforms are computed and the resulting power spectral density estimates are band averaged to obtain an even smoother result. In both the periodogram and modified periodograms, the estimate of the power spectral density corresponding to 0 $Hz$ is not included as this is the mean.

### 3.6.5 Results of power spectral analysis

Power spectral density graphs are given in Figures A.24 to A.35 for the east-west and north-south velocity components as well as for the longshore and cross-shore velocity components. Modified periodograms exhibit good frequency resolution with clear spectral peaks, while the unmodified periodograms exhibit a lot of activity with fast fluctuations. From examining the periodograms for all the periods and velocity components, there are four common periods with high peaks . The periods are: approximately 24 hours, 12 hours, 8 hours and 6 hours which can be attributed to tidal variations. These periods are easily identifiable in the east-west and cross-shore velocity components.

#### East-west and north-south currents

In addition to the periods already identified as high peaks in all the plots, others are worth mentioning. Period 1 and 2 exhibit high peaks at 5.68 days in both east-west and north-south velocity components. Period 3 exhibits a high peak at 9.48 days and 4.74 days in both east-west and north-south velocity components. Period 4 exhibits a high peak at 4.06 days in both components. Period 5 and 6 exhibit high peaks at 4.37 days and 5.17 days in both components respectively.

#### Longshore and cross-shore currents

Periodograms of longshore velocity components indicate less variation relative to cross-shore components. Modified periodograms of longshore velocity components are inspected first. For period 1, 2 and 3 a high peak is observed at 5.7 days, 3.6 days and 5.7 days, respectively. For period 4 and 5 the high peak is observed at 4.1 days while for period 6 the high is at 5.2 days.

Cross-shore components show 12.2 hours to be a predominant period with the highest power spectral density for period 1 to 5. For period 6 the predominant period is 24 hours followed by 10 days and then 6.3 hours. A periodicity of 4.1 days is also observed in the cross-shore velocity components of period 5.

## 3.7 Summary

This chapter discussed and presented current data. Some elements of time series analysis are presented and univariate time series analysis is applied to the current data. Due to the cumbersome nature of the data, only three levels of measurements were considered for analysis, namely, 2.42 m, 8.92 m and 15.92 m from ADCP. Missing records were identified in the data and list-wise deletion was used for the fourteen day long time series starting on the 8th of June 2012. Shorter missing records were overpassed and available records

were analysed. The current data was divided into six sections that are individually analysed. Summary statistics of the current data are computed and studied. Current speeds increase with increasing distance from the sea bed to the surface. Speed measurements at the surface are faster than those at the bottom and middle. Variation of the speed measurements also follows the same pattern.

Current speed and direction measurements are resolved into north-south and east-west velocity components. These are further resolved into longshore and cross-shore velocity components. Longshore velocity components are predominant relative to cross-shore velocity components. Progressive vector diagrams of the data are constructed. The currents tend to move in a north-eastern and south-western direction, which are near parallel to the coast. Autocorrelation is applied to the data and it reveals periodicities in the data. Approximately 12 hours is present in all the studied sections at 15.92 m. Spectral analysis is also performed on the data. This analysis reveals more periodicities in the data, including 12 hours, 24 hours, 4 days, 10 days and more.

# Chapter 4

# Tidal Analysis

## 4.1 Introduction

This chapter seeks to explore the effects of tides on both water levels and currents. The process of investigating the responses of water levels and currents to the action of tidal forces is called tidal analysis. The chapter commences with an introduction to tides, describing their generation and factors that influence them. A methodology of analysis is then outlined. Water levels are then analysed followed by currents in both east-west and north-south velocity components as well as cross-shore and longshore velocity components. As a tide causes a vertical motion of the water mass, a horizontal motion also takes place, this horizontal movement of water caused by tidal action is called a tidal current. The tidal current is indicated by $u_t$ in Equation (1.2.1).

### 4.1.1 The generation of tides

Tides are the variations in sea level as a result of the gravitational forces induced mainly by the sun and the moon. The variation in sea levels are periodic and this periodicity renders tides predictable with some level of accuracy (Wright et al., 1999; Parker, 2007).

The manner in which gravitational forces generate tides can be explained using the equilibrium theory of tides. On the side of the earth facing the moon (or the sun), the moon (or the sun) pulls water on the surface of the earth towards it. On the opposite side of this, centrifugal forces also pull water away from the surface of the earth. These causes two "bulges" on the two opposite ends with a depression between them (Thompson, 2015; Wright et al., 1999).

Since the moon is closer to the earth compared to the sun, it has a greater impact on the generation of tides. As a result, tidal patterns follow the pattern of revolution of the moon. Following the revolution of the moon around the earth every 24 hours and 50 minutes, there are two high tides in a lunar day

every 12 hour and 25 minutes and two low tides. These high tides occur as a location on earth has to face the moon once in a lunar day experiencing a "bulge" due its gravitational force. The location also faces away from the moon in that day, hence it will experience another "bulge" due to centrifugal forces.

These tides that occur twice a day in a location twice a day as the earth rotates under the moon experiencing bulges and depressions through a lunar day are called semi-diurnal tides. A semi-diurnal tidal system comprises two high tides and two low tides every 24 hours and 50 minutes. South African waters are characterized by a small tidal range with semi-diurnal tides (SANHO, 2014).

The generation of tides by the sun and the moon does not occur in isolation, but tides are influenced by other factors as well. These factors include (but are not limited to) the depth of the ocean, latitude and the structure of land-masses. Tides can be considered as shallow water waves, even in the open ocean as their wavelengths are higher than the ocean depth. As a result, tides are slowed down and move slower than the rotational velocity of the earth. So when the moon is overhead some place on the earth, the place does not experience a high tide immediately, but the high tide lags behind. In addition to this, when tides propagate into shallow water, as in nearshore areas, they are slowed down even further and their form gets distorted. This means that tides behave differently in shallow water to the way they behave in the open ocean (SANHO, 2014).

Tides behave differently at different latitudes as well. At high latitudes, tides follow the rotational velocity of the earth and when the moon is overhead a place the place experiences a high tide at that time. Tides are also affected by landmasses, and these prevent the earth from experiencing tidal "bulges" and depressions freely. For instance, large continents prevent free motion of tides from east to west and this results in complex patterns getting formed in various regions of the ocean. Many other factors influence tides but going through all of them is beyond the scope of this study.

Other characteristics of tides are spring tide and neap tides. Spring tides occur when the moon and the sun are aligned and the tidal forces from the two bodies add together. This occurs during new and full moon. They are characterized by reinforced high waters and low waters. The occurrence of high waters is during local noon and midnight. These above average tides occur about two days after the beginning of the alignment of the sun and the moon owing to the inertia of the water mass and repeats fortnightly (Hicks, 2006; Pinet, 2011). Neap tides occur when the sun and the moon are orthogonal to each other and the tidal forces from the two bodies counteract each other. The results are lower than average tide levels. They occur during the first and third quarter of the moon (Hicks, 2006; Pinet, 2011).

## 4.2 Analysis

Spectral analysis or Fourier analysis considers frequencies that are equally spaces, i.e., $f_1, f_2, f_2, ..., f_{\text{Nyquist}}$. In case of tides that are periodic and as a results have known frequencies, applying the entire band of frequencies as in Fourier analysis is not favourable. Harmonic analysis becomes an appropriate route of analysis. Harmonic analysis can determine coefficients to predetermined frequencies where each frequency presents a tidal constituent. The application of Harmonic analysis in tidal analysis is explained in detail in (Foreman, 1977; Godin, 1991)

To be able to determine $M$ harmonic constituents, the time series, say $z(t_n)$, can be be fitted with

$$z(t_n) = \bar{z} + \sum_{m=1}^{M} C_m \cos(2\Pi f_m t_n - \phi_m) + z_r(t_n), \tag{4.2.1}$$

where $\bar{z}$ is the mean of the series, $z_r(t_n)$ the residual series after the fitting and $f_m$ is the frequency at the $m$th specific constituents. Equation (4.2.1) can be represented as

$$z(t_n) = \bar{z} + \sum_{m=1}^{M} [A_m \cos(2\Pi f_m t_n) + B_m \sin(2\Pi f_m t_n)] + z_r(t_n). \tag{4.2.2}$$

From which,

$$\left.\begin{aligned} C_m &= \sqrt{(A_m^2 + B_m^2)} \\ \phi_m &= \tan^{-1}(B_m/A_m) \end{aligned}\right\}, \tag{4.2.3}$$

where $C_m$ represents amplitude and $\phi_m$ the phase lag. Least squares is used to minimize the variance of the residual series, which is

$$\begin{aligned} s^2 &= \sum_{n=1}^{M} {z_r}^2(t_n) \qquad (4.2.4) \\ &= \sum_{n=1}^{M} \left\{ z_n - \left[ z_0 + \sum_{m=1}^{R} [A_m \cos(2\Pi f_m t_n) + B_m \sin(2\Pi f_m t_n)] \right] \right\}^2. \end{aligned}$$

By taking the partial derivatives of $s^2$ with respect to the unknown coefficients, $A_m$ and $B_m$, $2M + 1$ simultaneous equations for $m = 1 : M$ constituents can be obtained to derive all the coefficients.

Given many frequencies, the standard criterion used to decide on which of the components with close frequencies to search for is the Rayleigh criterion. A constituent is included in the analysis provided that

$$|f_m - f_R|T = |\triangle f|T > R$$

where $R$ is the Rayleigh constant and $T$ is the record length. If this criterion is not satisfied the largest frequency is pursued (Emery & Thomson, 2004; Foreman, 1977).

## 4.3 Methodology

The objective of tidal analysis in this study is to separate tidal and non-tidal effect in order to understand the importance of tides in a current time series. In this study, T_Tide is utilized to carry out tidal analysis. T_Tide is a Matlab toolbox that synthesizes tidal data and it was developed by Pawlowicz et al. (2002). It solves a number of shortcomings of classical harmonic analysis. One of them being that, harmonic analysis ignores the modulation of perihelion requiring a time series of approximately 18.6 years in order to resolve all frequencies. In practice, however, record lengths are about 1 year or shorter periods. T_Tide can resolve frequencies given a short time series. T_Tide assumes the ocean responds in a similar manner at similar frequencies and then applies nodal rectifications and inference to resolve frequencies that may be unresolvable due to time series length restriction. One other advantage of T_Tide is the availability of shallow water constituents. These constituents are important as they account for the fact that in coastal regions, tidal response is in the form of a wave propagating onshore and the different topography in these regions affect the behaviour of the wave.

T_Tide first removes means from the records and then proceeds with harmonic analysis. For the water level time series, T_Tide outputs encompasses tidal constituents, amplitude and phase lags with 95% confidence estimates limits, and a time series of the tidal elevation produced using the tidal constituents with signal-to-noise ratio (snr) $> 1$. An output of T_Tide including the aforementioned is provided in Figure D.1. For current velocity components the output of T_Tide comprises ellipse parameters, i.e., major axis, minor axis and inclination as well as GMT phase with 95 % confidence estimate limits. An output of T_Tide including the aforementioned is provided in Figure D.2 and Figure D.3. A time series of the tidal currents produced using the tidal constituents with signal-to-noise ratio (snr) $> 1$ is also produced.

T_Tide is applied to the whole time series with missing records and then the missing records are filled with a new harmonic tidal signal in the predicted tidal signal. The reason for computing tidal prediction from a series with

missing records is because the tidal signal is more likely to be correct when more constituents are used, the recommended number of constituents being 60 (Hoang, 2012). The six short periods used, results in only 18 constituents at most, in exception of period 4 which is 39 days long and gives 35 constituents. A long time series allows for the resolution of more constituents and a more accurate tidal signal.

## 4.4 Discussion of results

### 4.4.1 Tidal analysis of water level series

Table 4.1 provides summary statistics for the water level series. For all the six periods, the range (maximum value - minimum value) is approximately 2 m, confirming the microtidal range mentioned in Chapter 2. The means across all the periods is approximately 16 m and the variances do not vary much from 0.20 $m^2$. The rest of the summary statistics for all six periods also do not vary much from each other. This indicates an absence of outliers or odd events in the data.

**Table 4.1:** The mean, variance, minimum, maximum values and range of water level measurements.

| Period | Length | Mean (m) | Variance ($m^2$) | Min (m) | Max (m) | Range (m) |
|---|---|---|---|---|---|---|
| 1 | 1801 | 16.35 | 0.19 | 15.37 | 17.21 | 1.84 |
| 2 | 1811 | 16.28 | 0.22 | 15.29 | 17.34 | 2.05 |
| 3 | 1810 | 16.40 | 0.25 | 15.24 | 17.46 | 2.22 |
| 4 | 2813 | 16.43 | 0.24 | 15.36 | 17.53 | 2.17 |
| 5 | 2315 | 16.27 | 0.22 | 15.36 | 17.40 | 2.04 |
| 6 | 2313 | 16.42 | 0.22 | 15.34 | 17.52 | 2.18 |

The output of T_Tide which comprised a time series of predicted water level elevations and residual water level elevations were divided into six time series that are individually analysed. Table 4.2 lists the variances of the water level measurements and the variances of the predicted tides, as well as the percentage contribution of tides to the water level variance for the six periods. Approximately 96% of the variance is due to tides during the first and third period, about 97% during the second period, about 99% during the fourth and fifth period and about 98% in the sixth period. From this table alone it can be concluded that the variation in water level is primarily due to tides.

**Table 4.2:** Comparison of variances of water level measurements with variances of predicted tides.

| Period | Variance (m) | Tidal variance (m) | Tidal percentage (%) |
|---|---|---|---|
| 1 | 0.192 | 0.184 | 96.1 |
| 2 | 0.225 | 0.217 | 96.7 |
| 3 | 0.252 | 0.242 | 96.3 |
| 4 | 0.242 | 0.240 | 98.8 |
| 5 | 0.216 | 0.214 | 98.8 |
| 6 | 0.218 | 0.214 | 97.9 |

Figure 4.1 shows predicted tidal signals computed using all the water level data with gaps included. In addition to tidal predictions computed using T_Tide, a second series of tidal predictions was computed using constituents given in Rosenthal & Grant (1989). The tidal predictions were computed through the use of a software called DElFT-3D and a graph of these tidal predictions is also included in Figure 4.1. The DELFT-3D tidal predictions were compared to the T_Tide tidal predictions to test the accuracy of T_Tide results. Apart from slight difference in amplitudes, the computations are synchronized and similar.

The fortnightly variation, indicating spring and neap tides is clear in the elevations. The graphs indicate that the variation in water level is mainly due to tidal action, the residual water levels have minimal variation relative to the original water levels.

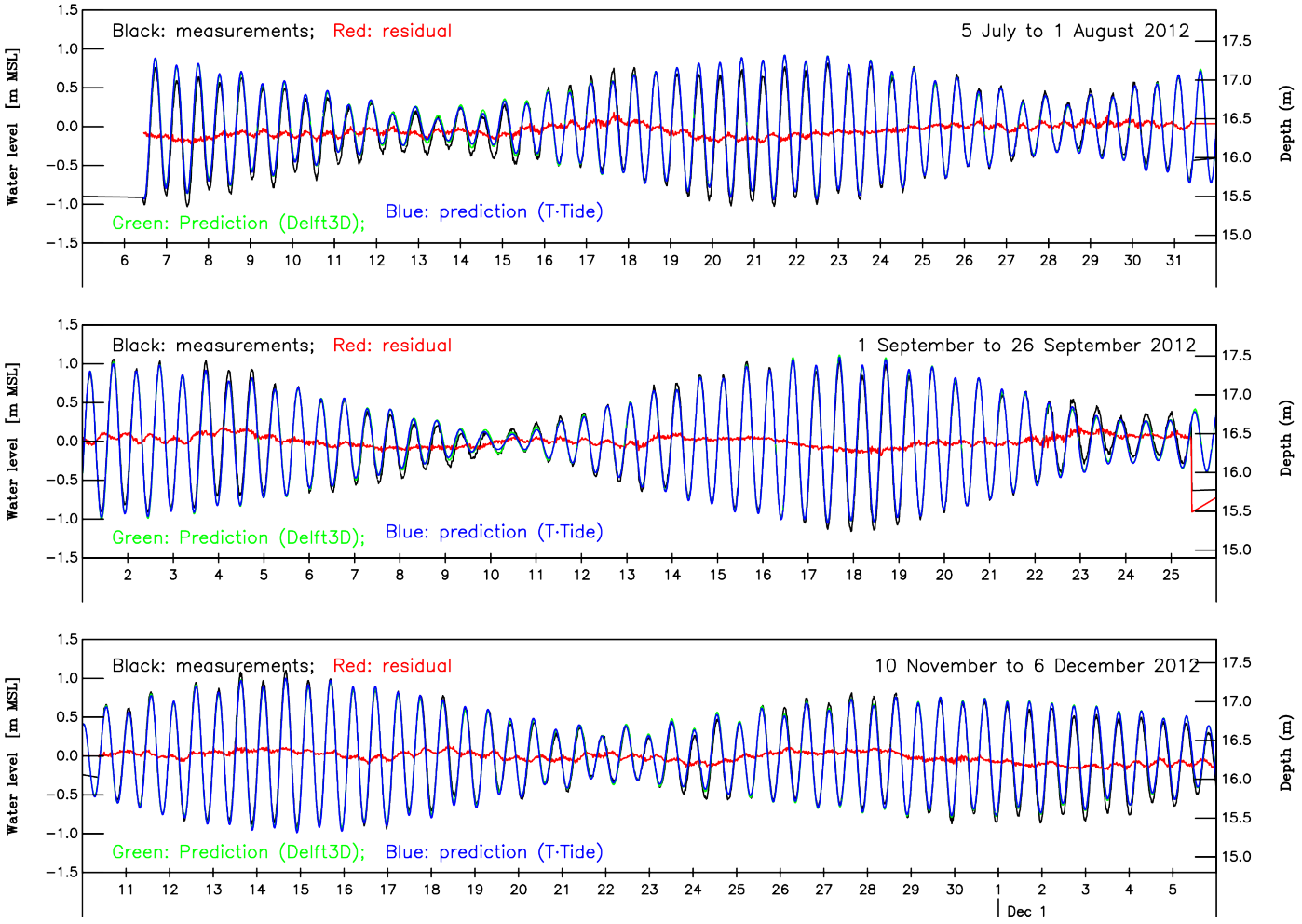


**Figure 4.1:** Plots of predicted water levels by T_Tide and DELFT-3D as well as the residual water levels

Figure E.1 shows the power spectral density of the original water level signals and the residual signals for the whole periods. Inspection of the power spectral density graphs indicate that the variation in the residual signal is less than that in the original signal, approximately 43% of the power spectral density remains in the residual signal at 12.4 hours. The peaks at 12.4 hours and 23.7 hours, which coincides with a semi-diurnal tide and diurnal tide respectively, are noticeably reduced. The peak at 23.7 hours is about non-existent in the residual graph. The reduction in the size of the 12.4 hour peak (and not complete absence) in the residual signals indicate the presence of other periodic events with the same period.

All in all, the variation in water level is from tidal action. The waters are characterized by a semi-diurnal tidal system.

### 4.4.2 Tidal analysis on current series

Tidal analysis is performed on current measurements in both north-south/east-west and longshore/cross-shore directions. The discussion commences with the tidal analysis of north-south and east-west velocity components, these components were inserted into T_tide and treated as vectors. After this, the tidal analysis of longshore and cross-shore components is discussed. The longshore and cross-shore components are inserted into T_tide as scalars.

#### Tidal analysis of north-south and east-west velocity components

The analysis is performed on the whole time series including missing records and then the results are divided into six time series which are then discussed. Table 4.3 to 4.8 give variances of east-west and north-south velocity components and combined (total) variances with fractions (in percentages) of each variance due to tidal constituents.

**Table 4.3:** Variances of east-west (East) and north-south (North) current components and combined (total) variance with the fraction (in percentage) of each variance due to the tidal constituents presented for the three current records for the first period. Variances are given in $(cm/s)^2$.

| Period 1 | | | |
|---|---|---|---|
| Depth | East(%) | North(%) | Total (%) |
| 2.42 m | 80.9(3.8%) | 33.9 (5.6%) | 114.8(4.3%) |
| 8.92 m | 22.5(3.6%) | 64.6(3.8%) | 87.1(3.8%) |
| 15.92 m | 267.6(24.2%) | 326.6(8.0%) | 594.2(15.3%) |

Table 4.3 gives the contribution of tidal constituents to the variance of east-west and north-south velocity components for period one. Tidal contribution to variance decreases from 2.42 m to 8.92 m , but increases from 8.92 m to 15.92 m. The tidal contribution is largest at 15.92 m which is near the surface, the largest contribution being in the east-west velocity components. For depths 2.42 m and 8.92 m, tidal contribution is larger in the north-south velocity components, while it is larger in the east-west velocity components at the near surface.

**Table 4.4:** Variances of east-west and north-south current components and combined (total) variance with the fraction (in percentage) of each variance due to the tidal constituents presented for the three current records for the second period. Variance given in $(cm/s)^2$.

| Period 2 | | | |
|---|---|---|---|
| Depth | East(%) | North(%) | Total (%) |
| 2.42 m | 27.0(8.5%) | 29.5 (6.7 %) | 56.5(7.5%) |
| 8.92 m | 36.1(2.8 %) | 51.7(6.1 %) | 87.9(4.8%) |
| 15.92 m | 300.0(25.6 %) | 273.7(13.9 %) | 573.7(20.0%) |

Table 4.4 gives tidal contribution to variance for east-west and north-south velocity components during period two. This period exhibit some similarities to period one, in that the tidal contribution is larger at 8.92 m than it is 2.42 m, and the largest tidal contribution is observed at 15.92 m. For depths 2.42 m and 15.92 m the largest tidal contributions are observed in the east-west velocity components, while for 8.92 m the largest tidal contribution to variance is observed in the north-south velocity components. The largest tidal contribution to variance for the whole period is observed at 15.92 m in the east-west velocity components.

**Table 4.5:** Variances of east-west and north-south current components and combined (total) variance with the fraction (in percentage) of each variance due to the tidal constituents presented for the three current records for the third period. Variances are given in $(cm/s)^2$.

| Period 3 | | | |
|---|---|---|---|
| Depth | East(%) | North(%) | Total (%) |
| 2.42 m | 22.3(7.7 %) | 64.2 (3.8 %) | 86.4(4.8%) |
| 8.92 m | 32.8(4.0 %) | 140.4(3.1 %) | 173.2(3.2%) |
| 15.92 m | 297.5(28.4 %) | 591.2(7.2 %) | 888.7(14.3%) |

Table 4.5 gives tidal contribution to variance for east-west and north-south velocity components for period three. The table gives the same pattern as was observed in Table 4.3 and 4.4, the largest tidal contribution to variance is observed at 15.92 m, followed by 2.42 m and the lowest tidal contribution occurs at 8.92 m. The contribution of tides to variance are higher in east-west velocity components than they are in the north-south velocity components for all depths. Once again, the largest tidal contribution to variance for the whole period is observed at 15.92 m in the east-west velocity components.

**Table 4.6:** Variances of east-west and north-south current components and combined (total) variance with the fraction (in percentage) of each variance due to the tidal constituents presented for the three current records for the fourth period. Variances are given in $(cm/s)^2$.

| Period 4 | | | |
|---|---|---|---|
| Depth | East(%) | North(%) | Total (%) |
| 2.42 m | 23.1(9.4 %) | 29.2 (11.7 %) | 52.3(10.7%) |
| 8.92 m | 39.1(3.6 %) | 74.8(6.4 %) | 113.8(5.4%) |
| 15.92 m | 349.1(22.9 %) | 476.0(8.1 %) | 825.1(14.4 %) |

Table 4.6 gives tidal contribution to variance for east-west and north-south velocity components for period four. In this period, tidal contributions to variance are larger at 2.42 m than they are at 8.92 m. The largest tidal contribution to variance is observed at 15.92 m in the east-west components. The tidal contribution to variance is larger in the north-south components at 2.42 m and 8.92 than it is in the east-west components, the opposite is true at 15.92 m.

**Table 4.7:** Variances of east-west and north-south current components and combined (total) variance with the fraction (in percentage) of each variance due to the tidal constituents presented for the three current records for the fifth period. Variances are given in $(cm/s)^2$.

| Period 5 | | | |
|---|---|---|---|
| Depth | East(%) | North(%) | Total (%) |
| 2.42 m | 21.4(13.6 %) | 79.4 (3.8 %) | 100.9(5.9%) |
| 8.92 m | 27.9(3.9 %) | 172.2(2.1 %) | 200.1(2.3%) |
| 15.92 m | 283(29.1 %) | 714.6(3.0 %) | 997.7(10.4%) |

Table 4.7 gives tidal contributions to variance for east-west and north-south velocity components during period five. Th highest tidal contribution is observed at the near surface in the east-west velocity component. The tidal contribution in both components are larger at 2.42 m than they are at 8.92 m. The contribution to variance is larger in east-west velocity components than it is in north-south velocity components for all the depths.

**Table 4.8:** Variances of east-west and north-south current components and combined (total) variance with the fraction (in percentage) of each variance due to the tidal constituents presented for the three current records for sixth period. Variances are given in $(cm/s)^2$.

| Period 6 | | | |
|---|---|---|---|
| Depth | East(%) | North(%) | Total (%) |
| 2.42 m | 38.1(7.9 %) | 47.1 (5.2 %) | 85.3(6.4%) |
| 8.92 m | 55.2(1.4 %) | 107.9(2.3 %) | 163.0(2.0%) |
| 15.92 m | 468.4(16.3 %) | 354.4(5.4 %) | 882.9(11.6%) |

The results in Table 4.8 do not differ greatly from results in the previous tables discussed earlier. The tidal contribution increases from 8.92 m, then 2.42 m and and then it is largest at 15.92 m in both east-west and north-south velocity components. The tidal contribution at 2.42 and 15.92 in the east-west velocity components exceed those in the north-south components, while the opposite is true at 8.92 m. The largest tidal contribution occurs at 15.92 m in the east-west velocity components.

The results in Table 4.3 to 4.8 indicate an insignificant contribution to current velocities by tidal action, in terms of east-west and north-south orientations. The largest contributions of tides to variances are observed in the east-west velocity components at 15.92 m. The range of the fractions of contributions are as follows, 24.2%, 25.6%, 28.4 %, 22.9 %, 29.1% and 16.3 % from period one through to six. For the whole period of data collection, the maximum tidal contribution to variance is 23.2%, taken from Table E.1.

Figure E.2 and Figure E.3 show the power spectral density graphs of the original east-west and north-south velocity signals and the corresponding residual signals for the whole period at 2.42 m and 8.92 m. The inspection of the power spectral density graphs indicate that the variation in the residual signal is similar to that in the original signal, except at around two frequencies which correspond with 12.4 hours and 23.7 hours. At these two periods, the peaks in the residual signals are smaller than those in the original signal.

Figure E.4 shows the power spectral density graphs of the original east-west and north-south velocity signals and the corresponding residual signals for the whole period at 15.92 m. There seems to be much more tidal impact in both velocity components 15.92 m away from the ADCP. Many more tidal constituents have a significant contribution to the currents, this is indicated by many more visible tidal peaks and their reduction in the residual signals. The additional periodicities include, 8.2, 6.2 as well as 4.1 hours. The tidal peaks are predominant and thus much more reduced in the east-west velocity than

in the north-south velocity components.

Figures 4.2 to 4.7 depict north-south and east-west velocity components of currents, velocity due to tidal action and the residual velocities for the whole time series with missing records included.

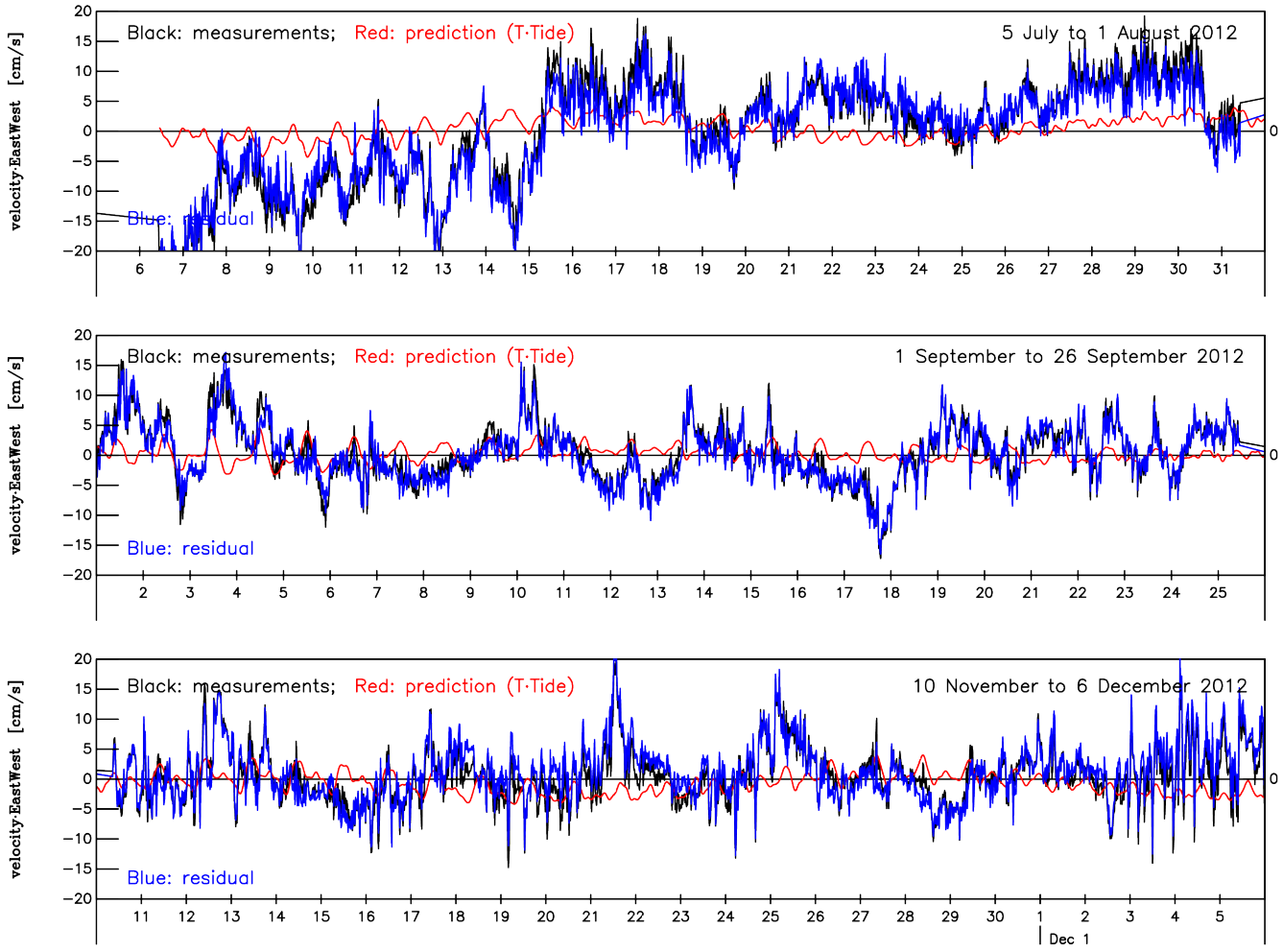


**Figure 4.2:** East-west velocity components of current at 2.42 m. The graphs show the original velocity, tidal velocity and the residual velocity.

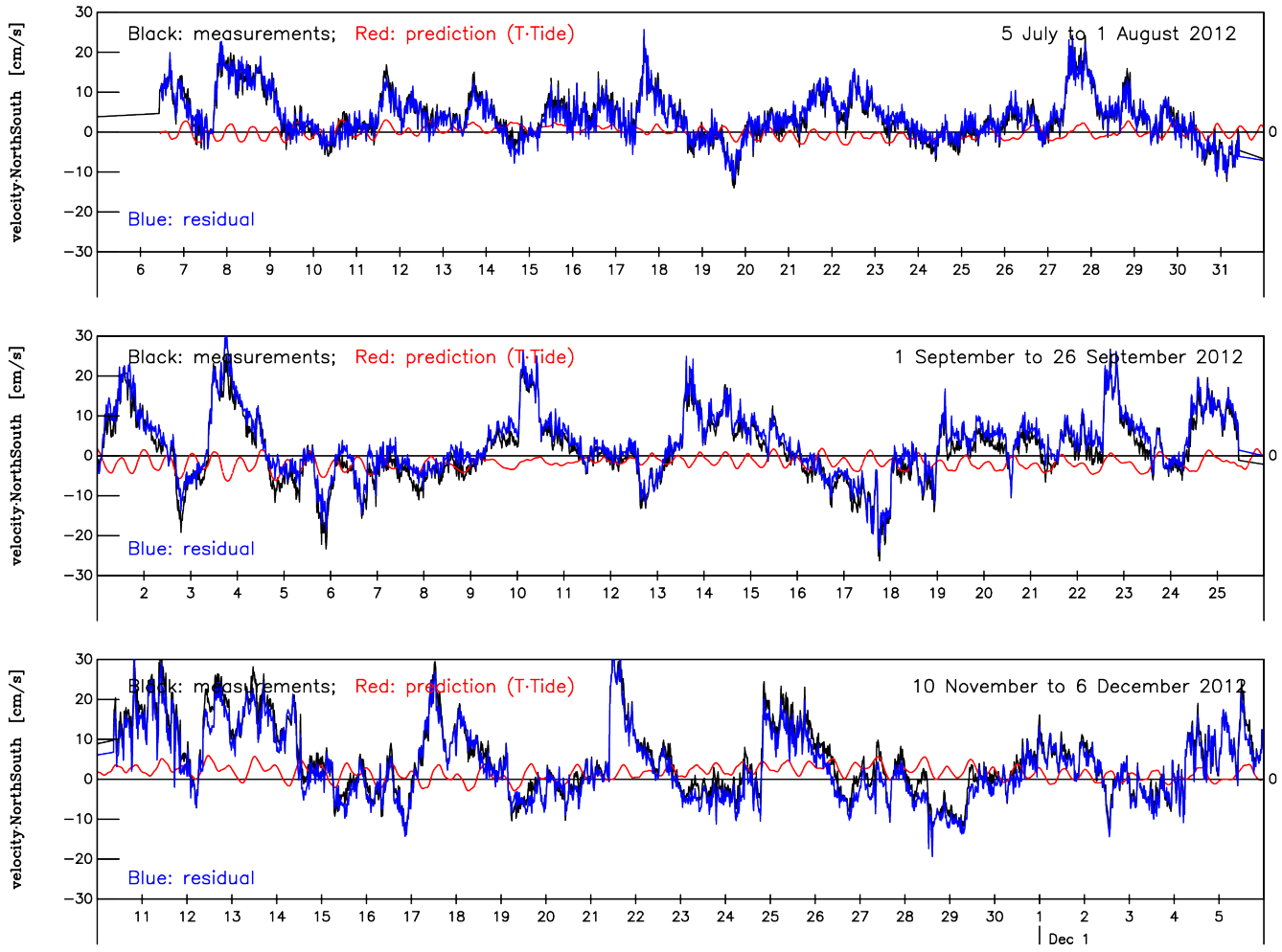


**Figure 4.3:** North-south velocity components of current at 2.42 m. The graphs show the original velocity, tidal velocity and the residual velocity.

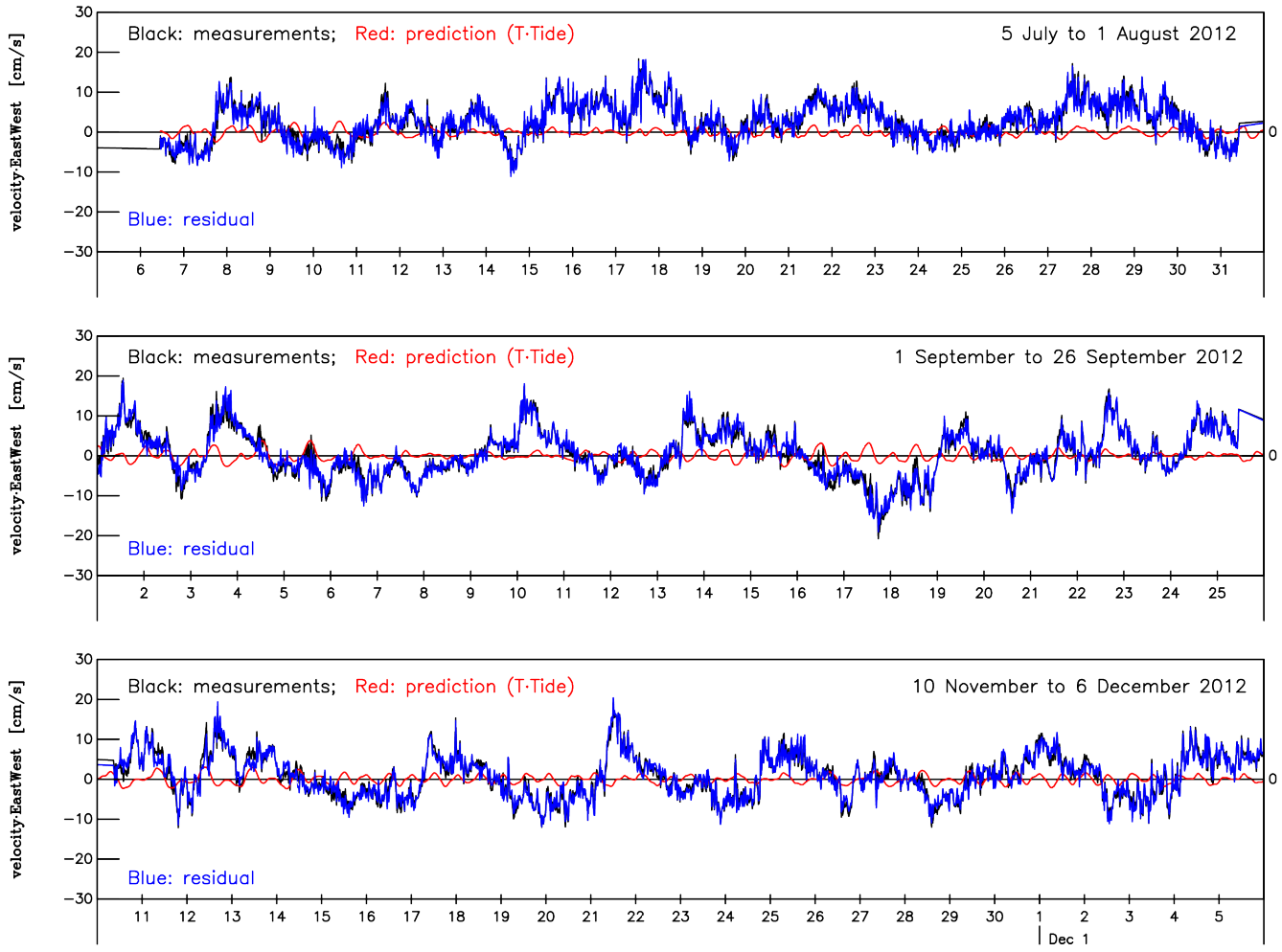


**Figure 4.4:** East-west velocity components of current at 8.92 m. The graphs show the original velocity, tidal velocity and the residual velocity.

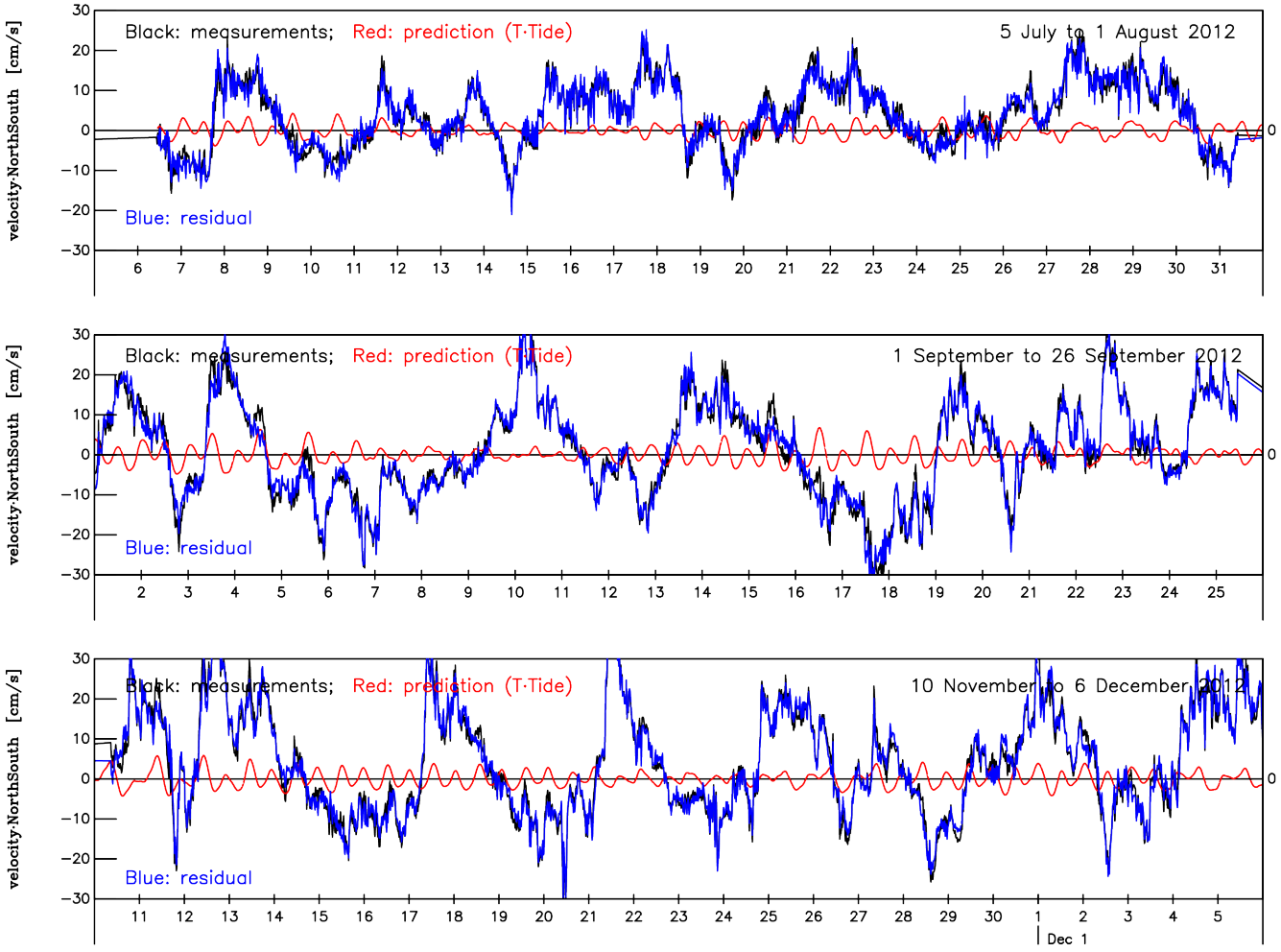


**Figure 4.5:** North-South velocity components of current at 8.92 m. The graphs show the original velocity, tidal velocity and the residual velocity.

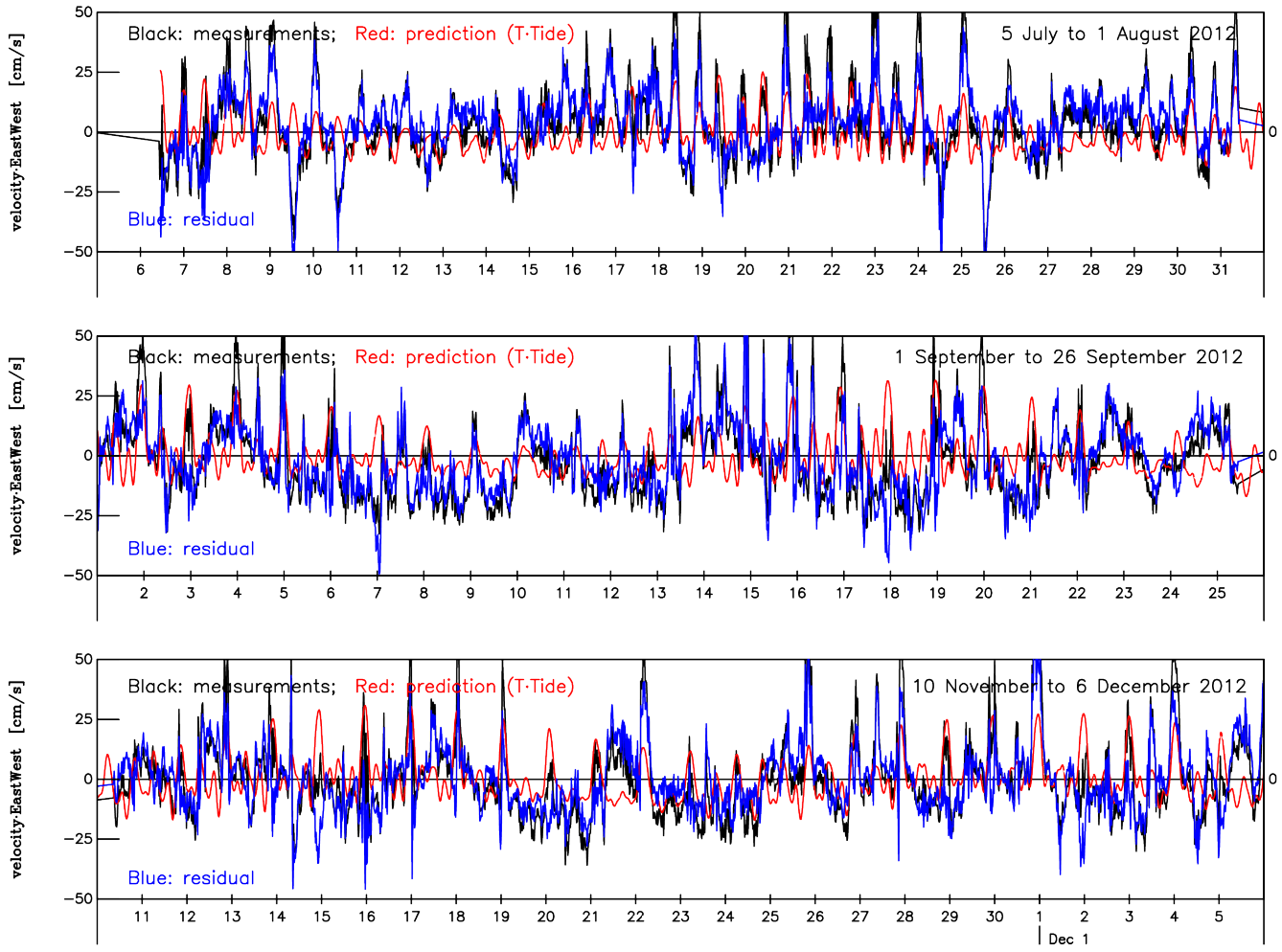


**Figure 4.6:** East-west velocity components of current at 15.92 m. The graphs show the original velocity, tidal velocity and the residual velocity.

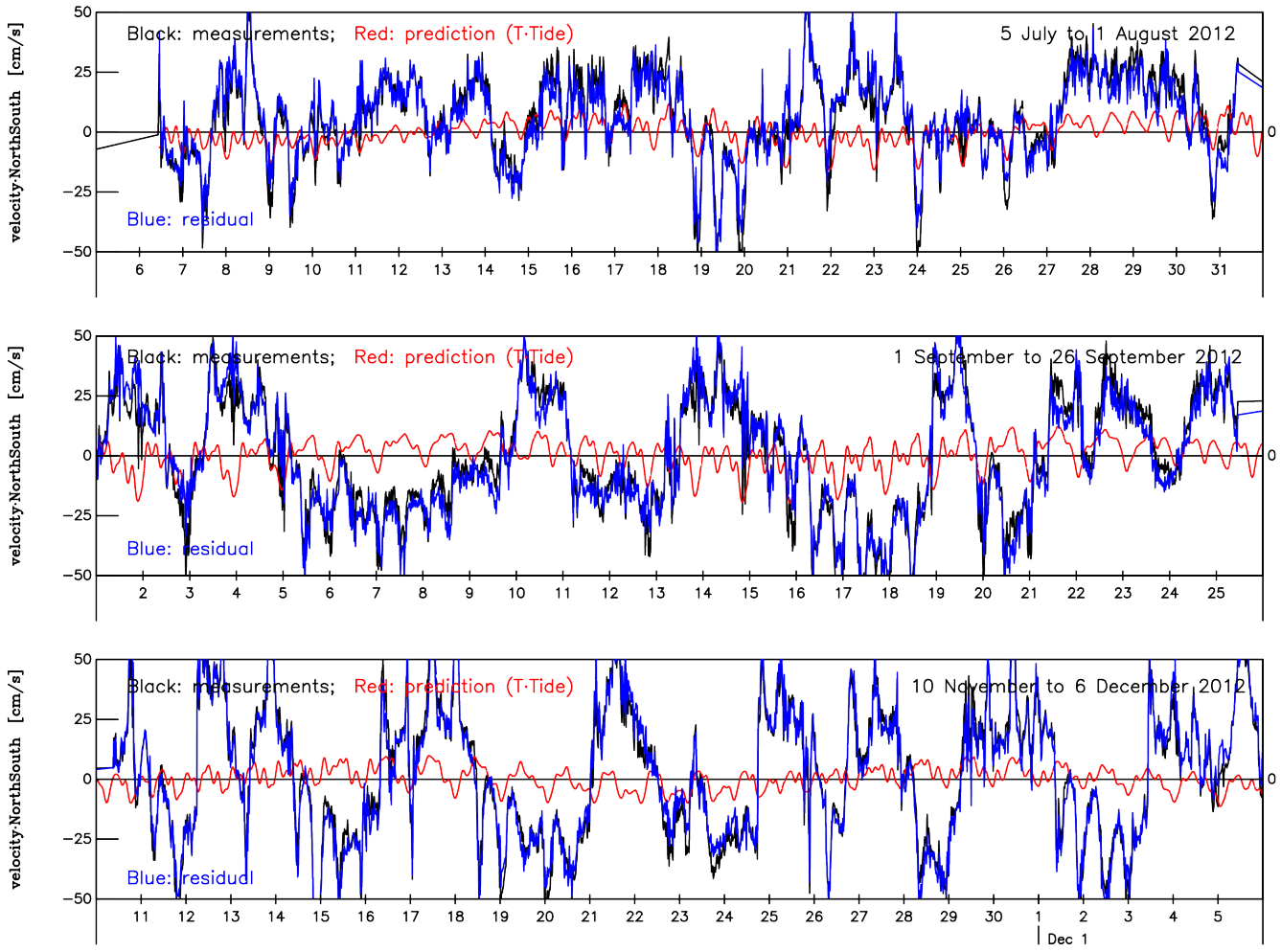


**Figure 4.7:** North-south velocity components of current at 15.92 m. The graph shows the original velocity, tidal velocity and the residual velocity.

The graphs in Figure 4.2 to 4.7 supplement Tables 4.3 to 4.8. They indicate that the effect of tides on current velocity is limited. The tide tend to have a stronger effect at the surface in the east-west direction while the effect is minimal everywhere else.

### Tidal analysis of longshore and cross-shore velocity components

Tidal analysis is also performed on longshore and cross-shore currents as these are the most appropriate orientations with respect to the coast. This analysis follows the same pattern as was conducted for the north-south and east-west velocity components.

Table 4.9 to 4.14 give variances of longshore and cross-shore velocity components with fractions (in percentages) of each variance due to tidal constituents.

**Table 4.9:** Variances of longshore and cross-shore current components with the fraction (in percentage) of each variance due to the tidal constituents presented for the three current records for the first period. Variances are given in $(cm/s)^2$.

| Period 1 | | |
|---|---|---|
| Depth | Longshore(%) | Cross-shore(%) |
| 2.42 m | 52.8 (5.8 %) | 62.2 (1.2 %) |
| 8.92 m | 79.4 (3.4 %) | 7.7 (3.8 %) |
| 15.92 m | 322.4 (3.5 %) | 271.8 (24.5 %) |

Table 4.9 gives the contribution of tides to the variance of longshore and cross-shore currents for period one. The table presents tidal contribution to variance to be increasing from the bottom (2.42 m) towards the surface (15.92 m) in the cross-shore velocity components. In the longshore components, the smallest tidal contribution is observed at 8.92 m and the highest contribution is observed at 2.42 m. The highest tidal contribution for the period occurs in the cross-shore components at the near surface.

**Table 4.10:** Variances of longshore and cross-shore current components with the fraction (in percentage) of each variance due to the tidal constituents presented for the three current records for the second period. Variances are given in $(cm/s)^2$.

| Period 2 | | |
|---|---|---|
| Depth | Longshore(%) | Cross-shore(%) |
| 2.42 m | 42.1 (7.8 %) | 14.3 (3.8 %) |
| 8.92 m | 83.2 (4.3 %) | 4.7 ( 5.6 %) |
| 15.92 m | 402.5 (2.2 %) | 171.2 (56.7 %) |

Table 4.10 gives tidal contribution to variance of longshore and cross-shore components velocity during the second period. Tidal contribution to variance decreases from 2.42 m to 15.92 m in the longshore velocity components. In the cross-shore velocity components, the tidal contribution increases from 2.42 m to 15.92 m. The largest tidal contribution occurs at the near surface, i.e, 15.92 m in the cross-shore velocity components.

**Table 4.11:** Variances of longshore and cross-shore current components with the fraction (in percentage) of each variance due to the tidal constituents presented for the three current records for the first period. Variances are given in $(cm/s)^2$.

| Period 3 | | |
|---|---|---|
| Depth | Longshore(%) | Cross-shore(%) |
| 2.42 m | 75.8 (5.1 %) | 10.6 (5.3 %) |
| 8.92 m | 159.8 (3.1 %) | 13.4 (2.6 %) |
| 15.92 m | 627.4 (1.3 %) | 261.4 (43.3 %) |

Table 4.11 gives tidal contribution to variance in longshore and cross-shore velocity components for period three. Similar to period two, tidal contribution to variance decreases from 2.42 m through 8.92 m to 15.92 m in the longshore velocity components. In the cross-shore velocity components, the tidal contribution to variance is the smallest at 8.92 m and highest at the near surface. The highest tidal contribution is found at the near surface in the cross-shore velocity components.

**Table 4.12:** Variances of longshore and cross-shore current components with the fraction (in percentage) of each variance due to the tidal constituents presented for the three current records for the first period. Variances are given in $(cm/s)^2$.

| Period 4 | | |
|---|---|---|
| Depth | Longshore(%) | Cross-shore(%) |
| 2.42 m | 43.1 (10.0 %) | 9.2 (10.0 %) |
| 8.92 m | 107.7 (5.1 %) | 6.1 (8.6 %) |
| 15.92 m | 620.4 (1.8 %) | 204.6758 (46.0 %) |

The tidal contribution to variance in longshore and cross-shore velocity components are given in Table 4.12. The tidal contribution to variance at 2.42 m is the same in both longshore and cross-shore velocity components, being 10.0 %. In the longshore velocity components, tidal contribution to variance decreases from the bottom, i.e., 2.42 m through 8.92 m to the near surface, i.e., 15.92 m. In the cross-shore velocity components, the lowest tidal contribution is in the middle, 8.92 m, while the largest tidal contribution is at the near surface, which is also the largest tidal contribution for the whole period.

**Table 4.13:** Variances of longshore and cross-shore current components with the fraction (in percentage) of each variance due to the tidal constituents presented for the three current records for the first period. Variances are given in $(cm/s)^2$.

| Period 5 | | |
|---|---|---|
| Depth | Longshore(%) | Cross-shore(%) |
| 2.42 m | 76.3 (4.8 %) | 24.6 (1.2 %) |
| 8.92 m | 176.2 (2.3 %) | 23.9 (1.3 %) |
| 15.92 m | 727.6974 (2.1 %) | 270.0 (26.6 %) |

Table 4.13 gives tidal contribution to variance for longshore and cross-shore velocity components. In the longshore velocity components, tidal contribution to variance decreases from 2.42 m to 15.92 m. The decrease from 8.92 m to 15.92 m is slight being only 0.1 %. In the cross-shore velocity components , tidal contribution to variance increases from the bottom to the near surface. The increase from 2.42 m to 8.92 m is also slight, also being 0.1 %. The highest tidal contribution is at the near surface in the cross-shore velocity components.

**Table 4.14:** Variances of longshore and cross-shore current components with the fraction (in percentage) of each variance due to the tidal constituents presented for the three current records for the first period. Variances are given in $(cm/s)^2$.

| Period 6 | | |
|---|---|---|
| Depth | Longshore(%) | Cross-shore(%) |
| 2.42 m | 67.6 (4.9 %) | 17.7 (3.9 %) |
| 8.92 m | 155.6 (1.8 %) | 7.5 (4.7 %) |
| 15.92 m | 619.9 (2.2 %) | 203.0 (34.0 %) |

Table 4.14 gives tidal contribution to variance in the longshore and cross-shore velocity components for period six. The highest tidal contribution to variance in the longshore velocity components is at 2.42 m , while the smallest contribution is at 8.92 m. In the cross-shore components tidal contribution to variance increases from the bottom to the near surface, the contribution at the near surface is the highest for the whole period.

Inspection of the results presented in Table 4.9 to 4.14 indicate that for the six periods, variance due to tidal action for levels 2.42 m and 8.92 m never exceed 10.0%. The difference in tidal contribution to variance at the bottom (2.42 m), middle (8.92 m) and that of the near surface (15.92 m) cross-shore components can be quite large such as 3.8 % at 2.42 m and 56.7 % at 15.92 m.

The largest tidal contribution in the longshore velocity components are found near the bottom, i.e, at 2.42 m, for the whole period. This is opposite to what happens in the cross-shore velocity components, where the largest tidal contribution to tides occurs at the near surface. For all the six periods, variances due to tidal action are relatively higher towards the surface, at 15.92 m, in the cross-shore velocity components. Towards the surface, at 15.92 m, in the cross-shore velocity components, the lowest percentage of tidal contribution occurs in the first period (24.5%), while the highest percentage occurs in the second period (56.7%). From Table E.2 the largest contribution to tidal variance for the whole period is 37.1 % which is somewhat significant.

Figure E.5 shows the power spectral density graphs of the original longshore and cross-shore velocity signals and the corresponding residual signals for the whole period at 2.42 m. The inspection of the power spectral density graphs indicate that the variation in the residual signal is similar to that in the original signal, except at around two frequencies which correspond with 12.4 hours and 23.7 hours. At these two periods, the peaks in the residual signals are smaller than those in the original signal. The tidal peaks are much larger in the longshore velocity components, more than they are in the cross-shore velocity components, especially at 12.4 hours. Figure E.6 shows the power spectral density graphs of the original longshore and cross-shore velocity signals and the corresponding residual signals for the whole period at 8.92 m. The graphs look similar to those in Figure E.5.

Figure E.7 shows the power spectral density graphs of the original longshore and cross-shore velocity signals and the corresponding residual signals for the whole period at 15.92 m. Many more tidal constituents have a significant contribution to the currents than at 2.42 m and 8.92 m, this is indicated by many more visible tidal peaks and their reduction in the residual signals. The additional periodicities include, 16.1 days, 8.2, 6.2 as well as 4.1 hours. The tidal peaks are predominant and thus much more reduced in the residual signals in the cross-shore velocity components than in the longshore velocity components.

Figures 4.8 to 4.13 depict longshore and cross-shore velocity components of currents, velocity due to tidal action and the residual velocities for the whole time series with missing records included.

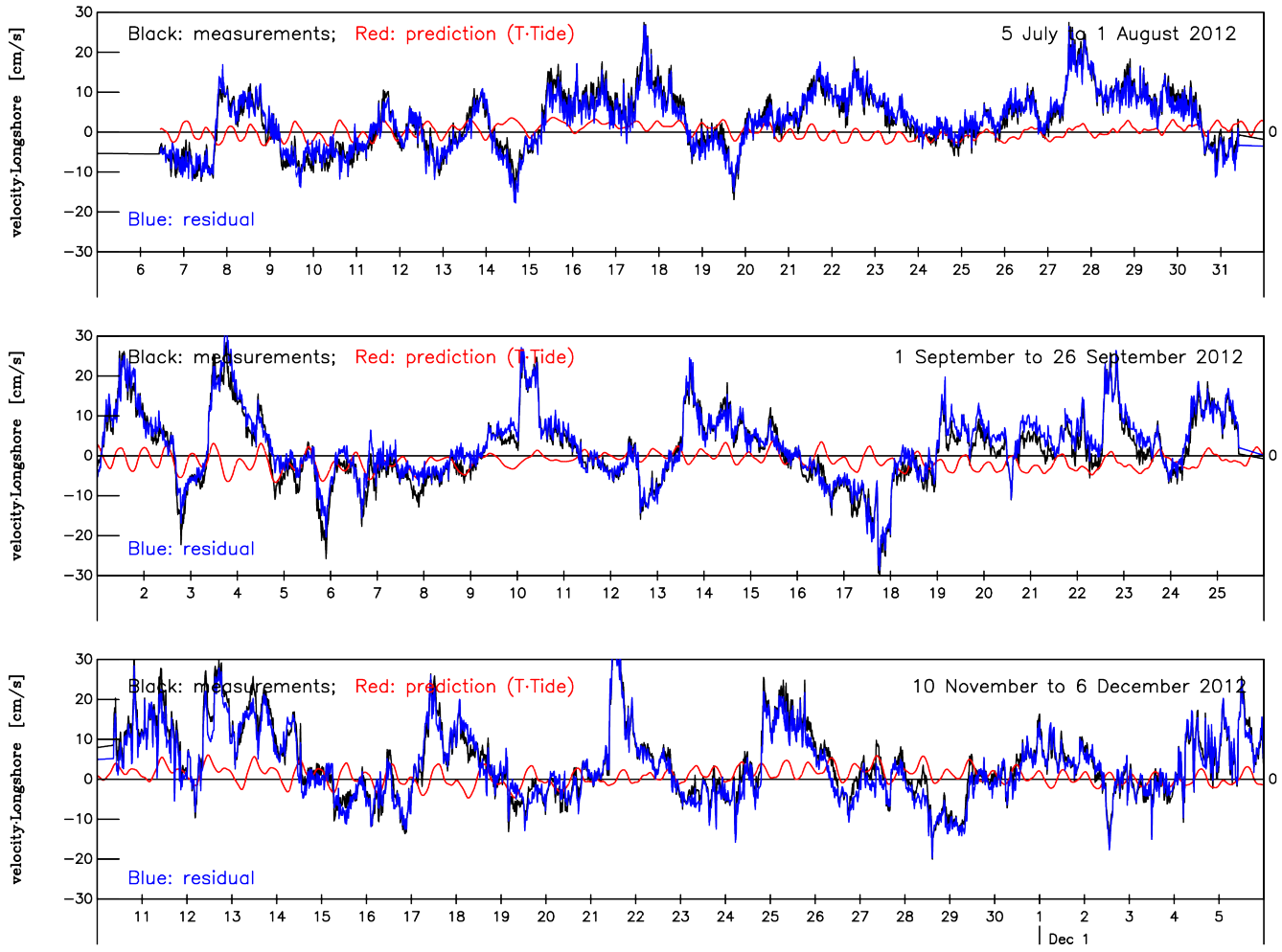


**Figure 4.8:** Longshore velocity components of current measurements at 2.42 m. The graphs show the original velocity, tidal velocity and the residual velocity.

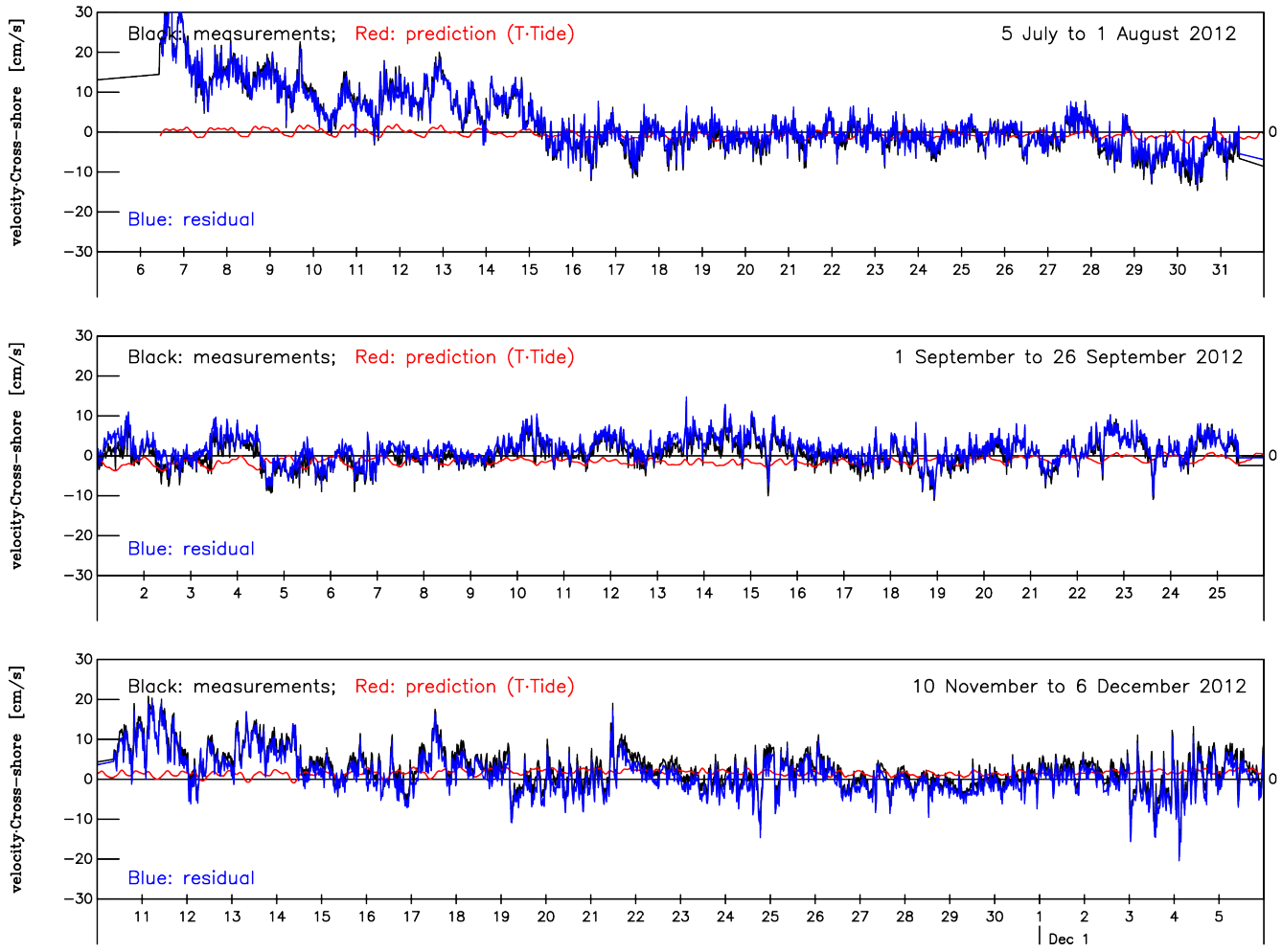


**Figure 4.9:** Cross-shore velocity components of current measurements at 2.42 m. The graphs show the original velocity, tidal velocity and the residual velocity.

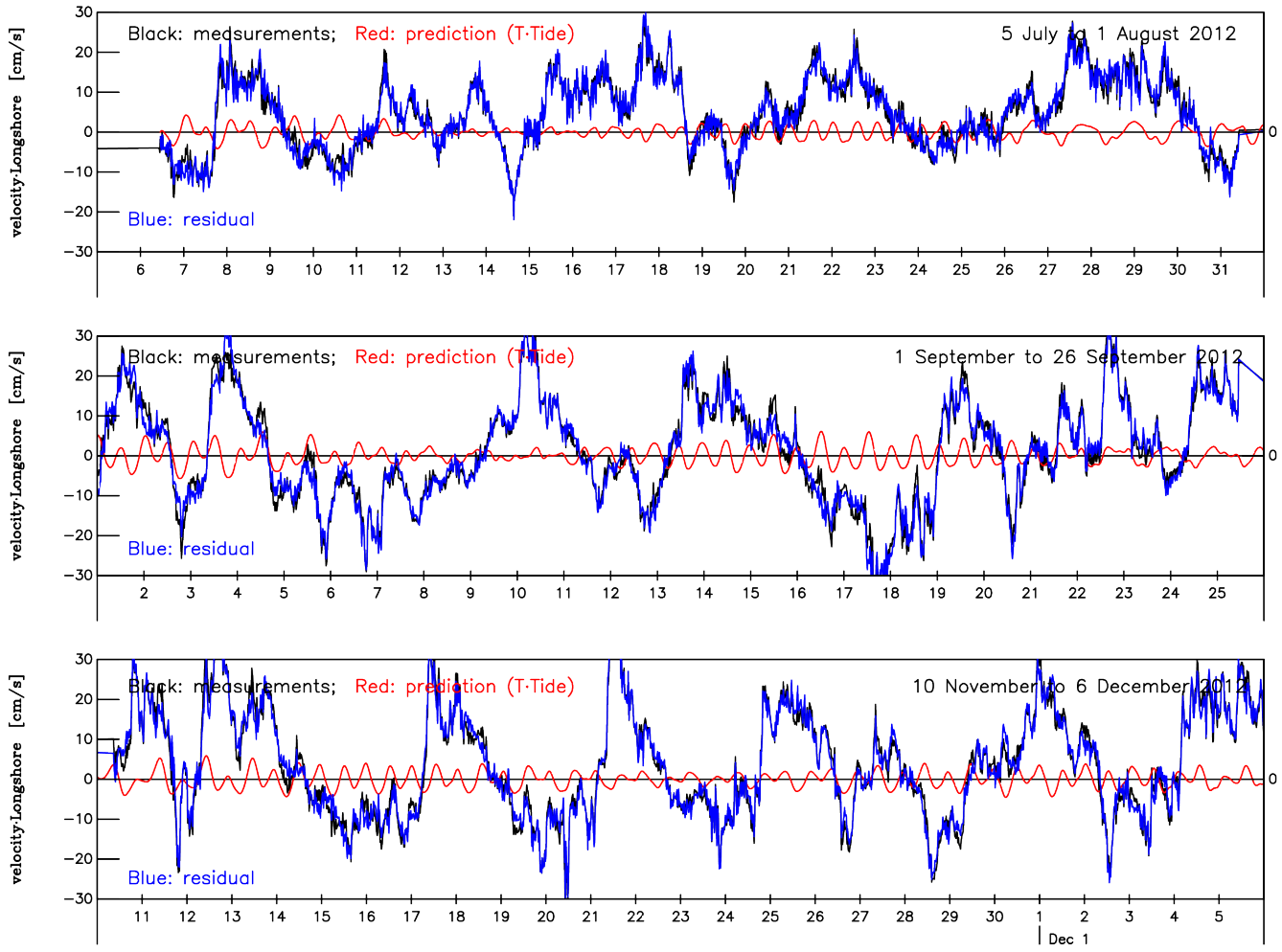


**Figure 4.10:** Longshore velocity components of current measurements at 8.92 m. The graphs show the original velocity, tidal velocity and the residual velocity.

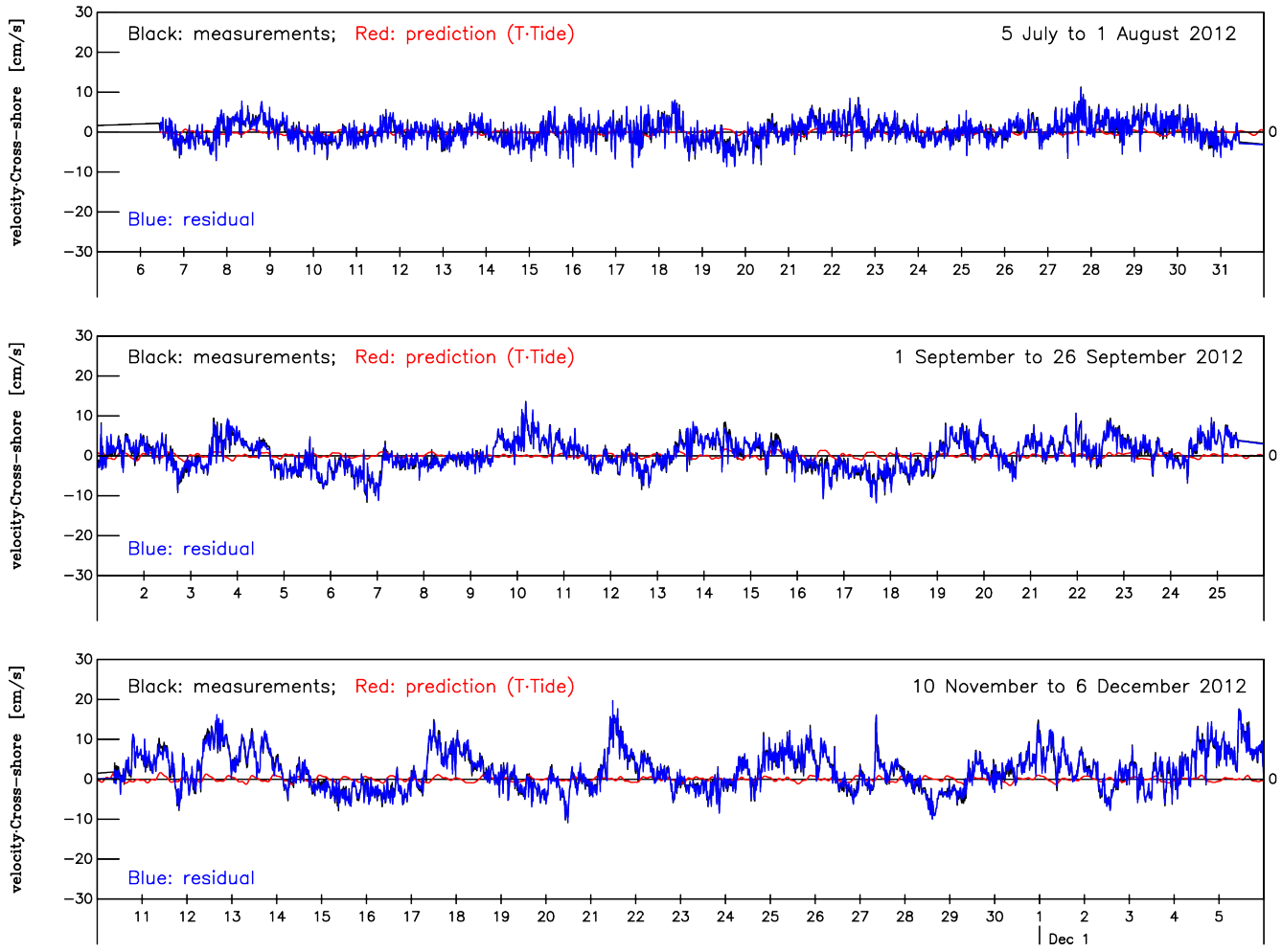


**Figure 4.11:** Cross-shore velocity components of current measurements at 8.92 m. The graphs show the original velocity, tidal velocity and the residual velocity.

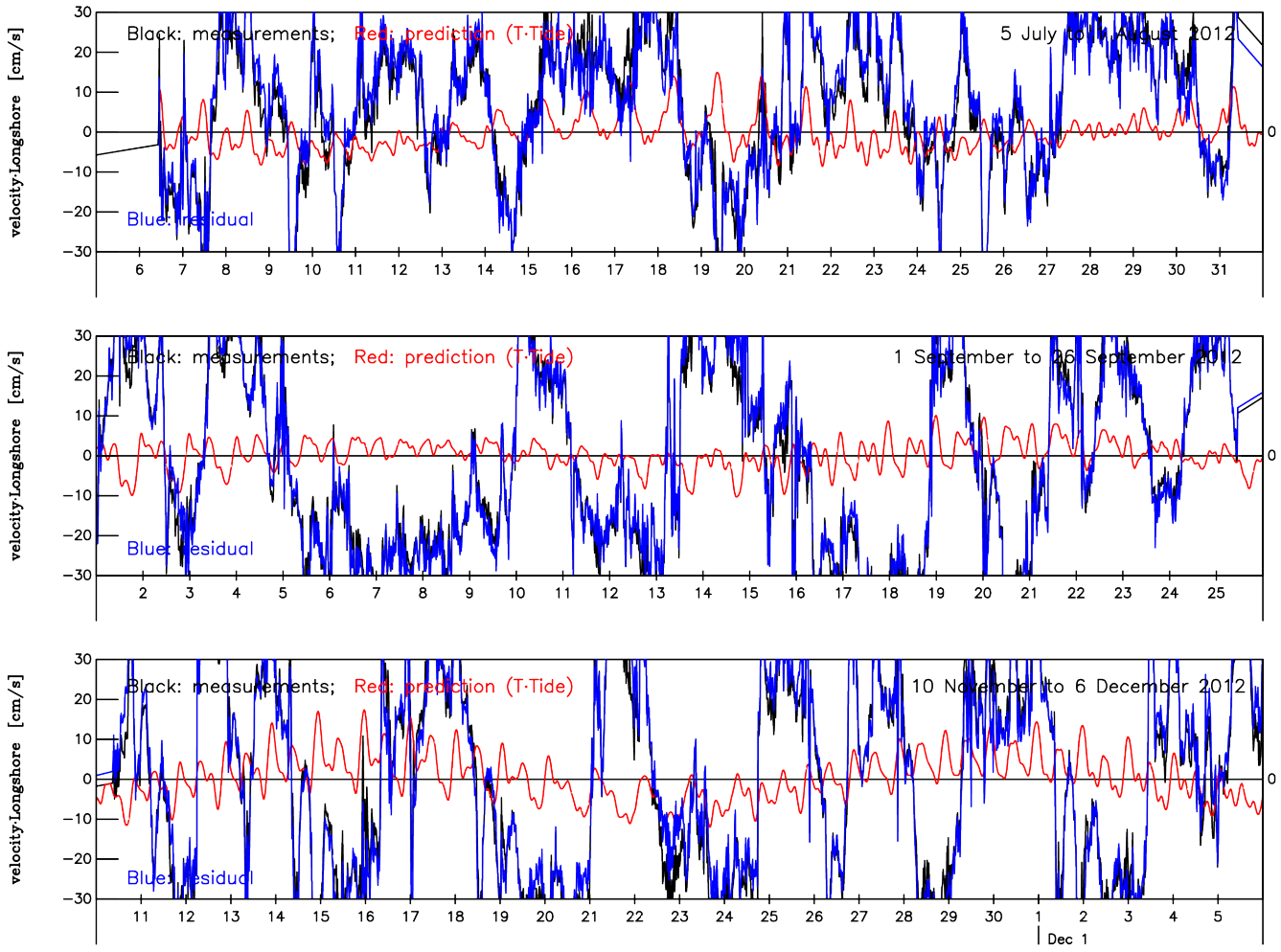


**Figure 4.12:** Longshore velocity components of current measurements at 15.92 m. The graphs show the original velocity, tidal velocity and the residual velocity.

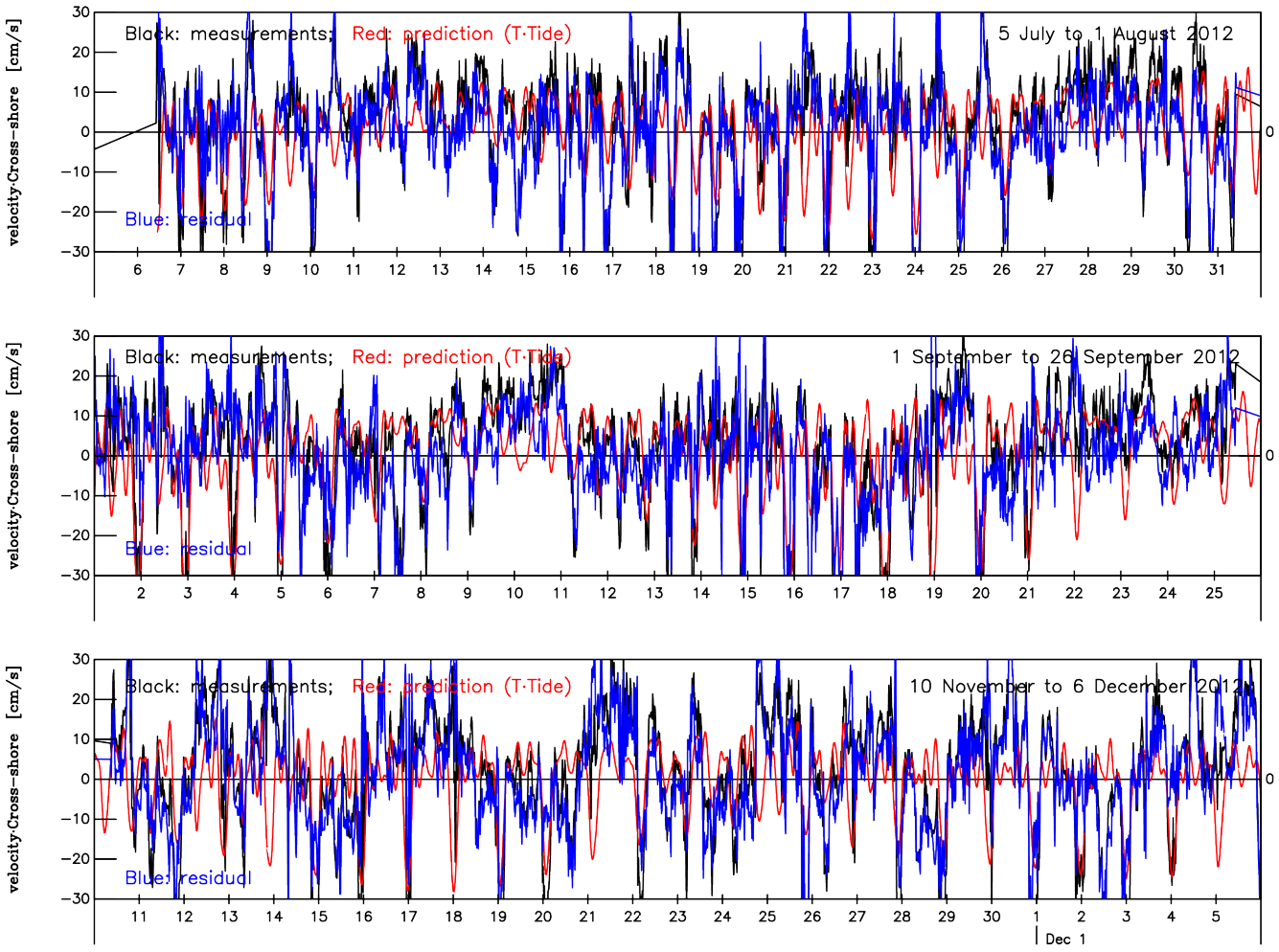


**Figure 4.13:** Cross-shore velocity components of current measurements at 15.92 m. The graphs show the original velocity, tidal velocity and the residual velocity.

Figures 4.8 to 4.13 show graphs of longshore and cross-shore velocity components, predicted tidal velocity components and residual velocity components. Figures 4.8 and 4.9 show the components at 2.42 m, in the alongshore and across-shore directions respectively. Figures 4.10 and 4.11 show the components at 8.92 m, in the alongshore and across-shore directions respectively. Finally, Figures 4.12 and 4.13 show the components at 15.92 m, in the alongshore and across-shore directions respectively.

The figures substantiate what was previously discussed with regards to Table 4.9 to 4.14. The tidal velocity components are smaller towards the sea bed (2.42 m) and the middle waters (8.92 m) in the cross-shore velocity components than they are in the longshore ones. The highest predicted tidal velocity components are observed in Figure 4.13, the residual velocity components are

noticeably reduced in the figure. Cross-shore tidal velocity components are higher relative to longshore tidal velocity components.

## 4.5 Summary

This chapter presented a brief introduction of tides and harmonic analysis as a technique that can be used to analyse tides. Tides are the variations in sea level as a result of the gravitational forces induced mainly by the sun and the moon. The variations are periodic rendering tides predictable with some level of accuracy. T_Tide was used to analyse tides in both water level and current level measurements.

Water level measurements substantiate the micro-tidal range that was established in Chapter 2. Tides are responsible for most of the variation in water levels for the duration of data collection, tidal variation accounts for at least 96% of the variance of water level measurements.

Tidal analysis was performed on both north-south and east-west velocity components as well as longshore and cross-shore velocity components. Tidal velocity components are predominant in the east-west components relative to north-south components. Tidal velocity components are highest near the surface and lowest in the middle waters as well as near the bottom in the east-west components. Tidal action also seem to have a predominant effect in the cross-shore velocity components as opposed to longshore ones near the surface. All in all, tidal velocity accounts for a limited portion of the current velocities. The highest contribution to variance by tidal currents is at most 37.1%, which occurs at the surface in the cross-shore direction.

# Chapter 5

# Wave data and Stokes drift analysis

## 5.1 Introduction

Ocean waves give rise to a variety of currents including longshore currents, cross-shore currents and Stokes drift. This chapter focuses on Stokes drift. Stokes drift is defined and estimated using measured wave data, and its contribution to the overall current is evaluated.

### 5.1.1 Definition of Stokes drift

Stokes drift is one of the manifestations of surface gravity waves, and can be intuitively visualised as the near surface current induced by wave action. This current is indicated by $u_s$ in (1.2.1). Academically, Stokes drift at a point is defined as the net motion of a fluid particle, generally, in the direction of wave propagation. This motion can be observed by tracing the motion of a fluid particle over a wave period. The fluid particle would move in an open orbital path, with a net forward flow in the direction of propagation of the wave. This motion was first theoretically described by George Gabriel Stokes in 1847, hence the drift bearing his name (Heath, 2011; Hoang, 2012; Monismith & Fong, 2004).

Stokes drift is also defined as the difference between the mean Eulerian flow velocity of a fluid particle at a fixed position and the mean Lagrangian flow velocity of a fluid particle. It diminishes with depth from the surface to the sea bed (Craik, 1988). Stokes drift is actually Stokes drift velocity, however it is commonly referred to as Stokes drift.

## 5.2 Estimation technique

The estimation of Stokes drift involves the use of a directional wave spectrum. There are various types of wave spectra, a commonly used one is the monochromatic spectrum (Webb & Fox-Kemper, 2011; Hoang, 2012). This spectrum is composed of one frequency and one wavenumber. For the computation of Stokes drift, either the wave spectrum is used directly through software or parameters from the wave spectrum are used. In this study the parameters have been provided. Stokes drift for a monochromatic wave for arbitrary depth can be computed using,

$$\vec{U}_s = \frac{a^2 \omega k \cosh[2k(z+h)]}{\sinh^2(kh)} \hat{\mathbf{e}}^{\mathrm{w}}, \tag{5.2.1}$$

where $a$ is wave amplitude, $\omega$ is angular wave frequency, $k$ is wavenumber, $\hat{\mathbf{e}}^{\mathrm{w}}$ is a unit vector in the direction of wave propagation, $z$ is depth from the surface and $h$ is the average water level (Teixeira, 2012; Monismith & Fong, 2004). The angular wave frequency and the wavenumber are related through the dispersion relationship,

$$\omega^2 = gk \tanh(kh). \tag{5.2.2}$$

## 5.3 Data

The wave data that was collected for this study was measured every 60 minutes. It comprises significant wave heights ($H_s$) in meters, peak wave period ($T_p$) and mean period ($T_{mean}$) in seconds, mean wave directions ($D_{mean}$) and peak wave direction ($D_p$) in degrees as well as water level measurements in metres. The directions are given as incoming wave directions, these are the directions in which waves are provided as the directions from which the waves approach.

Figures 5.1 to 5.6 show the measured significant wave heights ($H_s$) and incoming peak wave directions ($D_p$) for periods one to six.

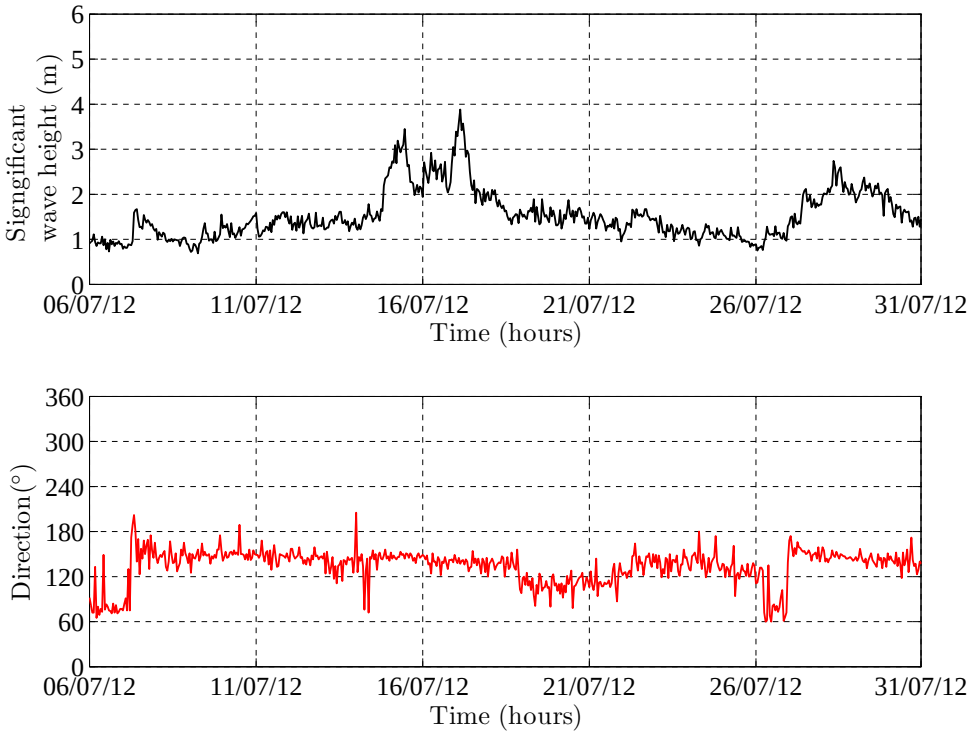


**Figure 5.1:** Significant wave height (top panel) and peak wave directions (bottom panel) during period 1.

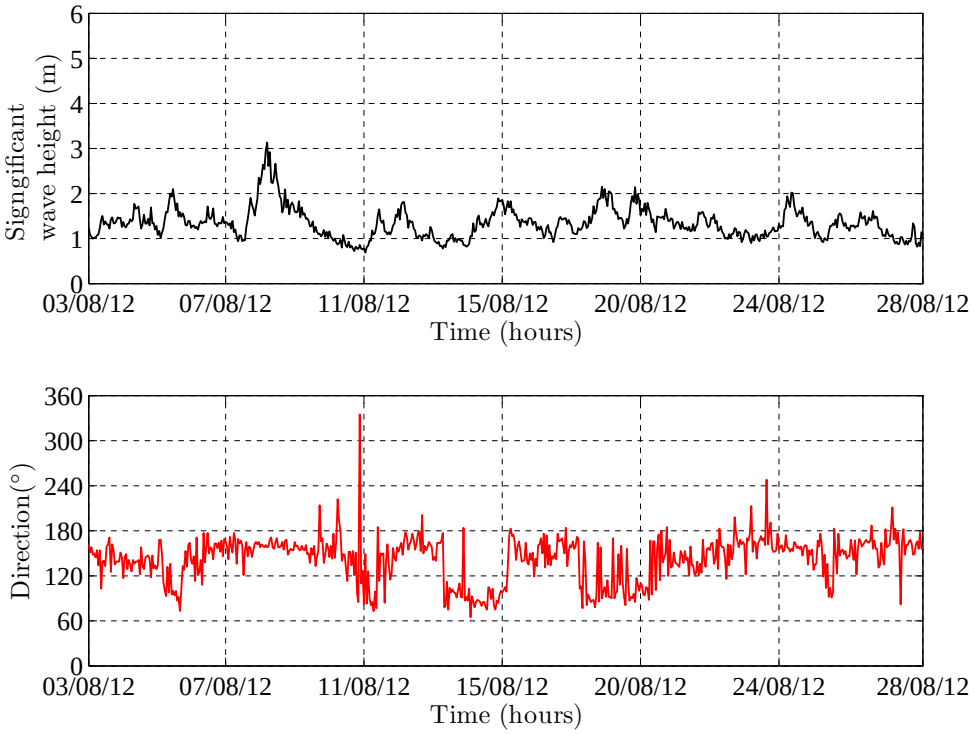


**Figure 5.2:** Significant wave height (top panel) and peak wave directions (bottom panel) during period 2.

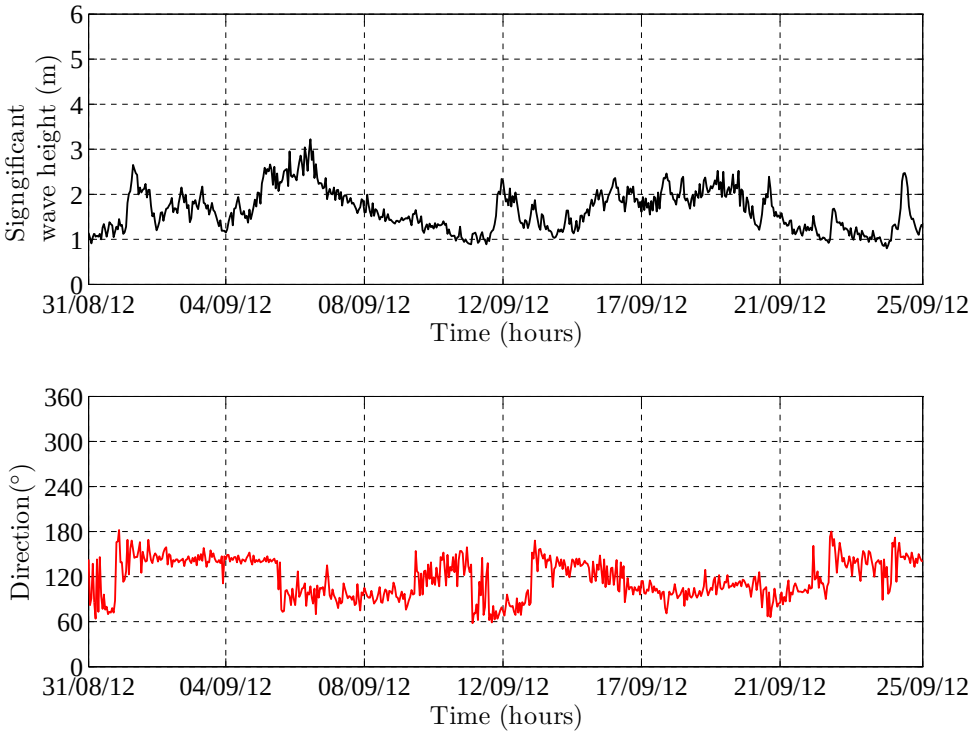


**Figure 5.3:** Significant wave height (top panel) and peak wave directions (bottom panel) during period 3.

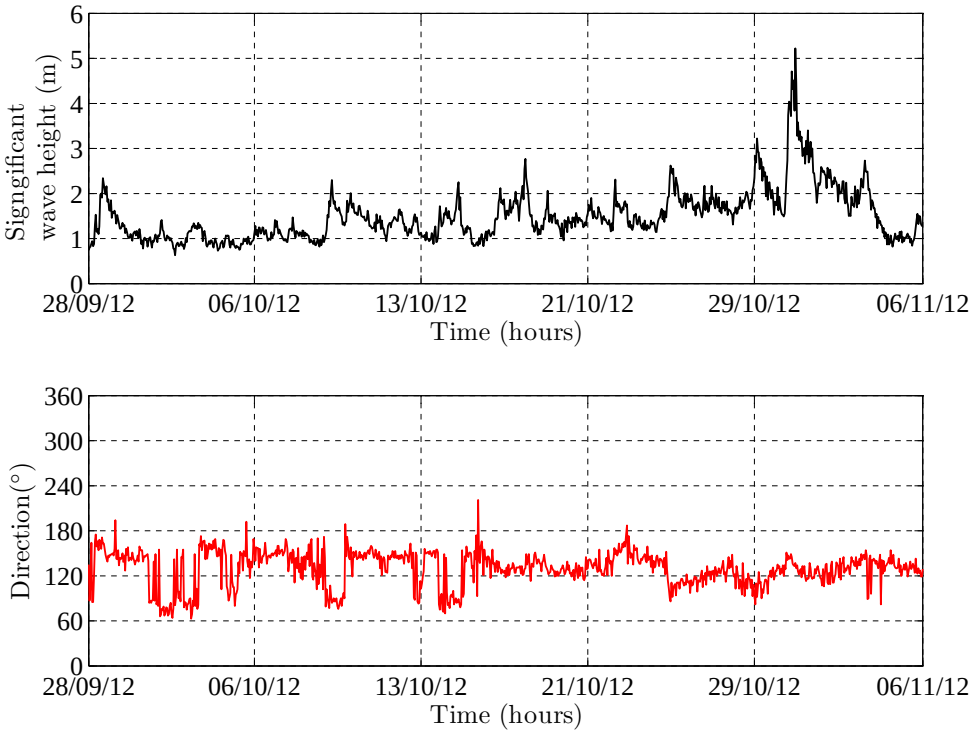


**Figure 5.4:** Significant wave height (top panel) and peak wave directions (bottom panel) during period 4.

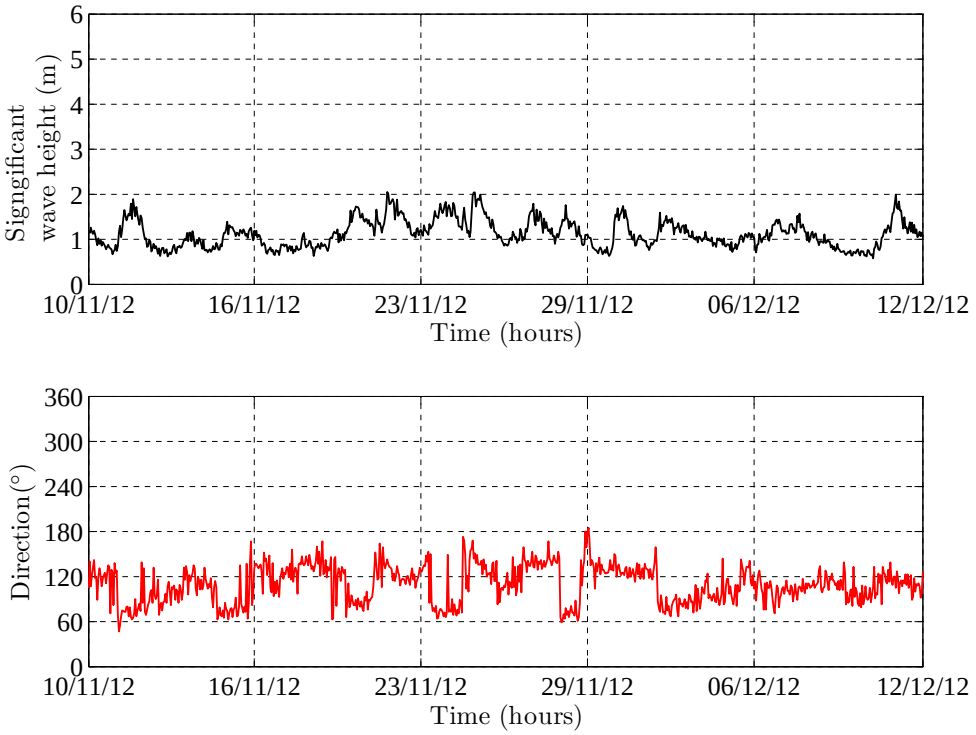


**Figure 5.5:** Significant wave height (top panel) and peak wave directions (bottom panel) during period 5.

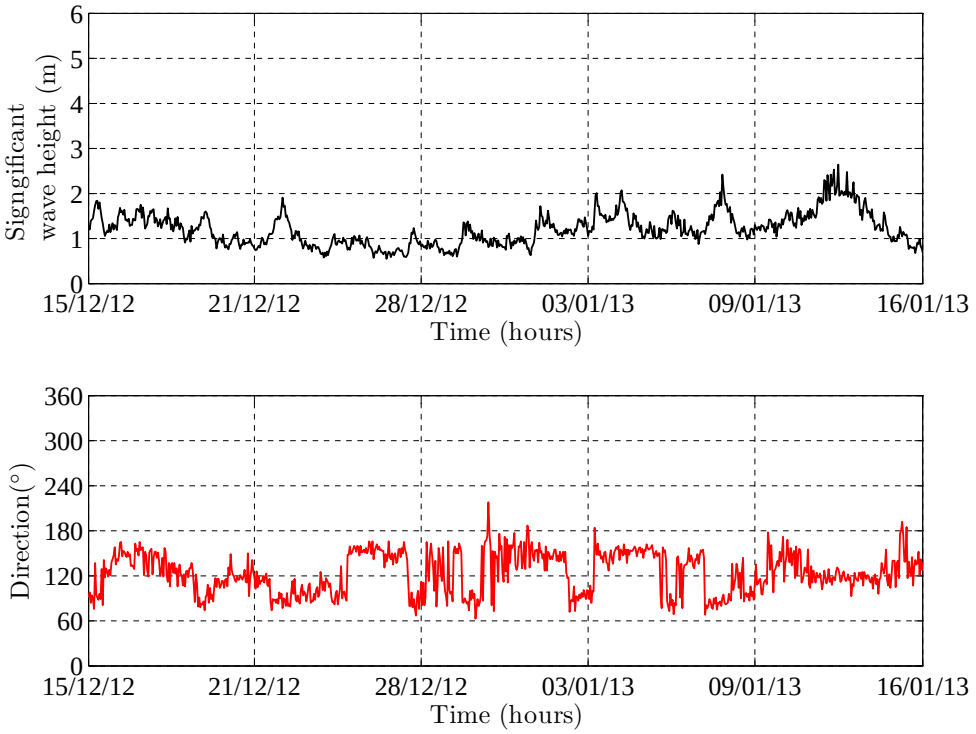


**Figure 5.6:** Significant wave height (top panel) and peak wave directions (bottom panel) during period 6.

Period 1 has two events of high significant wave heights, one from 15 July to 18 July 2012, ($< 4$ m) and between 26th July to 28th July 2012 ($< 3$ m), these can be seen in Figure 5.1. In this period waves mostly come from the south-eastern direction followed by the eastern direction. The average significant wave height is 1.53 m. Most of the measurements are between 1 m and 2 m (70.8%) with a maximum significant wave height of 3.88 m from the south-eastern direction. These measurements were taken during the winter season.

Figure 5.2 shows significant wave heights and directions for period 2, which is also a winter period. This period has one event of high significant wave heights from the 8th August to 9th August 2012 (just above 3 m). Mostly, waves come from the south-east, followed by the southern direction and then from the east. Most of the measurements are between 1 m and 2 m (85.9%). The average significant wave height is 1.34 m and the maximum one is 3.13 m and comes from the southern direction.

Period 3, which is in the beginning of Spring, has one period of high significant wave heights between 6th September to 9th September 2012 (just above 3 m). This event can be seen in Figure 5.3. Most of the measurements are between 1 m and 2 m (70.5%). Waves equally came from the south eastern and eastern direction and they seldom came from the southern direction. The average significant wave height is 1.65 m and maximum significant wave height is 3.22 m, which comes from the eastern direction.

During period 4 one event with the highest significant wave heights of all the periods occurs. This event started on the 31st October and ends on the 2nd November 2012, the highest significant wave height in this period exceeds 5 m (5.22 m). The wave measurements for this period are give in Figure 5.4. Most of the measurements are between 1 m and 2 m (73.0%) and the average significant wave height is 1.50 m. Waves primarily come from the south-eastern direction, followed by eastern direction and then seldom came from the southern direction. This period is at the beginning of spring time.

Period 5 is characterised by low significant wave heights, shown in Figure 5.5. Significant wave heights during this period do not exceed 3 m. The maximum significant wave height is 2.05 and comes from the south-eastern direction and the average significant wave height is 1.13 m. The majority of the measurements lie between 1 m and 2 m (66.8%). The waves in this period mainly come from the eastern direction, followed by south-east. Occasionally, waves come from the southern direction.

Figure 5.6 show significant wave heights and incoming wave directions for period 6. Significant wave heights measurements during period 6 are similar

to those collected during period 5, the measurements in both periods do not exceed 3 m. This period is in the beginning of the summer season. The maximum significant wave height is 2.64 m and comes from the eastern direction, and the average is 1.21 m. Most of the significant wave height measurements are between 1 m and 2 m (69.0%). Waves come from south-east, followed by east and seldom come from the southern direction.

**Table 5.1:** Summary statistics of significant wave heights.

| Period | Min $H_s$ (m) | Max $H_s$ (m) | Mean $H_s$ (m) |
|---|---|---|---|
| 1 | 0.69 | 3.88 | 1.53 |
| 2 | 0.69 | 3.13 | 1.34 |
| 3 | 0.80 | 3.22 | 1.65 |
| 4 | 0.63 | 5.22 | 1.50 |
| 5 | 0.58 | 2.05 | 1.12 |
| 6 | 0.55 | 2.64 | 1.21 |

Table 5.1 presents some summary statistics of the wave data which have just been discussed.

### 5.3.1 Adjustment and filtering of data

For computational purposes incoming peak wave directions are converted to scientific notation through the relation,

$$\beta = \frac{3\pi}{2} - \theta \tag{5.3.1}$$

as shown in (Brown et al., 1996), where $\beta$ is the direction towards which waves are going and $\theta$ is the incoming wave direction.

Near surface current measurements (15.92 m away from ADCP) are converted from centimetres per second to metres per second and also sub-sampled to hourly values for comparison with wave data. The 20 minutes current records were filtered using a Cosine-Lanczos filter with 37 weights and a half-power point at 0.535 cycles per hour before sub-sampling to hourly values. The filtering was done to avoid aliasing that may result from direct sub-sampling. Aliasing occurs when high frequencies are masked as lower frequencies, distorting a signal (Price, 1985).

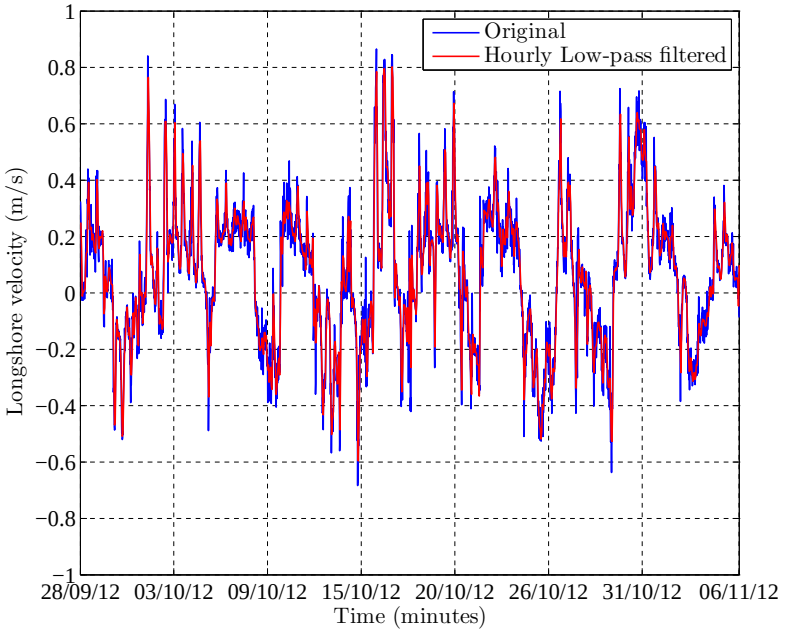


**Figure 5.7:** Graphs of original 20 minutes longshore current observations and sub-sampled, hourly observations.

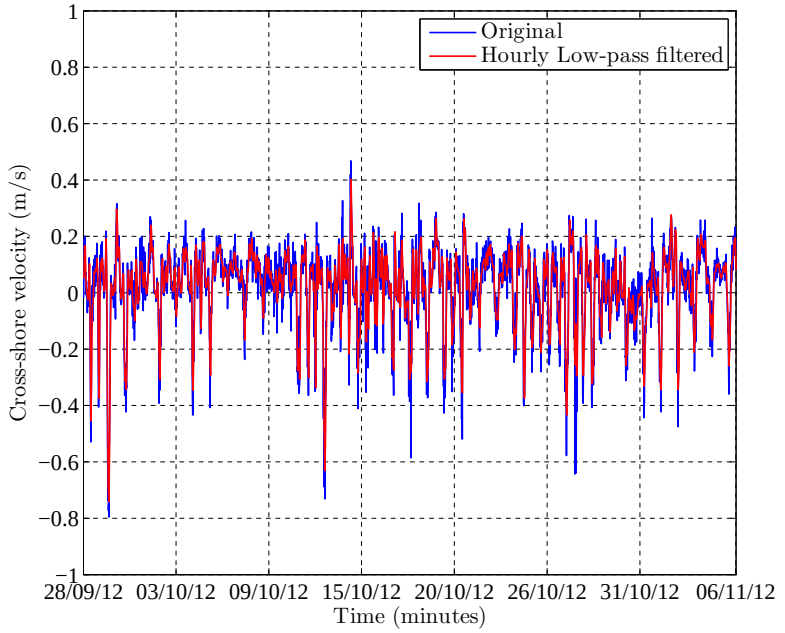


**Figure 5.8:** Graphs of the original 20 minutes cross-shore current observations and sub-sampled, hourly observations.

Figures 5.7 and 5.8 show graphs of 20 minutes current observation and sub-sampled, filtered hourly current observations, the sub-sampled series are noticeably smoother. The figures exhibit current observations from period 4, which was chosen for its extended length of 39 days.

## 5.4 Computation of Stokes drift

Stokes drift is computed using Equation 5.2.1 for the six periods in MATLAB using the converted wave directions ($\beta$), significant wave heights ($H_s$), angular wave frequency ($\omega$), wavenumber $k$, and average sea level $h = 16.42$ m. The wave amplitude, $a$, is substituted by measured significant wave height, where,

$$a = \frac{H_s}{2}.$$

The angular wave frequency, $\omega$, is computed from

$$\omega = 2\pi f_{p,}$$

where,

$$f_p = \frac{1}{T_p}.$$

The wavenumber $k$ is computed using Equation 5.2.2, through the use of Newton-Raphson method in MATLAB. In the end, equation 5.2.1 becomes,

$$\vec{U}_s = \frac{1}{2}\frac{H_s^2 \pi f_p k \cosh[2k(z+h)]}{\sinh^2(kh)}\hat{\mathbf{e}}^{\mathrm{w}}. \tag{5.4.1}$$

The Stokes drift components $\vec{U}_s$ computed here were computed as north-south and east west velocity components using $\sin(\beta)$ and $\cos(\beta)$, respectively, for $\hat{\mathbf{e}}^{\mathrm{w}}$. These components are resolved into longshore and cross-shore components using Equation 3.3.5 in Chapter 3.

### 5.4.1 Analysis and results

The average significant wave height ($H_s$) for the whole data collection period is 1.4 m, the average peak period ($T_p$) is 9.7 s, the average incoming peak wave direction ($D_{peak}$) is 127° which is south-east. These averages do not differ much from those calculated by Corbella & Stretch (2012) using 18 year long data. Those found by Corbella & Stretch (2012) are, $H_s = 1.65$ m, $T_p = 10$ s and $D_{peak} = 130°$. The slight differences in the averages may be explained by the short length of data used in this study.

Stokes drift estimations are computed at four depths, with $z = 0$ at the surface, $z = -0.5$ as 0.5 m away from the surface, $z = -7.5$ as 7.5 m from the surface

and $z = -14.0$ as 14 m from the surface. The Stokes drift estimations are provided in Figure 5.9 to 5.14. The figures show both the longshore and cross-shore components of Stokes drift for the six periods of data collection.

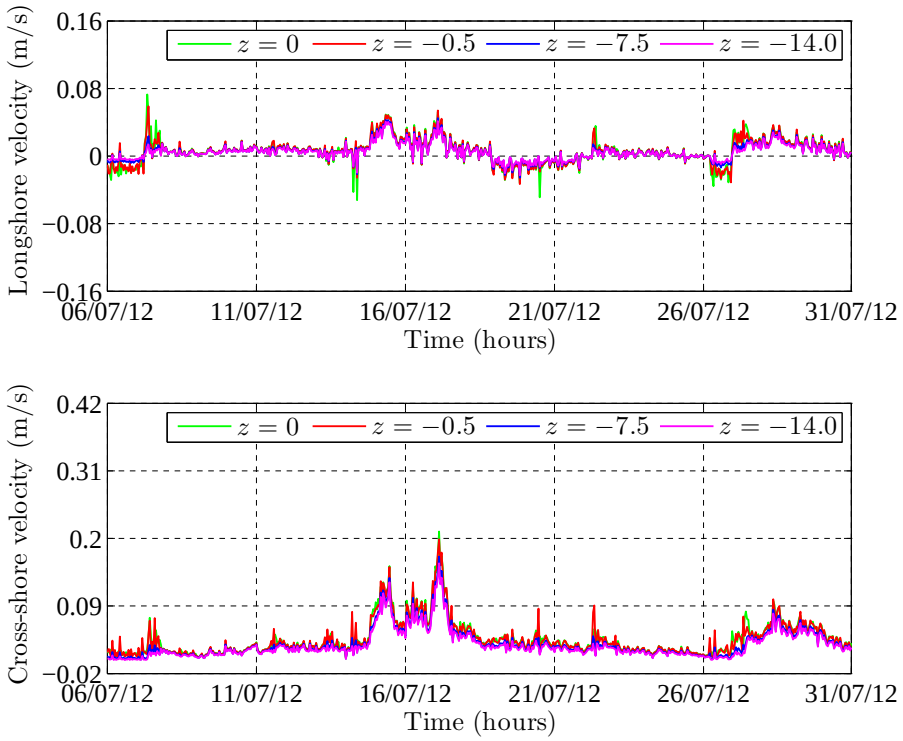


**Figure 5.9:** Longshore (top panel) and cross-shore (bottom panel) Stokes drift estimation for period 1.

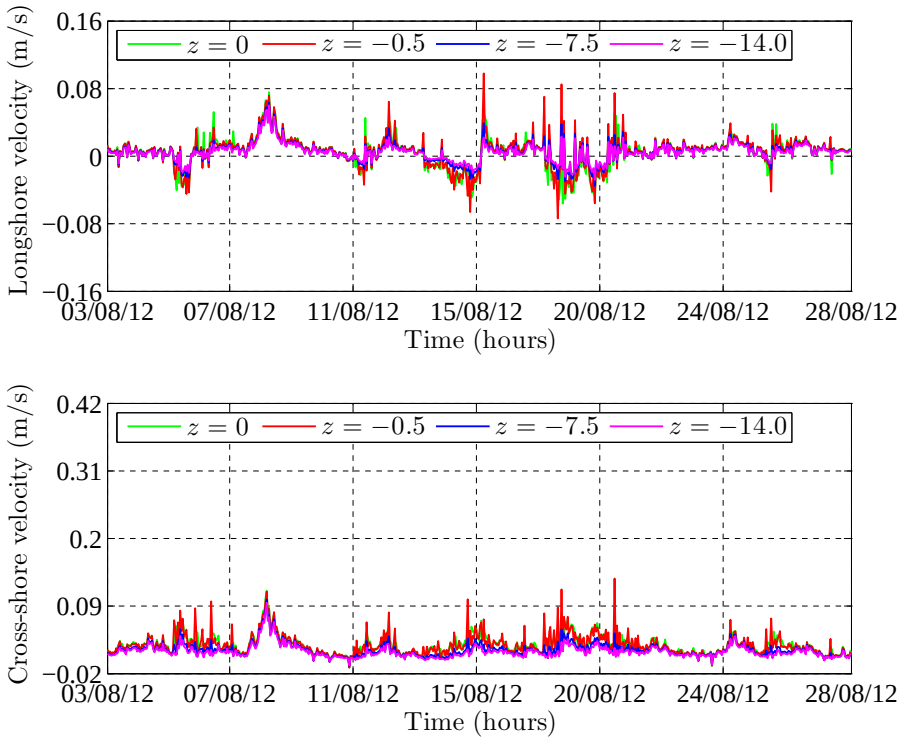


**Figure 5.10:** Longshore (top panel) and cross-shore (bottom panel) Stokes drift estimation for period 2.

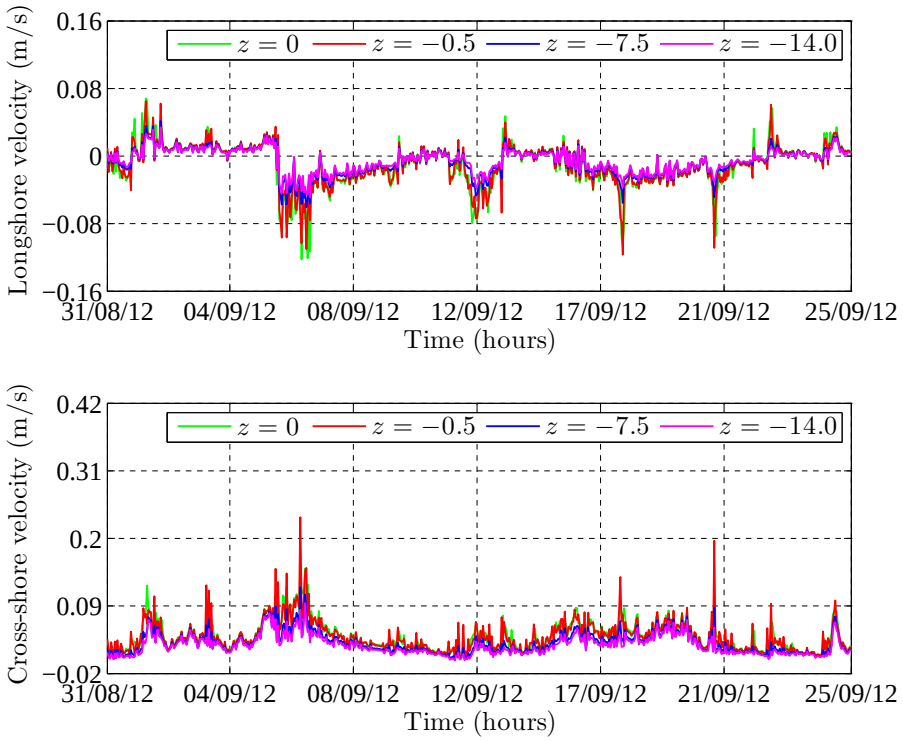


**Figure 5.11:** Longshore (top panel) and cross-shore (bottom panel) Stokes drift estimation for period 3.

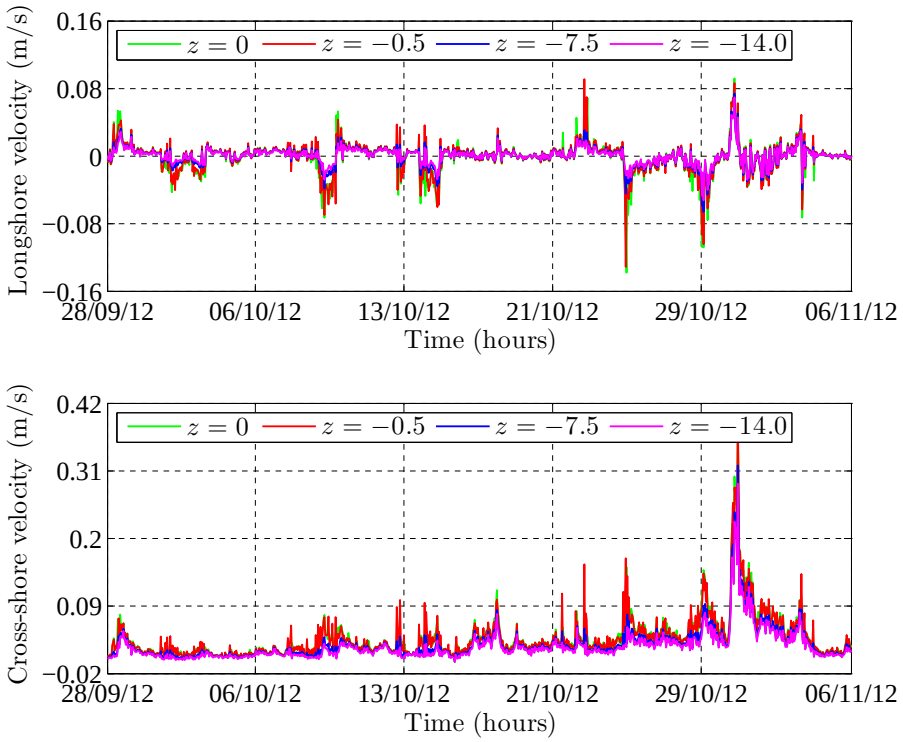


**Figure 5.12:** Longshore (top panel) and cross-shore (bottom panel) Stokes drift estimation for period 4.

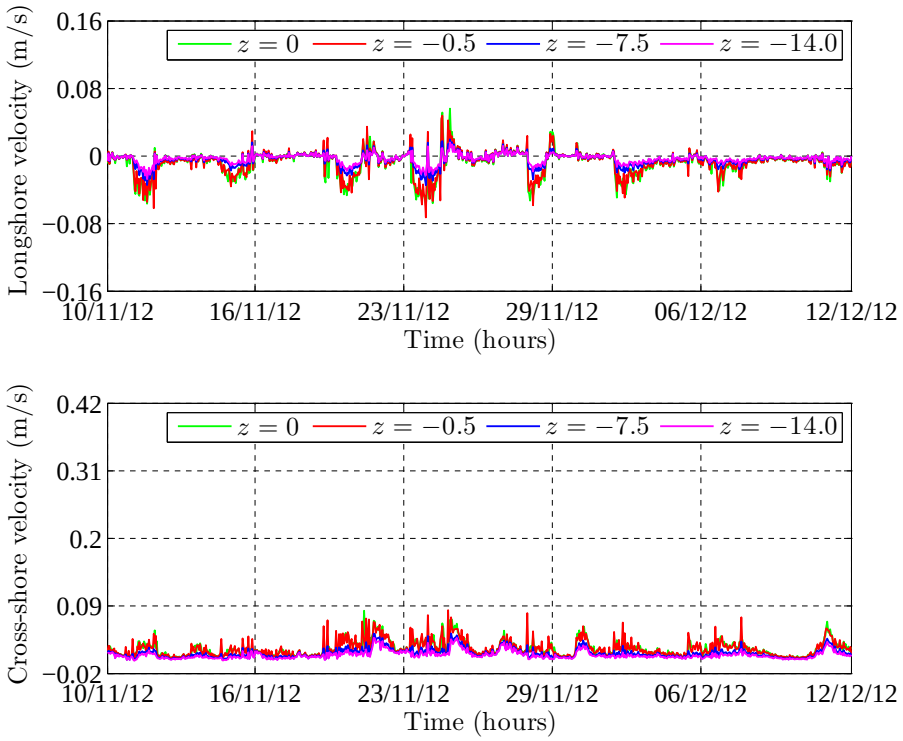


**Figure 5.13:** Longshore (top panel) and cross-shore (bottom panel) Stokes drift estimation for period 5.

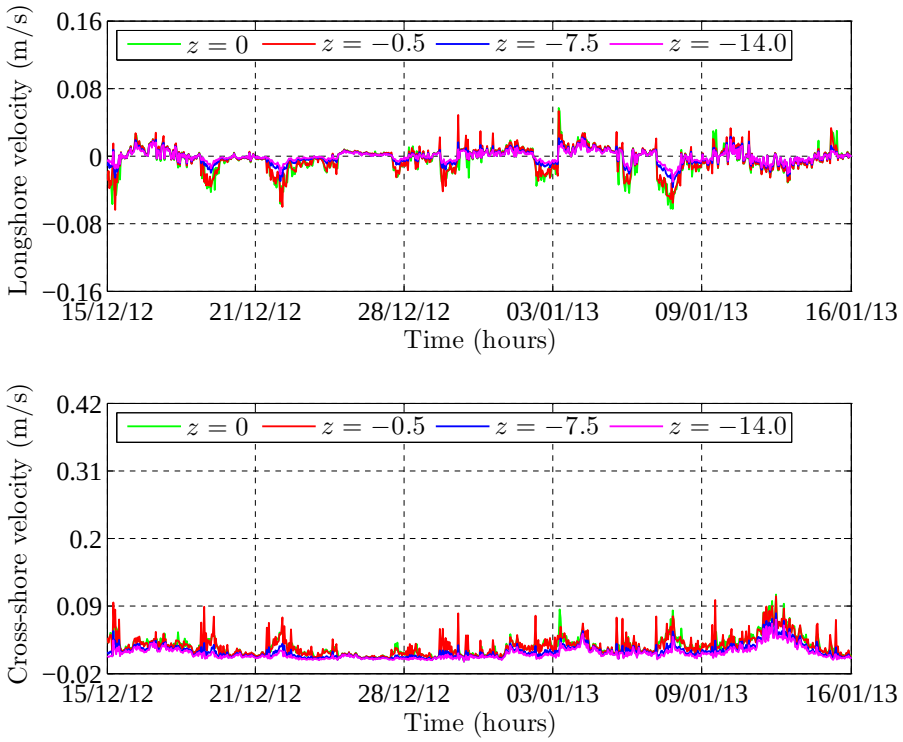


**Figure 5.14:** Longshore (top panel) and cross-shore (bottom panel) Stokes drift estimation for period 6.

Longshore components indicate movement in both directions along the coast. On the other hand, cross-shore components are primarily unidirectional, going towards the coast. This is in the exception of period 2, which also has motion away in an offshore direction. Stokes drift tends to be higher in the cross-shore velocity components as opposed to the longshore components. The highest Stokes drift velocities are observed during period 4, with maximum cross-shore velocity component being 0.38 m/s shore-wards while maximum longshore velocity component is -0.14 m/s. This is also the period with the highest significant wave heights. The Stokes drift estimations at the surface and 1/2 m from the surface, are noticeably higher compared to the estimations at $7\frac{1}{2}$ m and 14 m away from ADCP.

For period 1, 2 and 3, maximum longshore velocity components are 0.07 m/s, 0.08 m/s and -0.12 m/s respectively while maximum cross-shore velocity components are 0.21 m/s, 0.11 m/s and 0.15 m/s towards the shore, respectively. Both period 5 and 6 have Stokes drift velocity components which hardly exceed 0.1 m/s in magnitude. The maximum longshore velocity component is -0.06 m/s for both periods, the maximum cross-shore velocity components are 0.082 m/s and 0.11 m/s towards the shore. These make the cross-shore Stokes drift components in these periods, the lowest of all six periods.

Figures 5.15 to 5.20 show de-tided near surface (15.92 m away from ADCP) longshore and cross-shore velocity components compared with residual velocity components after the removal of surface Stokes drift. Surface Stokes drift correspond to $z = 0$. The figures indicate that Stokes drift causes a small change in the currents, especially in the longshore velocity components.

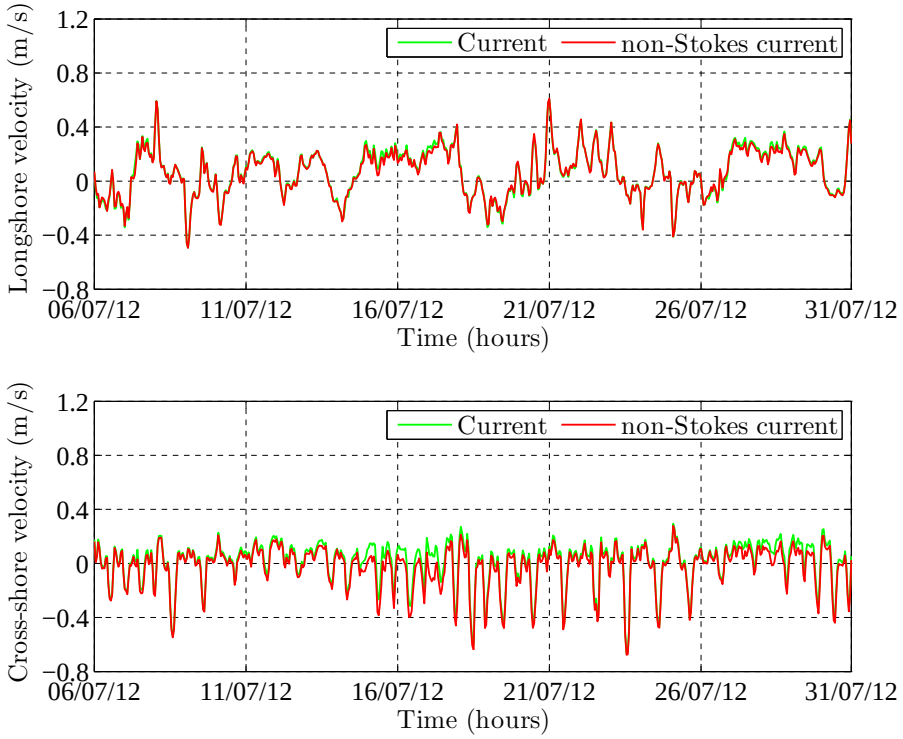


**Figure 5.15:** Longshore (top panel) and cross-shore component (bottom panel) of de-tided current and non-Stokes residual current during period 1.

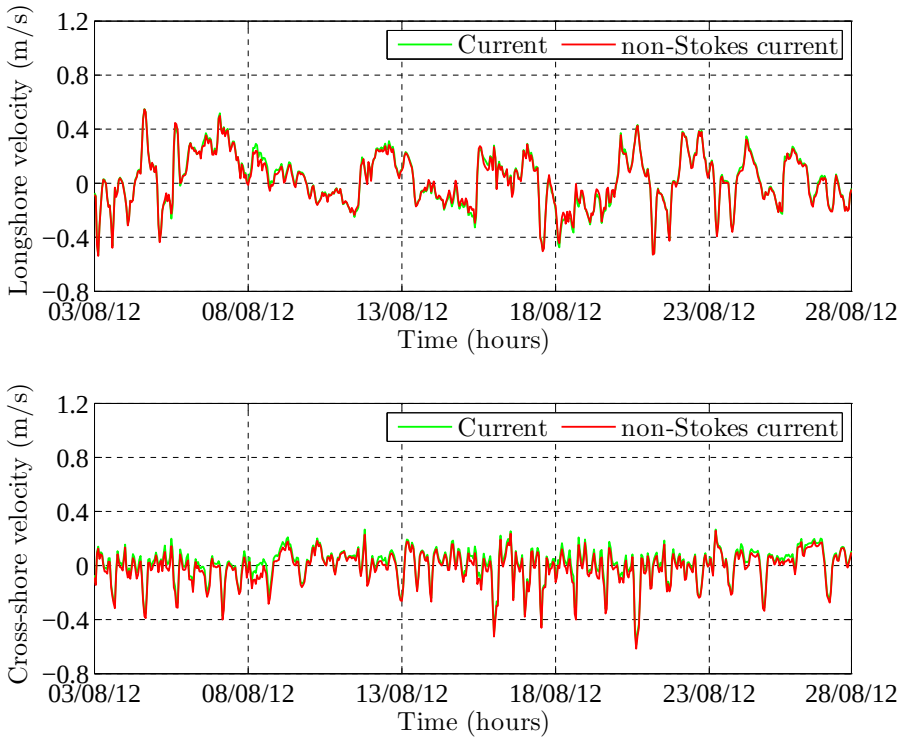


**Figure 5.16:** Longshore (top panel) and cross-shore component (bottom panel) of de-tided current and non-Stokes residual current during period 2.

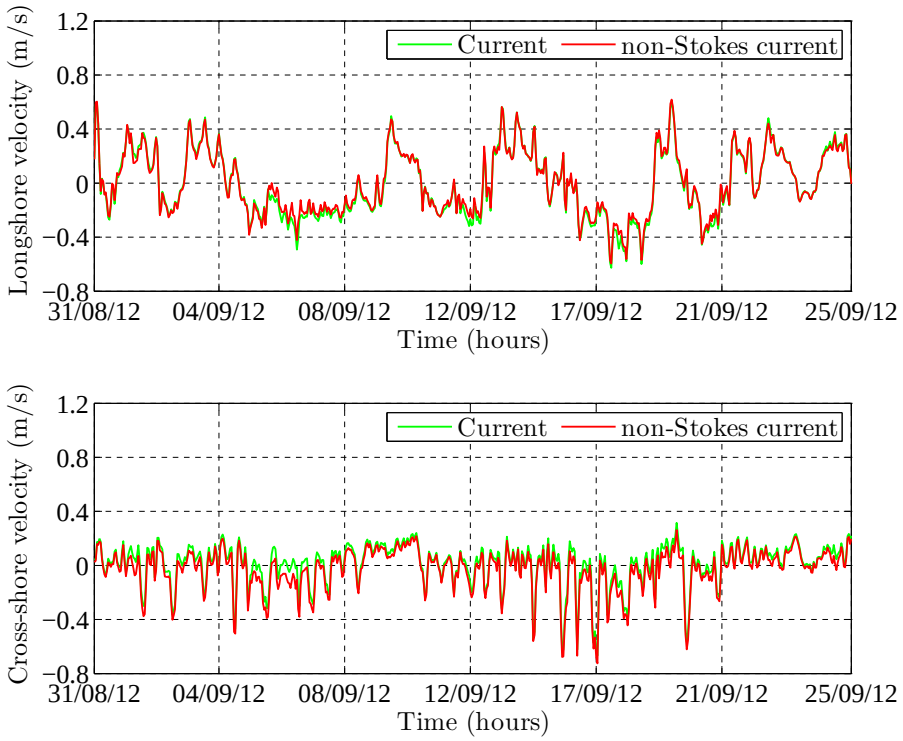


**Figure 5.17:** Longshore (top panel) and cross-shore component (bottom panel) of de-tided current and non-Stokes residual current during period 3.

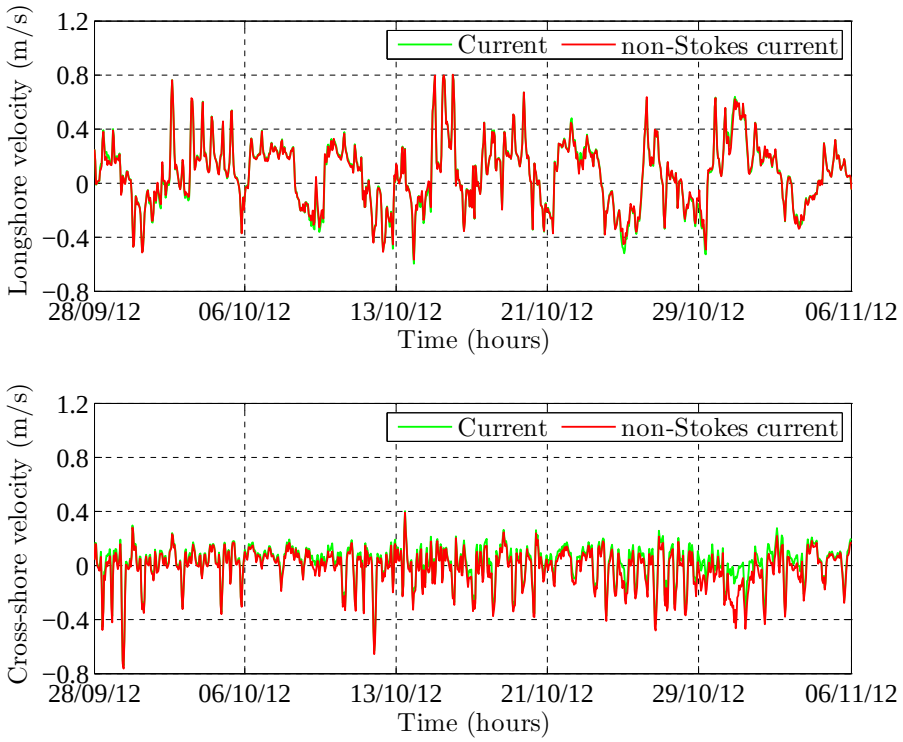


**Figure 5.18:** Longshore (top panel) and cross-shore component (bottom panel) of de-tided current and non-Stokes residual current during period 4.

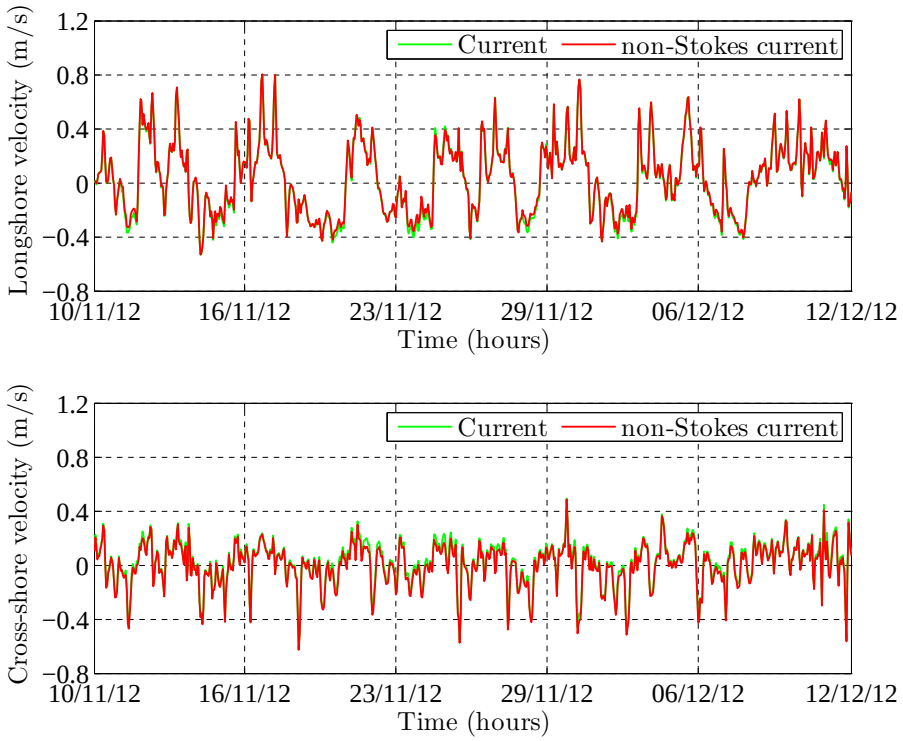


**Figure 5.19:** Longshore (top panel) and cross-shore component (bottom panel) of de-tided current and non-Stokes residual current during period 5.

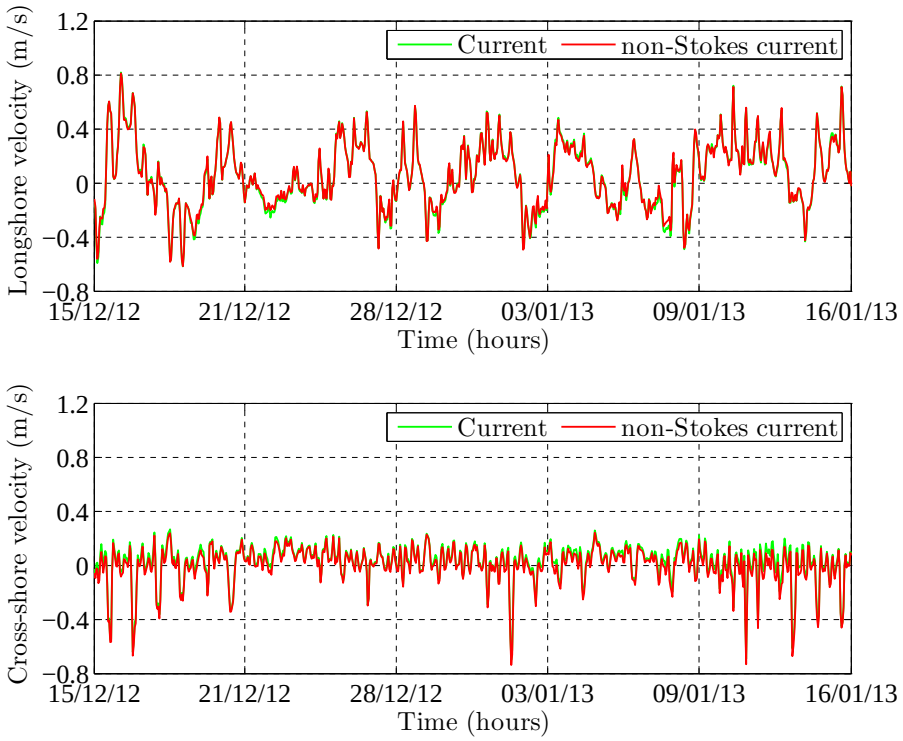


**Figure 5.20:** Longshore (top panel) and cross-shore component (bottom panel) of de-tided current and non-Stokes residual current during period 6.

These finding are confirmed by Table 5.2 which shows the variance in the de-tided velocity components and those in residual components. The contribution to variances by Stokes drift are higher in the cross-shore components while lower in the longshore components. The maximum contribution of Stokes drift to the variance is 6.70% in the cross-shore components and 1.04% in the longshore components. The percentage contribution of Stokes drift towards the near surface currents is less than that of tides discussed in Chapter 4.

**Table 5.2:** Variances of de-tided near surface currents and those of residual currents after the removal of Stokes drift.

| **Variance** | | | |
|---|---|---|---|
| Longshore $(m/s)^2$ | | Cross-shore $(m/s)^2$ | |
| Original | **Non-Stokes** | Original | **Non-Stokes** |
| 0.0252(0.71%) | **0.0251** | 0.0307(3.13%) | **0.0287** |
| 0.0153(0.87%) | **0.0156** | 0.0387(1.41%) | **0.0361** |
| 0.0239(1.04%) | **0.0255** | 0.0604(2.19%) | **0.0546** |
| 0.0184(0.59%) | **0.0207** | 0.0598(6.70%) | **0.0569** |
| 0.0248(0.30%) | **0.0248** | 0.0704 (0.58%) | **0.0671** |
| 0.0184(0.38%) | **0.0190** | 0.0598 (1.26%) | **0.0567** |

Stokes drift is of minimal importance in this study as the period during which data was collected is not characterised by large wave events. The season of possible large wave events is autumn in the Durban area and the data being studied was collected during late winter, spring and early summer (Corbella & Stretch, 2012). The minimal contribution of Stokes drift to the overall current is in line with the findings from a study that was conducted by Godin (1948) in Canadian coastal waters, where he concluded that Stokes drift is of below secondary importance in coastal waters, in the exception of coastal waters that are characterised by high amplitude waves or fast currents.

## 5.5 Summary

This chapter investigated the effect of Stokes drift on near surface currents. Stokes drift at a point is defined as the net motion of a fluid particle, generally, in the direction of wave propagation. The estimation of Stokes drift included the use of significant wave heights, peak periods and incoming wave directions. The average significant wave height for the whole data collection period is 1.4 m, the average peak period is 9.7 s, the average incoming peak wave direction is 127° which is south-east.

Stokes drift velocities never exceed 0.38 m/s towards the shore in cross-shore velocity components at the surface and 0.14 m/s in longshore components. This maximum velocity is observed in period 4, during which Stokes drift does contribute significantly. This is due to the fact that the mean surface current recorded was 25.36 cm/s and the maximum surface current recorded was 112.4 cm/s for period 4. These velocities occurred in period 4. For period 1, 2 and 3, longshore Stokes drift velocity components hardly exceed 0.1 m/s while cross-shore components do not exceed 0.21 m/s. Period 4 has the highest Stokes drift contribution and the highest significant wave heights. Period 5 and 6 have both Stokes drift velocity components hardly exceeding 0.1 m/s. These are thus the periods with the lowest Stokes drift components.

The contribution of Stokes drift towards currents is minimal. Tidal contribution towards variance never exceeds 6.70% and this value is for cross-shore velocity components. In the longshore direction the contribution is much less, the maximum tidal contribution to variance being 1.04%. Stokes drift has a larger impact in the direction towards the shore as opposed to along the shore. The contribution of Stokes drift towards the generation of surface currents is less than that of tides.

# Chapter 6

# The effect of wind on currents

## 6.1 Introduction

Surface currents and circulations of the ocean are to an extent determined by the wind. The currents tend to move in the general direction of the wind. Near-shore currents on the east coast of South Africa are known to be driven by the wind and the Agulhas current. This chapter addresses the effect of local wind speed, duration and direction on nearshore surface currents. The analysis is done only for the surface current as currents below 2 to 3 meters from the surface are not dependent on local wind conditions (Funke & Stretch, 2002). The current considered in this chapter is indicated by $u_w$ in Equation (1.2.1).

This chapter will address questions which include:

- To what extent does the wind affect surface currents?
- How long does it take for currents to respond to the wind?
- What is the dominant direction of the wind, and what is its relationship with the current?

### 6.1.1 Background on the effect of wind on nearshore currents

Wind generates a continuous motion of the surface layer of water in the general direction that it is blowing towards. This movement is communicated to layers that are beneath the surface by internal shear stress. This stress acts parallel to the plane along which the stress is being imposed. As the water starts moving the Coriolis acceleration also starts influencing it. The Coriolis acceleration is the seeming deflection of a body that is in a state of motion relative to the earth, as perceived by an observer on the earth, due to the Coriolis force. The force is brought on by the earth's rotation. The deflection

is to the left in the Southern hemisphere (Bowden, 1983).

Overall, wind results in a propagation of surface water elevations that that are superimposed on currents and tides. The surface elevations that are set in motion by the wind differ in speed, direction, depth and are also different from one position to the next. The wind induced currents move in approximately the same direction as the wind at an approximate speed of 3% of the wind speed. This applies to wind speed that have been measured 10 m above the mean sea surface (Bowden, 1983; Schwartz, 2006).

## 6.2 Methodology

Wind data was obtained for the same period as the currents from the port of Durban. The wind data includes wind speeds and directions at 20 minute intervals. There are occurrences of missing records in the wind data. Table 6.1 provides a summary of the periods of continuous records.

**Table 6.1:** Periods of continuous wind records.

| Order | Start | End | Duration |
|---|---|---|---|
| 1 | 2012/07/06 10:20:00 | 2012/07/29 19:40:00 | 23 days, 9 hours & 20 minutes |
| | 2012/07/30 16:00:00 | 2012/07/31 08:40:00 | 16 hours & 40 minutes |
| 2 | 2012/08/03 08:00:00 | 2012/08/28 11:00:00 | 25 days, 3 hours & 20 minutes |
| 3 | 2012/08/31 08:00:00 | 2012/09/25 11:00:00 | 25 days & 3 hours |
| 4 | 2012/09/28 09:40:00 | 2012/09/29 21:40:00 | 1 day & 12 hours |
| | 2012/10/01 00:00:00 | 2012/10/15 03:00:00 | 14 days & 3 hours |
| | 2012/10/24 11:40:00 | 2012/11/06 11:00:00 | 12 days, 23 hours & 20 minutes |
| 5 | 2012/11/10 08:40:00 | 2012/12/12 12:00:00 | 32 days, 3 hours & 20 minutes |
| 6 | 2012/12/15 07:20:00 | 2013/01/16 10:00:00 | 32 days, 2 hours & 40 minutes |

The periods one to six correspond with the study periods of available current records in Chapter 3. The wind speed is measured in m/s and the directions are in degrees. North is at 0° and wind measurements follow a clock-wise direction. By convention currents are provided with the direction, which they are flowing towards, while winds are described using the direction they are blowing from.

The length of period four for currents is approximately 39 days. There are approximately 12 days missing in the wind records for the period and the 1, 14 and 12 days available with gaps in between them are too short for any deductive analysis. Period four wind records are thus not included in the analysis.

Wind speed was measured at a height of 80 m above sea level. For correct computations, the wind power law is used to adjust the wind measurement from 80 m to 10 m above sea level. The wind power law is given by

$$\frac{u}{u_r} = \left(\frac{z}{z_r}\right)^{\alpha} \tag{6.2.1}$$

where $u_r$ is the given measured velocity at a given height, $z_r$, and $u$ is the unknown velocity at the new reference height $z$ (Emeis & Türk, 2007). Other wind profile laws, such as the logarithmic wind law, are available for use. However, the wind power law is chosen here for its mathematical simplicity and the fact that it gives acceptably accurate adjustments (Hsua et al., 1994). The standard power used in this calculation is

$$\alpha = \frac{1}{7},$$

referred to as the $\frac{1}{7}$th wind power law and is given by,

$$\frac{u}{u_r} = \left(\frac{z}{z_r}\right)^{\frac{1}{7}}. \tag{6.2.2}$$

Wind measurements are provided as $N$ pairs of observations, $(V_i, \phi_i)$ where $i = 1, 2, ..., N$, and $V_i$ is wind speed while $\phi_i$ is direction. The wind measurements are resolved into north-south and east-west velocity components as follows:

$$\begin{aligned} u_i &= V_i \sin(\phi_i - 180) \\ v_i &= V_i \cos(\phi_i - 180) \end{aligned} \tag{6.2.3}$$

where $u_i$ is the east-west component and $v_i$ is the north-south component (Longhurst & Brebbia, 2014). The components were resolved into longshore and cross-shore velocity components using Equations (3.3.5) in Chapter 3. This mathematical convention is only used in progressive vector diagrams, lagged correlation analysis and power spectral analysis.

The methodology is hereby illustrated by a detailed analysis of wind and current measurements during period five, the data in period five is chosen because the wind data is the same length as the current data without any missing records.

### 6.2.1 Analysis of direction, speed and duration

Joint analysis of direction, speed and duration of the wind and current measurements are carried out. Only the top-most layer of detided current measurements is used (15.92 m away from the ADCP). Stokes drift has not been removed from the currents as it effects to the generation of currents is negligible. The first part of the analysis is done by the use of current and wind roses. The wind roses and current roses are produced using WRPLOT View, a product of Thé et al. (2011).

#### Wind rose and current rose analysis

A wind rose provides a brief yet informative summary of the distribution of wind speed and direction at a given location. It gives a circular presentation of the frequencies of winds blowing from various directions. How long each "spoke" is, gives the frequency that wind comes from a particular direction. Every one of the concentric circles of the wind rose gives a representation of a different frequency, the frequencies blow from the centre, zero, and increase towards the outer circles. Every one of the spokes is split down into different categoric frequencies showing duration percentages that winds come from varying directions in particular speed ranges. The wind roses in this study are constructed with 16 cardinal directions. A wind rose and current rose for period five are provided in Figure 6.1

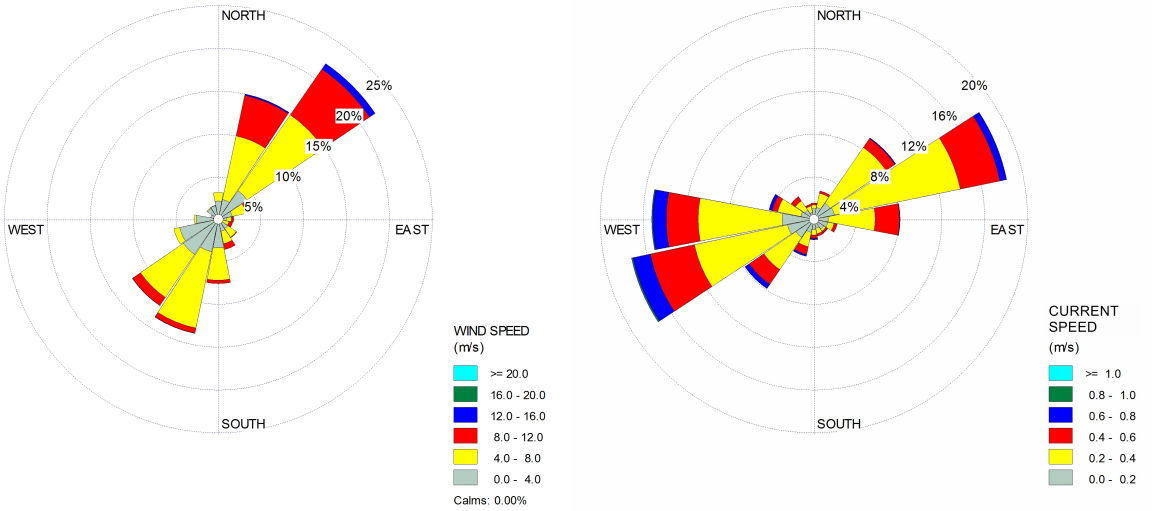


**(a)** Wind rose **(b)** Current rose

**Figure 6.1:** Wind rose and current rose for period five.

The wind rose in Figure 6.1 shows that the wind predominantly blows from a north-easterly direction followed by a south-westerly direction. The modal wind speed is in the 4-8 m/s range. The current rose shows the predominant direction of flow for the current to be south-west followed by north-east direction. The modal current speed is in the 0.2-0.4 m/s range. From these wind rose and current rose, the due directions of the wind and flow directions of the currents appear, suggesting a possible connection between the wind and current.

### Frequency distribution analysis

Frequency distribution analysis of both currents and winds are carried out from wind rose results. This is to determine the average duration that the wind blows from a particular direction as well as the average duration that the current flows towards a particular direction. If the analysis brings out a common tendency for the two variables (wind and current) this would imply an interdependency of the two variables (Funke & Stretch, 2002).

The daily average wind durations are computed from frequency distribution tables by multiplying each of the frequency distribution percentages by 24 hours. Two tables, one for wind frequency distribution and another for current frequency distribution that were produced by WRPLOT are presented in Table 6.2 and 6.3. These tables were used to compute the daily average wind durations in Table 6.4 and 6.5, by multiplying each of the values in the tables with 24 hours. This technique of duration analysis does not take into account the persistence of the wind or currents, i.e, whether the wind blows from one direction continuously or changes direction frequently into the same direction is not considered. However it does give an impression of the common direction.

**Table 6.2:** Wind frequency distribution for period five.

| Speed (m/s) | NNE (h) | ENE (h) | ESE (h) | SSE (h) | SSW (h) | WSW (h) | WNW (h) | NNW (h) |
|---|---|---|---|---|---|---|---|---|
| 0.01-4.0 | 0.043 | 0.065 | 0.019 | 0.022 | 0.065 | 0.091 | 0.056 | 0.027 |
| 4.0-8.0 | 0.038 | 0.165 | 0.016 | 0.021 | 0.086 | 0.117 | 0.004 | 0.001 |
| 8.0-12.0 | 0.008 | 0.108 | 0.005 | 0.007 | 0.009 | 0.016 | | |
| $\geq$ 12.0 | 0.001 | 0.010 | | | | 0.001 | | |

**Table 6.3:** Current frequency distribution for period five.

| Speed (m/s) | NNE (h) | ENE (h) | ESE (h) | SSE (h) | SSW (h) | WSW (h) | WNW (h) | NNW (h) |
|---|---|---|---|---|---|---|---|---|
| 0.00-0.2 | 0.022 | 0.035 | 0.030 | 0.022 | 0.021 | 0.040 | 0.049 | 0.022 |
| 0.2-0.4 | 0.011 | 0.124 | 0.115 | 0.007 | 0.012 | 0.080 | 0.144 | 0.024 |
| 0.4-0.6 | 0.004 | 0.024 | 0.050 | 0.003 | 0.009 | 0.043 | 0.052 | 0.008 |
| 0.6-0.8 | | 0.005 | 0.003 | | 0.002 | 0.011 | 0.027 | |
| $\geq$ 0.8 | | | | | | | 0.002 | |

**Table 6.4:** Daily average wind duration for period five.

| Speed (m/s) | NNE (h) | ENE (h) | ESE (h) | SSE (h) | SSW (h) | WSW (h) | WNW (h) | NNW (h) |
|---|---|---|---|---|---|---|---|---|
| 0.5-4.0 | 1.04 | 1.56 | 0.46 | 0.52 | 1.57 | 2.19 | 1.35 | 0.64 |
| 4.0-8.0 | 0.92 | 3.96 | 0.38 | 0.50 | 2.07 | 2.81 | 0.10 | 0.02 |
| 8.0-12.0 | 0.20 | 2.58 | 0.11 | 0.17 | 0.21 | 0.37 | | |
| $\geq$ 12.0 | 0.02 | 0.24 | | | | 0.02 | | |

**Table 6.5:** Daily average current duration for period five.

| Speed (m/s) | NNE (h) | ENE (h) | ESE (h) | SSE (h) | SSW (h) | WSW (h) | WNW (h) | NNW (h) |
|---|---|---|---|---|---|---|---|---|
| 0.00-0.2 | 0.53 | 0.85 | 0.71 | 0.53 | 0.50 | 0.96 | 1.18 | 0.52 |
| 0.2-0.4 | 0.27 | 2.97 | 2.76 | 0.16 | 0.28 | 1.93 | 3.45 | 0.57 |
| 0.4-0.6 | 0.09 | 0.58 | 1.19 | 0.06 | 0.22 | 1.03 | 1.24 | 0.19 |
| 0.6-0.8 | | 0.12 | 0.07 | 0.01 | 0.04 | 0.26 | 0.65 | 0.01 |
| $\geq$ 0.8 | | | | | | 0.01 | 0.04 | |

The longest average span for the wind was 4.0 hours in the ENE segment. This was for wind speed in the 4-8 m/s range. For the surface current the longest average duration is 3.5 hours in the WNW segment for speeds in the 0.2-0.4 m/s range. There is no direct link between the direction of flow of the currents and that of the winds. The next long average period that the wind blew was 2.8 hours from the WSW direction, this can also be assumed to be due ENE. The currents flowed towards ENE for an average duration of 3.0 hours. The speed ranges from 0.2 to 0.4 m/s. The duration periods have a 0.2 hour difference, a slight difference which demonstrates that wind-driven currents have reasonable response times to changes in wind conditions.

### 6.2.2 Progressive vector diagram analysis

The wind is also analysed using a progressive vector diagram (PVD). Each PVD is built by progressively combining estimations of $u_i$ (east-west) velocity, and $v_i$ (north-south) velocity components of currents or winds. The PVDs begin at (0,0). The wind progressive vector diagrams describe wind in the direction towards which it is going. A detailed description of a PVD is given in Section 3.4 in Chapter 3. A PVD for wind is provided in Figure 6.2 and one for current is provided in Figure 6.3.

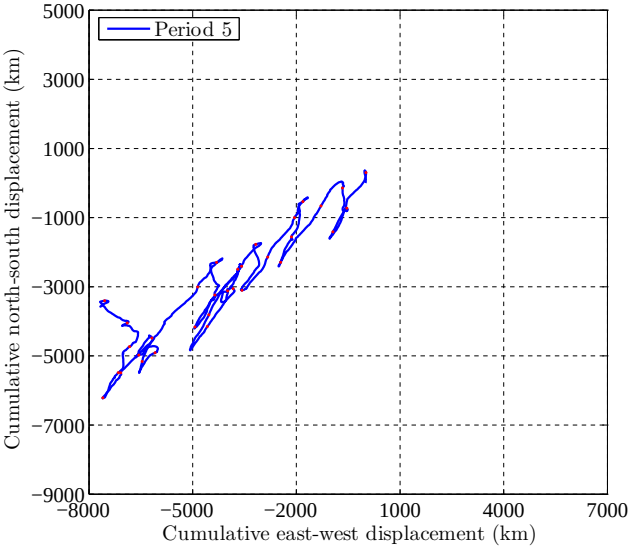


**Figure 6.2:** PVD of wind

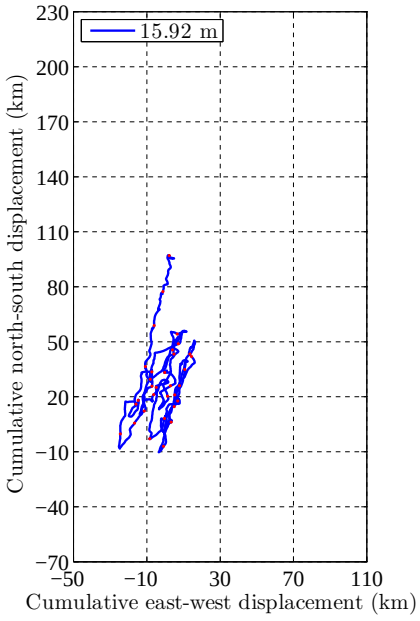


**Figure 6.3:** PVD of current

The wind follows a north-easterly direction. It changes direction in a pseudo-periodic manner. It blows from the north-easterly direction for some period, then it blows from the south-westerly direction for some period, and then it

keep changing directions in this pattern. The current also follows north-east and south-west directions, which are approximately parallel to the shoreline. The current changes direction more often and randomly into these two directions until it eventually flows consistently in the north-east direction. The direction of the current seem to be deflected towards the north relative to the direction of the wind. There is detectable similitude in the overall directions of current flow and the directions that the wind is blowing towards, except that the wind is deflected to the north.

### 6.2.3 Lagged correlation analysis of wind and current

#### Autocorrelation analysis

This analytical method gives the value of interdependence between the wind and current. The wind and current are independently analysed with the autocorrelation coefficient of which a detailed definition is given in Section 3.5 in Chapter 3. The lag that it takes for the autocorrelation coefficient to drop down to insignificance is taken as the characteristic time scale of the wind or current. These time scales can be compared and similarity can be used to deduce if the wind is the main driving force of the current (Funke & Stretch, 2002).

The autocorrelation coefficients are computed for longshore and cross-shore velocity components. Figure 6.4 shows a cross-shore wind correlogram while Figure 6.5 shows a cross-shore current one. On the other hand, Figure 6.6 shows a longshore wind correlogram while Figure 6.7 shows a longshore current one.

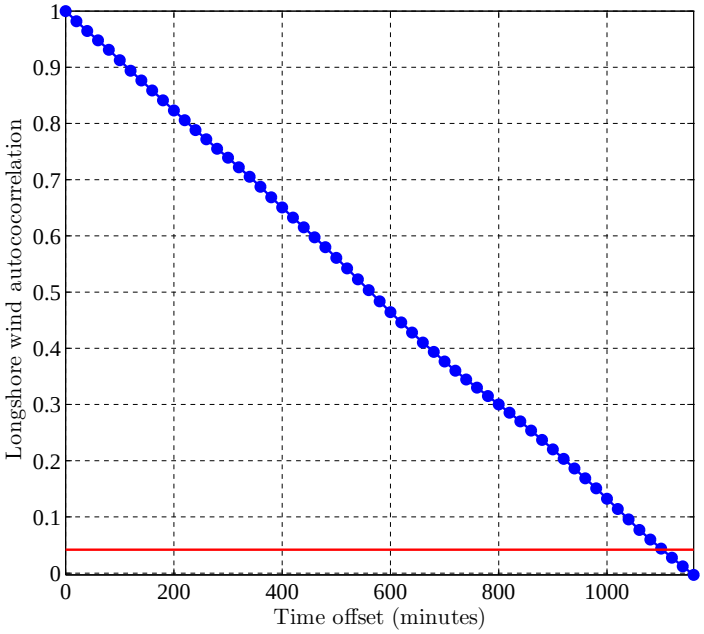


**Figure 6.4:** Longshore wind autocorrelation.

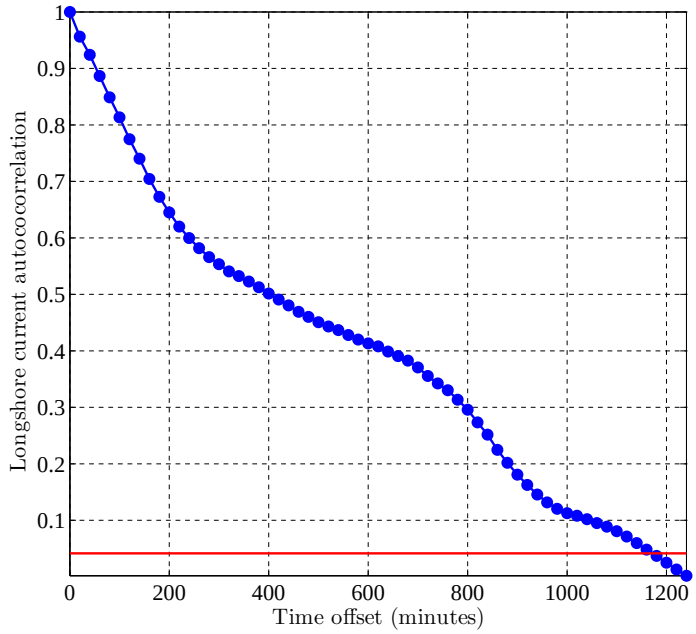


**Figure 6.5:** Longshore current autocorrelation.

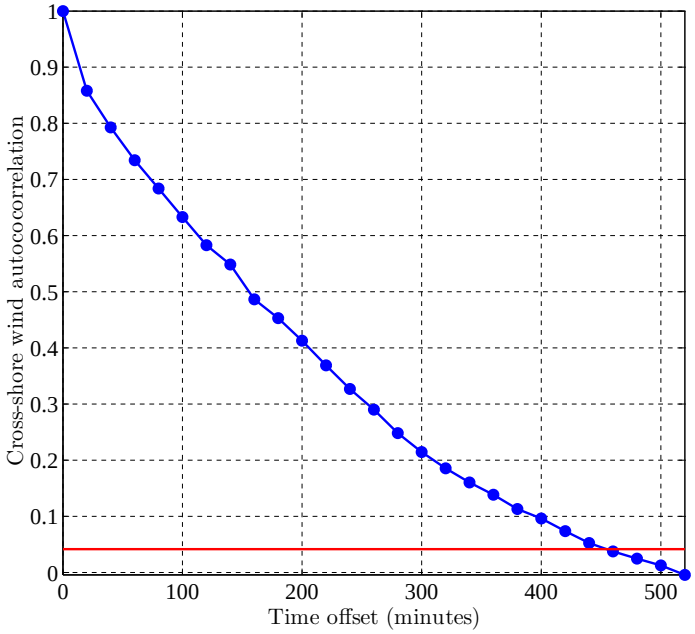


**Figure 6.6:** Cross-shore wind autocorrelation.

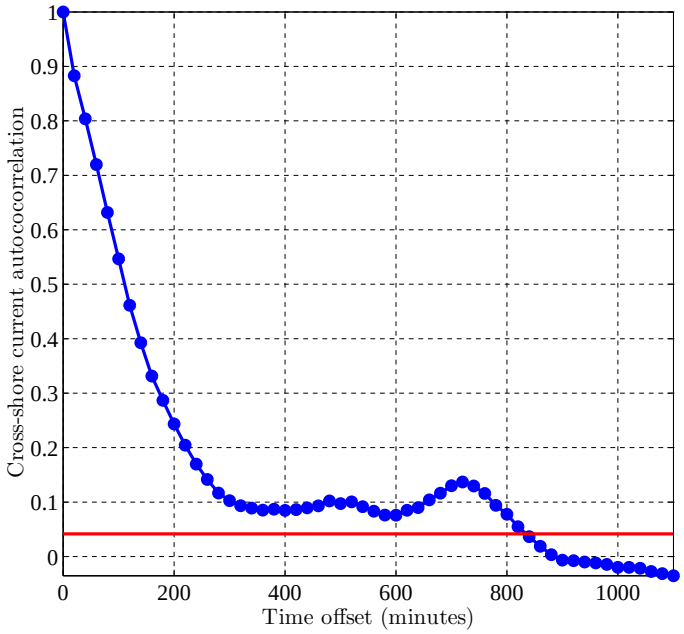


**Figure 6.7:** Cross-shore current autocorrelation.

The longshore wind time scale leads the current by an hour. The wind drops down to insignificance at 18.3 hours (1098 minutes, where graph cuts significance line in Figure 6.4), while the current drops down at 19.3 hours (1158

minutes, where graph cuts significance line in Figure 6.5) hours. On the other hand, the cross-shore current time scale is 14 hours while for the cross-shore wind, it is 7.7 hours. There is therefore similarity in the autocorrelation time scales of the wind and surface current in the longshore direction, suggesting further that the wind in the location may be a driving force for the surface currents. The same cannot be said with regards to the cross-shore direction.

**Lagged cross-correlation coefficients.**

Cross-correlation is performed on the wind and current data. Given a pair of $N$ observations $\{(x_i, y_i) \quad i = 1, ..., N\}$ the cross-correlation coefficient is based on the cross-covariance which is given by,

$$c_{xy}(k) = \begin{cases} \sum_{t=1}^{N-k} (x_t - \bar{x})(y_{t+k} - \bar{y}) & k = 0, 1, ..., N-1, \\ \sum_{t=1-k}^{N} (x_t - \bar{x})(y_{t+k} - \bar{y}) & k = -1, -2, ..., -(N-1), \end{cases} \tag{6.2.4}$$

where $k$ is the lag and $t$ is the time step. The cross-correlation function is then given by

$$r_{xy}(k) = \frac{c_{xy}(k)}{\sqrt{c_{xx}(0)c_{yy}(0)}}. \tag{6.2.5}$$

In equation (6.2.5), $c_{xx}(0)$ is the variance of $x_t$ and $c_{yy}(0)$ is the variance of $y_t$. In this study $x_t$ refers to the wind and $y_t$ is used for the current. The MATLAB function CROSSCORR is used for this analysis.

The current and wind, determined into longshore and cross-shore components are analysed utilizing lagged cross-correlation.

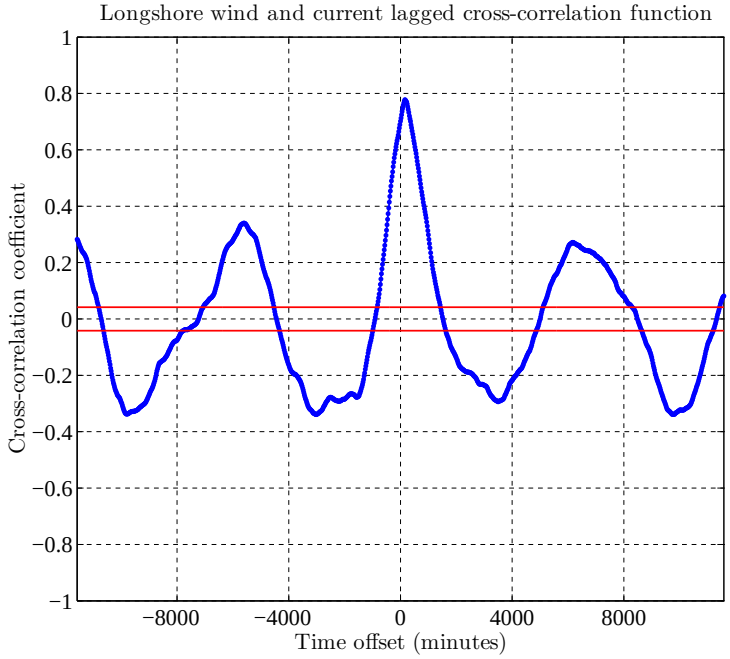


**Figure 6.8:** Lagged cross-correlation function of wind and currents for longshore components.

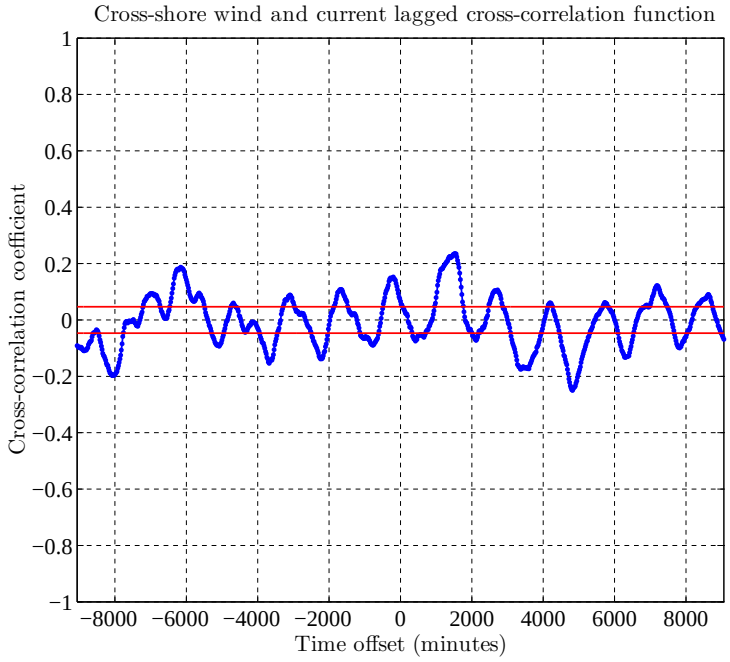


**Figure 6.9:** Lagged cross-correlation function of wind and currents for cross-shore components.

The cross-correlation functions for longshore wind and currents are depicted in Figure 6.8 for period five. When the surface current and the wind were analysed satisfactory cross-correlation coefficients were obtained, being 0.78 at a time lag of 2.7 hours. This confirms the dependence of surface currents on local wind conditions. However, a different conclusion was reached with regards to cross-shore wind and current components. The cross-correlation functions for cross-shore wind and currents are depicted in Figure 6.9 for period five.The maximum cross-correlation in the cross-shore direction is 0.35 at -20 minutes, indicating lack of possible dependence of the currents on the wind.

### 6.2.4 Power spectral analysis

Power spectral density plots are constructed following the description in Section 3.6 in Chapter 3. The power spectral density computations are made on the wind data resolved into longshore and cross-shore components.

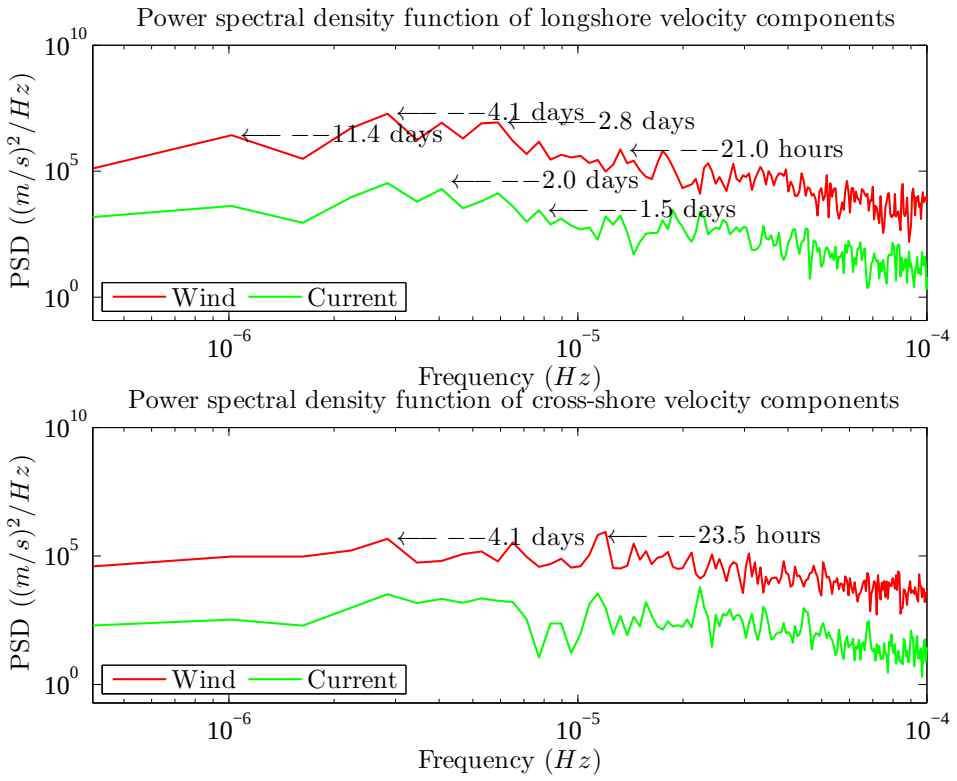


**Figure 6.10:** Modified periodogram and of currents and wind for period five.

The graphs depicting periods of common dominant periodicities in the wind and currents are shown in Figure 6.10. The graphs have common periodicities

between the wind currents indicated. The 24 hour period which corresponds to land and sea breeze is highly emphasized in the cross-shore wind and current power spectra. Many other periods are indicated in the longshore wind and power spectra, indicating common oscillations between the wind and surface current. These may indicate common driving factors for the wind and current, but no more deductions can be made.

## 6.3 Results and discussions

### 6.3.1 Analysis of direction, speed and duration

Before any involved analysis, the 3% rule of thumb can be applied to deduce if wind in the study location can have any significant impact on the generation of currents. From Section 2.4 in Chapter 2, the average wind speed is estimated to be 11 m/s and the maximum speed is 16.6 m/s. These equate to a potential current of 33.3 to 49.8 cm/s. This is significant considering that the mean surface (15.92 m) current speed recorded was between 20.69 to 36.67 cm/s and the maximum surface current recorded was between 74.8 to 112.4 cm/s.

Wind and current roses for periods one, two, three and six are shown in Figure 6.11 and Figure 6.12. A wind rose is shown on the right while a current rose for the same period is shown on the left.

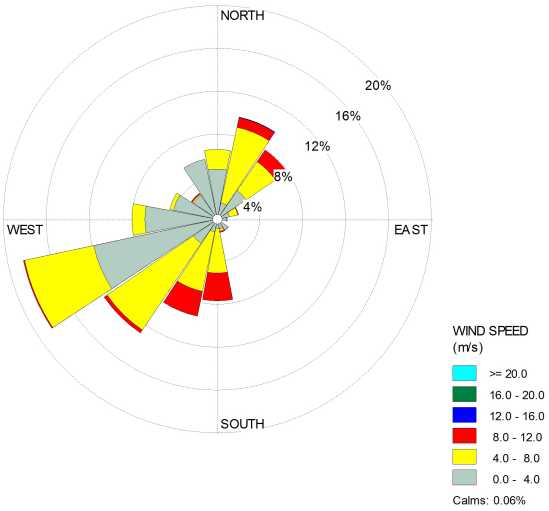


**(a)** Wind rose for period one.

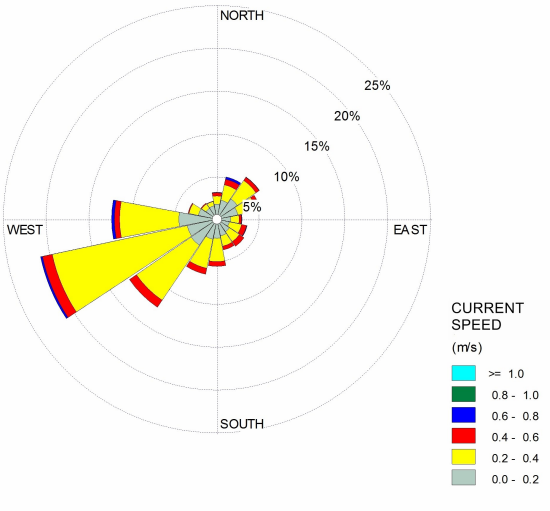


**(b)** Current rose for period one.

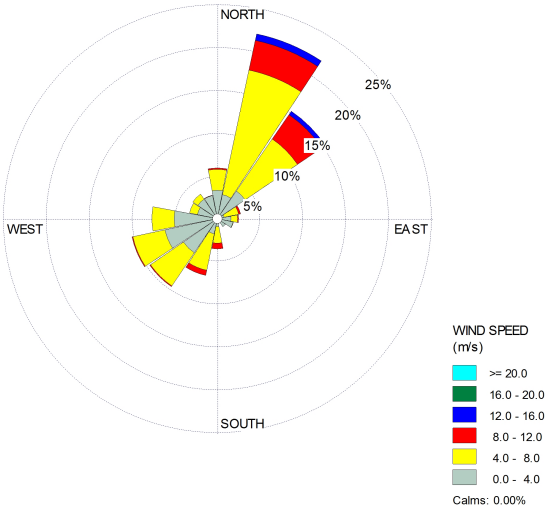


**(c)** Wind rose for period two.

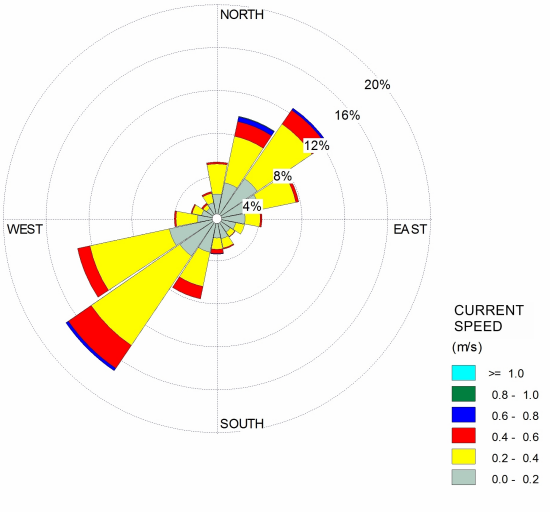


**(d)** Current rose for period two.

**Figure 6.11:** Wind rose and current rose for periods one and two.

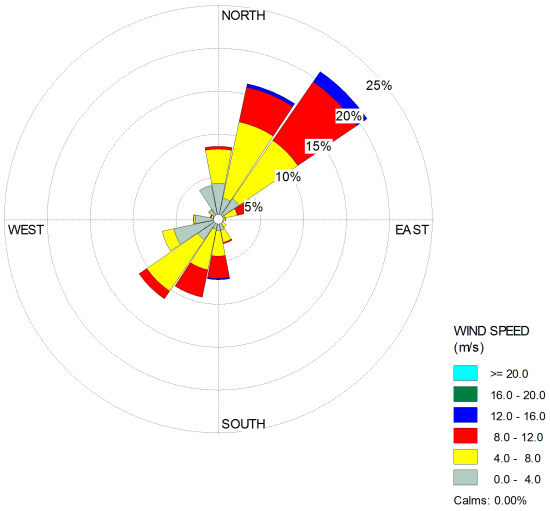


**(a)** Wind rose for period three.

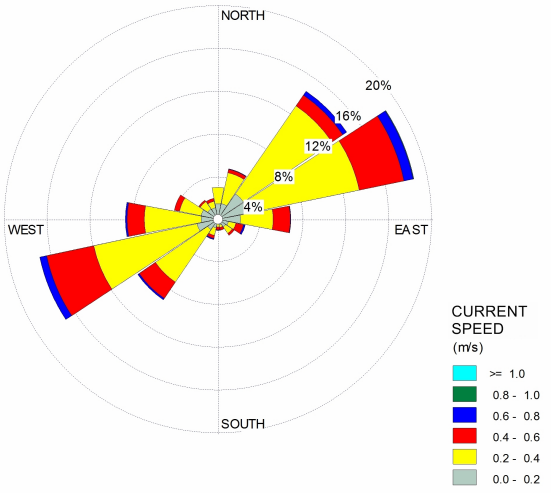


**(b)** Current rose for period three.

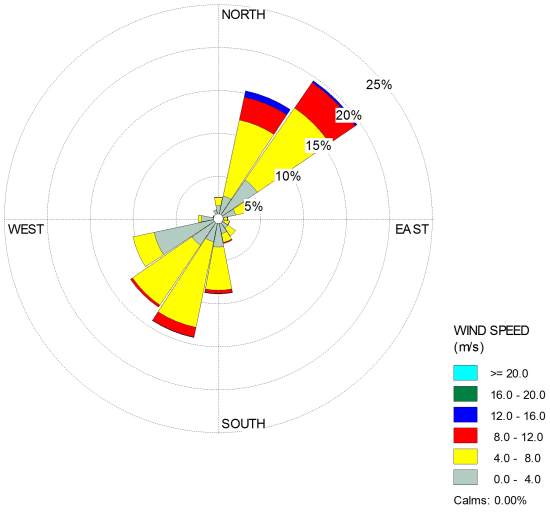


**(c)** Wind rose for period six.

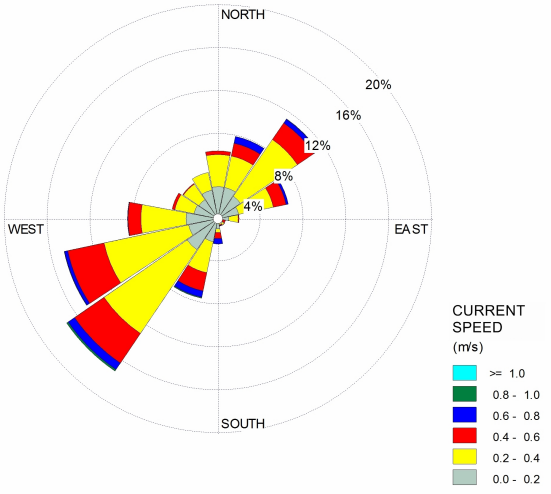


**(d)** Current rose for period six.

**Figure 6.12:** Wind roses and current roses for periods three and six.

Figure 6.11a and Figure 6.11b depict a wind rose and current rose, respectively, for period one. Wind speeds in this period do not exceed 12 m/s. This is the period with the weakest winds compared to all the other periods. The majority of the wind records originated from south-west. A weak WSW component dominates the wind rose. Winds from all other directions were recorded, with the least records from the south-east direction. A current rose is also displayed in Figure 6.11, it depicts a WSW current component being predominant. The majority of the currents tend to flow towards south-west, although currents flowing towards other directions are recorded. Currents with speeds up to 0.8 m/s are only recorded in the south-west and north-east directions, these directions are alongshore.

Figure 6.11c and Figure 6.11d show a wind rose and current rose , respectively, for period two. North-westerly winds are predominant during the period, with wind speeds up to 16 cm/s recorded from this direction. The main wind originating direction is ENE. The next major winds are south-easterly. The current rose shows the majority of the currents flowing towards south-west followed by north-east. Currents flowing towards WSW are predominant. Current speeds up to 0.8 m/s are recorded in the south-west and north-east directions. Currents flowing towards other directions are also recorded, however their speeds do not exceed 0.6 m/s.

Figure 6.12a and Figure 6.12b depicts a wind rose and current rose, respectively, for period three. The ENE wind component dominates the wind rose. Wind speeds going up to 16 m/s are recorded from north-easterly and southerly components only. The majority of winds are recorded in the south-west and north-east components. The current rose is also dominated by an ENE component. The majority of current speeds are recorded in north-east and south-west directions. Current speeds do not exceed 0.8 m/s.

Figure 6.12c depicts a wind rose and Figure 6.12d depicts a current rose for period six. The majority of wind speeds in this period are recorded from the north-east direction, with the ENE component being predominant, with wind speeds reaching up to 16 m/s. Wind records not exceeding 12 m/s are recorded in the south-west direction. There are records in all directions of the wind rose. The current rose show currents flowing towards the south-west to be predominant. This direction is followed by north-east, with speeds up to 0.8 m/s. Current speeds not exceeding 0.6 m/s are recorded in the north-west direction and the least amount of records are found in the south-east directions.

The predominant direction from which the wind blew is from the south-westerly and north-north-easterly directions. These are the directions of the prevailing winds in the location (DN & SDCEA, 2004). There were no occur-

rences of wind speeds exceeding 20 m/s in the studied wind records. Predominant directions of flow for the currents is south-west and north-east which are similar to due wind directions. An exception is seen in period one, which is a rather calm period, the maximum wind speed is 11.32 m/s (the lowest maximum of all the periods) and is predominantly from the south-westerly direction. The current also flows in all directions except in the south-easterly direction. Similarity in corresponding current roses and due directions in wind roses proposes that the wind can be a driving mechanism of currents, further analysis may confirm this.

### 6.3.2 Duration analysis

Average wind durations in a day in different directions are shown in Table 6.6 to Table 6.12. Discussions for the five periods are discussed one at a time.

#### Duration analysis for period one

Table 6.6 and Table 6.7 give the average wind and current durations in a day in different directions for period one.

**Table 6.6:** Wind duration for period one.

| Speed (m/s) | NNE (h) | ENE (h) | ESE (h) | SSE (h) | SSW (h) | WSW (h) | WNW (h) | NNW (h) |
|---|---|---|---|---|---|---|---|---|
| 0.01-4.0 | 2.21 | 1.18 | 0.39 | 0.43 | 0.57 | 2.05 | 3.66 | 1.69 |
| 4.0-8.0 | 1.09 | 2.03 | 0.04 | 0.01 | 1.76 | 4.06 | 0.82 | 0.08 |
| 8.0-12.0 | 0.01 | 0.54 | | | 0.93 | 0.40 | | 0.03 |
| $\geq$ 12.0 | | 0.01 | | | | | | |

**Table 6.7:** Current duration for period one.

| Speed (m/s) | NNE (h) | ENE (h) | ESE (h) | SSE (h) | SSW (h) | WSW (h) | WNW (h) | NNW (h) |
|---|---|---|---|---|---|---|---|---|
| 0.00-0.2 | 0.92 | 1.36 | 0.76 | 0.88 | 1.09 | 1.60 | 1.83 | 0.89 |
| 0.2-0.4 | 0.43 | 1.20 | 0.63 | 0.68 | 1.15 | 4.28 | 3.72 | 0.32 |
| 0.4-0.6 | 0.13 | 0.29 | 0.19 | 0.32 | 0.25 | 0.43 | 0.36 | 0.03 |
| $\geq$0.6 | 0.07 | 0.03 | 0.01 | 0.01 | | 0.01 | 0.12 | |

The longest average span for the wind during period one was 4.06 hours in the WSW (the corresponding due direction is ENE) segment (45° segments are used). For the surface current, the longest average duration is 4.28 hours in the WSW segment for speeds in the 0.2-0.4 m/s range. The maximum duration of 4.28 hours for the surface current is not consistent with the 4.06 hours found for the wind.

### Duration analysis for period two

Average wind and current durations in a day in different directions for period two are given in Table 6.8 and 6.9.

**Table 6.8:** Wind duration for period two.

| Speed (m/s) | NNE (h) | ENE (h) | ESE (h) | SSE (h) | SSW (h) | WSW (h) | WNW (h) | NNW (h) |
|---|---|---|---|---|---|---|---|---|
| 0.01-4.0 | 1.48 | 1.39 | 0.80 | 0.53 | 0.48 | 2.11 | 2.44 | 1.25 |
| 4.0-8.0 | 2.27 | 3.91 | 0.33 | | 0.91 | 2.23 | 1.19 | 0.23 |
| 8.0-12.0 | 0.28 | 1.48 | 0.04 | | 0.23 | 0.12 | 0.01 | |
| $\geq$ 12.0 | | 0.30 | | | | | | |

**Table 6.9:** Current duration for period two.

| Speed (m/s) | NNE (h) | ENE (h) | ESE (h) | SSE (h) | SSW (h) | WSW (h) | WNW (h) | NNW (h) |
|---|---|---|---|---|---|---|---|---|
| 0.00-0.2 | 1.25 | 1.95 | 1.42 | 0.83 | 0.98 | 1.98 | 1.20 | 0.65 |
| 0.2-0.4 | 1.22 | 2.57 | 0.82 | 0.28 | 0.77 | 3.88 | 1.36 | 0.27 |
| 0.4-0.6 | 0.13 | 0.70 | 0.05 | 0.01 | 0.23 | 0.98 | 0.15 | 0.07 |
| 0.6-0.8 | 0.01 | 0.15 | | | 0.01 | 0.07 | | |
| $\geq$ 0.8 | | 0.01 | | | | | | |

The longest average span for the wind during period two was 3.91 hours in the ENE segment, this was for wind speed in the 4-8 m/s range. For the surface current the longest average duration is 3.88 hours in the WSW segment, the speed is in the 0.2-0.4 m/s range. The current duration and wind duration are similar. This demonstrates that wind generated currents in this period have short, almost instantaneous response times to changes in wind conditions.

### Duration analysis for period three

Average wind and current durations in a day in different directions for period three are given in Table 6.10 and 6.11.

**Table 6.10:** Wind duration for period three.

| Speed (m/s) | NNE (h) | ENE (h) | ESE (h) | SSE (h) | SSW (h) | WSW (h) | WNW (h) | NNW (h) |
|---|---|---|---|---|---|---|---|---|
| 0.01-4.0 | 1.84 | 1.15 | 0.23 | 0.32 | 0.64 | 1.54 | 1.39 | 0.88 |
| 4.0-8.0 | 2.08 | 3.24 | 0.30 | 0.32 | 1.50 | 2.56 | 0.16 | 0.07 |
| 8.0-12.0 | 0.42 | 2.89 | 0.11 | 0.01 | 1.06 | 0.64 | 0.03 | 0.01 |
| $\geq$ 12.0 | | 0.50 | 0.08 | | 0.04 | | | |

**Table 6.11:** Current duration for period three.

| Speed (m/s) | NNE (h) | ENE (h) | ESE (h) | SSE (h) | SSW (h) | WSW (h) | WNW (h) | NNW (h) |
|---|---|---|---|---|---|---|---|---|
| 0.00-0.2 | 0.66 | 1.30 | 1.06 | 0.38 | 0.20 | 0.72 | 0.85 | 0.60 |
| 0.2-0.4 | 0.70 | 4.33 | 1.80 | 0.27 | 0.20 | 2.68 | 2.83 | 0.42 |
| 0.4-0.6 | 0.04 | 0.84 | 1.01 | 0.17 | 0.12 | 0.88 | 1.14 | 0.13 |
| 0.6-0.8 | | 0.25 | 0.11 | 0.03 | 0.03 | 0.13 | 0.12 | |
| $\geq$0.8 | | 0.01 | | | | | | |

The longest average span for the wind during period three was 3.24 hours in the ENE segment. This was for wind speed in the 4-8 m/s range. For the surface current the longest average duration is 4.33 hours in the ENE segment for speed in the 0.2-0.4 m/s range. There is also 2.68 hours in the due direction of the wind in the 0.2-0.4 m/s speed range. It takes 0.56 hours for wind-induced currents to respond to changes in wind conditions, which is a short reaction time.

### Duration analysis for period six

Average wind durations in a day in different directions for period six are given in Table 6.12 and 6.12.

**Table 6.12:** Wind duration for period six.

| Speed (m/s) | NNE (h) | ENE (h) | ESE (h) | SSE (h) | SSW (h) | WSW (h) | WNW (h) | NNW (h) |
|---|---|---|---|---|---|---|---|---|
| 0.01-4.0 | 0.81 | 2.09 | 0.42 | 0.60 | 1.48 | 2.13 | 1.54 | 0.20 |
| 4.0-8.0 | 1.02 | 4.10 | 0.26 | 0.40 | 2.32 | 3.92 | 0.27 | 0.04 |
| 8.0-12.0 | 0.18 | 1.44 | 0.02 | 0.02 | 0.31 | 0.16 | | |
| $\geq$ 12.0 | 0.02 | 0.22 | 0.02 | | 0.02 | | | |

**Table 6.13:** Current duration for period six.

| Speed (m/s) | NNE (h) | ENE (h) | ESE (h) | SSE (h) | SSW (h) | WSW (h) | WNW (h) | NNW (h) |
|---|---|---|---|---|---|---|---|---|
| 0.00-0.2 | 1.48 | 1.21 | 0.51 | 0.22 | 0.54 | 1.55 | 1.30 | 1.14 |
| 0.2-0.4 | 1.38 | 2.40 | 0.48 | 0.08 | 0.32 | 4.04 | 1.93 | 0.70 |
| 0.4-0.6 | 0.17 | 0.90 | 0.08 | 0.06 | 0.35 | 1.55 | 0.63 | 0.04 |
| 0.6-0.8 | 0.06 | 0.25 | | | 0.20 | 0.32 | 0.02 | |
| $\geq$ 0.8 | | 0.01 | | | | 0.07 | | |

The longest average span for the wind during period six was 4.1 hours in the ENE segment, which was for wind speed in the 4-8 m/s range. For the surface current the longest average duration was 4.04 hours in the WSW segment, the speed is in the 0.2-0.4 m/s range. This is consistent with the span of 4.1 hours in the WSW direction found for the wind. This demonstrates that wind generated currents have short reaction times to changes in wind conditions in this period.

The durations of the five periods were short (ranging from 23 days to 32 days) thus the variable response periods for the currents from the wind. The most common wind speed in this location is in the ENE direction segment with speed within a 4-8 m/s range. For the currents the common speed is in the WSW direction, and speed is in a 0.2-0.4 m/s range. From this analysis alone, wind seem to influence the direction of flow of the surface currents, they have short response times to changes in wind conditions. This conclusion is in agreement with that of Funke & Stretch (2002) who followed a similar technique.

## Progressive vector diagram analysis

PVDs for the current and wind are shown in Figure 6.13 to Figure 6.20. The PVDs are shown side by side for the six periods. A wind PVD is presented on the left and a corresponding current PVD is given on the right.

Figure 6.13 shows a PVD for period one. During the first period, the wind blows constantly from a south-westerly direction, changing direction to blow from a north-easterly direction. A short displacement is covered in the PVD indicating weak wind conditions. Figure 6.14 shows a current PVD for period one, the current starts off towards south-west, then north-east, continues changing direction and occasionally flows towards the south and north, ultimately, flowing in a north-east direction.

For period two, the wind starts blowing from a south-westerly direction, then blows from the east, and continues as a south-westerly wind. Ultimately the wind blows from a south-westerly direction and occasionally blows from a north-easterly and easterly direction. This is shown in Figure 6.15. The current in this period, shown in Figure 6.16, primarily flows towards north-east, it commences flowing in a south-western direction, then north-east for an extended period. Subsequently, the current changes direction regularly from north-east and south-west.

PVDs of wind and currents for period three are shown in Figure 6.17 and Figure 6.18. For period three, the wind commences blowing from a north-easterly direction. Subsequently, the wind blows from a south-westerly direction, occasionally changing direction to blow from a north-easterly direction. The

current on the other hand changes direction constantly. It commences in the south-west direction, then north-east and subsequently it flows towards north-west and changes into a number of other directions.

During the sixth period, the wind predominantly blows from a south-westerly direction. A number of changes of direction occurs from the north-easterly direction to the south-westerly directions as can be observed in the PVD in Figure 6.19. The current flows predominantly towards the north-east, with a number of changes towards south-west as can be observed in Figure 6.20.

The PVDs outline the behaviour of the prevailing winds during the period of data collection. Looking at the PVDs for the wind and current flows, there is a detectable similitude in the general due paths of the wind and the flow directions of the currents. The wind commonly blows towards south-west and north-east while the currents flow towards the same directions. This substantiates a connection between the local wind and the currents.

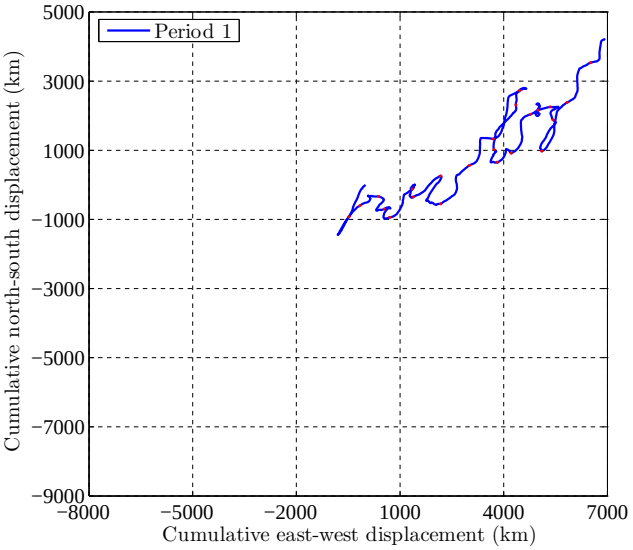


**Figure 6.13:** PVD of wind (1)

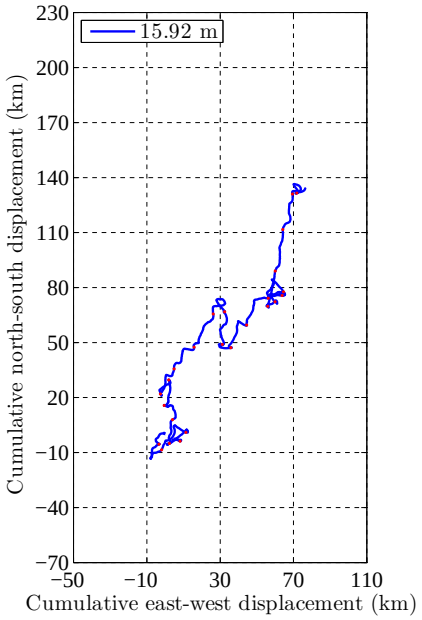


**Figure 6.14:** PVD of current (1)

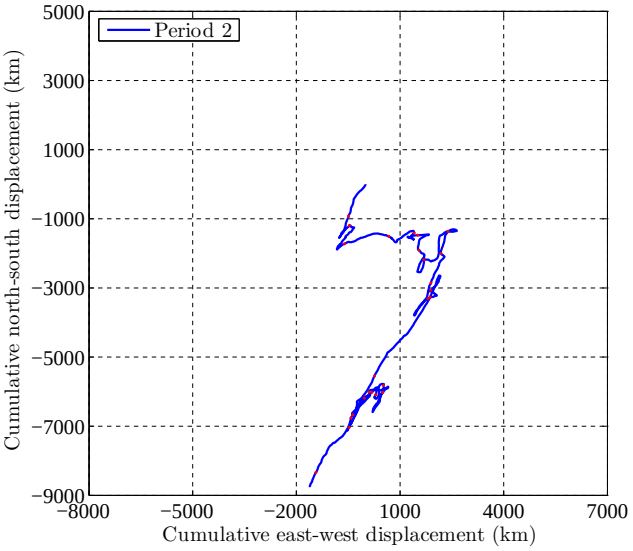


**Figure 6.15:** PVD of wind (2)

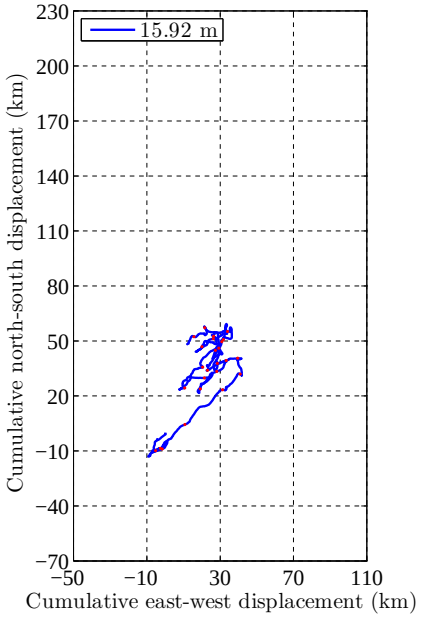


**Figure 6.16:** PVD of current (2)

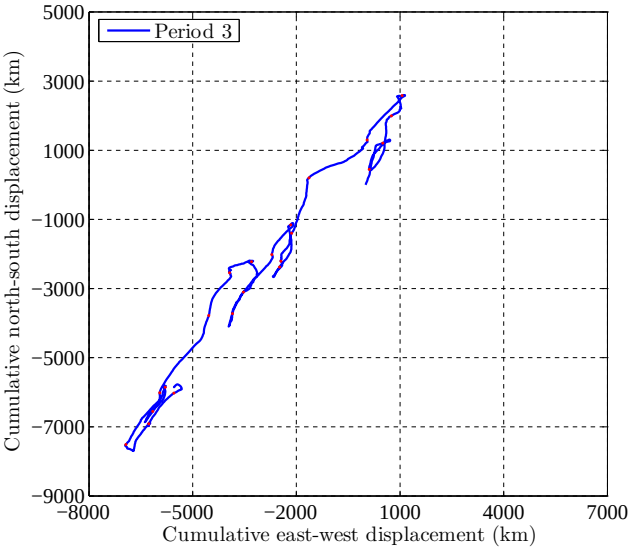


**Figure 6.17:** PVD of wind (3)

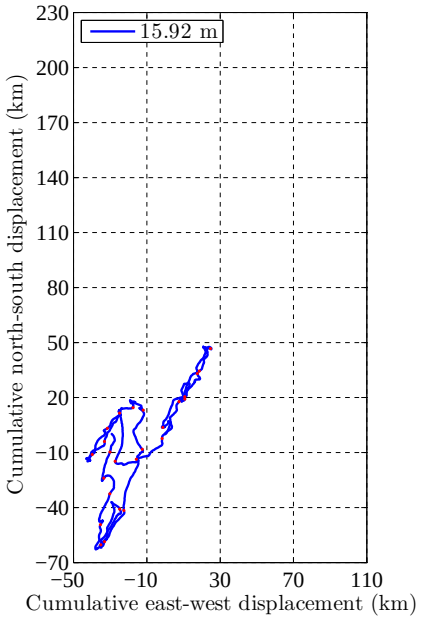


**Figure 6.18:** PVD of current (3)

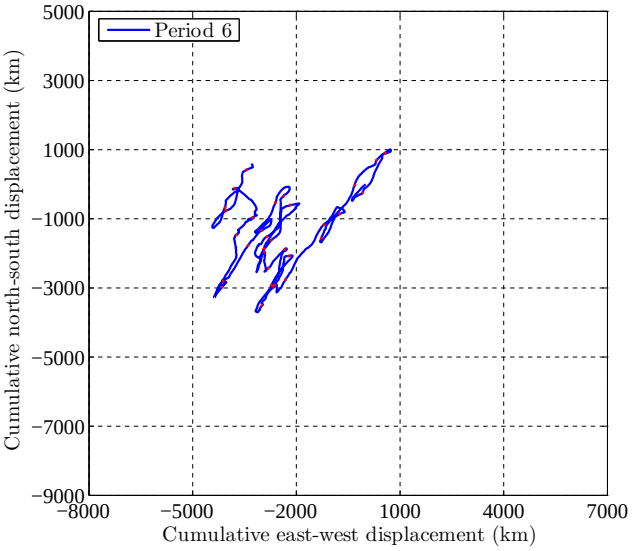


**Figure 6.19:** PVD of wind (6)

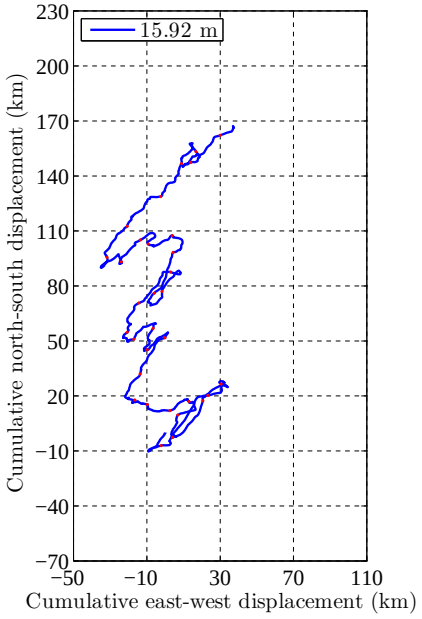


**Figure 6.20:** PVD of current (6)

## Autocorrelation analysis

Correlograms of the wind and current data resolved into longshore and cross-shore components are given in Appendix F, in Figure F.1 to Figure F.24 and also in Figure 6.6 for period five. The times when the autocorrelation coefficient drops down to insignificance are given in Table 6.14 and Table 6.15.

**Table 6.14:** Long-shore autocorrelation averages.

| Period | Longshore wind (h) | Longshore current (h) |
|---|---|---|
| 1 | 18.3 | 20.3 |
| 2 | 19 | 27 |
| 3 | 24 | 25.7 |
| 5 | 18.3 | 18.7 |
| 6 | 18.7 | 21.3 |

**Table 6.15:** Cross-shore autocorrelation averages.

| Period | Cross shore wind (h) | Cross shore current (h) |
|---|---|---|
| 1 | 6 | 3.5 |
| 2 | 6.3 | 4.7 |
| 3 | 10.6 | 20.7 |
| 5 | 7.7 | 19.3 |
| 6 | 7.3 | 4 |

The difference between the time it takes for the longshore wind to drop down to insignificance and the longshore current to drop down for all the periods is at most 2.6 hours. This is with the exception of the second period. In all these periods, the current lags the wind. There is therefore a small difference in the correlation time scales of the wind and the current. This affirms the conclusion that the wind is one of the fundamental generating forces for the current. For the cross-shore components, the difference between the time it takes for the wind to drop down to insignificance and the current to drop down for all the periods is at most 3.3 hours. This is with the exception of the third and fifth period, where the the difference exceed 10 hours.

## Lagged cross-correlation

Current and wind measurements, resolved into into longshore and cross-shore components were analysed utilizing lagged cross-correlation. The maximum cross-correlation results for the five periods are included in Table 6.16 for longshore velocity components. Corresponding lagged cross-correlation graphs are included in Figure F.25, Figure 6.8 and Figure F.26.

**Table 6.16:** Maximum longshore wind-current cross-correlations and corresponding lag times.

| Period | Cross-correlation coefficient | Lag time |
|---|---|---|
| 1 | 0.78 | 2.7 hours |
| 2 | 0.60 | 26.3 hours |
| 3 | 0.83 | 26.7 hours |
| 5 | 0.78 | 2.7 hours |
| 6 | 0.73 | 2.7 hours |

When surface currents and wind measurements were analysed, maximum cross-correlation coefficients which are significantly different from zero were obtained. These were reasonable results. The maximum longshore wind and current cross-correlation coefficients and corresponding lag times are provided in Table 6.16. A lag time of 2.7 hours gave a maximum correlation coefficient of 0.78. Period two and three indicates an even higher time lag for maximum correlation coefficients, the time lags in both periods are above 26 hours. The high correlation coefficients between the wind currents confirms the dependence of surface currents on local wind conditions. It should be recalled that the directions of prevailing winds are roughly along the shore.

From Table 6.16 it is evident that it takes a short time scale for strong winds to have a significant effect on the currents, this is indicated for period one, five and six. For periods two and three, longer time scales are identified. The cross-correlation between the wind and the currents are significant, positive and above 0.5 for all the periods indicating a strong correlation between the wind and current at the specified lags. This indicates a direct interdependent relationship between the wind and current in the alongshore direction.

**Table 6.17:** Maximum cross-shore wind-current cross-correlations and corresponding lag times.

| Period | Cross-correlation coefficient | Lag time |
|---|---|---|
| 1 | 0.38 | 1.3 hours |
| 2 | 0.26 | 26.3 hours |
| 3 | 0.24 | 3.35 days |
| 5 | 0.35 | -20 minutess |
| 6 | 0.27 | 1.3 hours |

For cross-shore components the maximum lagged cross-correlations are significant yet close to zero. For periods, one and six, the maximum cross-correlation coefficient is identified at a short time lag of 1.3 hours. For period three, the

time lag is longer than three days. This would mean that the wind has to consistently blow in a particular direction at given speed ranges for three days for it to be positively aligned with the current. Period five indicates a maximum cross-correlation coefficient at a negative lag. This indicates the absence of a positive linear relationship between the currents and the wind in the period. Figures F.27 and F.28 confirm that cross-shore winds and currents have a weak positive relationship. The currents are driven by the wind to a minimal extent in the cross-shore direction. These results are not surprising as from the wind roses and current roses as well as progressive diagrams, the dominant directions followed by winds and currents are south-west and north-east, which are both along the shore. There has also been indications of dependence of currents on winds in the alongshore direction in all previous analysis and not in the cross-directions.

### Power spectral analysis

Power spectral density graphs are included in Appendix F. Power spectral density graphs for longshore and cross-shore wind and current velocity components are included in Figure F.29, Figure 6.10 and Figure F.30. Winds are strongly impacted by the diurnal cooling and warming of the land and ocean so a diurnal peak of about 24 hours in the cross-shore components is expected. This is confirmed by the 24 hour peak, present in both the detided current power spectral graphs as well as the wind ones. The 24 hour peak occurs in all the cross-shore power spectral graphs and sometimes in the longshore power spectral graphs. This is to be expected as wind-generated current due to land/sea breeze magnifies the diurnal tidal current ($K_1$) for the same period. This is identifiable in the amplitude which spans 23.93 hours (Yanagi, 1999).

## 6.4 Summary

This chapter investigated the relationship between the wind and currents. The investigation was done through the use of wind and current roses, autocorrelation and cross-correlation analysis, comparison of progressive vector diagrams and power spectral analysis. The investigation was performed on the time series for all the periods except for period four as this period had many missing wind records in it.

Wind roses revealed similitude in the due directions of the wind and flow direction of currents, which were for all the periods except for period one. Duration analyses which were performed using results of current and wind roses substantiated this. The most common wind speed in the study is in the ENE (due WSW) direction segment with speed within a 4-8 m/s range. For the currents the common speed is in the WSW direction, and speed is in a 0.2-0.4 m/s

range. From this analysis alone, there are indications that the wind influence the direction of flow of surface currents.

Autocorrelation analysis substantiated the driving of currents by the wind especially in the alongshore direction. Cross-correlation analyses substantiated that currents are driven by the wind. In the longshore components, for all the five periods the maximum cross-correlation coefficient was above 0.60. The cross-correlation coefficients were weak in the cross-shore components. This may be due to the fact that land and sea breezes, although regular across the shore, are weak, while prevailing winds are known to blow along the shore around the ADCP mooring site (Schumann, 1988; DN & SDCEA, 2004; Cooper, 1991). Progressive vector diagrams further substantiated that currents are driven by the wind in the north-east and south-west direction. These directions are roughly alongshore.

A combination of all the techniques which were used in the wind and current analyses played different roles in bringing out the conclusion that winds are a driving mechanism of currents in the study location. Wind roses gave a general impression of the wind currents and the duration analysis showed how currents respond to changes in wind condition. Progressive vector diagram gave a further visual impression of the wind and currents, separately, allowing for comparison. Lagged correlation analysis quantified the dependence relationship of currents and winds, the agreement of this analysis with all other previous analyses confirm the dependence of the currents on the wind. Power spectral analysis explored common oscillations between currents and winds.

# Chapter 7

# Effect of the Agulhas current on measured currents

## 7.1 Introduction

The Agulhas Current is the western boundary current of the South Indian Ocean. It flows south-westwards along the East coast of South Africa from: 27°S to 40°S (Gordon, 1985). It is a fast flowing current reaching speeds up to 200 cm/s and transports large volumes of water. Sources of the Agulhas current include the Mozambique channel eddies, the East Madagascar Current and the Indian Ocean sub-gyre. It flows close to the shore along the narrow shelf of the East coast until it reaches the Natal Bight where it diverges from the shore. The configuration of the Bight causes the Agulhas current to move offshore (Pearce, 1977). The divergence and destabilization results in the formation of Natal pulses in the Natal Bight (Lutjerharms & De Ruijter, 1994). These are large, irregular and desolate meanders that progress at 5 cm/s in the Natal Bight (Lutjerharms & Roberts, 1988).

The data used in this study was measured in the Natal Bight, which is a shallow region of the KwaZulu-Natal coast with a width of 50 km. In this region the Agulhas current is known to move away from the shore and flow farther offshore, its mean axis is about 50 km offshore. A large cyclonic system called the Natal gyre occurs in the Natal Bight. The Natal gyre is created by the separation of the Agulhas current from the shoreline (Harris, 1978b).

## 7.2 Discussion

This chapter investigates the currents indicated by $u_b$ in Equation (1.2.1). The data in this study was measured approximately 500 m from the shoreline. Since the Agulhas current flows farther offshore at this location, it would be unlikely for it to have any direct influence on the currents measurements. However, the

Natal gyre and the anti-cyclonic systems that are caused in its presence can influence currents in the region (Van der Westhuysen, 2002; Harris, 1978b). The Natal pulse that also originates in the Natal bight with counter currents can also affect nearshore currents (Lutjerharms & De Ruijter, 1994). Figure 7.1 shows the ADCP mooring site with respect to the shoreline.


**Figure 7.1:** ADCP mooring site.

Approximately 42.3% of the measured currents flow towards the south-west and south-south-west for the whole duration of data collection. This directions corresponds with the direction of flow of the Agulhas current. Based on the findings by Harris (1978b) the region is influenced by the Natal gyre and the flow of currents in a south-western direction could be due to an influence of a counter current in the Natal bight.

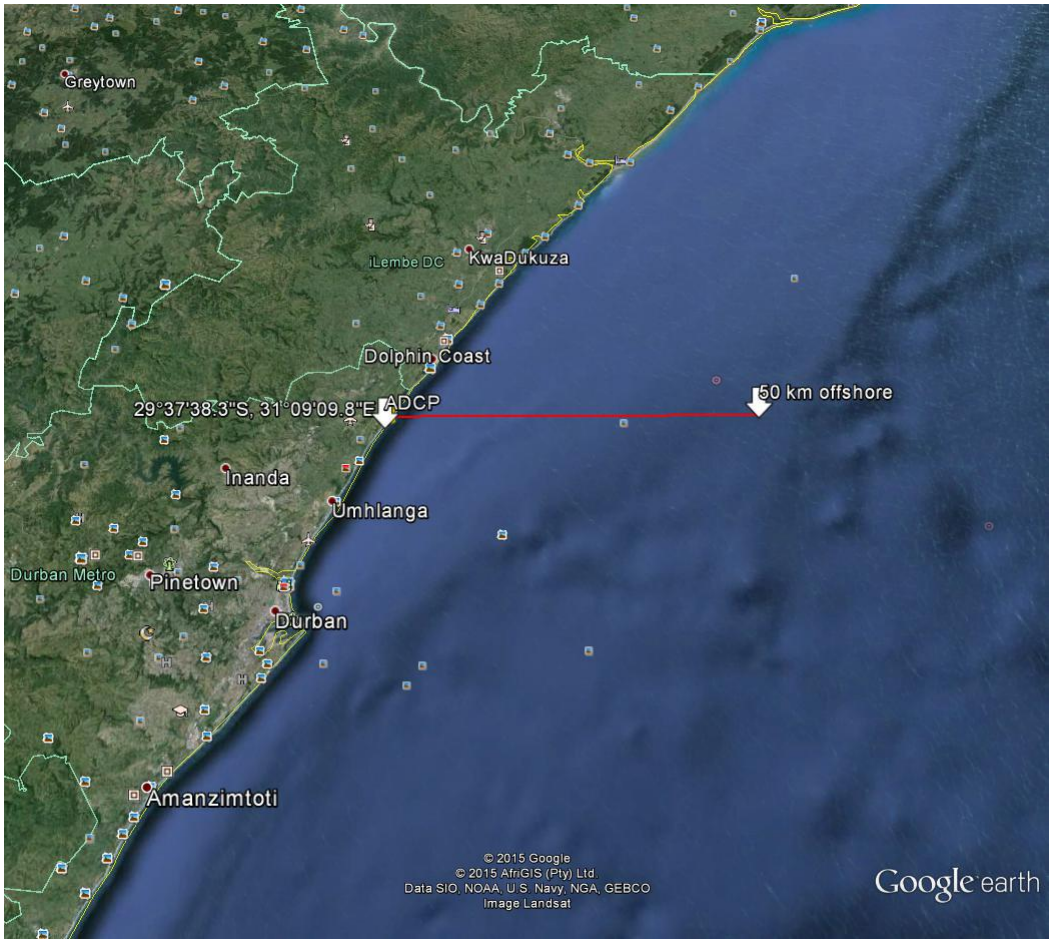


**Figure 7.2:** ADCP mooring site

Figure 7.2 shows the ADCP mooring site compared with a distance that extends 50 km offshore. That the Agulhas current does not have direct influence on currents was also established by (Harris, 1978b).

Preliminary analyses in Chapter 3 and Chapter 6 revealed that some of the largest energy in the ADCP current velocity spectra could be attributed to lower frequency processes associated with periods of five days or greater. No deductions were made with regards to the cause of this periodicities. The effect of Natal pulses or counter currents associated with them could not be analysed given the limited data. Satellite images could have made identification of the Natal pulses possible.

Measurements of temperatures at the ADCP mooring site could not be used to make any deduction about the Agulhas current or natal pulses either, as the temperature measurements where collected at one fixed position only. The temperature measurements change with seasonal changes and they are the only

measurements available for the study. No other temperature measurements from a proximate place were available for comparison. Given that the only information available in this study consisted of Eulerian current measurements, wave and water level measurements, not much can be deducted about the Agulhas current.

# Chapter 8

# Conclusion

In this study the driving forces of currents in a nearshore area are investigated. The study employs current data that was measured over approximately six and a half months. Based on literature, some forces including tides, wind, Stokes drift and the Agulhas current are considered as possible generating forces. These forces are considered for possibility of driving currents and their contribution in the generation of the currents is evaluated.

## 8.1 Brief summary of study

The coastal zone is an attractive area that is sought after for residence, sewage disposal, building of power plants and many more interests. This area also supports a variety of fauna and flora. Thus it is in need of protection and preservation. Any information that aids in the understanding of this zone is of value to society.

A general discussion of the nearshore area, including its location, the ecosystems it supports as well as the dynamics that are particular to it were presented in Chapter 1. Chapter 2 described the driving forces of currents in detail, as well as consider previous studies of these driving forces in the areas in proximity to the ADCP mooring site.

The measured current data were plotted and inspected, autocorrelation analysis followed by spectral analysis were performed on the current data. Three levels of current measurements were used at a distance 2.42 m (bottom), 8.92 m (middle) and 15.92 m (near surface) away from the ADCP. The current speeds and directions were resolved into north-south and east-west velocity components as well as longshore and cross-shore velocity components. Various methods of data presentation were used including summary statistics and progressive vector diagrams. Autocorrelation and power spectral analysis revealed the periodic nature of the data which led to tidal analysis and other

analysis.

In Chapter 4, tidal analysis was performed on water levels and currents using T_Tide. Periodograms of water level measurements revealed that most of the variation in the water level measurements is concentrated around 12 hours and a small amount at 24 hours. These substantiated previous studies that revealed the semi-diurnal tidal nature of the study area (Schumann & Perrins, 1982; Harris, 1978b). Tidal analysis confirmed that the variation in water levels for the entire study period was due to tidal action. The analysis on currents involved analysing currents as velocity vectors and evaluating the variance of measured currents as well as the variance of predicted tidal velocity components to assess the contribution of tides to the generation of the currents. Tides did not contribute significantly to the generation of nearshore currents.

Chapter 5 explores the effect of Stokes drift on the driving of the currents. Stokes drift is computed from collected wave data which includes significant wave heights, peak wave period and wave directions. The standard deviations of the Stokes drift are compared with the standard deviations of the measured current velocities and the importance of Stokes drift in current velocities is evaluated. It was found that the Stokes drift has a negligible contribution to the nearshore currents.

The effect of the wind on surface currents is analysed through the employment of wind roses and the duration that the wind blows from a particular direction is compared with the duration that the current flow towards a particular direction. Common tendencies may imply dependence of the current on the wind. In addition, progressive vector diagrams of currents and winds are also utilized to provide visual comparison. Correlograms of currents and winds are also analysed, significant time scales of the wind and current are compared for any similarity for further substantiation of whether the wind is a driving force of the currents. Lagged cross-correlation between the two variables are also computed to evaluate the response time of the current to changes in the wind, and levels of correlation. Lastly periodograms of currents and winds are compared to observe any similarity in variation. These analyses were performed in Chapter 6, where wind was found to be a driving force of surface currents.

This study is concluded by a small section in Chapter 7 discussing the Agulhas current. Given the limited data used in this study, no educated deductions could be made with regards to the Agulhas current. The tendency of the nearshore current to flow in the general direction of the Agulhas current and results found in literature are used to make an assumption that the Agulhas current may be indirectly influencing nearshore currents.

## 8.2 Findings

The measurements at 2.42 m had an average speed of 7.73 cm/s and the currents mainly flowed towards the south-west more often followed by north-east. At 8.92 m, the currents flow towards the south-west followed by north-east. The flow in other directions was very minimal and the average speed was 10.15 cm/s. At 15.92 m, the currents also flowed towards the south and south-south-west, followed by the north-east direction. The average speed is 24.71 cm/s. Standard deviations from the mean current velocities varied from 18.07 cm/s near the surface to 5.82 cm/s at the bottom. These high standard deviations from mean current velocities indicated the swift changing nature of the water flow at the ADCP mooring site, such that the currents experienced sudden and recurrent changes in both speed and direction.

The techniques used in the various chapters for analysis were not all equally useful, so their effectiveness can be discussed. Progressive vector diagrams were reliable for short periods of time and showed the intensity of currents and their general directions. Autocorrelation was not very useful in the periodic unfiltered time series of currents as it only revealed periodicities which were properly brought out by power spectral analysis. Power spectral analysis is also better carried out using a modified periodogram. T_Tide was useful and gave satisfactory results in the analysis of tides. Stokes drift estimation technique was also efficient. In the analysis of wind and surface currents, wind and current roses together with duration analysis provided a rough idea of how the wind and currents related while progressive vector diagrams substantiated the relation. Autocorrelation was slightly beneficial, and lagged cross-correlation was very important in drawing conclusion on wind and currents. Power spectral analysis was not useful with regards to wind and current analysis. Finally, the conclusion that the Agulhas current is an indirect generator of nearshore currents is based on previous studies as there was not enough information in this study to draw any concrete conclusion.

### Tides

Tidal analysis on water levels revealed recognizable variability at the 12 hour period which coincides with semi-diurnal tides. Almost all the variability in water levels were caused by tides. The waters are dominated by a semi-diurnal and micro-tidal system as tidal amplitude hardly exceeds 2 m.

Tidal analysis on currents produced other results. Tidal velocities were small, but increased from the sea bed towards the surface. Tidal action also seem to have a predominant effect in the cross-shore velocity components as opposed to longshore ones near the surface. All in all, tidal velocity accounts for a limited portion of current velocities. The highest contribution to variance

by tidal currents is at most 37.1%, which occurs at the surface in the cross-shore direction. The findings in this study agrees with previous studies which discovered the limited role of tides in the generation of currents (Schumann & Perrins, 1982; Harris, 1978b).

## Stokes drift

Stokes drift is of minimal importance in the generation of currents at the ADCP mooring site. Estimates of Stokes drift are of very little magnitude compared to the magnitude of the currents. Its effect to variability of nearshore currents is negligible, contributing by at most 6.7% to the variance of currents in the cross-shore direction. The findings are in agreement with the findings by Godin (1948) that in areas that are not characterized by high tides and high amplitude waves Stokes drift is of less than secondary importance.

## Wind

There is a high correlation between the wind and currents. During the period of data collection winds predominantly blew from east-north-east while currents flowed towards west-south-west. That the wind is a driving force of currents is established although the extent was not exactly quantified. The findings agree with those established by Schumann (1988) and Harris (1978b) with regards to winds being driving forces of currents at the ADCP mooring site.

## Agulhas current

The modal direction of flow of the currents in this study was towards the south-west (regardless of weather conditions), which is the same direction followed by the offshore Agulhas current and counter currents opposite to the Natal gyre. Based on previous studies, the Natal gyre and the counter-clockwise currents formed in the Natal Bight do influence the nearshore currents (Harris, 1978b).

By reviewing the results of all the analysis in this study with regards to Equation (1.2.1), it is clear that the techniques chosen only resulted in the quantification of tidal currents ($u_t$) and the wave phenomenon called Stokes drift ($u_s$). Wind currents ($u_w$) could not be quantified and currents driven by the Agulhas current ($u_b$) could not be resolved. In order of importance, $u_w > u_t > u_s$, $u_b$ cannot be quantified as there was not enough information in this study for an in depth analysis.

## 8.3 Future recommendations

- Investigate if the linear addition that was provided in Equation (1.2.1) is appropriate. The reason for this is that currents are vectors and currents resulting from different contributors move in different directions.
- Use sea surface temperature (SST) and altimetry to observe the presence of natal pulses and any variability related to the Agulhas current.
- Use a longer data set to allow for the resolution of more tidal constituents and the the ability to identify the effect of seasonal variations.
- Apply cross-spectral analysis to wind and currents data.

# Appendices

# Appendix A

# Current data

**Figure A.1:** A depiction of some of the current and water level measurements in original file.

Series Data
Broadband 614.4 kHz
Pings/Ens =
Time/Ping = 00:01.00
First Ensemble Date = 12/06/08
First Ensemble Time = 09:00:00.00
Ensemble Interval (s) =
1st Bin Range (m) =
Bin Size (m) =

| Ens | | Tem | Dep | 2.42 | 2.92 | 3.42 | 3.92 | 4.42 | 4.92 | 5.42 | 5.92 | 6.42 | 6.92 | 7.42 | 7.92 | 8.42 | 8.92 | 9.42 | 9.92 | 10.42 | 10.92 | | |
|---|---|---|---|---|---|---|---|---|---|---|---|---|---|---|---|---|---|---|---|---|---|---|---|
| | | deg | m | Mag | Mag | Mag | Mag | Mag | Mag | Mag | Mag | Mag | Mag | Mag | Mag | Mag | Mag | Mag | Mag | Mag | Mag | | |
| | | | | mm/s | mm/s | mm/s | mm/s | mm/s | mm/s | mm/s | mm/s | mm/s | mm/s | mm/s | mm/s | mm/s | mm/s | mm/s | mm/s | mm/s | mm/s | | |
| | | | | 1 | 2 | 3 | 4 | 5 | 6 | 7 | 8 | 9 | 10 | 11 | 12 | 13 | 14 | 15 | 16 | 17 | 18 | | |
| 1 | 2012/06/08 | 09:00 | | 21.56 | 16.516 | 4.9 | 3.7 | 3.3 | 5.7 | 3.5 | 3 | 2.8 | 4.3 | 2.2 | 3.3 | 3.7 | 3 | 4.1 | 4.4 | 2.3 | 1.9 | 1.3 | 1.4 |
| 2 | 2012/06/08 | 09:20 | | 21.75 | 16.086 | 3.1 | 4.5 | 5.7 | 4.4 | 4.3 | 2.8 | 2.9 | 3.9 | 4.4 | 3.8 | 3.6 | 3.1 | 2.1 | 2.3 | 2.6 | 3.8 | 2.9 | 1.1 |
| 3 | 2012/06/08 | 09:40 | | 21.82 | 15.97 | 4.7 | 3.2 | 4.7 | 6.6 | 7.7 | 6.1 | 6.4 | 1 | 3.3 | 4.4 | 5.2 | 2.8 | 3.1 | 2.5 | 2.8 | 4.7 | 2.2 | 2.4 |
| 4 | 2012/06/08 | 10:00 | | 21.9 | 15.846 | 1.9 | 0.4 | 4.9 | 3.9 | 3.3 | 6 | 6.3 | 5.2 | 4.9 | 1.1 | 0.9 | 1.1 | 1.1 | 1.8 | 2.1 | 0.7 | 3 | 3.5 |
| 5 | 2012/06/08 | 10:20 | | 21.96 | 15.726 | 2.2 | 2.4 | 2.4 | 3.7 | 4.8 | 4.3 | 3.4 | 2.7 | 2.6 | 2.7 | 1.4 | 1.4 | 2.8 | 3 | 1 | 2.2 | 3 | 3.5 |
| 6 | 2012/06/08 | 10:40 | | 21.95 | 15.638 | 3.1 | 1.7 | 3.6 | 5.6 | 6.2 | 5.6 | 6.1 | 6.5 | 6.6 | 4.1 | 3.9 | 4.5 | 2.5 | 2.8 | 5.7 | 2.5 | 5.1 | 4.7 |
| 7 | 2012/06/08 | 11:00 | | 21.96 | 15.546 | 3.9 | 3.2 | 4.8 | 4 | 5.4 | 4.2 | 6.7 | 5.8 | 6.4 | 3.3 | 3.7 | 7.9 | 4.7 | 6.6 | 5.1 | 4.9 | 6.9 | 4.1 |
| 8 | 2012/06/08 | 11:20 | | 21.94 | 15.466 | 4.7 | 5.9 | 4.4 | 5.8 | 4.3 | 5.2 | 3.7 | 4.1 | 4.5 | 5.8 | 6.7 | 5.8 | 6.3 | 6.3 | 6.2 | 6.1 | 5.4 | 5.9 |
| 9 | 2012/06/08 | 11:40 | | 21.96 | 15.403 | 7 | 4.6 | 5.1 | 3.8 | 7.5 | 7.4 | 8.3 | 5 | 4.7 | 7.2 | 2.1 | 4.4 | 6.3 | 5.6 | 7 | 8.2 | 6.8 | 5.1 |
| 10 | 2012/06/08 | 12:00 | | 21.94 | 15.418 | 2.7 | 4.5 | 3.2 | 5.7 | 5.1 | 5.7 | 4.2 | 5.2 | 4.1 | 4.4 | 5.9 | 7.6 | 8.5 | 7 | 6.6 | 7.8 | 4.2 | 6.9 |
| 11 | 2012/06/08 | 12:20 | | 21.89 | 15.368 | 5.3 | 8.4 | 8.8 | 11 | 10 | 8.5 | 9.3 | 10.7 | 8.7 | 8.7 | 6.1 | 7.2 | 6.3 | 8.5 | 5.2 | 6.2 | 4.5 | 8.1 |
| 12 | 2012/06/08 | 12:40 | | 21.84 | 15.371 | 5 | 8.6 | 9.9 | 9.7 | 9.9 | 9.4 | 10.4 | 9.1 | 6.3 | 9.2 | 6.1 | 5.2 | 6.5 | 7.4 | 8 | 7.2 | 6.9 | 5.9 |
| 13 | 2012/06/08 | 13:00 | | 21.85 | 15.398 | 10.1 | 7.9 | 7.6 | 8.4 | 8.9 | 8.5 | 7.4 | 9.9 | 7.2 | 7.4 | 7.6 | 7 | 5.5 | 6.6 | 8.2 | 5.5 | 5 | 5.8 |
| 14 | 2012/06/08 | 13:20 | | 21.86 | 15.467 | 7.6 | 6.4 | 6.7 | 7.2 | 7.5 | 8 | 8.8 | 6.9 | 7.2 | 8 | 7 | 7.9 | 6.6 | 6.6 | 6.9 | 8.6 | 7.5 | 9.3 |
| 15 | 2012/06/08 | 13:40 | | 21.89 | 15.572 | 4.7 | 4.2 | 8.1 | 9.9 | 9.7 | 7.7 | 7.3 | 8.6 | 5.3 | 6.2 | 8.9 | 6.6 | 6.3 | 8.3 | 7.5 | 5.4 | 8.5 | 5.4 |
| 16 | 2012/06/08 | 14:00 | | 21.92 | 15.616 | 6.6 | 7 | 9.4 | 9.3 | 7.2 | 9.2 | 10.3 | 8.3 | 7.9 | 7.2 | 8.1 | 7.4 | 4.6 | 8.1 | 9.2 | 6.7 | 6.5 | 7.6 |
| 17 | 2012/06/08 | 14:20 | | 21.96 | 15.735 | 5.8 | 6.4 | 6.2 | 6.8 | 5.8 | 6.1 | 5.4 | 5.3 | 6.4 | 7 | 5.9 | 5.1 | 7 | 5.6 | 2.9 | 5.8 | 6.1 | 8.3 |
| 18 | 2012/06/08 | 14:40 | | 22.01 | 15.798 | 7.8 | 7.5 | 7.6 | 7.6 | 8.7 | 8.3 | 5.1 | 5.4 | 5.7 | 5.6 | 6 | 7.5 | 5.9 | 4.2 | 6.3 | 6.9 | 6.2 | 7.4 |
| 19 | 2012/06/08 | 15:00 | | 22.03 | 15.947 | 8.2 | 4.9 | 7.9 | 9.6 | 6.9 | 7.5 | 6.9 | 6.1 | 5.7 | 6.8 | 6.4 | 4.1 | 6.3 | 3 | 5.3 | 7.6 | 4.9 | 3.9 |
| 20 | 2012/06/08 | 15:20 | | 22.04 | 16.079 | 6.3 | 5 | 6 | 6.6 | 5.5 | 4.9 | 3.2 | 5.7 | 5.6 | 4.6 | 1.9 | 2.3 | 3.3 | 2.7 | 6.1 | 6.2 | 5.8 | 4 |
| 21 | 2012/06/08 | 15:40 | | 22.07 | 16.165 | 4 | 5.7 | 5.3 | 7.9 | 5.9 | 5.2 | 8 | 6.7 | 5.4 | 3.5 | 5.6 | 4.9 | 6.1 | 5.9 | 5.6 | 3.6 | 3.2 | 4.4 |
| 22 | 2012/06/08 | 16:00 | | 22.08 | 16.312 | 5.3 | 4.3 | 4.5 | 5 | 5.6 | 4.1 | 4.8 | 3.3 | 7.5 | 1.8 | 2.8 | 4.3 | 2.8 | 5.1 | 2.8 | 4 | 3.4 | 4.4 |
| 23 | 2012/06/08 | 16:20 | | 22.09 | 16.43 | 4.9 | 4 | 6.1 | 5.8 | 4.7 | 5.2 | 6.6 | 3.9 | 2.1 | 5.8 | 4.1 | 1.5 | 2.1 | 3.8 | 2.7 | 3.5 | 1.4 | 3.2 |
| 24 | 2012/06/08 | 16:40 | | 22.11 | 16.56 | 7.1 | 5.6 | 3.5 | 4.7 | 3.7 | 8.2 | 5.6 | 5.2 | 3.7 | 4.2 | 5.1 | 5.3 | 4.8 | 1 | 3.8 | 4.3 | 3 | 1.9 |
| 25 | 2012/06/08 | 17:00 | | 22.13 | 16.618 | 3.5 | 2.5 | 4.3 | 5.4 | 5.2 | 5.3 | 4.3 | 6.6 | 3.4 | 2.1 | 2 | 5.7 | 2.7 | 3.2 | 5.2 | 3.3 | 2.5 | 3.4 |
| 26 | 2012/06/08 | 17:20 | | 22.14 | 16.705 | 5.7 | 2.8 | 2.9 | 2.7 | 3 | 1.3 | 5.7 | 2.9 | 1.8 | 2.5 | 2.4 | 3 | 4.6 | 2.9 | 3 | 3.1 | 3.3 | 3.1 |
| 27 | 2012/06/08 | 17:40 | | 22.16 | 16.793 | 6.5 | 5.4 | 3.7 | 5.7 | 3.8 | 1.9 | 4.4 | 3.8 | 1.5 | 5.9 | 1.8 | 2.6 | 2.8 | 3.3 | 1.2 | 0.5 | 2.2 | 4.3 |
| 28 | 2012/06/08 | 18:00 | | 22.17 | 16.826 | 5.5 | 4.4 | 2.4 | 2 | 0.5 | 0.9 | 0.6 | 0.6 | 1.6 | 3.6 | 3.4 | 1.1 | 1.7 | 2.2 | 1.4 | 3.6 | 0.5 | 3.5 |
| 29 | 2012/06/08 | 18:20 | | 22.17 | 16.834 | 7.2 | 3.7 | 0.8 | 1.9 | 3.7 | 0.8 | 5.4 | 2.7 | 1.8 | 1.7 | 3 | 0.7 | 1 | 2.2 | 0.9 | 0.1 | 1.4 | 1.9 |
| 30 | 2012/06/08 | 18:40 | | 22.18 | 16.88 | 5.4 | 1.5 | 2.7 | 1.1 | 3.7 | 2.1 | 2.7 | 0.3 | 3.1 | 0.6 | 1.3 | 1.7 | 0.4 | 0.1 | 0.8 | 2.9 | 0.4 | 1.5 |
| 31 | 2012/06/08 | 19:00 | | 22.2 | 16.859 | 6.7 | 1.8 | 3 | 3.9 | 4.1 | 3.4 | 4 | 1.4 | 1.3 | 1.1 | 3.8 | 3.8 | 2.2 | 2 | 1.5 | 3.6 | 2.8 | 2.6 |
| 32 | 2012/06/08 | 19:20 | | 22.2 | 16.833 | 5.4 | 2.9 | 1.3 | 2.6 | 2.3 | 1.6 | 3 | 1.2 | 2.3 | 3.4 | 0.7 | 2 | 1.9 | 2.2 | 1.6 | 3.7 | 2.2 | 1.7 |
| 33 | 2012/06/08 | 19:40 | | 22.2 | 16.808 | 5.2 | 3.2 | 2.3 | 3.7 | 1.9 | 2.6 | 0.5 | 3.6 | 3.8 | 4.7 | 2.5 | 3.9 | 3.3 | 2.5 | 4.5 | 2.6 | 3 | 2.8 |
| 34 | 2012/06/08 | 20:00 | | 22.23 | 16.707 | 6.1 | 3.1 | 2.9 | 0.9 | 2.8 | 3.5 | 1.4 | 3 | 2.6 | 1.2 | 3.3 | 1.6 | 4.2 | 1.6 | 3.2 | 3.2 | 2.5 | 2.8 |
| 35 | 2012/06/08 | 20:20 | | 22.22 | 16.634 | 7.3 | 5.6 | 1.1 | 4.7 | 2.7 | 3 | 3 | 1.3 | 2.1 | 2.6 | 1 | 4.7 | 2.2 | 2.8 | 2.1 | 3.4 | 4.1 | 2.5 |
| 36 | 2012/06/08 | 20:40 | | 22.25 | 16.533 | 8.4 | 4.4 | 0.8 | 2.8 | 2.8 | 3.8 | 1.9 | 1.4 | 3.2 | 2.1 | 2.7 | 1.4 | 0.3 | 2.8 | 3.1 | 4 | 4.3 | 2.1 |
| 37 | 2012/06/08 | 21:00 | | 22.26 | 16.454 | 5.1 | 2.4 | 2.5 | 1.8 | 1.2 | 0.2 | 1.5 | 3.2 | 1.9 | 1.8 | 0.7 | 1.5 | 1.2 | 3.6 | 3.2 | 3.5 | 1.8 | 3.1 |
| 38 | 2012/06/08 | 21:20 | | 22.26 | 16.326 | 5.3 | 0.6 | 2 | 2.1 | 1.7 | 2.9 | 2.4 | 3 | 2.7 | 2.2 | 3.3 | 0.9 | 3.3 | 1.1 | 2.8 | 2.7 | 1.7 | 2.9 |
| 39 | 2012/06/08 | 21:40 | | 22.26 | 16.215 | 4.8 | 1.7 | 0.6 | 1.6 | 1.7 | 1.4 | 2.1 | 1.1 | 2.1 | 2.7 | 1.2 | 3 | 0.9 | 2.8 | 1.7 | 1.6 | 1.6 | 2.4 |
| 40 | 2012/06/08 | 22:00 | | 22.28 | 16.119 | 5.6 | 1.9 | 2.3 | 3 | 2.1 | 3.4 | 2 | 2.7 | 3.1 | 1.6 | 0.9 | 2.3 | 2.5 | 2.9 | 1.4 | 3.9 | 0.7 | 0.6 |

**Table A.1:** The mean speeds for all seven periods at all twenty nine bins or distances measured from the ADCP.

| Mean peed (cm/s) | | | | | | | |
|---|---|---|---|---|---|---|---|
| Level | Period 0 | Period 1 | Period 2 | Period 3 | Period 4 | Period 5 | Period 6 |
| 2.42 m | 7.55 | 9.81 | 6.68 | 7.63 | 5.85 | 8.76 | 8.20 |
| 2.92 m | 7.49 | 8.23 | 6.77 | 7.87 | 6.13 | 8.51 | 8.40 |
| 3.42 m | 7.60 | 7.76 | 6.61 | 8.14 | 6.17 | 8.65 | 8.65 |
| 3.92 m | 7.81 | 7.86 | 6.63 | 8.45 | 6.40 | 8.93 | 8.86 |
| 4.42 m | 8.01 | 7.90 | 6.73 | 8.69 | 6.64 | 9.22 | 9.10 |
| 4.92 m | 8.32 | 7.99 | 6.88 | 8.95 | 6.81 | 9.57 | 9.41 |
| 5.42 m | 8.47 | 8.08 | 7.05 | 9.25 | 7.07 | 9.90 | 9.65 |
| 5.92 m | 8.67 | 8.18 | 7.18 | 9.49 | 7.27 | 10.22 | 9.89 |
| 6.42 m | 8.90 | 8.31 | 7.38 | 9.73 | 7.51 | 10.53 | 10.15 |
| 6.92 m | 8.91 | 8.38 | 7.46 | 9.95 | 7.74 | 10.89 | 10.46 |
| 7.42 m | 9.18 | 8.47 | 7.62 | 10.24 | 7.99 | 11.25 | 10.78 |
| 7.92 m | 9.31 | 8.62 | 7.72 | 10.47 | 8.26 | 11.54 | 11.08 |
| 8.42 m | 9.48 | 8.69 | 7.89 | 10.74 | 8.59 | 11.90 | 11.37 |
| 8.92 m | 9.61 | 8.80 | 8.05 | 10.93 | 8.89 | 12.26 | 11.67 |
| 9.42 m | 9.75 | 8.94 | 8.12 | 11.22 | 9.21 | 12.63 | 11.94 |
| 9.92 m | 10.01 | 9.00 | 8.28 | 11.40 | 9.53 | 13.01 | 12.29 |
| 10.42 m | 10.02 | 9.06 | 8.40 | 11.64 | 9.91 | 13.35 | 12.59 |
| 10.92 m | 10.25 | 9.21 | 8.56 | 11.90 | 10.29 | 13.74 | 12.93 |
| 11.42 m | 10.37 | 9.23 | 8.67 | 12.15 | 10.67 | 14.14 | 13.28 |
| 11.92 m | 10.41 | 9.26 | 8.82 | 12.42 | 11.05 | 14.59 | 13.61 |
| 12.42 m | 10.54 | 9.39 | 9.00 | 12.62 | 11.52 | 15.00 | 13.95 |
| 12.92 m | 10.62 | 9.60 | 9.13 | 12.90 | 11.92 | 15.46 | 14.36 |
| 13.42 m | 10.77 | 9.61 | 9.26 | 13.20 | 12.41 | 15.94 | 14.98 |
| 13.92 m | 10.98 | 9.72 | 9.47 | 13.52 | 13.14 | 16.62 | 15.42 |
| 14.42 m | 11.14 | 9.99 | 9.87 | 14.18 | 14.03 | 17.35 | 16.05 |
| 14.92 m | 12.28 | 11.67 | 11.27 | 15.89 | 15.90 | 18.17 | 17.06 |
| 15.42 m | 14.41 | 14.65 | 14.41 | 20.37 | 18.53 | 20.19 | 19.31 |
| 15.92 m | 23.03 | 21.89 | 20.69 | 26.57 | 25.36 | 27.71 | 24.87 |
| 16.42 m | 35.41 | 33.61 | 31.82 | 36.67 | 34.73 | 37.76 | 35.82 |

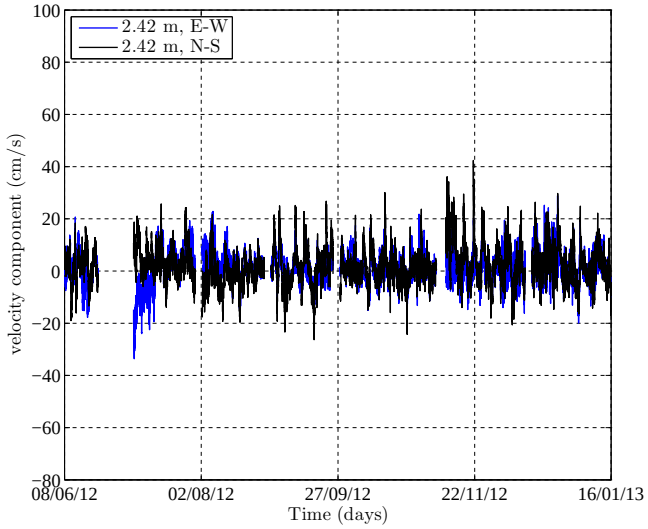


**Figure A.2:** Time series of the east-west and north-south velocity components at 2.42 m.

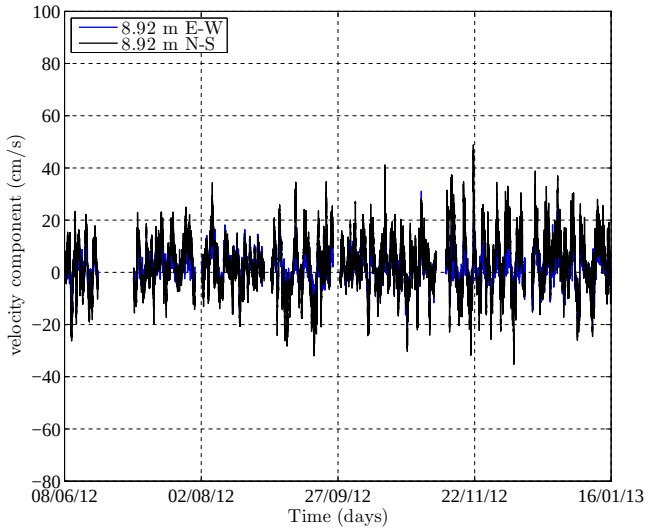


**Figure A.3:** Time series of the east-west and north-south velocity components at 8.92 m.

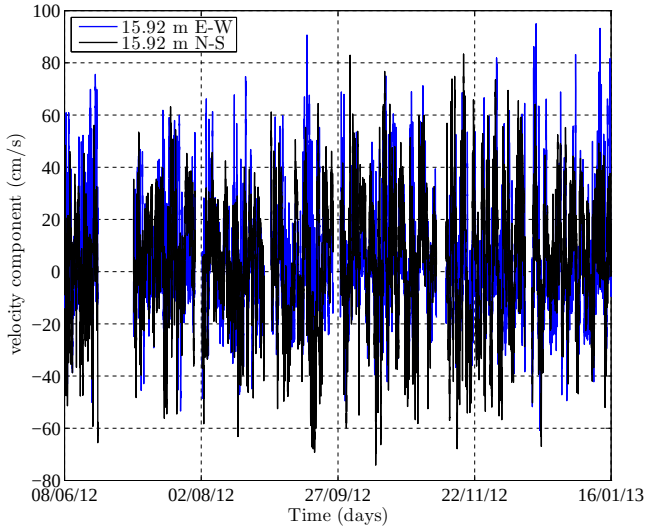


**Figure A.4:** Time series of the east-west and north-south velocity components at 15.92 m.


**Figure A.5:** Picture showing the orientation of the coast where data that is used in this study was collected.

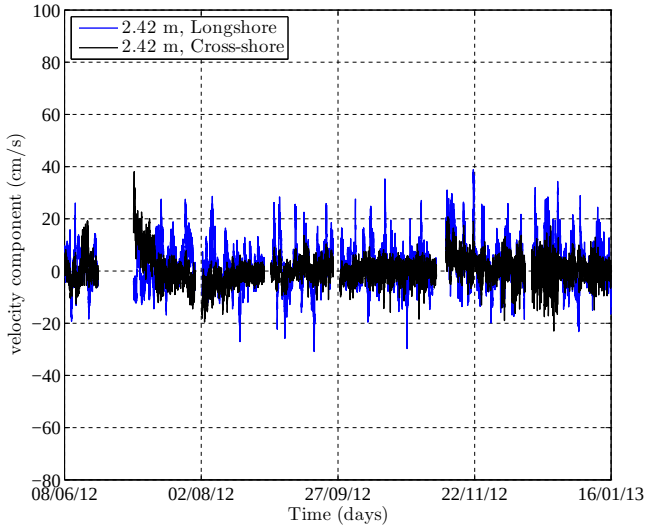


**Figure A.6:** Time series of the cross-shore and longshore velocity components at 2.42 m.

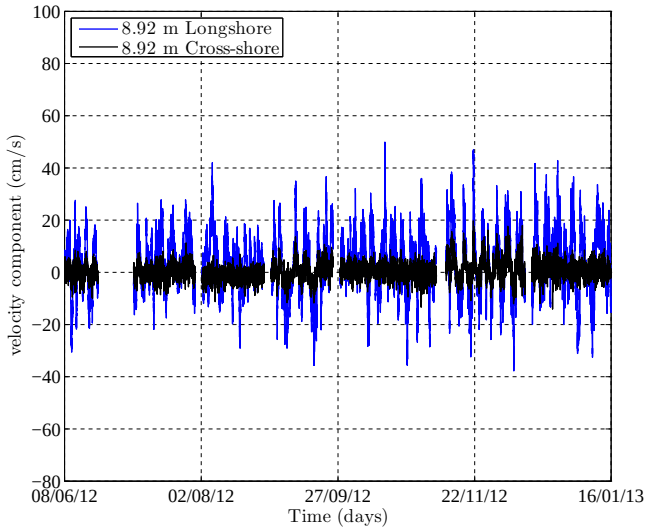


**Figure A.7:** Time series of the cross-shore and longshore velocity components at 8.92 m.

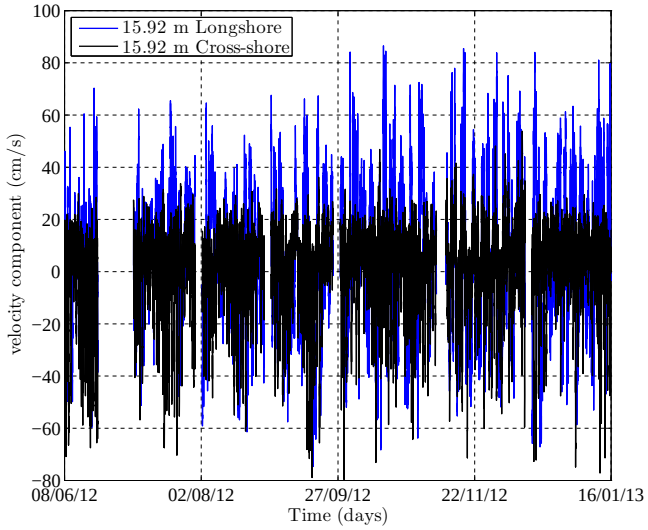


**Figure A.8:** Time series of the cross-shore and longshore velocity components at 15.92 m.

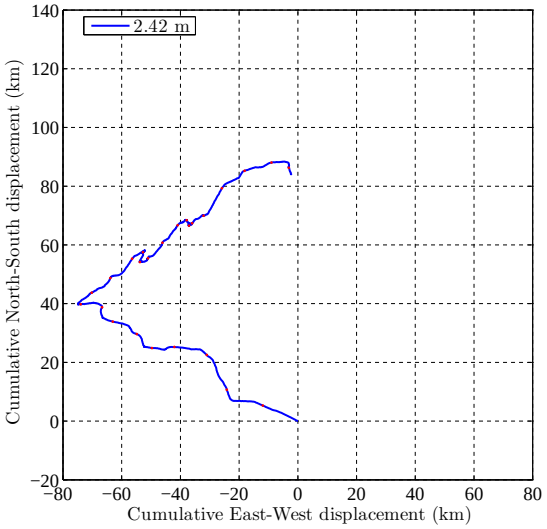


**Figure A.9:** PVD of the east-west and north-south velocity components at 2.42 m for period 1.

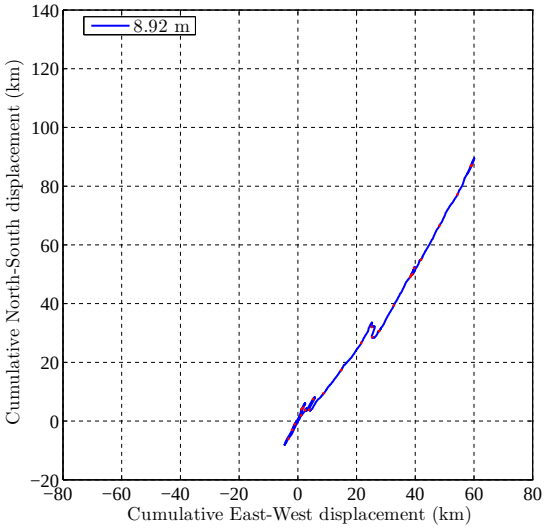


**Figure A.10:** PVD of the east-west and north-south velocity components at 8.92 m for period 1.

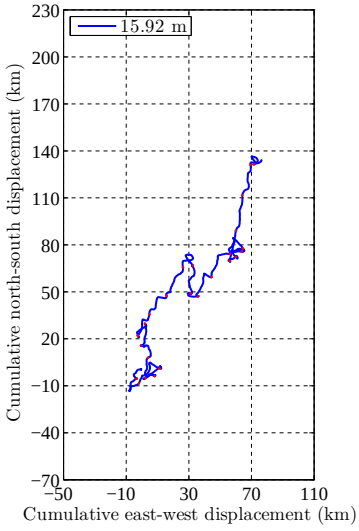


**Figure A.11:** PVD of the east-west and north-south velocity components at 15.92 m for period 1.

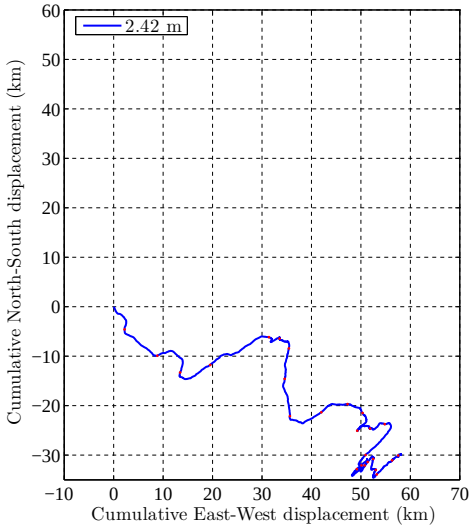


**Figure A.12:** PVD of the east-west and north-south velocity components at 2.42 m for period 2.

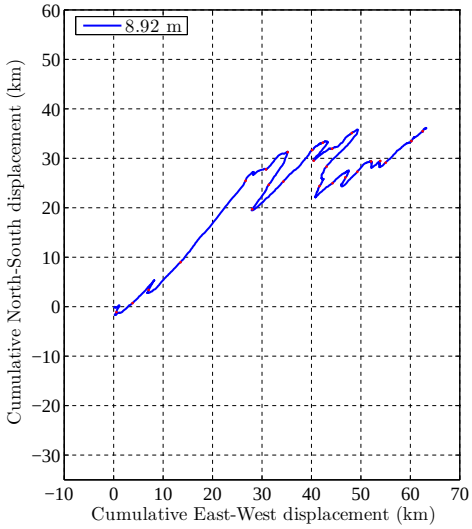


**Figure A.13:** PVD of the east-west and north-south velocity components at 8.92 m for period 2.

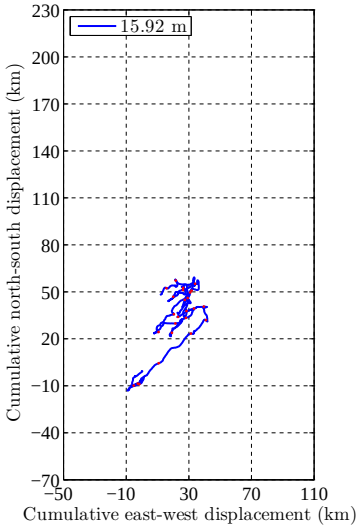


**Figure A.14:** PVD of the east-west and north-south velocity components at 15.92 m for period 2.

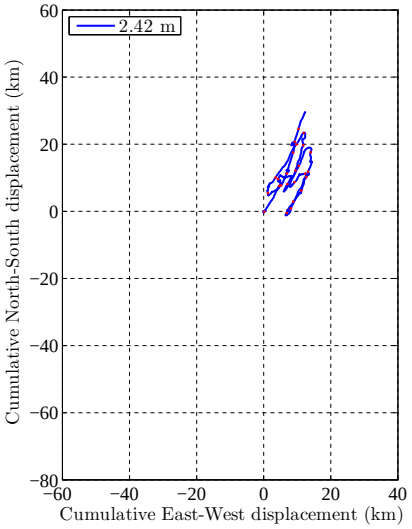


**Figure A.15:** PVD of the east-west and north-south velocity components at 2.42 m for period 3.

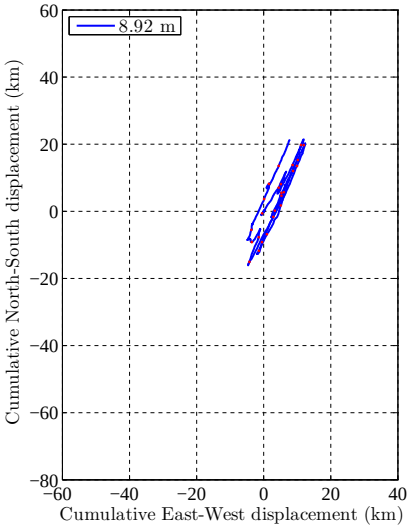


**Figure A.16:** PVD of the east-west and north-south velocity components at 8.92 m for period 3.

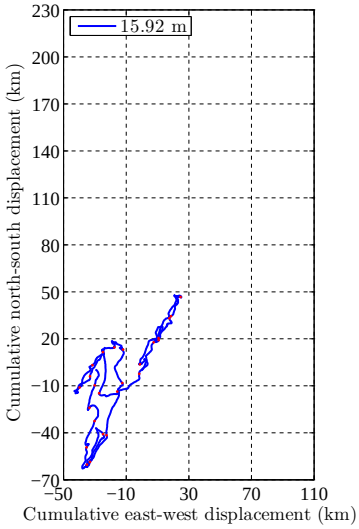


**Figure A.17:** PVD of the east-west and north-south velocity components at 15.92 m for period 3.

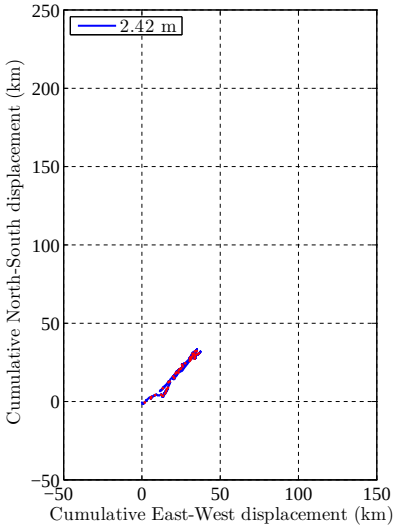


**Figure A.18:** PVD of the east-west and north-south velocity components at 2.42 m for period 4.

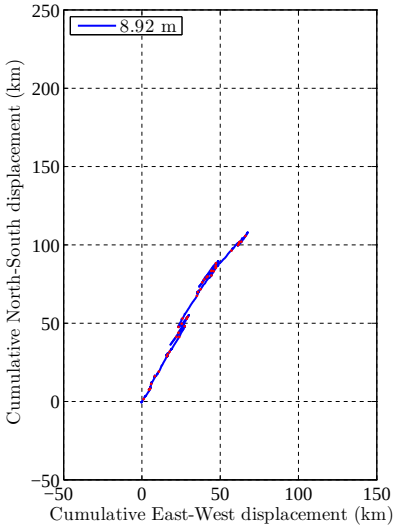


**Figure A.19:** PVD of the east-west and north-south velocity components at 8.92 m for period 4.

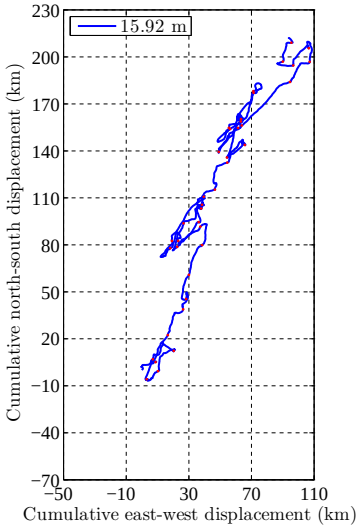


**Figure A.20:** PVD of the east-west and north-south velocity components at 15.92 m for period 4.

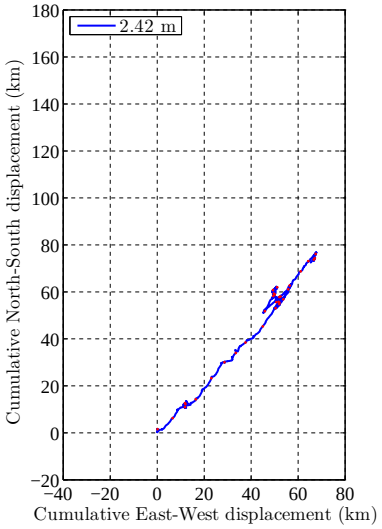


**Figure A.21:** PVD of the east-west and north-south velocity components at 2.42 m for period 6.

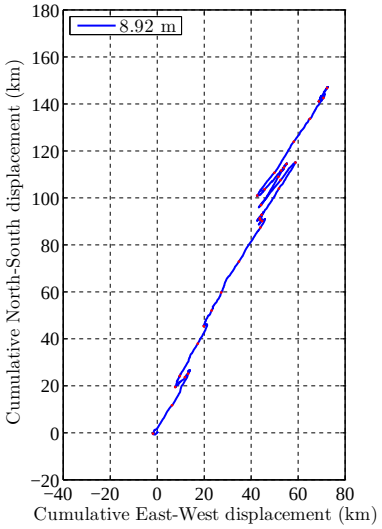


**Figure A.22:** PVD of the east-west and north-south velocity components at 8.92 m for period 6.

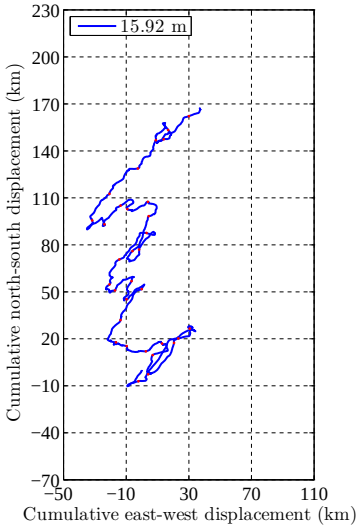


**Figure A.23:** PVD of the east-west and north-south velocity components at 15.92 m for period 6.

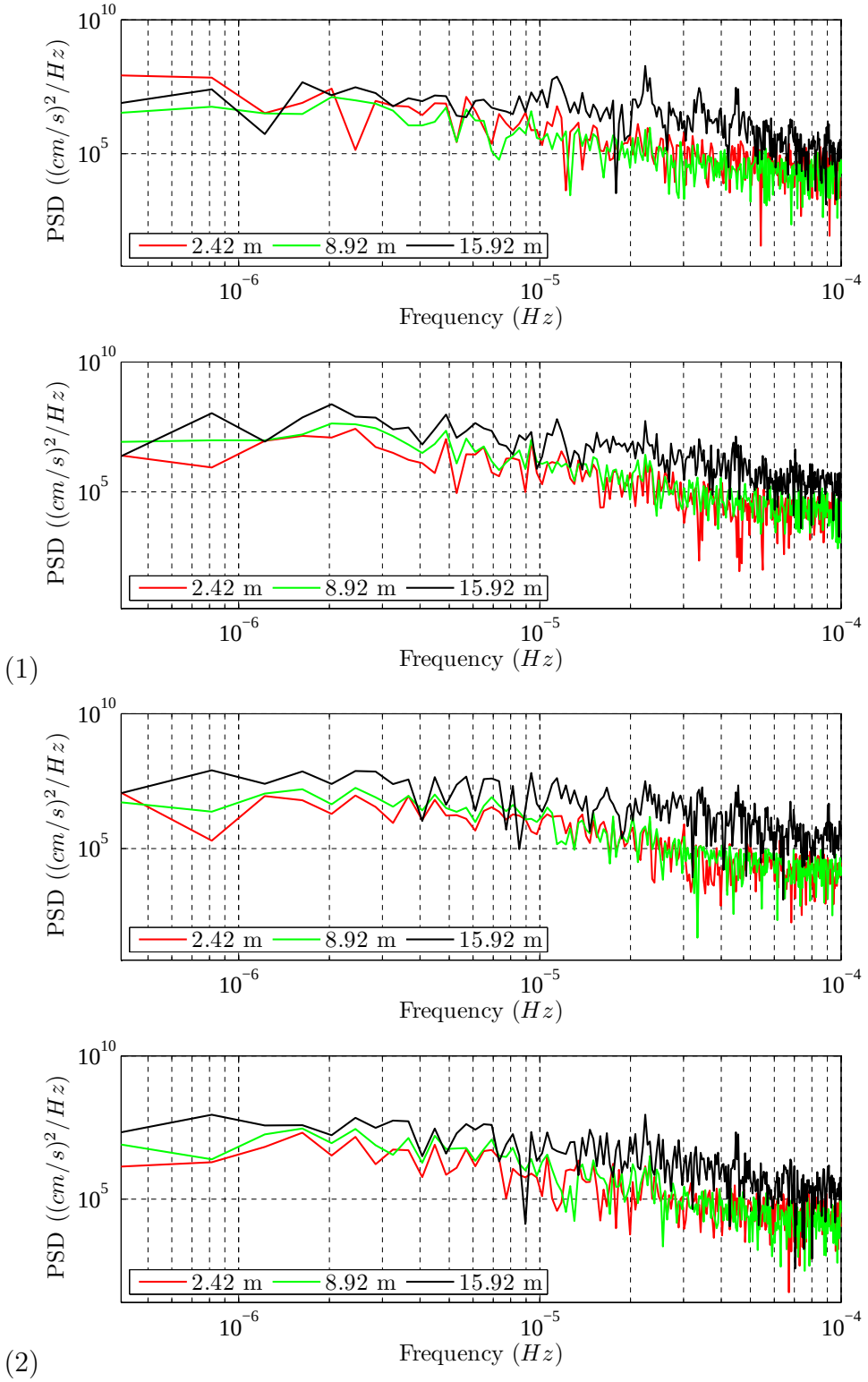


**Figure A.24:** Periodograms of currents for period one and two. In each figure, the top panel is of east-west velocity components and the bottom panel is of north-south velocity components.

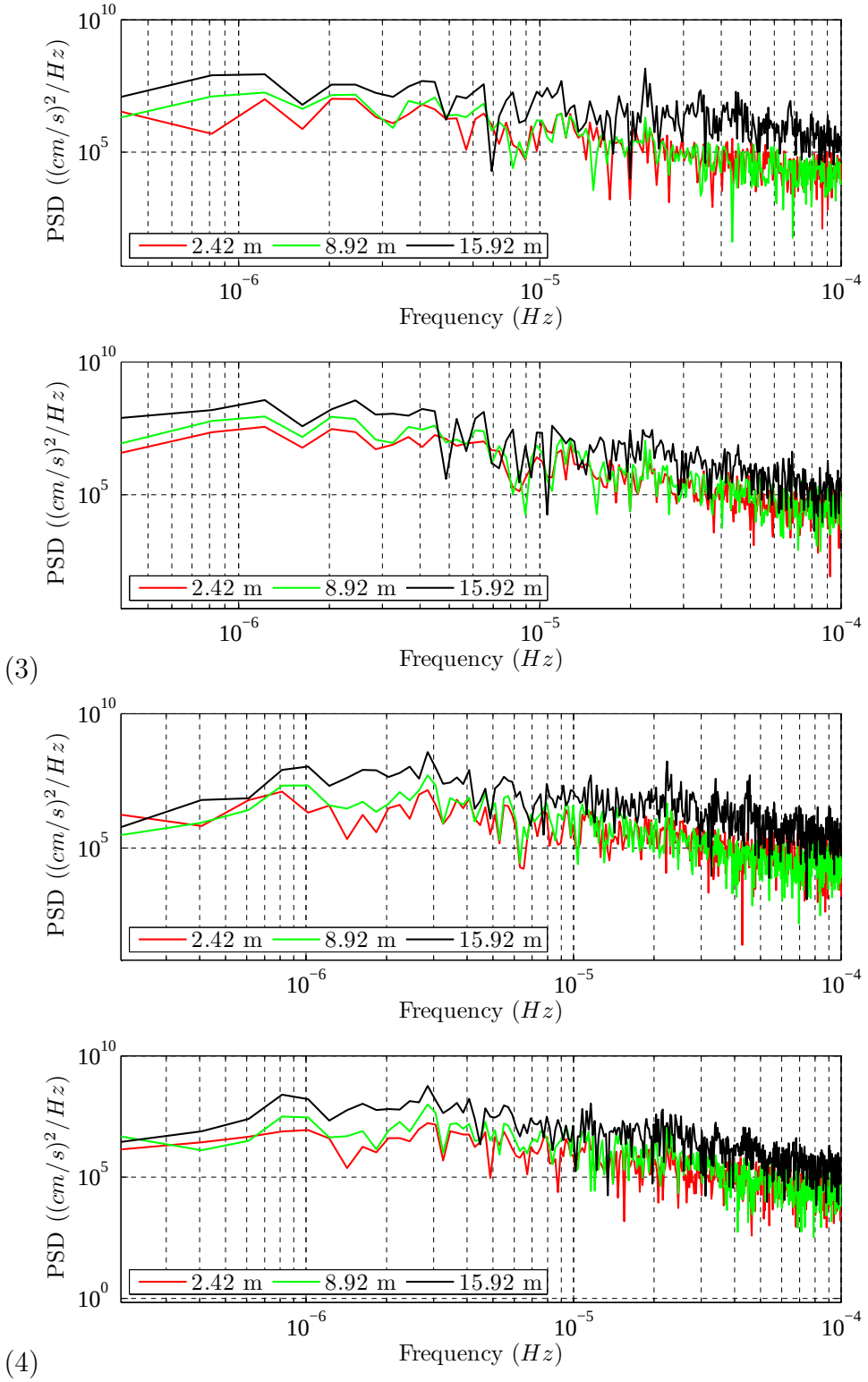


**Figure A.25:** Periodograms of currents for period three and four. In each figure, the top panel is of east-west velocity components and the bottom panel is of north-south velocity components.

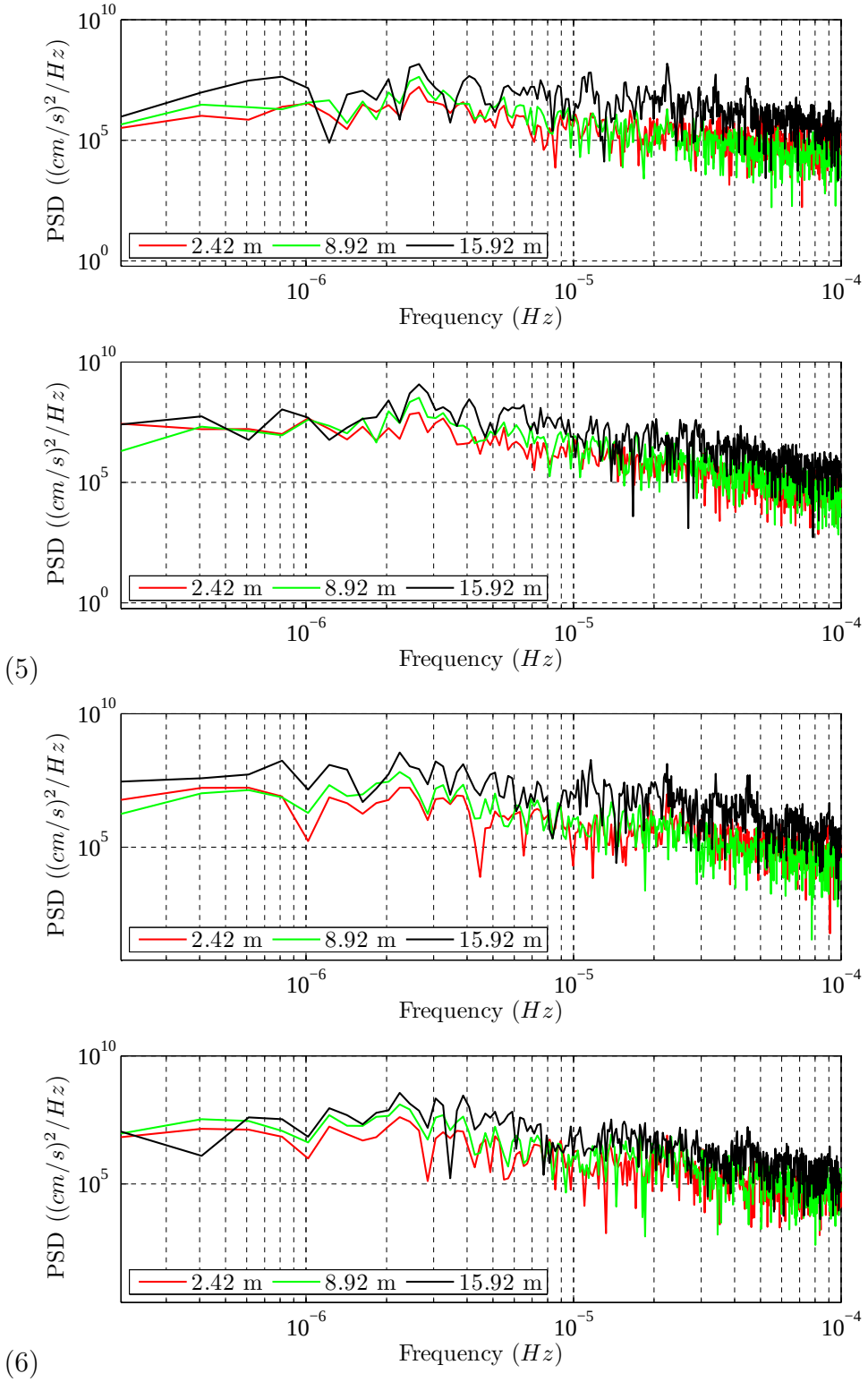


**Figure A.26:** Periodograms of currents for period five and six. In each figure, the top panel is of east-west velocity components and the bottom panel is of north-south velocity components.

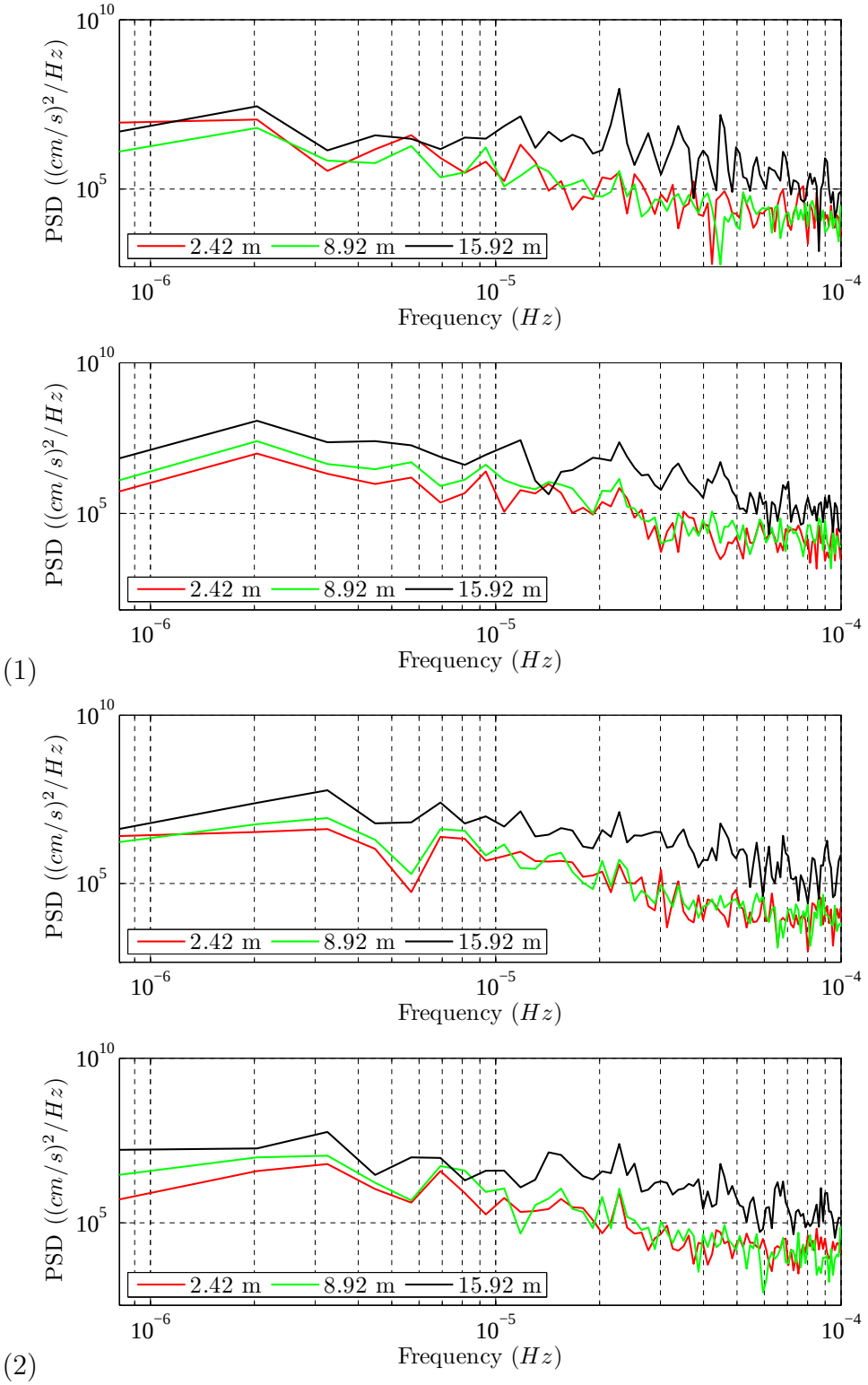


**Figure A.27:** Periodograms of currents for period one and two. In each figure, the top panel is of east-west velocity components and the bottom panel is of north-south velocity components. These were obtained through a modified periodogram.

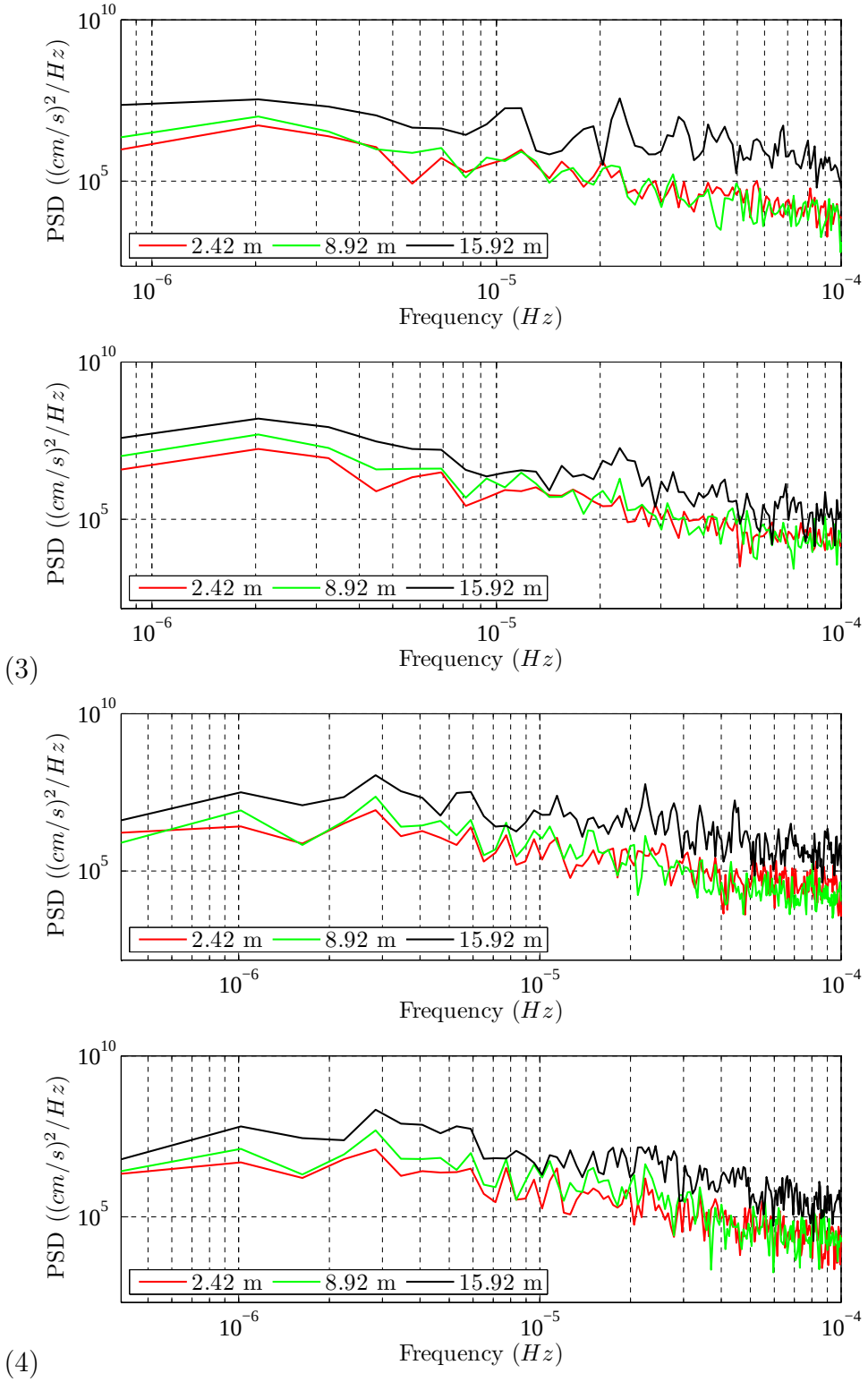


**Figure A.28:** Periodograms of currents for period three and four. In each figure, the top panel is of east-west velocity components and the bottom panel is of north-south velocity components. These were obtained through a modified periodogram.

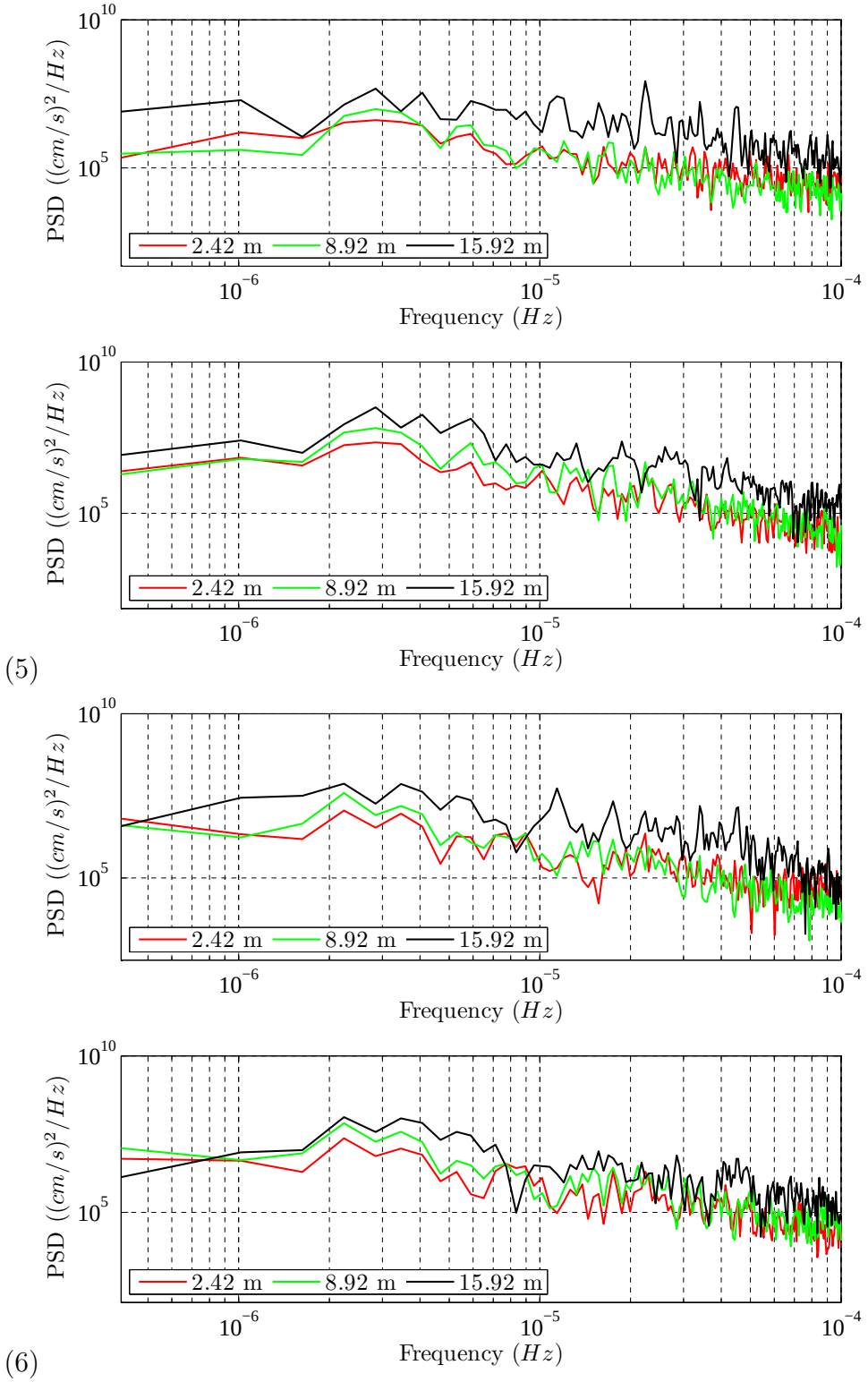


**Figure A.29:** Periodograms of currents for period five and six. In each figure, the top panel is of east-west velocity components and the bottom panel is of north-south velocity components. These were obtained through a modified periodogram.

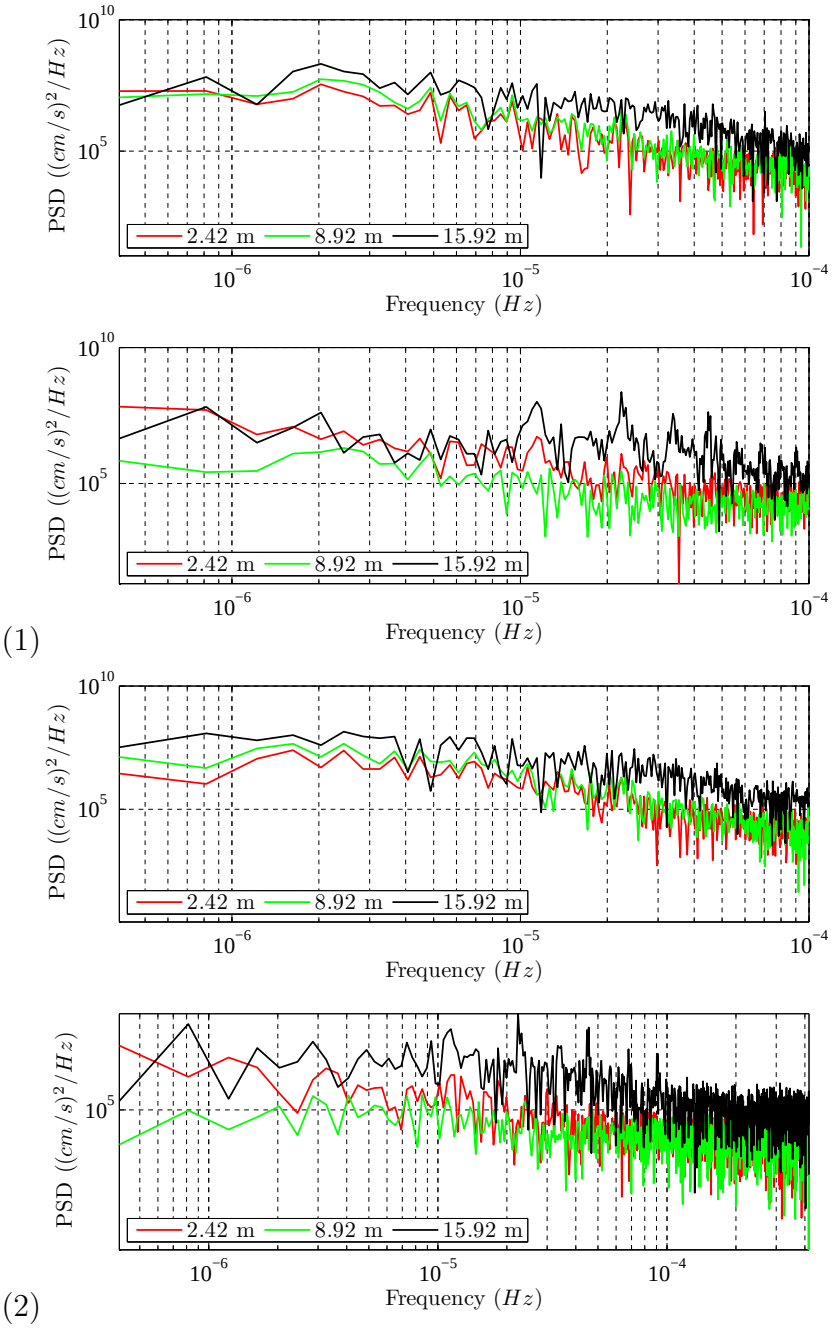


**Figure A.30:** Periodograms of currents for period one and two. In each figure, the top panel is of longshore velocity components and the bottom panel is of cross-shore velocity components.

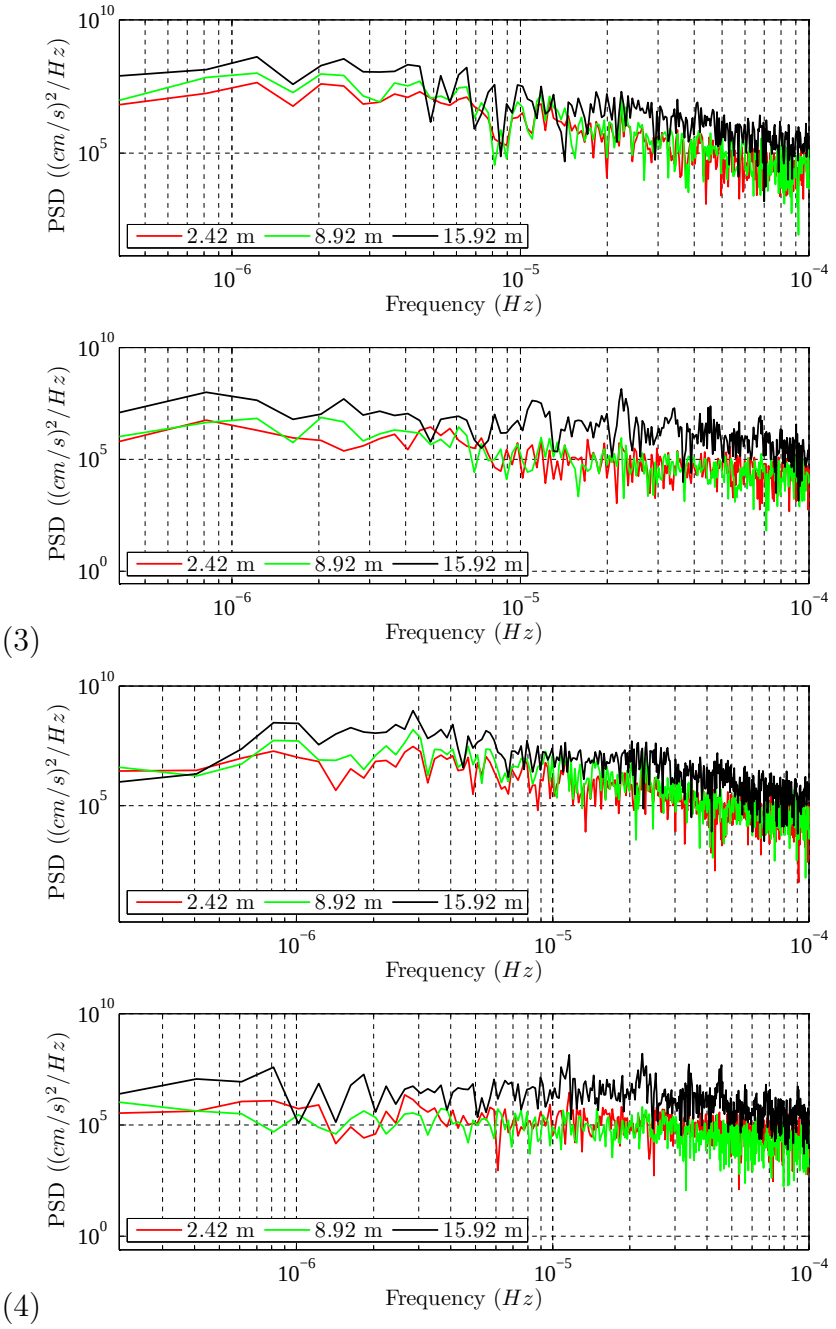


**Figure A.31:** Periodograms of currents for period three and four. In each figure, the top panel is of longshore velocity components and the bottom panel is of cross-shore velocity components.

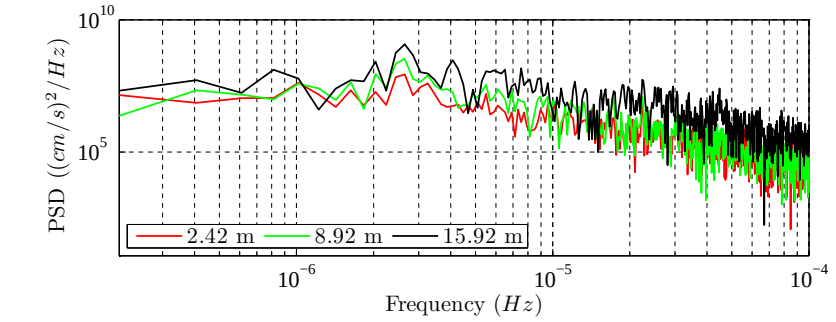


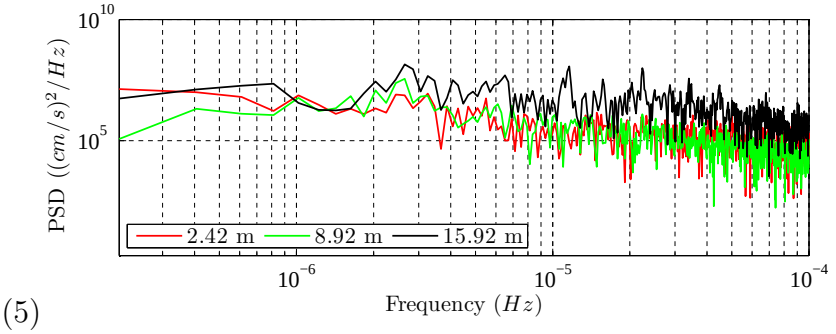


(5)

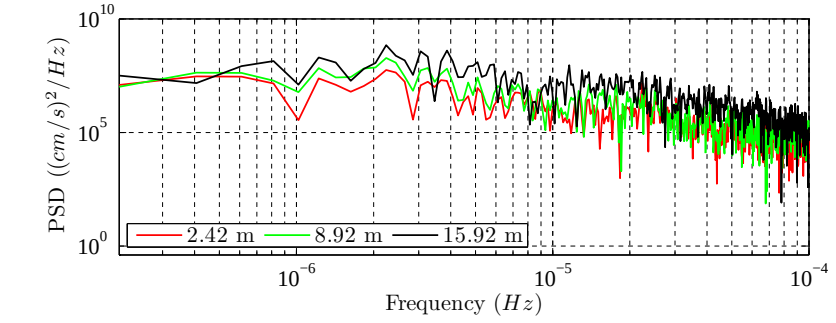


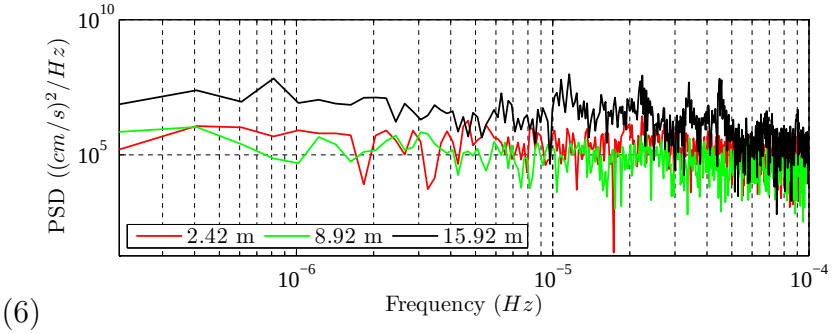


(6)

**Figure A.32:** Periodograms of currents for period five and six. In each figure, the top panel is of longshore velocity components and the bottom panel is of cross-shore velocity components.

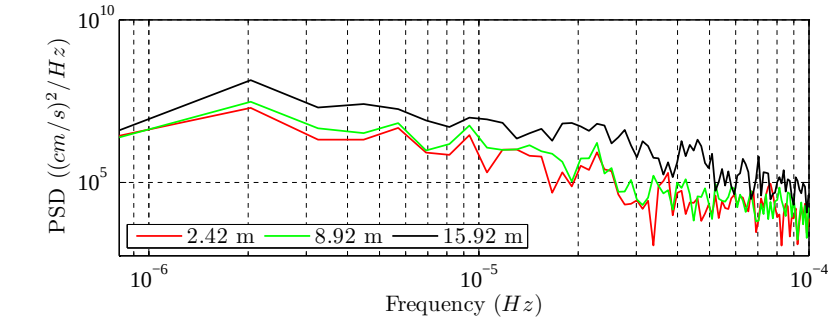


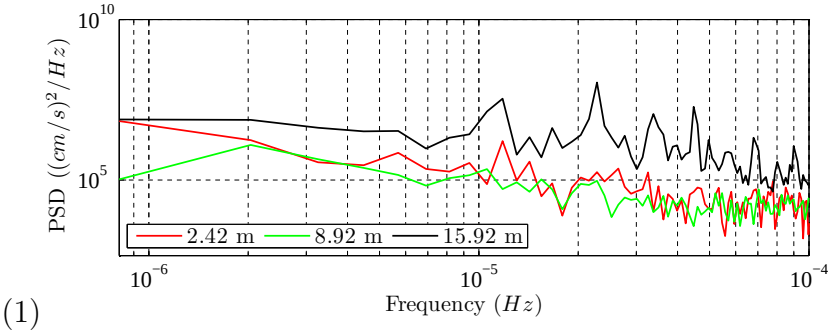


(1)

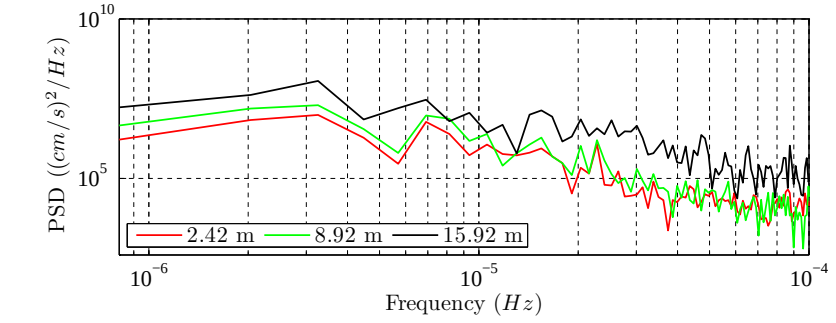


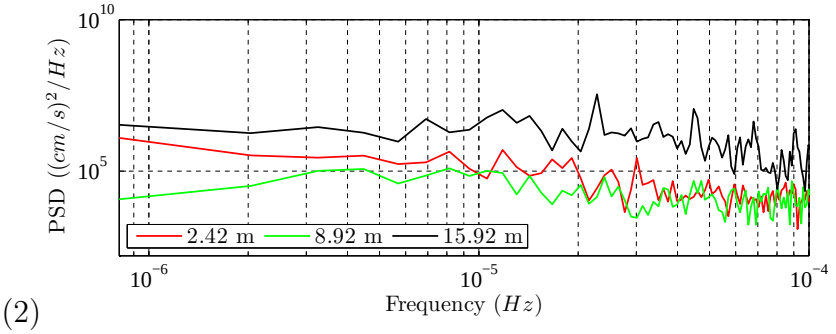


(2)

**Figure A.33:** Periodograms of currents for period one and two. In each figure, the top panel is of longshore velocity components and the bottom panel is of cross-shore velocity components. These were obtained through a modified periodogram.

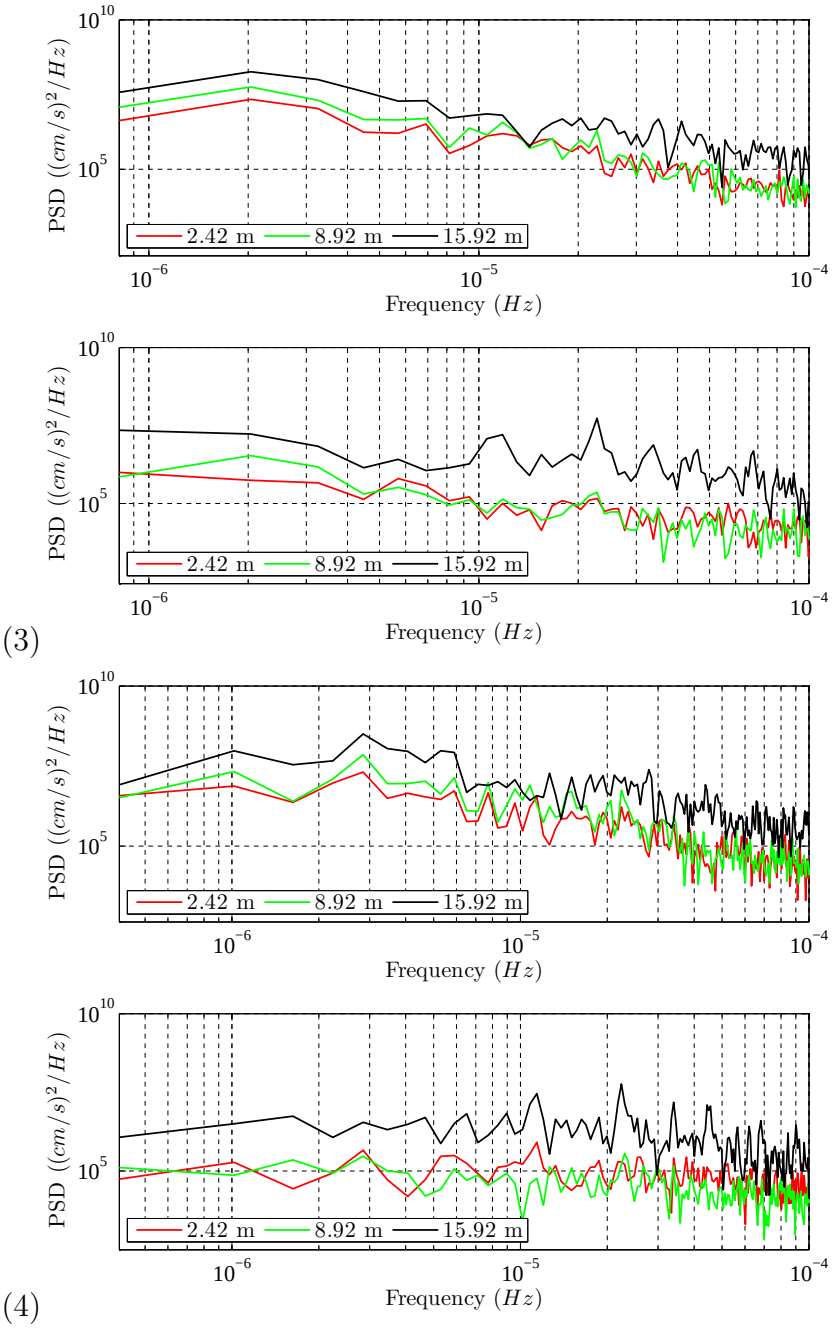


**Figure A.34:** Periodograms of currents for period three and four. In each figure, the top panel is of longshore velocity components and the bottom panel is of cross-shore velocity components. These were obtained through a modified periodogram.

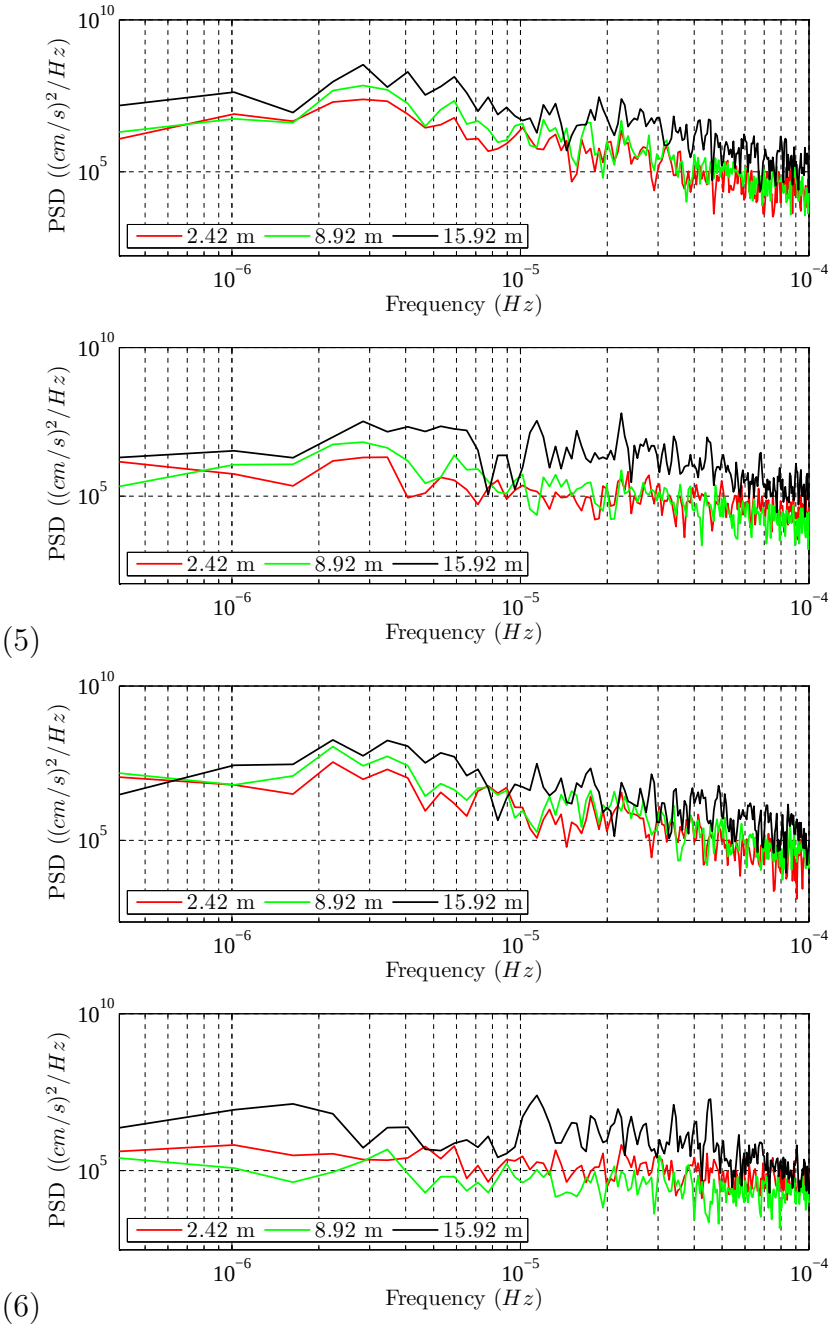


**Figure A.35:** Periodograms of currents for period five and six. In each figure, the top panel is of longshore velocity components and the bottom panel is of cross-shore velocity components. These were obtained through a modified periodogram.

# Appendix B

# Matlab autocorrelation code

```
function t = auto_c_f(x,n)
% auto_c_f — Calculate autocorrelations for n lags
% >> the_auto_cf = auto_c_f(x,n)
%
% Inputs:
% x — the series to calculate autocorrelation coefficients for,
    colum
% vector of size nx1
% n — length of lags, size 1x1 (integer)
%
% Output:
% THE_AUTO_CF —  vector of size nx1 containing autocorrelation
    coefficients
%       (First lag used in calculations is lag 1, 0th lag not
    used in calculations)
%
%
% Produces a bar graph of the autocorrelation coefficients.%
    Bartlett for testing individual autocorrelation coefficients
    = 0.
%
%
% ------------------------------------------------------
% Check Inputs
% ------------------------------------------------------

[p1, p2] = size(x) ;
if p2 ~=1
    error('Input x must be a column vector of size nx1')
end

[a_1, a_2] = size(n) ;
if ~((a_1==1 & a_2==1) & (n<p1))
    error('Input n is an integer, of size 1x1, and must be a
       length less than that m of series x')
end



% ------------------------------------------------------
%  Beginning of code
% ------------------------------------------------------
```

```
t = zeros(n,1) ;
global M
M = max(size(x)) ;
global xbar
xbar = mean(x);

% Collect autocorrelation coefficients at each ith lag
for i = 1:n
   t(i) = auto_c_f_k(x,i) ;
end

% Plot correlogram
% Plot Bartlet lines
% H_0: rho(tau) = 0 at alpha=0.05
bar(t)
Bart([0 n+.5], (1.96)*(1/sqrt(M))*ones(1,2))
Bart([0 n+.5], (-1.96)*(1/sqrt(M))*ones(1,2))

% Some figure properties
Bart_hi = (1.96)*(1/sqrt(M))+0.05;
Bart_lo = -(1.96)*(1/sqrt(M))-0.05;
bar_hi = max(t)+0.05 ;
bar_lo = -max(t)-0.05 ;

if (abs(Bart_hi) > abs(bar_hi)) % if Bartlett lines may not
   appear on graph
    axis([0 n+.60 Bart_lo Bart_hi])
else
    axis([0 n+.60 bar_lo bar_hi])
end
title('Autocorrelation coefficients')
xlabel('Lags ')
set(gca,'YTick',[-1:.20:1])
% set number of lag labels shown
if (n<28 & n>4)
    set(gca,'XTick',floor(linspace(1,n,4)))
elseif (n>=28)
    set(gca,'XTick',floor(linspace(1,n,8)))
end
set(gca,'TickLength',[0 0])
```

```
% ------------------------------------------------
% second function
% ------------------------------------------------
function t2 = auto_c_f_k(x,k)
% AUTO_C_F_K - Autocorrelation at the kth lag
% auto_c_f(x,k)
%
% Inputs:
% x - series to compute autocorrelation coefficients for
% k -the lag at which to compute autocorrelation coefficient
%
global xbar
global M
cross_sum = zeros(M-k,1) ;

% unscaled covariance as numerator,
for i = (k+1):M
    cross_sum(i) = (x(i)-xbar)*(x(i-k)-xbar) ;
end

% unscaled variance as denominator,
xvar = (x-xbar)'*(x-xbar) ;

t2 = sum(cross_sum) / xvar ;
```

# Appendix C

# Fast Fourier Transform and Gibb's phenomenon

## C.1 Fast Fourier transform

Fast Fourier transform (FFT) refers to a fast algorithm that calculates a discrete Fourier transform (DFT) or inverse DFT. For an even faster computation, the sample size, $N$, must be a power of 2. The series can be padded with zeroes to achieve this.

Given a series of $N$ observations for which $N = 2^p$ (where $p$ is a positive integer), the DFT of this series requires $N^2$ operations. On the other hand, the FFT algorithm requires only $Nlog_2N$ operations (Baher, 2012). This leads to a reduction in computational time, making FFT more efficient. This efficiency is important for large values of $N$, as the DFT has computational time of order $O(N)^2$ while the FFT has computational time of order $O(N)$ (Emery & Thomson, 2004). Following is a presentation of how FFT works.

Consider a time series, $x_t$ where $t = 1, 2, ..., N$. To obtain the discrete Fourier transform $X_k = X(k/N\Delta t)$ where $k = 0, 1, 2, ..., N$, the series is divided into 2 halves, $Y_t$ and $Z_t$, where $Y_t = x_{2t-1}$, $Z_t = x_{2t}$ and $t = 1, 2, ..., N/2$.

The DFTs are as follows:

$$\begin{aligned} Y_k^{N/2} &= \frac{2}{N}\sum_{t=1}^{N/2} y_t \exp\left[\frac{(-\mathrm{i}4\pi tk)}{N}\right] \\ Z_k^{N/2} &= \frac{2}{N}\sum_{t=1}^{N/2} z_t \exp\left[\frac{(-\mathrm{i}4\pi tk)}{N}\right]. \end{aligned}$$

The superscripts indicate the number of terms in the expansion. $X_t, Y_t$ and $Z_t$ are related since,

$$\begin{aligned} X_k^N &= \frac{2}{N}\sum_{t=1}^{N/2} y_t \exp\left[\frac{(-\mathrm{i}4\pi tk)}{N}\right] \\ &= \frac{1}{N}\sum_{t=1}^{N/2} y_t \exp\left\{\left[\frac{(-\mathrm{i}4\pi tk)}{N}(2t-1)\right] + \left[\frac{(-\mathrm{i}4\pi tk)}{N}(2t)\right]\right\} \\ &= \frac{1}{2}\exp\left[\frac{(\mathrm{i}2\pi k)}{N}\right] Y_k^{N/2} + \frac{1}{2}Z_k^{N/2} \text{ where } 0 \leq k \leq (N/2)-1, \end{aligned}$$

and

$$\begin{aligned} Y_{k+N/2}^N &= Y_k^{N/2}; \quad 0 \leq k \leq (N/2)-1 \\ Z_{k+N/2}^N &= Z_k^{N/2}; \quad 0 \leq k \leq (N/2)-1. \end{aligned}$$

This implies that:

$$\begin{aligned} X_{k+N/2}^N &= \frac{1}{2}\exp\left[\mathrm{i}\left(\frac{2\pi}{N}\right)\left(k+\frac{N}{2}\right)\right] Y_k^{N/2} + \frac{1}{2}Z_k^{N/2} \\ &= -\frac{1}{2}\exp\left[\mathrm{i}\left(\frac{2\pi k}{N}\right)\right] Y_k^{N/2} + \frac{1}{2}Z_k^{N/2}, \ 0 \ \leq k \leq (N/2)-1. \end{aligned}$$

As a result,

$$X_k^N = \frac{1}{2}\exp\left[\mathrm{i}\left(\frac{2\pi k}{N}\right)\right] Y_k^{N/2} + \frac{1}{2}Z_k^{N/2}, \ 0 \ \leq k \leq (N/2)-1$$

and

$$X_{k-N/2}^N = -\frac{1}{2}\exp\left[\mathrm{i}\left(\frac{2\pi k}{N}\right)\right] Y_k^{N/2} + \frac{1}{2}Z_k^{N/2}, \ 0 \ \leq k \leq (N/2)-1$$

This explains how a discrete Fourier transform is obtainable through the two half series, $Z_t$ and $Y_t$, and the advantage of DFT symmetry. Since the size of each of the series is an even number, $N/2$, the process can be repeated numerously, halving the computational cost each time, until the size of the series is 0 or a prime number.

## C.2 Gibb's phenomenon

A time series of real data $y(t_n)$ can be thought of as a time series of infinite length with a rectangular window that spans a duration of length $T = N\Delta t$ of the data. The estimated discrete PSD is then the convolution of the true power spectral density (PSD) with the Fourier transform of the rectangular window. With this window, only a section of the time series is used, as a result a distorted PSD is produced.

The distorted PSD has a wide central lobe which leaks into its side lobes. The distortion described here is Gibb's phenomenon (Emery & Thomson, 2004). The rectangular window is defined in equation as

$$\begin{aligned} w_R &= 1 \quad |k| \leq N/2 \\ &= 0 \quad |k| > N/2. \end{aligned} \tag{C.2.1}$$

The windowed result is,

$$d_k = w_R(k) Y_k,$$

and is graphically illustrated in Figure C.1.

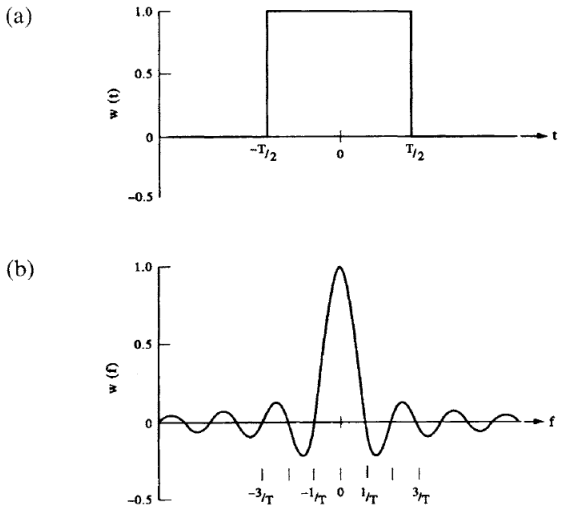


**Figure C.1:** A rectangular window w($t$). (a) shows the window w($t$) in a time domain, where w($t$) = 1 for $-T/2 \leq t \leq T/2$ and 0 otherwise. (b) shows the frequency response to the window in (a) (Emery & Thomson, 2004)

.

# Appendix D

# T_Tide outputs

```
file name: dbn_wl_02.txt
date: 03-Nov-2015
nobs = 13966,  ngood = 12860,  record length (days) = 193.97
start time: 06-Jul-2012 11:00:00
rayleigh criterion = 1.0
Greenwich phase computed with nodal corrections applied to
amplitude \n and phase relative to center time

x0= 4.02, x trend= 0

var(x)= 575.4326   var(xp)= 11.6826   var(xres)= 564.0556
percent var predicted/var original= 2.0 %

     tidal amplitude and phase with 95% CI estimates
```

| tide | freq | amp | amp_err | pha | pha_err | snr |
|---|---|---|---|---|---|---|
| SSA | 0.0002282 | 1.7409 | 4.218 | 191.10 | 138.83 | 0.17 |
| MM | 0.0015122 | 1.4396 | 4.218 | 73.30 | 167.89 | 0.12 |
| MSF | 0.0028219 | 2.2553 | 4.218 | 40.69 | 107.17 | 0.29 |
| MF | 0.0030501 | 3.6837 | 4.218 | 162.33 | 65.61 | 0.76 |
| *ALP1 | 0.0343966 | 1.1881 | 1.091 | 324.42 | 57.32 | 1.2 |
| 2Q1 | 0.0357064 | 0.1720 | 1.091 | 245.11 | 395.13 | 0.025 |
| Q1 | 0.0372185 | 0.1748 | 1.091 | 37.75 | 388.82 | 0.026 |
| O1 | 0.0387307 | 0.9938 | 1.091 | 242.56 | 68.25 | 0.83 |
| TAU1 | 0.0389588 | 0.9334 | 1.091 | 331.03 | 59.83 | 0.73 |
| *BET1 | 0.0400404 | 1.3771 | 1.091 | 216.52 | 50.42 | 1.6 |
| NO1 | 0.0402686 | 0.6650 | 1.091 | 247.78 | 148.71 | 0.37 |
| P1 | 0.0415526 | 0.6813 | 1.091 | 221.91 | 91.12 | 0.39 |
| *K1 | 0.0417807 | 1.6955 | 1.091 | 12.78 | 38.85 | 2.4 |
| *PHI1 | 0.0420089 | 1.4493 | 1.091 | 197.24 | 42.81 | 1.8 |
| J1 | 0.0432929 | 0.1957 | 1.091 | 21.98 | 336.07 | 0.032 |
| *SO1 | 0.0446027 | 1.2551 | 1.091 | 302.13 | 54.10 | 1.3 |
| OO1 | 0.0448308 | 0.6663 | 1.091 | 297.33 | 150.49 | 0.37 |
| UPS1 | 0.0463430 | 0.7801 | 1.091 | 342.76 | 117.28 | 0.51 |
| EPS2 | 0.0761773 | 0.2249 | 1.069 | 177.38 | 255.33 | 0.044 |
| MU2 | 0.0776895 | 0.4384 | 1.069 | 179.69 | 135.29 | 0.17 |
| N2 | 0.0789992 | 0.2108 | 1.069 | 252.87 | 285.66 | 0.039 |
| *M2 | 0.0805114 | 2.2345 | 1.069 | 291.58 | 26.85 | 4.4 |
| *MKS2 | 0.0807396 | 1.1382 | 1.069 | 77.16 | 61.09 | 1.1 |
| L2 | 0.0820236 | 0.5277 | 1.069 | 276.07 | 96.68 | 0.24 |
| *S2 | 0.0833333 | 1.9516 | 1.069 | 336.59 | 31.41 | 3.3 |
| K2 | 0.0835615 | 0.6564 | 1.069 | 66.33 | 107.96 | 0.38 |
| MSN2 | 0.0848455 | 0.1592 | 1.069 | 64.28 | 371.07 | 0.022 |
| ETA2 | 0.0850736 | 0.6164 | 1.069 | 151.39 | 110.00 | 0.33 |
| MO3 | 0.1192421 | 0.1370 | 0.525 | 319.20 | 233.44 | 0.068 |
| M3 | 0.1207671 | 0.3783 | 0.525 | 89.08 | 77.09 | 0.52 |
| *SO3 | 0.1220640 | 0.5565 | 0.525 | 352.01 | 58.70 | 1.1 |
| *MK3 | 0.1222921 | 1.1540 | 0.525 | 263.17 | 26.91 | 4.8 |
| *SK3 | 0.1251141 | 0.5801 | 0.525 | 252.65 | 54.67 | 1.2 |
| *MN4 | 0.1595106 | 0.6571 | 0.557 | 185.32 | 46.80 | 1.4 |
| *M4 | 0.1610228 | 0.8668 | 0.557 | 178.63 | 35.36 | 2.4 |
| SN4 | 0.1623326 | 0.3883 | 0.557 | 126.45 | 80.90 | 0.49 |
| *MS4 | 0.1638447 | 0.9701 | 0.557 | 219.34 | 32.27 | 3 |
| MK4 | 0.1640729 | 0.3310 | 0.557 | 5.07 | 109.36 | 0.35 |
| S4 | 0.1666667 | 0.2701 | 0.557 | 238.48 | 118.40 | 0.24 |
| SK4 | 0.1668948 | 0.5372 | 0.557 | 197.33 | 68.84 | 0.93 |
| *2MK5 | 0.2028035 | 0.3417 | 0.301 | 167.27 | 51.14 | 1.3 |
| 2SK5 | 0.2084474 | 0.1038 | 0.301 | 93.03 | 175.57 | 0.12 |
| 2MN6 | 0.2400221 | 0.1204 | 0.282 | 346.26 | 126.83 | 0.18 |
| M6 | 0.2415342 | 0.1620 | 0.282 | 263.97 | 93.95 | 0.33 |
| *2MS6 | 0.2443561 | 0.3287 | 0.282 | 282.87 | 47.30 | 1.4 |
| 2MK6 | 0.2445843 | 0.1403 | 0.282 | 196.64 | 128.15 | 0.25 |
| 2SM6 | 0.2471781 | 0.0440 | 0.282 | 142.19 | 360.95 | 0.024 |
| MSK6 | 0.2474062 | 0.2261 | 0.282 | 156.98 | 81.23 | 0.64 |
| 3MK7 | 0.2833149 | 0.1163 | 0.222 | 22.07 | 108.59 | 0.27 |
| *M8 | 0.3220456 | 0.2197 | 0.177 | 167.34 | 42.51 | 1.5 |

**Figure D.1:** T_Tide output for water levels.

```
file name: ux_uy_1592_fin01.txt
date: 26-Oct-2015
nobs = 13966,  ngood = 12860,  record length (days) = 193.97
start time: 06-Jul-2012 11:00:00
rayleigh criterion = 1.0
Greenwich phase computed with nodal corrections applied to
 amplitude \n and phase relative to center time

x0= 1.13, x trend= 0

var(x)= 335.5076   var(xp)= 77.6791   var(xres)= 258.2277
percent var predicted/var original= 23.2 %

y0= 4.22, x trend= 0

var(y)= 469.0296    var(yp)= 30.4179  var(yres)= 439.5029
percent var predicted/var original= 6.5 %

ellipse parameters with 95%% CI estimates

tide   freq      major  emaj    minor   emin     inc    einc     pha    epha      snr
 SSA  0.0002282  1.800   3.630  -0.454   2.52    67.27  91.22   187.17 125.23   0.25
 MM   0.0015122  1.441   3.379   0.083   2.85    54.92 113.95    73.47 134.93   0.18
*MSF  0.0028219  4.233   2.241  -0.106   3.81   174.17  51.63   222.97  30.37    3.6
*MF   0.0030501  4.239   3.798  -0.216   2.26    81.69  30.78   160.67  51.49    1.2
*ALP1 0.0343966  1.188   0.885   0.311   0.87    52.41  50.91   324.53  51.54    1.8
 2Q1  0.0357064  0.668   0.874   0.171   0.88   140.32  90.89   328.57  90.07   0.58
 Q1   0.0372185  0.507   0.878   0.166   0.88   135.31 127.33   108.02 127.27   0.33
*O1   0.0387307  2.571   0.867  -0.948   0.89   149.20  26.47   133.65  25.95    8.8
*TAU1 0.0389588  1.948   0.895   0.296   0.86   114.63  23.49   347.40  24.32    4.7
*BET1 0.0400404  1.380   0.881  -0.521   0.88    47.96  50.42   218.05  50.64    2.5
 NO1  0.0402686  0.784   0.902  -0.082   0.85    84.24 100.41   244.02 105.93   0.76
*P1   0.0415526  3.586   0.881   0.313   0.88   132.25  14.07   248.79  14.14     17
*K1   0.0417807  4.170   0.866   1.606   0.89   150.11  16.17   123.10  15.84     23
*PHI1 0.0420089  1.867   0.855   0.640   0.90     9.84  32.71   180.01  31.38    4.8
 J1   0.0432929  0.196   0.883   0.065   0.87    49.90 318.89    21.29 321.33  0.049
*SO1  0.0446027  1.362   0.866   0.191   0.89    28.88  41.94   298.70  40.76    2.5
*OO1  0.0448308  1.237   0.855   0.236   0.90   172.88  70.68    99.67  67.21    2.1
 UPS1 0.0463430  0.782   0.881   0.151   0.88    47.76  99.44   341.94  99.94   0.79
 EPS2 0.0761773  0.444   0.758  -0.199   1.05   157.45 167.78    55.68 135.19   0.34
*MU2  0.0776895  1.462   0.915   0.408   0.92   135.39  39.35   247.13  39.14    2.6
*N2   0.0789992  1.165   0.791  -0.020   1.03   152.37  49.83    78.34  38.29    2.2
*M2   0.0805114  7.312   0.746   0.435   1.06   159.47   8.20   100.88   5.77     96
*MKS2 0.0807396  1.210   1.082  -0.578   0.72    74.73  61.63    65.85  79.12    1.2
*L2   0.0820236  0.847   0.680  -0.075   1.11     0.25  62.96   282.45  39.01    1.6
*S2   0.0833333  3.487   0.692   1.085   1.10   171.31  20.39   127.60  14.06     25
*K2   0.0835615  2.296   0.984   0.071   0.85   125.48  24.53    72.31  28.46    5.4
 MSN2 0.0848455  0.219   0.683  -0.124   1.10   175.48 432.58   284.76 342.02    0.1
```

**Figure D.2:** Part 1 of T_Tide output for east-west and north-south velocity components at 15.92 m.

```
ETA2 0.0850736  0.616   0.973  -0.551   0.86    52.83 624.86   150.65 633.47    0.4
 MO3   0.1192421  0.492   0.518   0.131   0.52   137.28  71.57    32.02  71.45    0.9
*M3    0.1207671  0.712   0.512   0.069   0.52   173.66  41.53   260.10  40.52    1.9
*SO3   0.1220640  2.416   0.514  -0.014   0.52   155.31  13.46   173.40  13.23     22
*MK3   0.1222921  3.075   0.513   0.521   0.52   161.87  10.51    58.07  10.31     36
*SK3   0.1251141  1.820   0.513  -0.042   0.52   160.54  17.39    76.60  17.04     13
*MN4   0.1595106  1.560   0.507   0.165   0.50   166.20  18.00   352.07  18.25    9.5
*M4    0.1610228  3.520   0.506  -0.322   0.50   155.27   7.93    19.84   8.01     48
 SN4   0.1623326  0.442   0.500  -0.126   0.51    81.84  73.31   117.15  72.35   0.78
*MS4   0.1638447  3.494   0.507  -0.166   0.50   157.90   8.08    48.80   8.18     48
*MK4   0.1640729  1.508   0.503  -0.032   0.50   129.38  21.76   359.63  21.69      9
 S4    0.1666667  0.350   0.500  -0.200   0.51   102.68 142.14   203.56 141.09   0.49
*SK4   0.1668948  0.664   0.507   0.230   0.50    13.15  60.15   181.76  60.83    1.7
*2MK5 0.2028035  0.678   0.319   0.192   0.29   167.76  28.10   316.80  30.62    4.5
 2SK5 0.2084474  0.133   0.287  -0.062   0.32    97.21 201.56    67.78 188.20   0.22
*2MN6 0.2400221  0.461   0.328   0.044   0.29   156.14  33.97   145.69  38.95       2
*M6    0.2415342  0.651   0.324  -0.124   0.29   151.37  25.47   133.09  28.26       4
*2MS6 0.2443561  1.347   0.324  -0.247   0.29   151.42  12.52   150.73  13.90      17
*2MK6 0.2445843  0.372   0.292  -0.032   0.32   120.35  55.86   184.44  50.57     1.6
*2SM6 0.2471781  0.676   0.311   0.018   0.30   138.61  25.29   166.88  25.96     4.7
*MSK6 0.2474062  0.548   0.297   0.171   0.32   125.51  43.56   203.54  41.23     3.4
 3MK7 0.2833149  0.229   0.246   0.038   0.20   171.14  53.05   185.35  63.41   0.87
*M8    0.3220456  0.550   0.189  -0.168   0.17   157.69  18.64    34.78  20.73     8.5

total var= 804.5372   pred var= 108.097
percent total var predicted/var original= 13.4 %
```

**Figure D.3:** Part 2 of T_Tide output for east-west and north-south velocity components at 15.92 m.

# Appendix E

# Tidal analysis graphs and tables

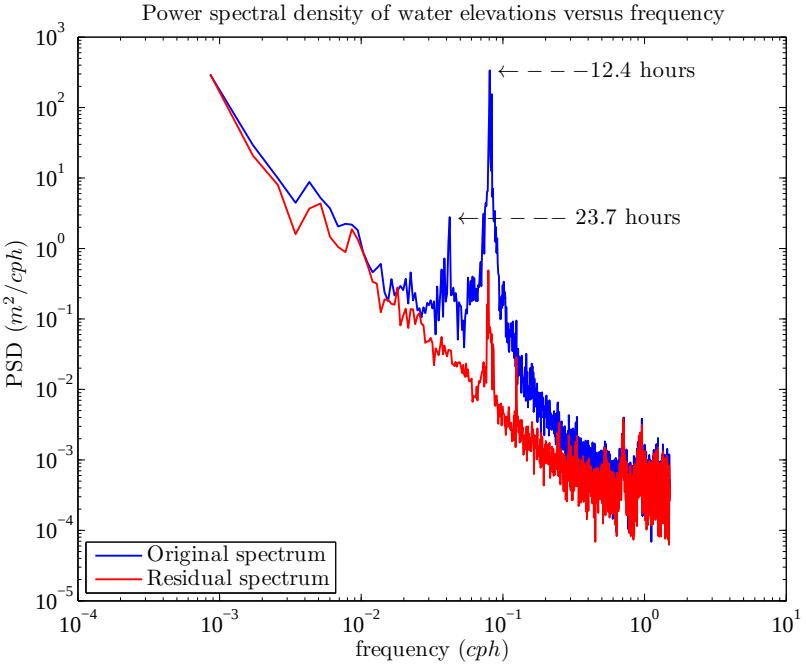


**Figure E.1:** Power spectral density graph of water level measurements and residual water levels after de-tiding for the whole period.

| Variances for the whole period | | | |
|---|---|---|---|
| Depth | East(%) | North(%) | Total (%) |
| 2.42 m | 35.0(7.9%) | 50.4( 8.2%) | 85.4(8.1%) |
| 8.92 m | 37.2(2.9%) | 104.8(3.4%) | 142.0(3.3%) |
| 15.92 m | 335.5(23.2%) | 469.0(6.5%) | 804.5(13.4%) |

**Table E.1:** Variances of East and North current components and combined (total) variance with the fraction (in percentage) of each variance due to the tidal constituents presented for the three current records for the whole period. Variance given in $(\mathrm{cm/s})^2$.

Table E.1 shows the variances of east-west and north-south velocity components, total variances and percentages of tidal contributions to the variances for the whole study period. The table presents an increase in tidal contribution to variance from the middle, through the bottom to the near surface in the east-west velocity components. In the north-south velocity components, tidal contribution to variance increases from the middle, through the near surface to the near bottom. The total contribution to variance is smallest at the middle and highest at the near surface.

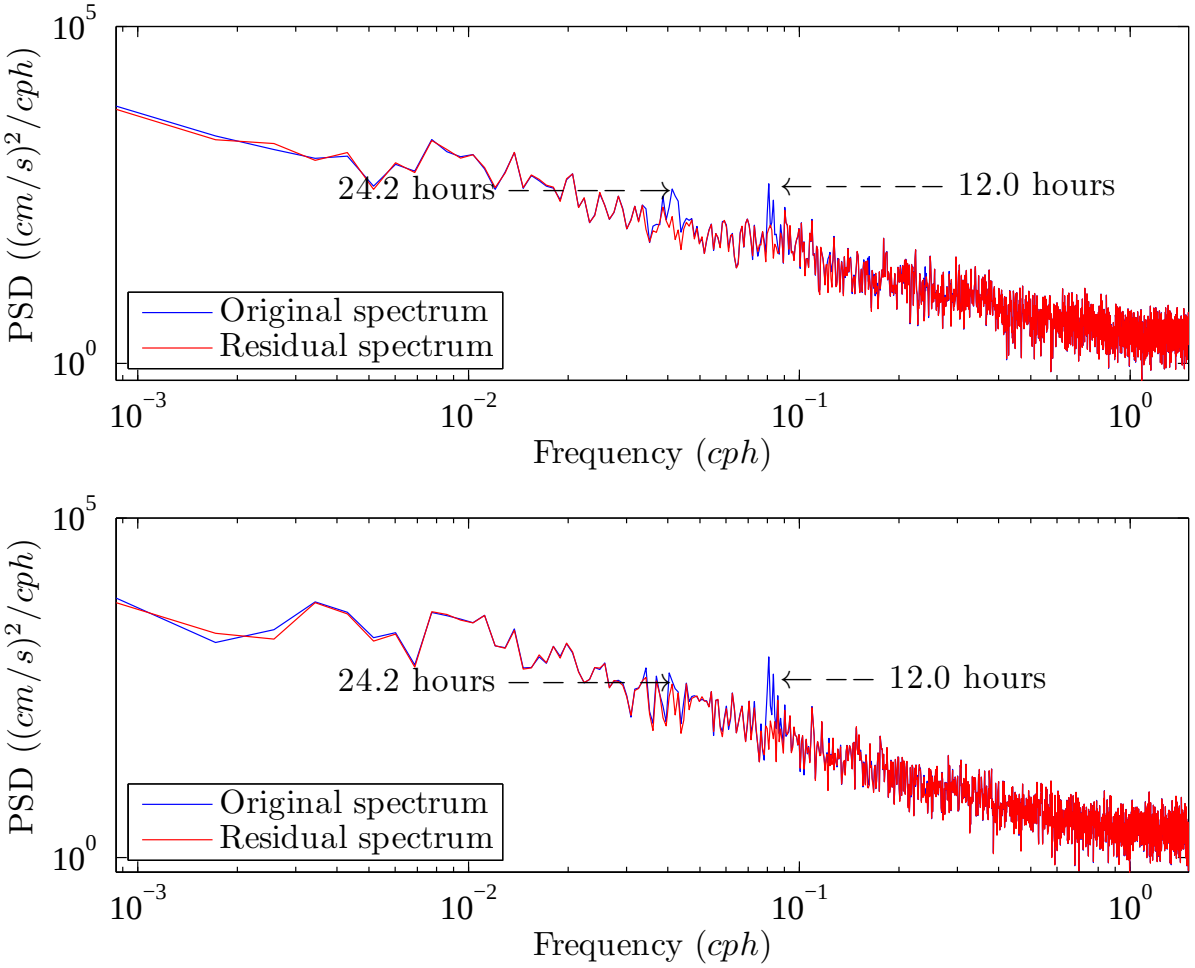


**Figure E.2:** Power spectral density plots of current measurements and residual currents for the whole period at 2.42 m. The top panel represents east-west velocity components and the bottom panel represents north-south velocity components.

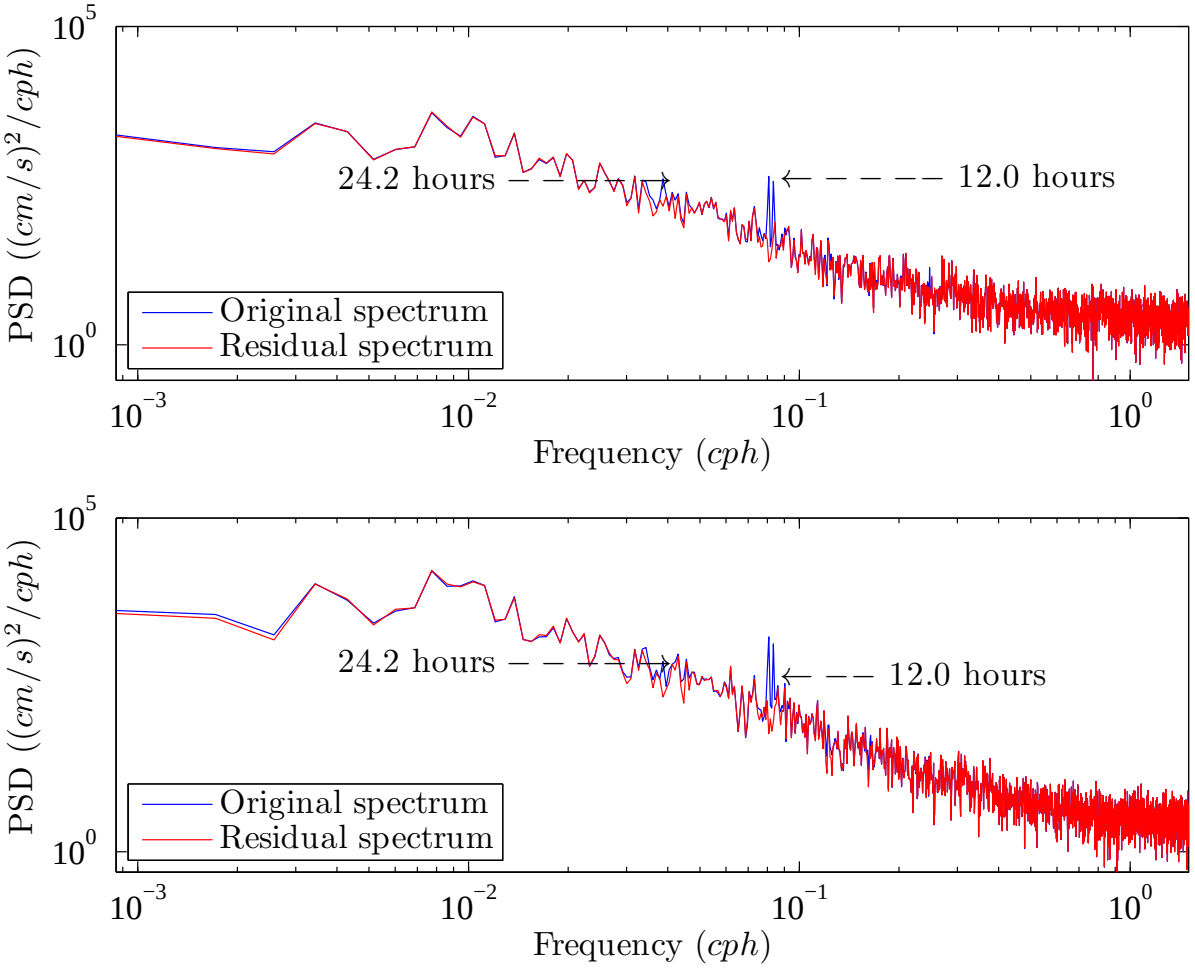


**Figure E.3:** Power spectral density plots of current measurements and residual currents for the whole period at 8.92 m. The top panel represents east-west velocity components and the bottom panel represents north-south velocity components.

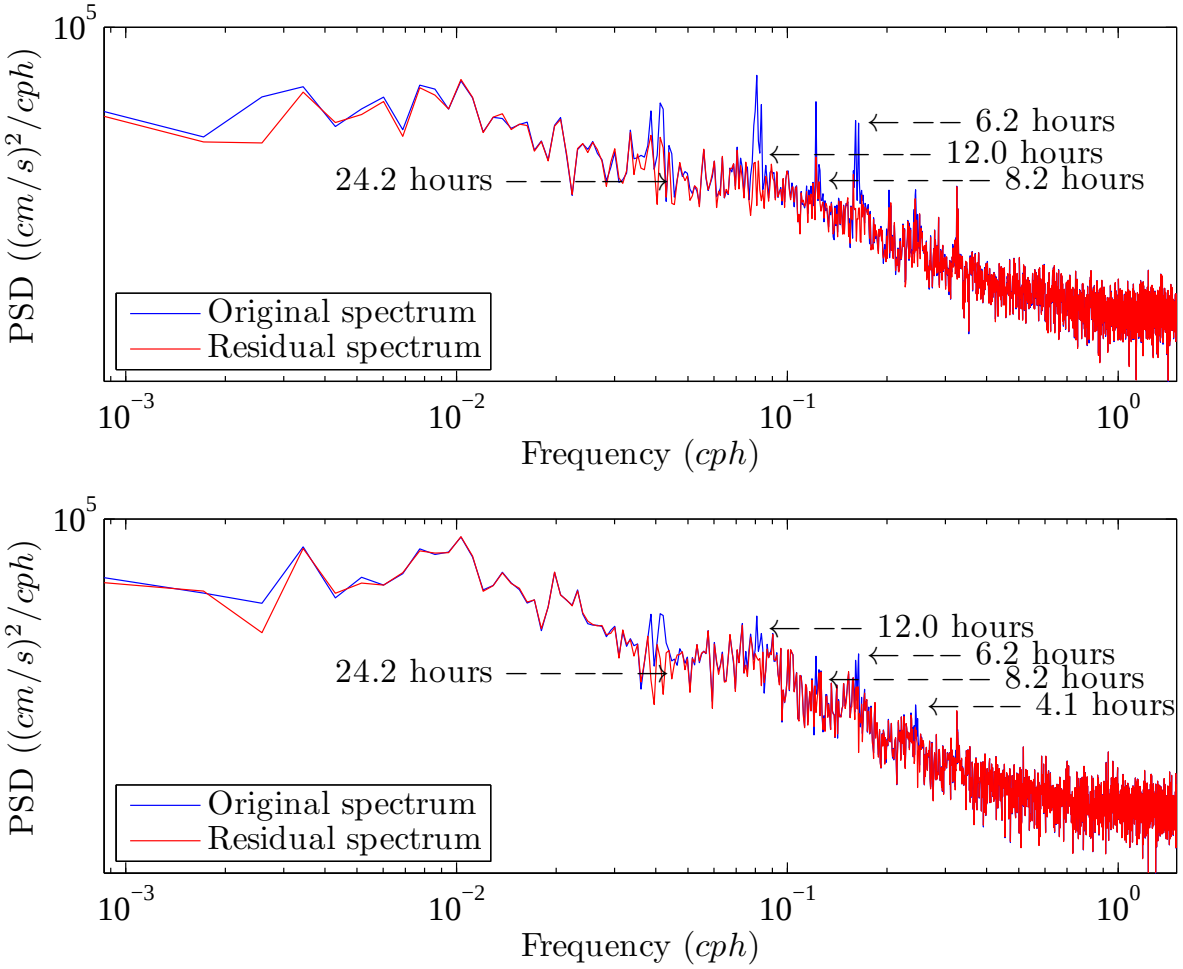


**Figure E.4:** Power spectral density plots of current measurements and residual currents for the whole period at 15.92 m. The top panel represents east-west velocity components and the bottom panel represents north-south velocity components.

| Variances for the whole period | | |
|---|---|---|
| Depth | Longshore(%) | Cross-shore(%) |
| 2.42 m | 60.6(6.0%) | 24.7( 7.4%) |
| 8.92 m | 3130.5(3.1%) | 11.5(7.7%) |
| 15.92 m | 575.4(2.1%) | 229.1(37.1%) |

**Table E.2:** Variances of longshore and cross-shore current components with a fraction (in percentage) of each variance due to tidal constituents presented for the whole period. Variance given in $(cm/s)^2$.

Table E.2 shows the variances of cross-shore and longshore velocity components, total variances and percentages of tidal contributions to the variances for the whole study period. The table presents tidal contribution to variance in the longshore velocity components to be largest at the bottom, followed by the middle and then it is smallest near the surface. In the cross-shore components the tidal contribution to variance is smallest at the bottom, followed by the middle, and then it is largest near the surface The table also show the effect of tides in the cross-shore velocity components to be larger than that in the longshore velocity components.

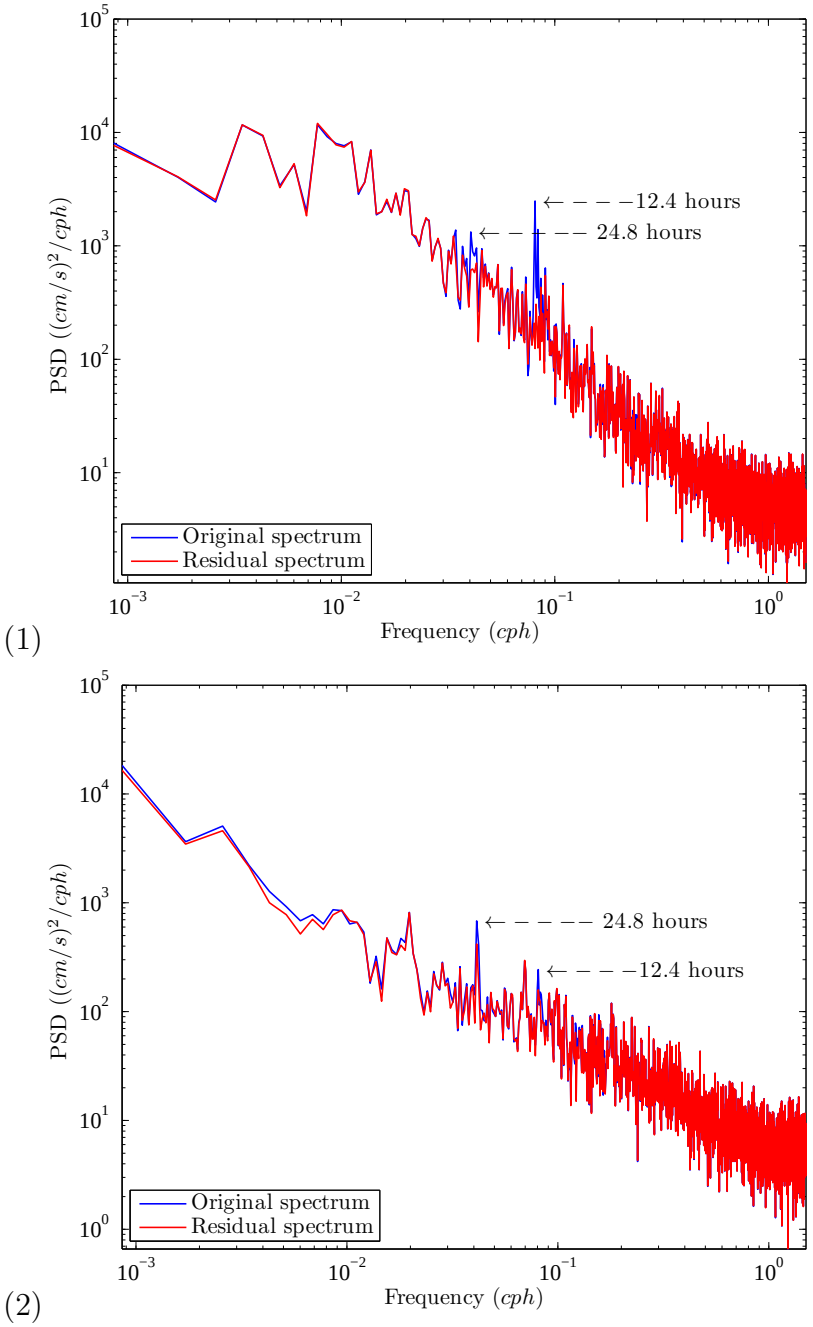


**Figure E.5:** Power spectral density plots of current measurements and residual currents for the whole period at 2.42 m. The top panel (1) represents longshore velocity components and the bottom panel (2) represents cross-shore velocity components.

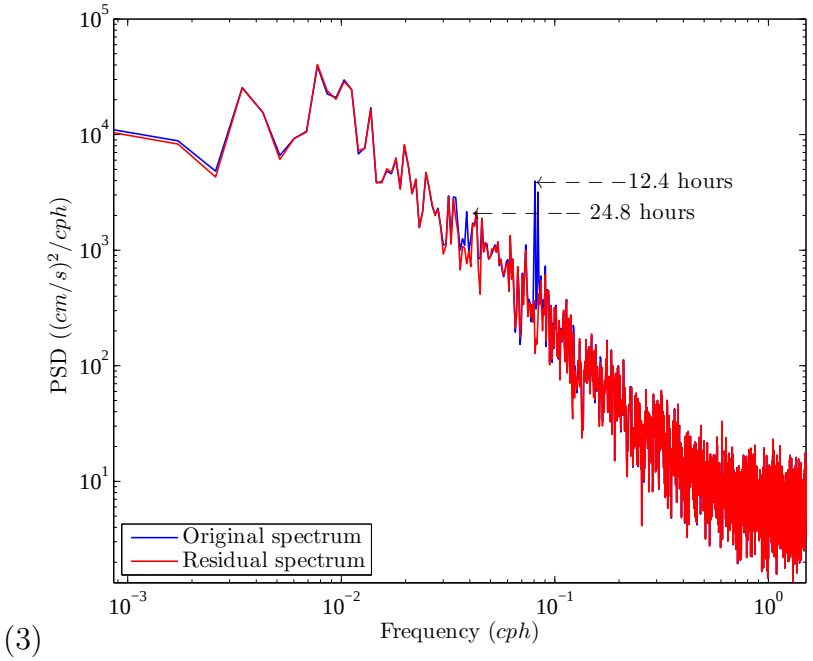


(3)

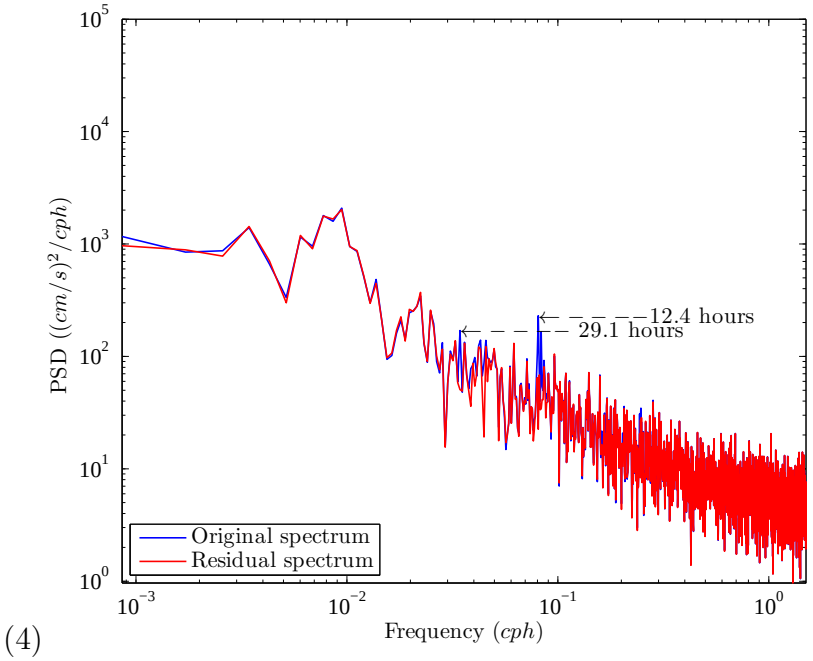


(4)

**Figure E.6:** Power spectral density plots of current measurements and residual currents for the whole period at 8.92 m. The top panel (3) represents longshore velocity components and the bottom panel (4) represents cross-shore velocity components.

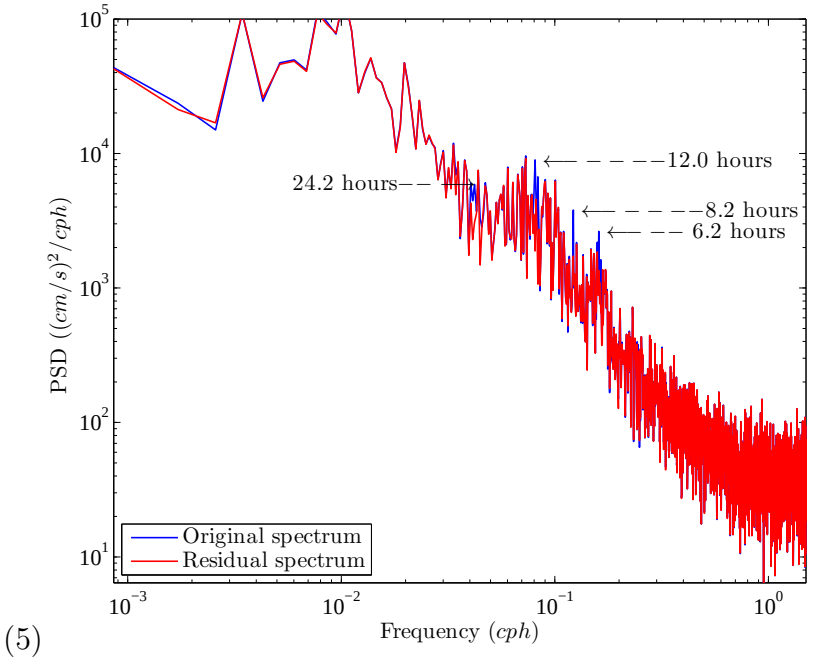


(5)

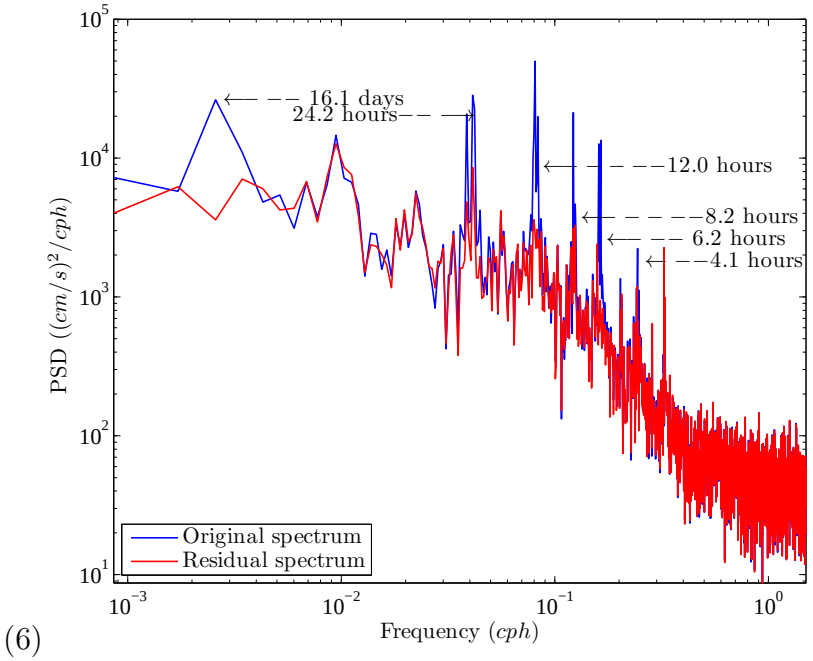


(6)

**Figure E.7:** Power spectral density plots of current measurements and residual currents for the whole period at 15.92 m. The top panel (5) represents longshore velocity components and the bottom panel (6) represents cross-shore velocity components.

# Appendix F

# Wind and currents analysis

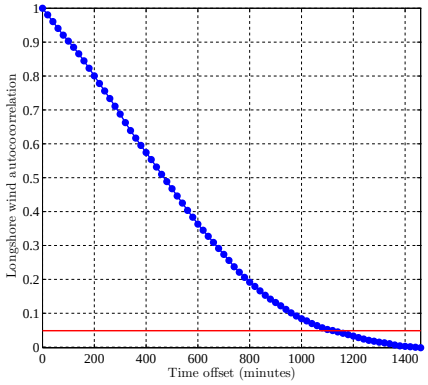


**Figure F.1:** LS Wind autocorrelation (1)

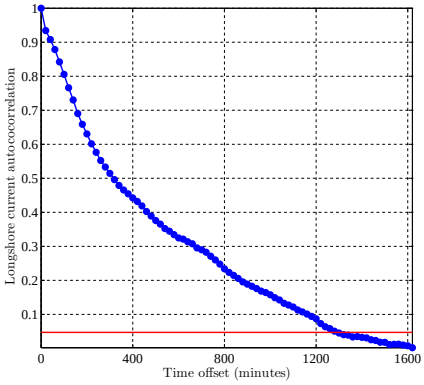


**Figure F.2:** LS Current autocorrelation (1)

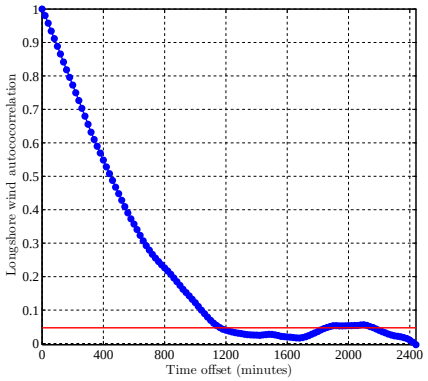


**Figure F.3:** LS Wind autocorrelation (2)

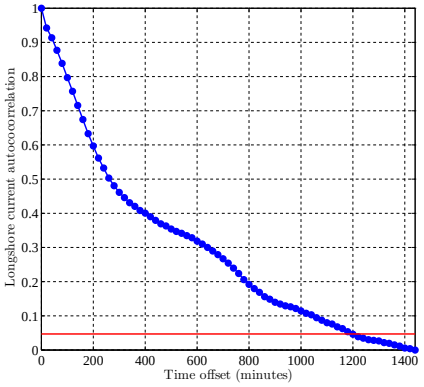


**Figure F.4:** LS Current autocorrelation (2)

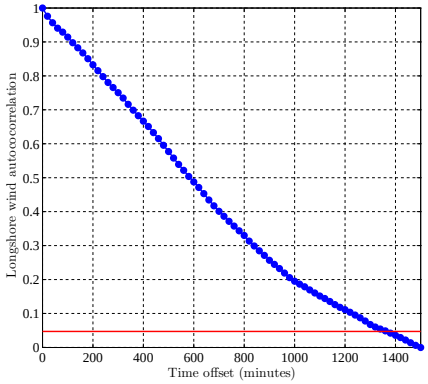


**Figure F.5:** LS Wind autocorrelation (3)

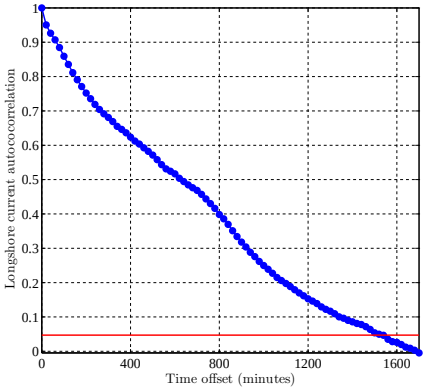


**Figure F.6:** LS Current autocorrelation (3)

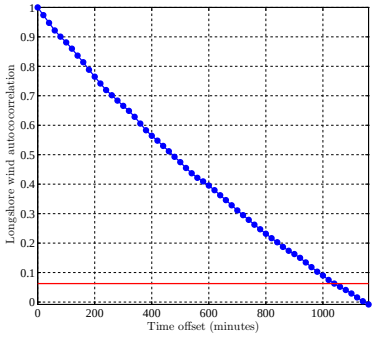


**Figure F.7:** LS Wind autocorrelation (4)

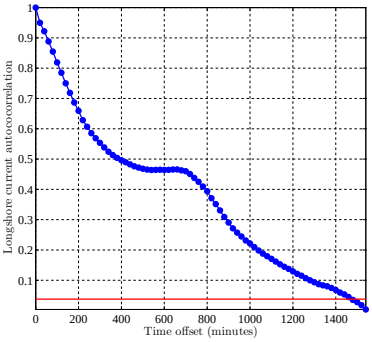


**Figure F.8:** LS Current autocorrelation (4)

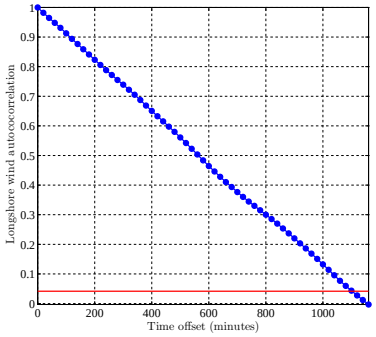


**Figure F.9:** LS Wind autocorrelation (5)

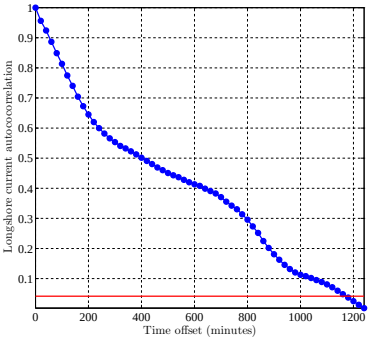


**Figure F.10:** LS Current autocorrelation (5)

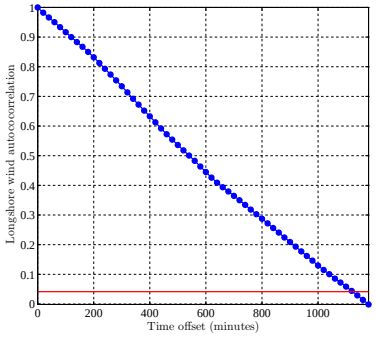


**Figure F.11:** LS Wind autocorrelation (6)

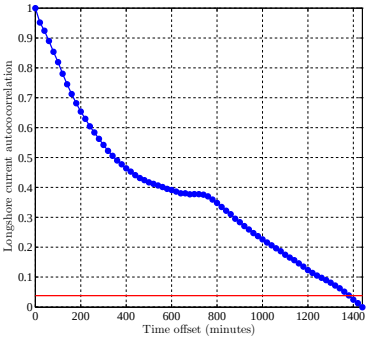


**Figure F.12:** LS Current autocorrelation (6)

**Figure F.13:** CS Wind autocorrelation (1)

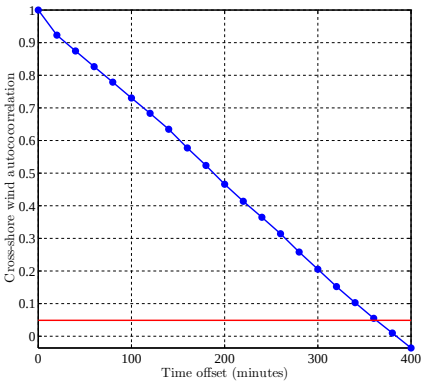


**Figure F.14:** CS Current autocorrelation (1)

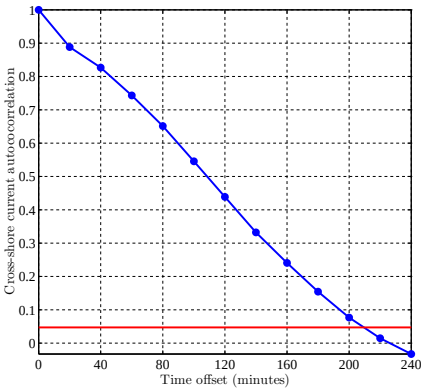


**Figure F.15:** CS Wind autocorrelation (2)

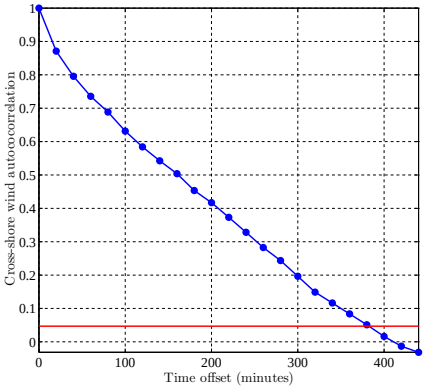


**Figure F.16:** CS Current autocorrelation (2)

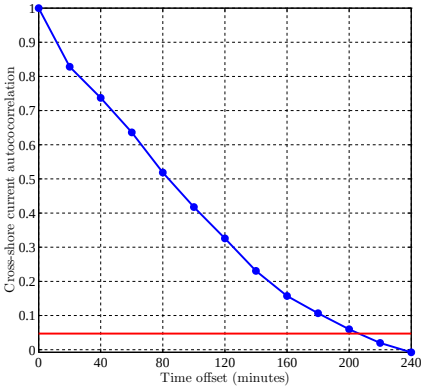


**Figure F.17:** CS Wind autocorrelation (3)

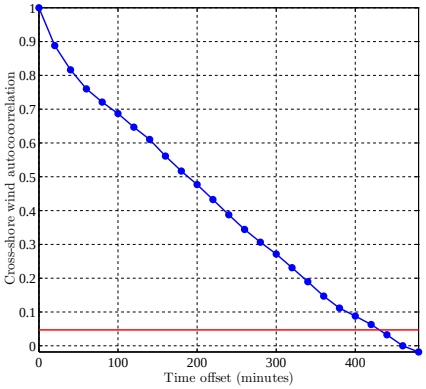


**Figure F.18:** CS Current autocorrelation (3)

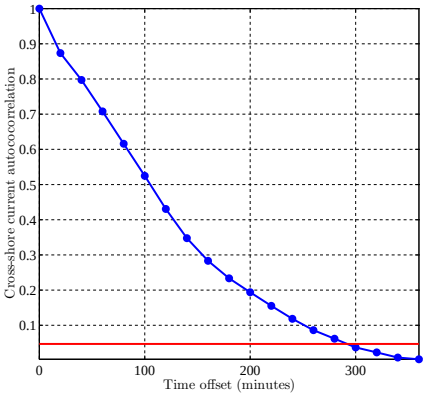

**Figure F.19:** CS Wind autocorrelation (4)

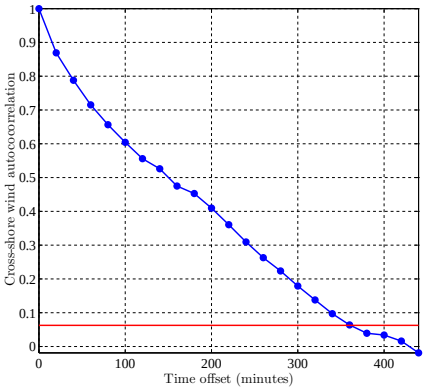


**Figure F.20:** CS Current autocorrelation (4)

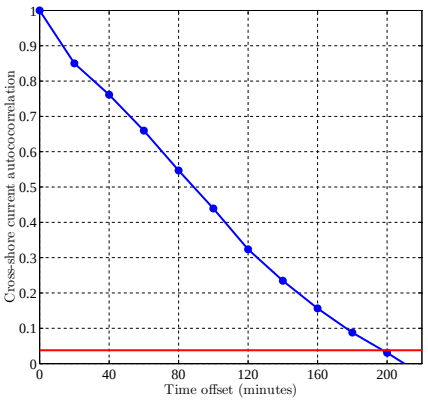


**Figure F.21:** CS Wind autocorrelation (5)

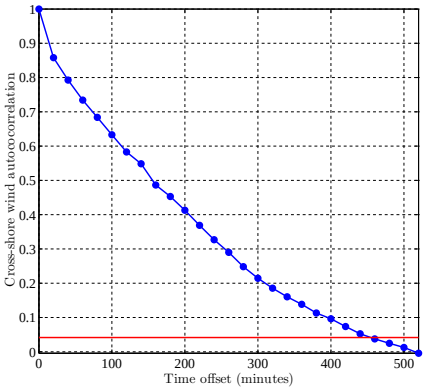


**Figure F.22:** CS Current autocorrelation (5)

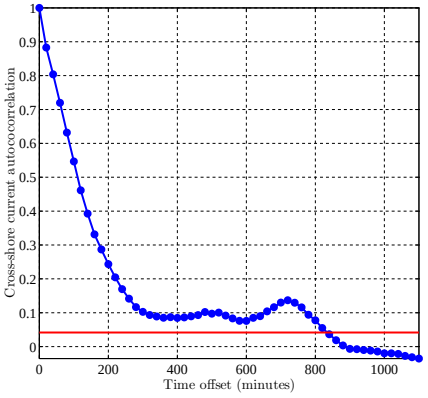


**Figure F.23:** CS Wind autocorrelation (6)

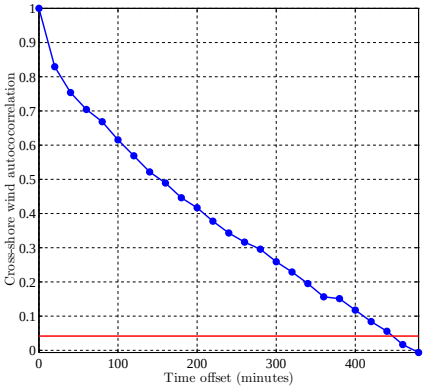


**Figure F.24:** CS Current autocorrelation (6)

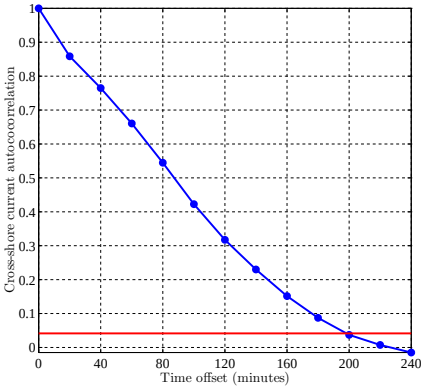

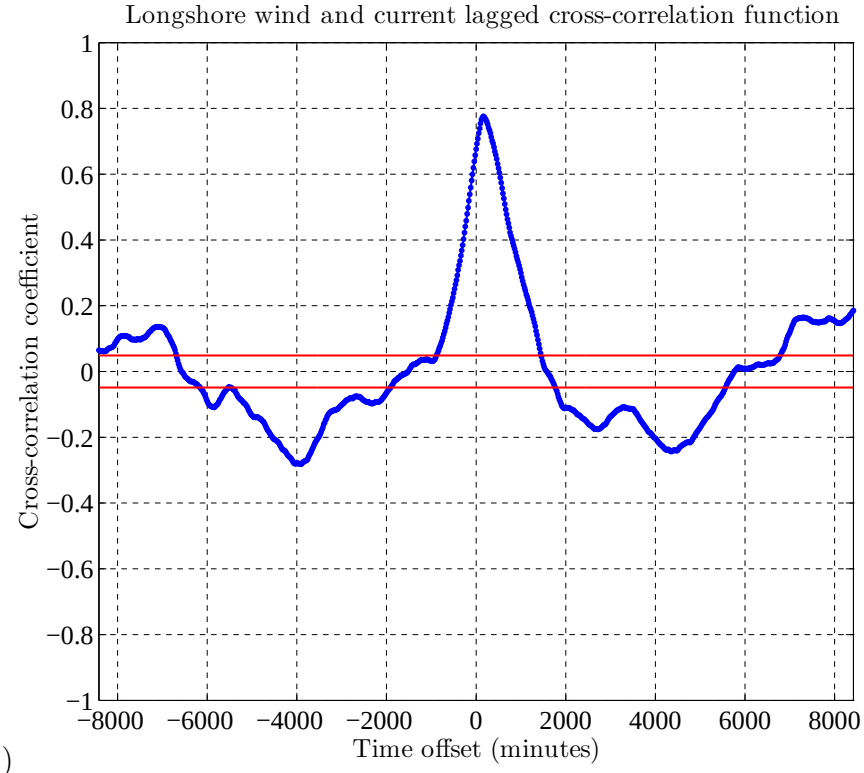


(1)

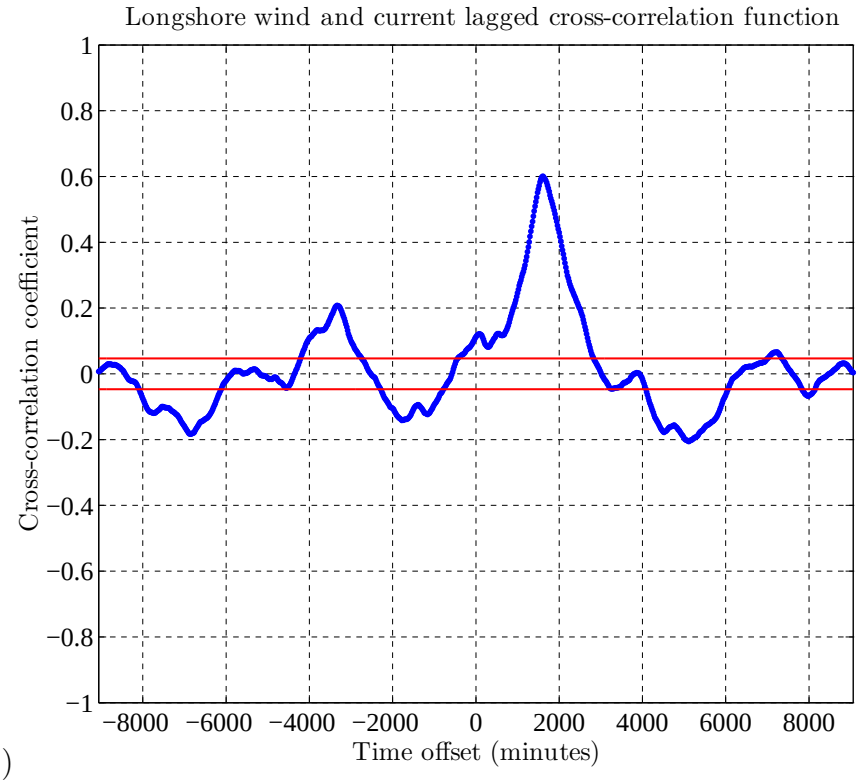


(2)

**Figure F.25:** Lagged longshore cross-correlation function of wind and currents for period one (1) and period two (2).

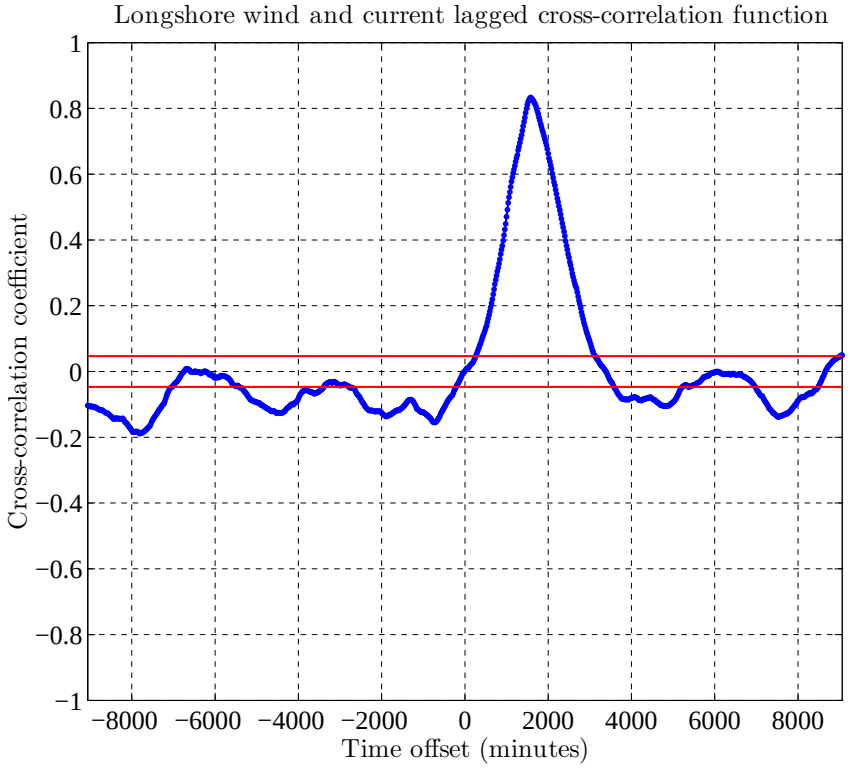


(3)

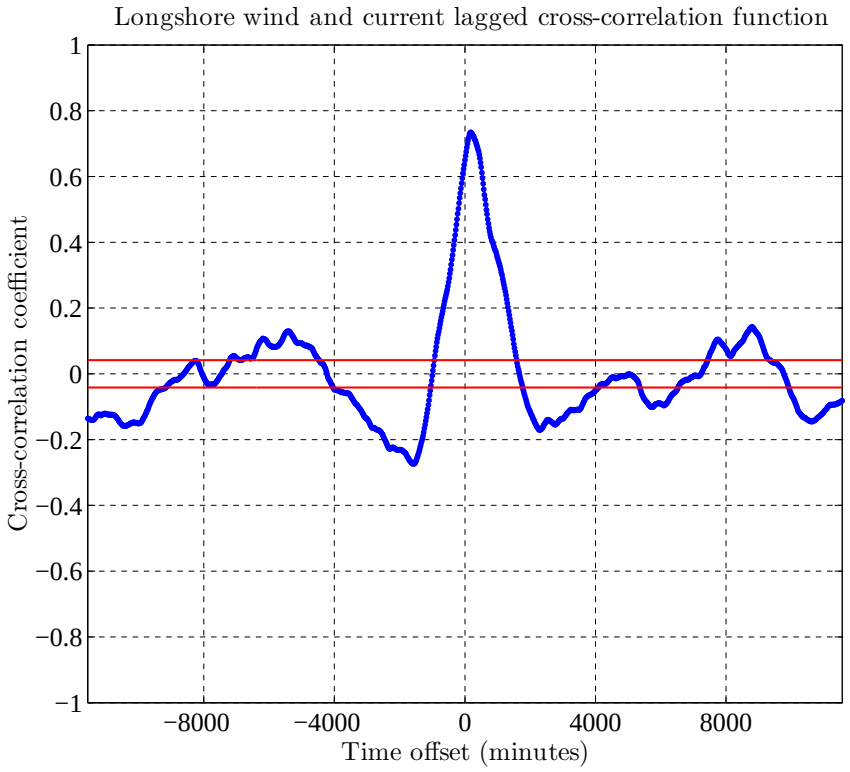


(4)

**Figure F.26:** Lagged longshore cross-correlation function of wind and currents for period three (3) and period six (4).

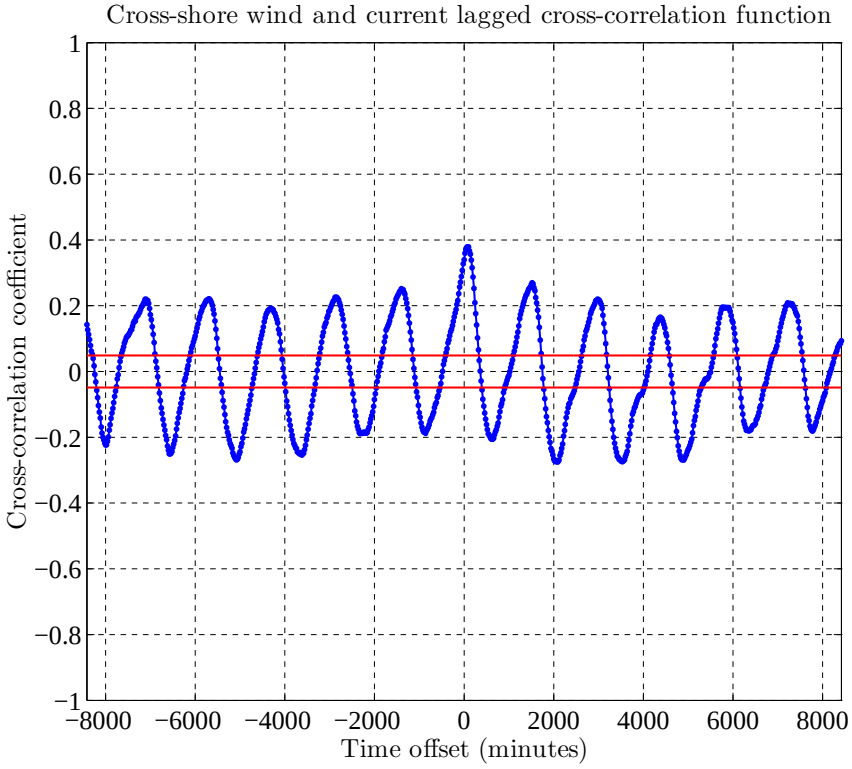


(1)

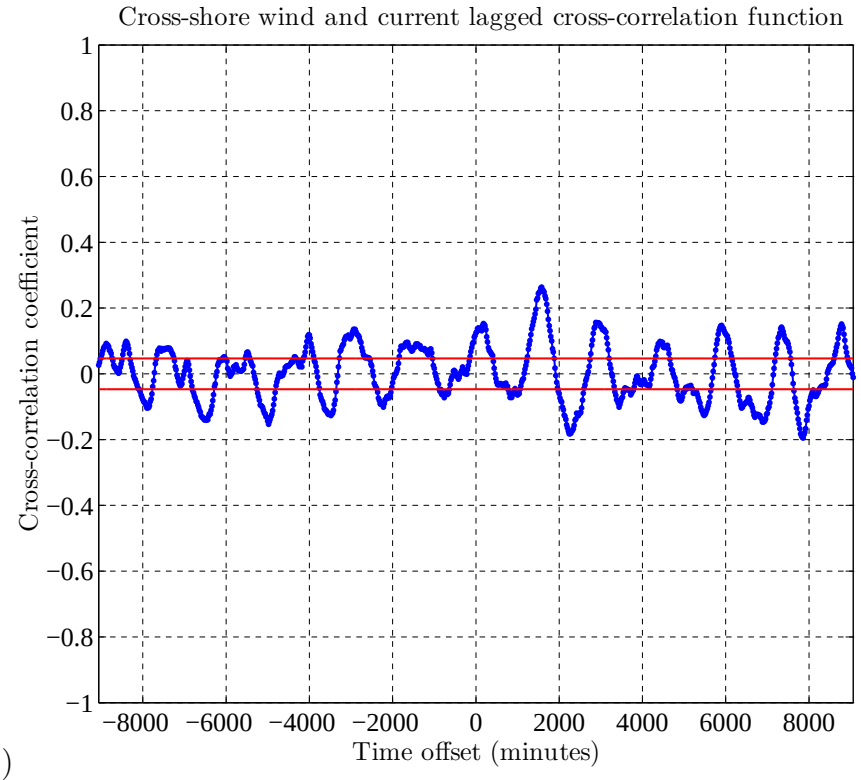


(2)

**Figure F.27:** Lagged cross-shore cross-correlation function of wind and currents for period one (1) and period two (2).

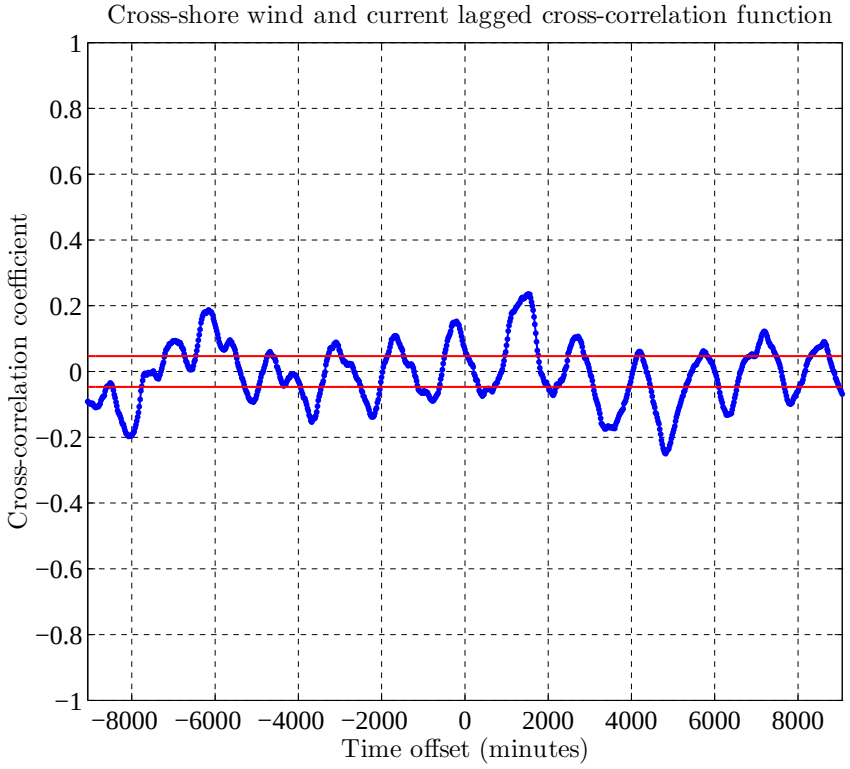


(3)

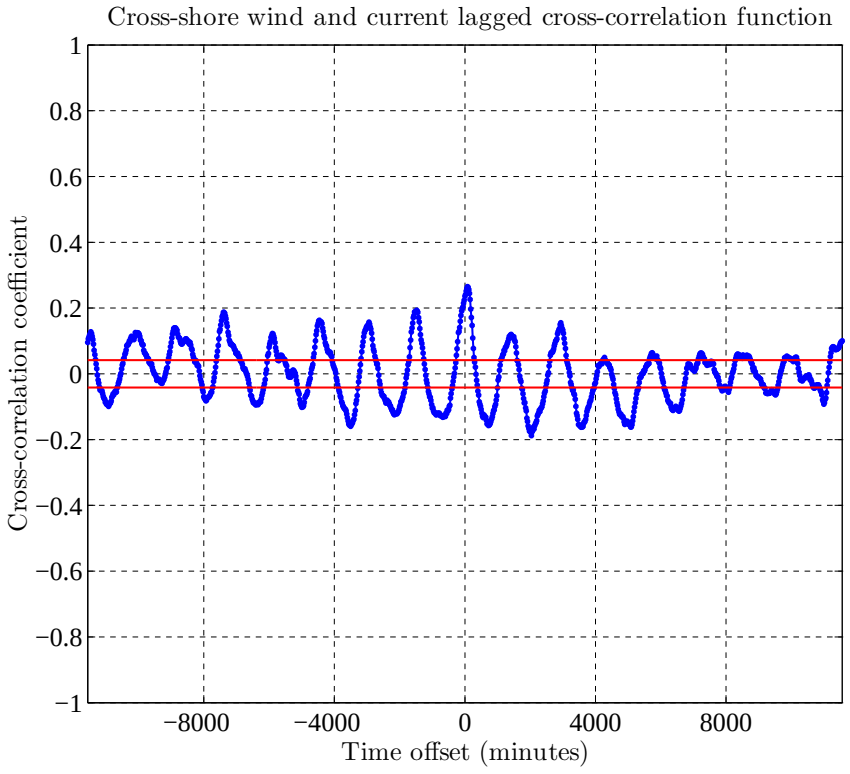


(4)

**Figure F.28:** Lagged cross-shore cross-correlation function of wind and currents for period three (3) and period six (4).

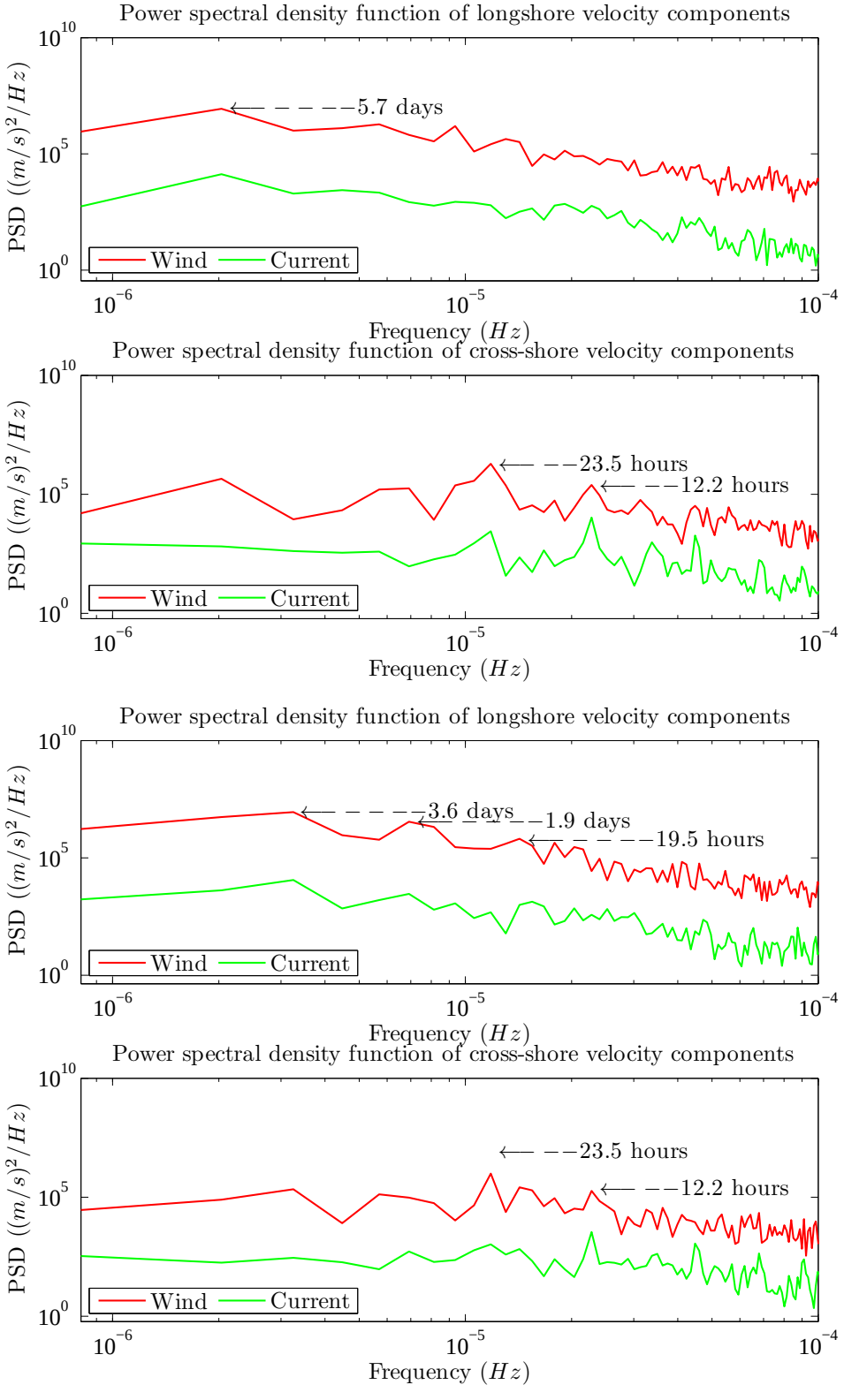


**Figure F.29:** Modified periodogram of currents and wind for period one (1) and period two (2).

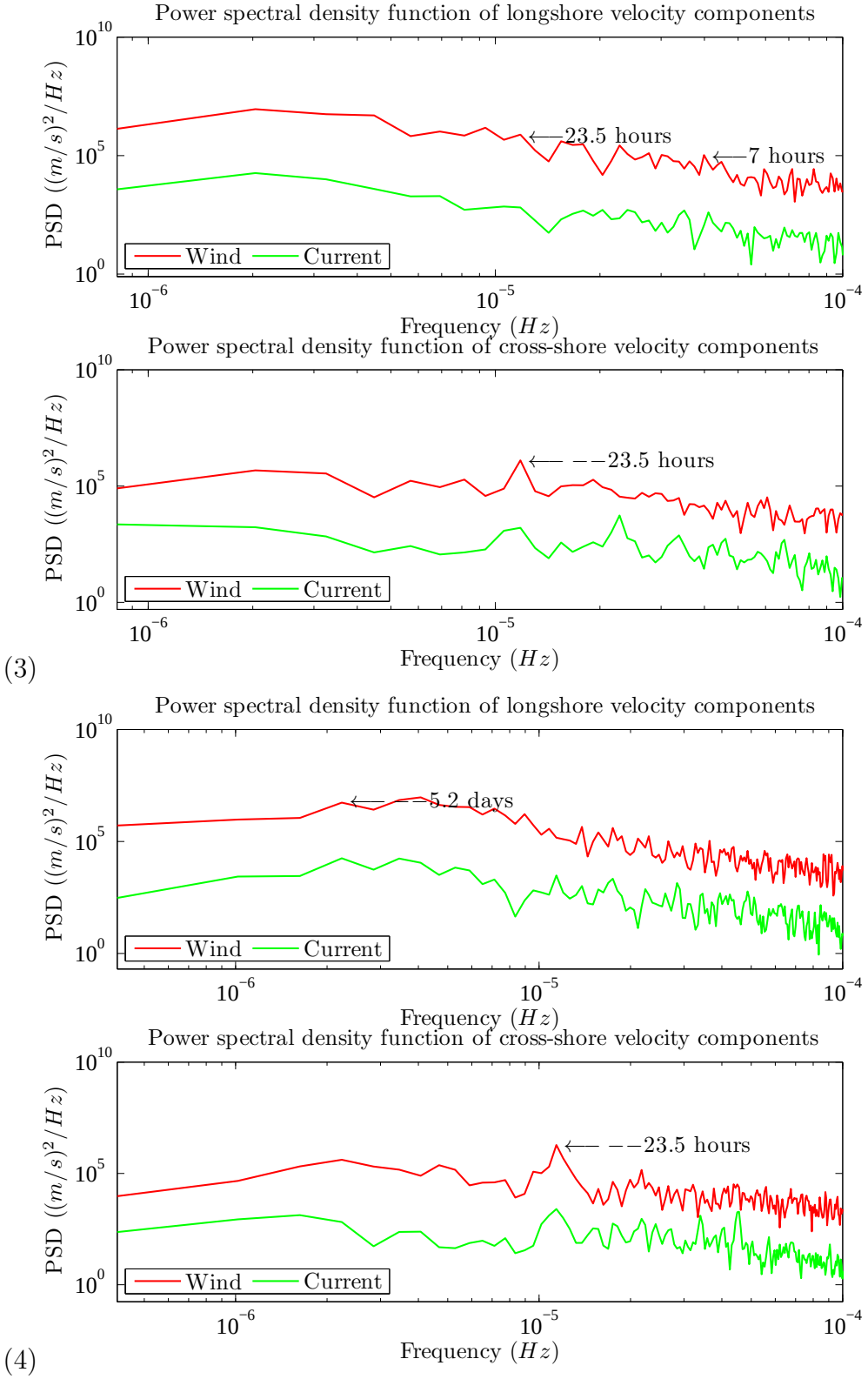


**Figure F.30:** Modified periodogram of currents and wind for period three (3) and period six (4).

# List of References

Aagaard, T. & Vinther, N. (2008). Currents in the surf zone: Rips or undertow. *Journal of Coastal Research, 24, No. 3*, 561–570.

Baher, H. (2012). *Signaliing processing and integrated circuits*. The Atrium, Southern Gate, Chichester, West Sussex, PO19 8SQ, United Kingdom: John Wiley & Sons, Ltd.

Bird, E. C. F. (1984). *Coasts: An introduction to coastal geomorphology* (3 ed.). United Kingdoms: Basil Blackwell Publishers Limited.

Boiten, W. (2003). *Hydrometry: IHE Delft lecture note series*. Lisse, The Netherlands: A.A Balkema publishers.

Bowden, K. F. (1983). *Physical oceanography of coastal waters*. Liverpool, Merseyside: Ellis Horwood Limited.

Brown, R., Baker, D. J., & McCall, J. C. (1996). Nondirectional and directional wave data analysis procedures. Technical Report 96-002(1), National Oceanic and Atmospheric Administration, Slidell, Louisiana.

Buttkus, B. (2012). *Spectral Analysis and Filter Theory in Applied Geophysics*. Springer Berlin Heidelberg.

CEM (2001). *Coastal Engeneering Manual*. Washington, D.C: U.S. Army Corps of Engineers.

Chatfield, C. (1989). *The Analysis of Time Series-An Introduction* (4 ed.). Washington D C.: Chapman and Hall.

Chatfield, C. (2004). *The Analysis of Time Series-An Introduction* (6 ed.). Boca Raton, Florida: CRC Press LLC.

Cooper, I. (1991). Shoreline changes on the Natal coast: Mkomazi river to Tugela river mouth. Technical report, Natal Town and Regional planning, KwaZulu-Natal, South Africa.

Corbella, S. & Stretch, D. D. (2012). The wave climate on the KwaZulu-Natal coast of South Africa. *Journal of the South African institution of civil engeneering, 54*(2), 45â–54.

Craik, A. (1988). *Wave Interactions and Fluid Flows*. Cambridge Monographs on Mechanics. Cambridge University Press.

Croninger, R. G. & Douglas, K. M. (2005). Missing data and institutional research. *New directions for institutional research*, *2005*(127), 33–49.

Cushanick, M. S. (2005). Analysis of nearshore contents near a submarine canyon. Master's thesis, Naval postgraduate school, Monterey, California.

Davidson-Arnott, R. G. D. & Greenwood, B. (2003). Waves and sediment transport in the nearshore zone. In F. I. Isla (Ed.), *Coastal zones and estuaries, Encyclopedia of Life Support Systems (EOLSS)* (pp. 43–60). Paris, France: Eolss Publishers. Developed under the auspices of the UNESCO.

DN & SDCEA (2004). *Applied meteorology and climatology in south Durban*. South Africa.: Danmarks Naturfredningsforening (DN) and south Durban Community Environmental Alliance (SDCEA).

Dong, Y. & Peng, C. J. (2013). Principled missing data methods for researchers. *Springer plus*, *2*(222). http://creativecommons.org/licenses/by/2.0.

Emeis, S. & Türk, M. (2007). Comparison of logarithmic wind profiles and power law wind profiles and their applicability for offshore wind profiles. In P. Schaumann, S. Barth, & J. Peinke (Eds.), *Wind energy-proceedings of the Euromech colloquium* (1 ed.)., volume 1 chapter 11, (pp. 61–64). Berlin, Heidelberg: Springer.

Emery, W. J. & Thomson, R. E. (2004). *Data analysis methods in physical oceanography* (2 ed.). Amsterdam, The Netherlands: B V. Elsevier.

Foreman, M. G. G. (1977). *Manual for tidal heights analysis and prediction*, volume 77. Sidney B.C.: Institute of Ocean Sciences, Patricia Bay.

Funke, E. R. & Stretch, D. D. (2002). The effects of wind speed, direction and duration on crosscurrents at the port of Durban entrance. *Proc. of the 1$^{st}$ Int. Conf. On Heat Transfer Fluid Mechanics, and Thermodynamics (HEFAT2002): Skukuza, Kruger National Park, South Africa, 8-10 April*.

Godin, G. (1948). Magnitude of Stokes drift in coastal waters. *Deutsche hydrographische zeitschrift*, *47*(1995), 227–286.

Godin, G. (1991). The analysis of tides and currents. *Tidal Hydronamics*, 675–709.

GoMA (2013). Doppler-based Velocimeters. `http://www.gulfofmaine-census.org/education/research-technology/acoustical-instruments/doppler-based-velocimeters/`.

Gordon, A. L. (1985). Indian-Atlantic transfer of thermocline water at the Agulhas retroflection. Technical report, Kwa Zulu Natal, South Africa.

Harris, F. J. (1978a). On the use of windows for harmonic analysis with the discrete fourier transform. *Proc. of the IEEE, volume 66, No. 1, January 1978*, *66*.

Harris, T. F. W. (1978b). Review of coastal currents in southern African waters. Technical Report 30, South African National Committee for Oceanographic Research.

Heath, N. (2011). Determining the effects of Stokes drift on the movement of oil in the Gulf of Mexico. Honor Theses. Paper 17. http://diginole.lib.fsu.edu/uhm/17.

Hicks, S. D. (2006). *Understanding tides*. U.S. DEPARTMENT OF COMMERCE, National Oceanic and Atmospheric Administration National Ocean Service.

Hoang, A. (2012). Resuspension of bottom sediment on inner shelf. a case study of North-Western coast of Taiwan. Master's thesis, National Central University, Graduate Institute of Hydrological and Oceanic Sciences, Taiwan.

Holthuijsen, L. H. (2007). *Waves in oceanic and coastal waters*. United Kingdoms: Cambridge University press.

Hsua, S. A., Meindlb, E. A., & Gilhousenb, D. B. (1994). Determining the power-law wind-profile exponent under near-neutral stability conditions at sea. *Journal of Applied Meteorology and Climatology*, *33*(6), 757–772.

Huang, H., Wang, F., & Zhanping, X. (2009). V-ADCP: A new acoustic doppler current profiler for measuring water velocity, level, and flow in open channels or large pipes. *Proc. of the 33rd IAHR Congress: Water Engineering for a Sustainable Environment, International Association of Hydraulic Engineering and Research (IAHR), Vancouver, Canada*, 4425–4432.

Kantz, H. & Schreiber, T. (2003). *Nonlinear Time Series Analysis*. United Kingdom: Cambridge University Press.

Longhurst, J. W. S. & Brebbia, C. A. (Eds.). (2014). *Air polution XXII*. United Kingdoms: WIT Press.

Lutjeharms, J. R. E., Valentine, H. R., & Van Ballegooyen, R. C. (2000). The hydrography and water masses of the Natal Bight, South Africa. *Continental Shelf Research*, *20*, 1907–1939.

Lutjerharms, J. R. E. & De Ruijter, W. P. M. (1994). The influence of the Agulhas current on the adjacent coastal ocean: possible impacts of climate change. *Journal of Marine Systems*, *7*(1996), 321–336.

Lutjerharms, J. R. E. & Roberts, H. R. (1988). The Natal pulse: an extreme transient on the Agulhas current. *Journal of geophysical research*, *93*(C1), 631–645.

Mecozzi, M. & Tomassetti, P. (2007). Handling of a large dataset: application of time series analysis to oceanographic studies. *International journal of Environment and Health*, *1*(3), 347–359.

Meyer, A. A., Lutjeharms, J. R. E., & Villiers, S. D. (2002). The nutrient characteristics of the Natal Bight, South Africa. *Journal of Marine Systems*, 11–37.

Meyer, I., Reinecke, J., Roberts, M., & Van Niekerk, J. L. (2013). Assessment of the ocean energy resources off the South African coast. Technical report, Centre for Renewable and Sustainable Energy Studies, Stellenbosch University, Stellenbosch, South Africa.

Monismith, S. G. & Fong, D. A. (2004). A note on the potential transport of scalars and organisms by surface waves. *Limnology and Oceanography*, *49*, 1214–1217. DOI: 10.4319/lo.2004.49.4.1214.

Parker, B. B. (2007). *Tidal Analysis and Prediction*. Silver Spring, Maryland. http://tidesandcurrents.noaa.gov.

Pawlowicz, R., Beardsley, B., & Lentz, S. (2002). Classical tidal harmonic analysis including error estimates in MATLAB using T_Tide. *Computers and Geosciences*, *28*, 929–937.

Pearce, A. E. (1977). The shelf circulation off the east coast of south africa. Master's thesis, University of Natal, Durban, South Africa.

Pinet, P. R. (2011). *Invitation to Oceanography* (2 ed.). Burlington, Massachusetts: Jones & Bartlett Publishers.

Price, J. F. (Ed.). (1985). *Fourier techniques and applications*. New York, United States of America: Springer Science and Business Media.

RDI (1996). *Acoustic Doppler Current Profiler principle of operation: A practical Primer*. Carlifonia: RDI.

Reddy, P. J. (1997). *Stochastic Hydrology* (1 ed.). Laxmi Publications.

Rosenthal, G. & Grant, S. (1989). Simplified tidal prediction for the south african coastline. *South African journal of Science*, *85*, 104–107.

Ross, S. M. (2010). *Introductory Statistics* (3 ed.). Kidlington, Oxford: Elsevier Inc.

SANHO (2014). Tidal theory. http://www.sanho.co.za/tides/tide _theory.PDF.

Schumann, E. H. (Ed.). (1988). *Coastal ocean studies off Natal, South Africa*, volume 26 of *Lecture notes on coastal and estuarine studies*. New York: Springer-Verlag.

Schumann, E. H. & Perrins, L. A. (1982). Tidal and inertial currents around South Africa. *Proc. of the Eighteenth International Coastal Engeneering Conference*, *18*, 562–2580.

Schwartz, M. (2006). *Encyclopedia of Coastal Science*. Tokyo/The Netherlands: Springer Science & Business Media.

Short, A. D. (2012). Coastal processes and beaches. *Nature Education Knowledge*, *3*(10), 15.

Shumway, R. H. & Stoffer, D. S. (2006). *Time series analysis and its applications with R examples* (2 ed.). United States of America: Springer Science and Business Media, LLC.

Southgate, H. N. (1988). A nearshore profile model of wave and tidal current interaction. *Coastal engeneering*, *13*, 219–245.

Steinberg, W. J. (2011). *Statistics Alive!* (2 ed.). United States of America: SAGE Publications, Inc.

Sutherland, J., Walstra, D. J. R., Van Rijn, L. C., & Southgate, H. N. (2003). Evaluation of modelling systems at an estuary mouth. *Coastal engeneering*, *51*, 119–142.

Teixeira, M. A. C. (2012). The influence of langmuir turbulence on the scaling for the dissipation rate in the oceanic boundary layer. *Journal of Geophysical Research: Oceans*, *117*(C5), n/a–n/a. C05015.

Thé, J. L., Thé, C. L., Johnson, M. A., Raskin, I., & Shatalov, O. (2011). WRPLOT View. `http://www.weblakes.com/products/wrplot/index.html`.

Thompson, L. (2015). Equilibrium tides. `http://faculty.washington.edu/luanne/pages/ocean420/notes/TidesIntro.pdf`.

Van der Westhuysen, A. J. (2002). The application of the numerical wind wave model SWAN to a selected field case on the South African coast. Master's thesis, Stellenbosch University, Stellenbosch, South Africa.

Walters, R. A. & Henston, C. (1981). Notes and correspondences, removing tidal-period variations from time series data using low pass filters. *Journal of Physical Oceanography*, *12*, 112–115.

Webb, A. & Fox-Kemper, B. F. (2011). Wave spectral moments and stokes drift estimation. *Ocean modelling*, *38*, 273–288.

Weller, R. A. & Davis, R. E. (1980). A vector measuring current meter. *Deep Sea Research Part A. Oceanographic Research Papers*, *27*(7), 565–582.

WHOI (2013). Acoustic doppler current profiler (ADCP). `http://www.whoi.edu/instruments/viewInstrument.do?id=819`.

Woodroffe, C. D. (2002). *Coasts: form, process and evolution.* United Kingdoms: Cambridge University press.

Wright, J., Colling, A., & Park, D. (1999). *Waves, Tides, and Shallow-water Processes* (2 ed.). Singapore: Gulf Professional Publishing.

Yanagi, T. (1999). *Coastal Oceanography.* Tokyo/The Netherlands: Terra Scientific Publishing Company/Kluwer Academic Publishers.